Lawrence Berkeley National Laboratory
Recent Work

Title
CHEMISTRY DIVISION ANNUAL REPORT, 1962

Permalink
https://escholarship.org/uc/item/0rx0s2s5

Author
Lawrence Berkeley National Laboratory

Publication Date
1963

eScholarship.org Powered by the California Digital Library
University of California

UCRL - 10624

# University of California

# Ernest O. Lawrence Radiation Laboratory

CHEMISTRY DIVISION ANNUAL REPORT, 1962

TWO-WEEK LOAN COPY

This is a Library Circulating Copy
which may be borrowed for two weeks.
For a personal retention copy, call
Tech. Info. Division, Ext. 5545

Berkeley, California

## DISCLAIMER

This document was prepared as an account of work sponsored by the United States Government. While this document is believed to contain correct information, neither the United States Government nor any agency thereof, nor the Regents of the University of California, nor any of their employees, makes any warranty, express or implied, or assumes any legal responsibility for the accuracy, completeness, or usefulness of any information, apparatus, product, or process disclosed, or represents that its use would not infringe privately owned rights. Reference herein to any specific commercial product, process, or service by its trade name, trademark, manufacturer, or otherwise, does not necessarily constitute or imply its endorsement, recommendation, or favoring by the United States Government or any agency thereof, or the Regents of the University of California. The views and opinions of authors expressed herein do not necessarily state or reflect those of the United States Government or any agency thereof or the Regents of the University of California.

UCRL-10624
UC-4 Chemistry
TID-4500 (19 Ed.)

UNIVERSITY OF CALIFORNIA
Lawrence Radiation Laboratory
Berkeley, California

Contract No. W-7405-eng-48

# CHEMISTRY DIVISION ANNUAL REPORT, 1962

January 1963

I. Perlman, Director, Chemistry Division
Editors: J. M. Hollander, F. L. Reynolds, and J. C. Wallmann

# CHEMISTRY DIVISION ANNUAL REPORT, 1962

Contents



*Preceding annual reports: UCRL-10023, UCRL-9566

D. PHYSICAL CHEMISTRY

# CHEMISTRY DIVISION ANNUAL REPORT, 1962

Lawrence Radiation Laboratory
University of California
Berkeley, California

January 1963

## INTRODUCTION

This report presents a review of the research progress made during the 1962 calendar year by the Nuclear Chemistry Division of the Lawrence Radiation Laboratory. Though the report is not exhaustive, an effort has been made to give a balanced view of the widely ranging research interests and problems of the Division. Contributors to this report include staff members of the Radiation Laboratory, graduate students, and visiting postdoctoral chemists and physicists from many laboratories, domestic and foreign.

Twelve Ph. D. degrees were awarded during 1962 to graduate students who did their research work in this Division, and six Master's degrees were given. Abstracts of the theses are included in this report.

# A. RADIOACTIVITY AND NUCLEAR STRUCTURE

## 1. HYPERFINE STRUCTURE OF THE LITHIUM ISOTOPES

Douglas W. McColm, Richard G. Schlecht, and Isaac Maleh

The lithium-6, 7 hyperfine structure anomaly has been measured by the atomic beams magnetic resonance method. The results are

$$\Delta\nu(Li^6) = 228.20528(10) \text{ Mc/sec},$$

$$\Delta\nu(Li^7) = 803.50404(50) \text{ Mc/sec},$$

$$_7\Delta_6 = -1.08(2)\times 10^{-4},$$

where the nuclear magnetic moment values of Bitter et al.[1] were used and where the quoted errors on the hfs values are approximately five times the statistical errors, and where the error on $\Delta$ arises primarily from that quoted by Bitter. These results are of interest because they give a measure of the distribution of magnetism inside the lithium nucleus to higher precision than previously obtained.[2] This particular nucleus is sufficiently simple that calculations of this distribution from L - S coupled nuclear wave functions of definite total isotopic spin can be performed; we expect to obtain information that will aid in the interpretation of the lithium-6 and lithium-7 magnetic moments.

---

1. F. Bitter, N. I. Adams, and T. F. Wimett, MIT Research Laboratory of Electronics Quarterly Progress Report [No. 21], April 15, 1951, p. 30.

2. P. Kusch and A. K. Mann, Phys. Rev. 76, 707 (1949).

## 2. HALF-LIFE OF FLUORINE-18(*)

John D. Mahony and Samuel S. Markowitz

The half-life of $F^{18}$ has been reported to have various values, ranging from 107 ± 4 to 115 ± 4 min. The accepted value[1] has been 112 min (more recently,[2] 111 min). Our studies of the reaction of $He^3$ with $O^{16}$ to produce this nuclide indicated that an even lower value would be more consistent with

---

*Brief version of a paper submitted to J. Inorg. Nucl. Chem. (UCRL-10512, Oct. 1962).

1. D. Strominger, J. M. Hollander, and G. T. Seaborg, Rev. Mod. Phys. 30, 585 (1958).

2. D. G. Goldman and J. R. Stehn, Chart of the Nuclides, General Electric Co., Schnectady, N. Y., 1961.

the experimental data. Because of (a) the need for an accurate value for the half-life of this nuclide in our activation-analysis studies,[3] (b) the abundance of data available from the determination of the excitation function for the production of $F^{18}$ from $O^{16}$ by using $He^3$ as the incident particle, and (c) the relative purity of the $F^{18}$ produced in this way, the evaluation of this half-life was here undertaken. In addition, there was available a computer program which gives an iterative least-squares fit, including the standard deviations, in $a_j$ and $\lambda_j$ of the function

$$A(t) = \sum_{j=1}^{10} a_j \exp(-\lambda_j t),$$

where t is elapsed time, $a_j$ is the activity of each component at t = 0, and $\lambda_j$ is the decay constant of component j. Additional half-life data were also taken on $F^{18}$ obtained from neutron and proton reactions, in order to afford a wider range of sampling and to eliminate impurities.

## Experimental Procedure

### Preparation and Isolation of Fluorine-18

Method A. Foils of 1/4-mil Mylar, a condensate of terphthalic acid and ethylene glycol containing 33.2% oxygen, were irradiated with $He^3$ ions of energy 1 to 31 MeV for about 15 min at the Berkeley heavy-ion linear accelerator (Hilac). The foils were left uncounted for about 4 hours to allow their shorter-lived activity time to decay. This represents a period 12 times the half-life of 20.4-min $C^{11}$, the longest-lived interfering nuclide. During this time the initial activity of $C^{11}$, approx $10^7$ counts/min, decreased to $2 \times 10^3$ counts/min, which is less than 1% of the $F^{18}$ activity counted at that time. The foils were mounted on 1/16-in. aluminum cards with double-faced Scotch tape and covered with a thin plastic foil.

Method B. Ten milligrams of $Li_2SO_4$ was irradiated with 44-MeV $He^4$ ions at the Berkeley 60-inch cyclotron. The $F^{18}$, produced mainly by the $\alpha, d$ and $\alpha, np$ reactions on $O^{16}$, was separated by dissolving the target in 1 M KOH and placing the solution on a 12-in.-long anion-exchange column filled with Dowex 1 (100–200 mesh), and eluting with 1 M KOH. The active material, which contained the $F^{18}$, came off the column within 3.0 to 3.8 ml. To this volume of eluent, which was collected in about 25 min, 0.5 ml of carrier containing about 9 mg of $F^-$ was added. The solution was made acid with HCl, and 20 mg of $NaH_2PO_4$ and 5 mg of $Fe^{+++}$ was introduced. $Fe(H_2PO_4)_3$ and $Fe(OH)_3$ precipitated when the solution was made basic with $NH_4OH$. [$Fe^{+++}$ was added to scavenge impurities produced by $S^{32}(\alpha, 3p)P^{33}$ and $S^{32}(n, p)P^{32}$ reactions.] After centrifuging, the supernatant solution was made acid with HCl, basic with KOH, and finally, acid again with acetic acid. Ten ml of 1 M $Ca(NO_3)_2$ was added to the warm solution and the resulting precipitate of $CaF_2$ was washed with water, alcohol, and acetone. The final acetone slurry was mounted directly on the aluminum cards.

---

3. S. S. Markowitz and J. D. Mahony, Anal. Chem. 34, 329 (1962).

Method C. Twelve milligrams of spectroscopically pure LiOH was irradiated at the Livermore neutron reactor in a flux of $5\times10^{12}$ n/cm$^2$-sec for 10 min. $F^{18}$ was produced by the two-step reaction, $Li^6(n, \alpha)H^3$ and $O^{16}(H^3, n)F^{18}$. The product was separated and mounted as described in method B except that the scavenging step was omitted.

Counting

The samples were counted with β end-window gas-flow proportional counters whose plateaus were tested for stability. Methane was the counter gas. The counters were periodically checked with a $Cl^{36}$ standard. As an additional control, annihilation radiation emitted by one of the samples was counted with a 3×3-in. NaI(Tl) scintillation counter and 256-channel pulse-height analyzer.

## Results

Each count rate and time datum was rounded to three-digit accuracy and the full set of data for each sample was analyzed with the aid of the FRENIC program (originally written[4] for the IBM-704 computer but adapted for use on the 709-7090). This program yielded a value for λ and also gave its standard deviation. The results of the 16 individual experiments are compiled in Table I. When the standard deviation of the half-life calculated for a particular set of data was greater than 0.7 min, that result was not included in the analysis; because of the small weighting factor in comparison with those listed in Table I, this would have a negligible effect on the weighted mean half-life.

The weighted mean half-life is given by[5]

$$m^w = \sum_{i=1}^{n} w_i x_i \Big/ \sum_{i=1}^{n} w_i ,$$

where $x_i$ represents the individual half-lives measured for the samples and $w_i$ are the weighting factors given by

$$w_i = 1/s_i^2 ,$$

where $s_i$ is the standard deviation of each half-life determination. The weighted standard deviation of the mean is given by[5]

$$s_{mw} = \left[ \sum w_i (x_i - m^w)^2 \Big/ \sum w_i \right]^{1/2} .$$

4. G. R. Keepin, T. F. Wimett, and R. K. Zeigler, J. Nucl. Energy 6, 1 (1957). Revised by R. W. Hoff and J. O. Rasmussen, Lawrence Radiation Laboratory, Berkeley, California.

5. L. G. Parratt, Probability and Experimental Error (John Wiley and Sons, Inc., New York, 1961), p. 118-120.

The results of the research presented here give, for the weighted mean half-life of $F^{18}$ and the weighted standard deviation of the mean,

$$109.7_4 \pm 0.21 \text{ min.}$$

Table I. Results of individual half-life determinations.

| No. of data points | $x_i$(min) | $s_i$(min) | $w_i = 1/s_i^2$ | Method |
|---|---|---|---|---|
| 5 | 109.12 | 0.53 | 3.56 | A |
| 5 | 109.29 | 0.30 | 11.11 | A |
| 5 | 109.36 | 0.22 | 20.66 | A |
| 95 | 109.52 | 0.09 | 123.46 | C |
| 141 | 109.63 | 0.08 | 156.25 | C |
| 104 | 109.66 | 0.10 | 100.00 | B |
| 165 | 109.69 | 0.16 | 39.06 | C |
| 6 | 109.72 | 0.12 | 69.44 | A |
| 91 | 109.86 | 0.11 | 82.65 | C |
| 5 | 109.87 | 0.55 | 3.31 | A |
| 70 | 110.02 | 0.09 | 123.46 | B |
| 5 | 110.03 | 0.38 | 6.93 | A |
| 6 | 110.10 | 0.18 | 30.86 | A |
| 5 | 110.18 | 0.37 | 7.31 | A |
| 12 | 110.27 | 0.30 | 11.11 | A |
| 16 | 110.29 | 0.55 | 3.31 | C(NaI) |

## 3. A SPIN-5 SENIORITY-4 STATE IN CHROMIUM-52(*)

Morton Kaplan and D. A. Shirley

In a paper on seniority coupling of nuclear shell-model states, Edmonds and Flowers showed that the $(f_{7/2})^4$ configuration should couple to states of character 2+, 4+, 5+, and 8+ in $Cr^{52}$.[1] The first three of these states should be observable in the decay of $Mn^{52}$. Recently, Wilson et al. have reported finding states of 2+ and 4+ character at about the expected energies.[2] They found a state of 5+ or 6+ character at the energy expected for the seniority-4 5+ state. Since the 2+ and 4+ states were predicted by several other theoretical calculations while the 5+ state was a unique feature of Edmonds and Flowers' model, it seemed important to determine the spin of this higher level.

*Condensed from a published paper, Nucl. Phys. 37, 522 (1952).

1. A. R. Edmonds and B. H. Flowers, Proc. Roy. Soc. (London) A215, 120 (1952).

2. R. R. Wilson, A. A. Bartlett, J. J. Kraushaar, J. D. McCullen, and R. A. Ristinen, Phys. Rev. 125, 1655 (1962).

The state in question, at 3.614 MeV, is depopulated by very weak γ transitions of 0.847 and 1.246 MeV to states of spin and parity 4+. These γ rays are almost imperceptible in the ordinary photon spectrum. We have studied the angular distribution following the decay of oriented $Mn^{52}$ nuclei. In the spectra taken along the direction of orientation the intensity of the stronger transitions is only 40% of that for isotropically oriented nuclei, while the 0.847- and 1.246-MeV γ rays are enhanced by 100%. This is a sufficient improvement of the peak-to-background ratio to permit good resolution of these two peaks (Fig. A. 3-1). The mere fact that the angular distribution of these peaks is different from that of the more intense peaks (in fact, the signs of the coefficients of $P_2(\cos\theta)$ are opposite) is sufficient to eliminate a spin of 6 for the 3.614-MeV level. Spins of 0, 2, and 4 are also easily eliminated. Thus, the spin of the 3.614-MeV state of $Cr^{52}$ is 5, and this state may be identified with the seniority-4 state predicted by Edmonds and Flowers.

## 4. THE NEUTRON-DEFICIENT YTTRIUM ISOTOPES $Y^{82}$, $Y^{83}$, AND $Y^{84}$(*)

V. Maxia,† William H. Kelly,‡ and Daniel J. Horen

Early attempts to study the decay of $Y^{82}$ revealed that its half-life was much shorter than the 70 minutes previously reported by Caretto and Wiig.[1] These authors also reported the half-life of $Y^{85}$ as 5 hours. From other work at this Laboratory, in which $Sr^{85m}$ was chemically separated from yttrium at regular intervals, it was found that $Y^{85}$ has a 3-h half-life.[2] The apparent disagreement in the half-life for $Y^{85}$ as found by Caretto and Wiig[1] and Kim et al.[2] has been resolved by the discovery of a 5-h isomeric state in $Y^{85}$.[3] The work presented here was undertaken in order to clarify the situation pertaining to the neutron-deficient yttrium isotopes with $A \leq 84$.

The Hilac was used to produce neutron-deficient yttrium isotopes by the reactions $As^{75}(C^{12}, xn)Y^{87-x}$ and $Ga^{69}(O^{16}, xn)Y^{85-x}$. For convenience, most of the data were obtained from bombardments of thick targets of powdered arsenic metal with about 120-MeV carbon ions, while other reactions were mainly used for corroborative purposes. The yttrium activities reported here were also produced by spallation of natural strontium with 240-MeV protons in the Berkeley 184-inch cyclotron. To aid in the identification of $Y^{84}$, a few milligrams of enriched $Sr^{84}$ (obtained from Separated Isotopes Division, Oak Ridge National Laboratory, Oak Ridge, Tennessee) was irradiated with 5- and 15-MeV deuterons in the Crocker 60-inch cyclotron.

*Condensed version of paper submitted to Inorg. Nucl. Chem. (UCRL-9995, Dec. 1961).

†Permanent address: Laboratorio di Radiochimica, Universitá di Pavia, Pavia, Italy.

‡Permanent address: Department of Physics and Astronomy, Michigan State University, East Lansing, Michigan.

1. A. A. Caretto, Jr., and E. O. Wiig, J. Am. Chem. Soc. 74, 5235 (1952).

2. Y. E. Kim, D. J. Horen, and J. M. Hollander, unpublished data.

3. D. J. Horen and W. H. Kelly, Bull. Am. Phys. Soc. 7, 341 (1962).

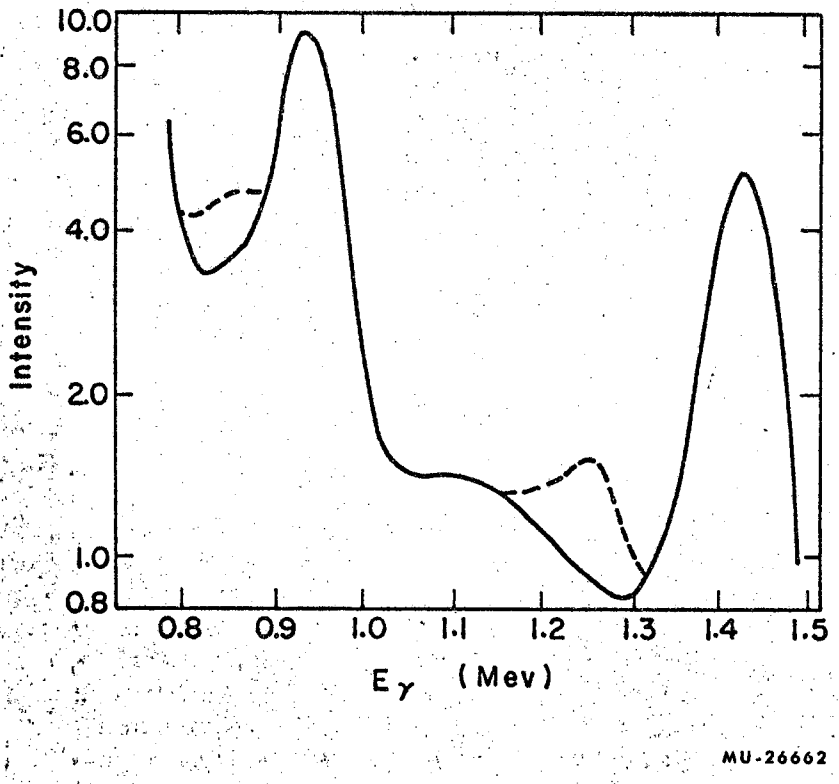


Fig. A. 3-1. Gamma-ray spectrum at 0° from the crystalline c axis of a cerium magnesium nitrate crystal, containing $Mn^{52}$, in an axial magnetic field of 200 gauss. The solid curve is the spectrum taken with the crystal at 1°K and the nuclei randomly oriented. The dotted curve is the spectrum taken at 0.0051°K, with the nuclei oriented. This curve has been normalized to the solid curve. (It has only 0.4 the intensity of the solid curve, unnormalized, because of the large γ-ray anisotropy). The two curves coincide everywhere except in the 0.85- and 1.25-MeV regions, where γ-ray peaks are clearly resolved in the 0.0051°K spectrum.

## Experimental Results

### Yttrium-82

After an irradiation of powdered arsenic metal with 120-MeV carbon ions, the genetic relationship of $Y^{82}$ to its daughter $Sr^{82}$ was established by a series of timed chemical separations (milkings). In these experiments yttrium was extracted into a solution of toluene and HDEHP while strontium was simultaneously back-extracted into 0.1 N HCl.

Several days after the milking experiments were performed, the strontium fractions were chemically isolated and measured with the scintillation spectrometer and proportional counter. From these measurements it was found that annihilation radiation, a weak 770-keV photon, and an approximately 3-MeV positron branch decayed with about a 25-d half-life. These data are attributable to the decay of $Sr^{82}$ - $Rb^{82}$ - $Kr^{82}$, since it is known that 25-d $Sr^{82}$ decays by electron capture to 1.3-min $Rb^{82}$, which in turn decays to $Kr^{82}$ with the emission of 3.1-MeV and 2.3-MeV positron branches and a weak 777-keV photon.[4] By counting the positrons with energies between 2 and 3 MeV, the yield of $Sr^{82}$ as a function of the time of the chemical separation of strontium from yttrium was obtained. Typical results are shown in Fig. A.4-1. From a number of such experiments, the average value obtained for the half-life of $Y^{82}$ is 9 ± 3 min.

### Yttrium-83

The γ-ray spectra of the strontium fractions milked from yttrium contained prominent peaks at 38, 375, 511, 770, 1160, and 1520 keV which decayed with a 34-h half life. This activity is assigned to $Sr^{83}$, since the latter is known to decay with a similar half-life with the emission of a 1.2-MeV positron branch.[5] Figure A.4-2 shows the yield of the 375-keV peak as a function of the time of the chemical separation of strontium from yttrium. Consideration of the data from several experiments utilizing different production modes of yttrium and different milking times leads to an average value of 8 ± 2 min for the half-life of $Y^{83}$.

### Yttrium-84

When the yttrium fraction obtained from the bombardment of arsenic with $C^{12}$ ions was chemically repurified approximately 2 hours after the irradiation, the γ-ray spectrum decayed with a 39 ± 2-min half-life. Strontium fractions chemically separated from the yttrium activity at fixed time intervals (40 min) contained only 150- and 235-keV photons arising from the decay of $Sr^{85m}$ and a very weak 513-keV photon from the decay of $Sr^{85}$. The half-life of $Y^{85}$ determined in this way is 3.0 ± 0.2 h, in good agreement with the results of Kim et al.[2] The 39-min yttrium activity was also produced by irradiating strontium enriched in $Sr^{84}$ with 15-MeV deuterons,

---

4. Nuclear Data Sheets, National Academy of Sciences - National Research Council, NRC 59-1-67 (National Research Council, Washington, D. C.)

5. S. V. Castner and D. H. Templeton, Phys. Rev. 88, 126 (1952).

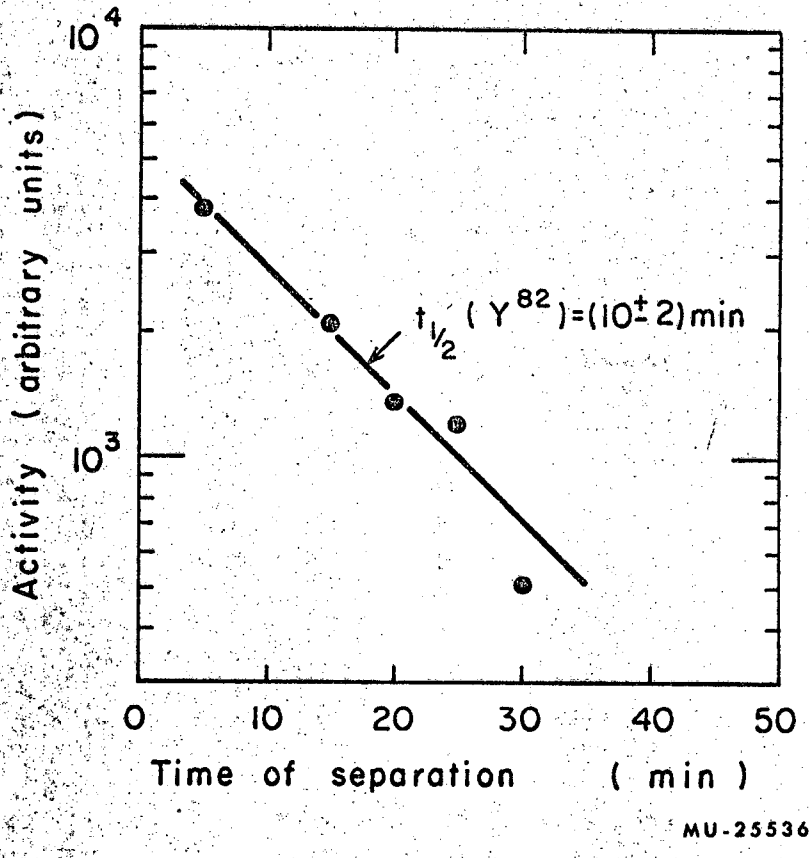


Fig. A. 4-1. Yields of 2.0- to 3.0-MeV positrons of $Sr^{82}$-$Rb^{82}$ decay as a function of time of chemical separation of strontium from yttrium parent.

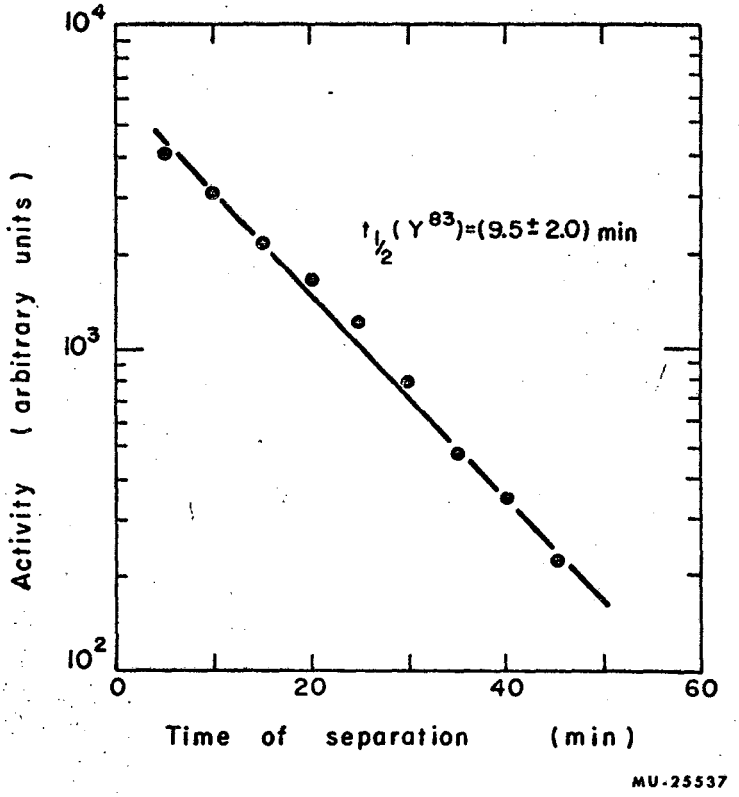


Fig. A. 4-2. Yields of the 375-keV $\gamma$ ray of $Sr^{83}$ as a function of time of chemical separation of strontium from the parent yttrium.

but not with 5-MeV deuterons. These data are consistent only with the assignment of the 39-min activity to $Y^{84}$. This half-life is in good agreement with that obtained by Yamazaki et al.[6]

6. T. Yamazaki, H. Ikegami, M. Sakai, K. Saito, Y. Hashimoto, M. Fujioka, H. Ohnuma, E. Takekoshi, J. Matsumoto, and A. Hashizume, (University of Tokyo Institute for Nuclear Studies) unpublished data; and private communication from M. Sakai, 1961.

## 5. ISOMERISM IN YTTRIUM-85(*)

Daniel J. Horen and William H. Kelly

Isomeric states with half-lives of 2.9 ± 0.3 h and 4.7 ± 0.2 h have been observed in $Y^{85}$. By use of a plastic scintillator, the end-point energy of the position spectrum associated with the 3-h level has been measured as 1.8 ± 0.4 MeV, and that with the 5-h state as 2.3 ± 0.3 MeV. By means of timed chemical separations of strontium from the parent yttrium, and γ-ray decay data, it was found that the 3-h state decays to $Sr^{85m}$ (spin and parity 1/2 -). In addition to the γ rays from the decay of $Sr^{85m}$, photons of energy 710 keV (probable) and 935 keV have been observed in the decay of the 3-h activity.

The scintillation spectrum of the 5-h activity is complex, consisting of more than 20 γ rays with energies between 228 and 2800 keV. Beta-gamma coincidence measurements show that there is direct population of the 228-keV level (7/2+) in $Sr^{85}$. Although the isomeric transition has not been observed, these data suggest that it is the (9/2+ → 1/2 -) M4 transition that has been observed in other odd-mass yttrium isotopes.

A tentative decay scheme with levels at 228, 235, 780, 1013, 1170, 1253, 2100, 2173, 2335, 2480, 2620, and 2754 keV has been constructed.

*Preliminary report presented at the Washington APS Meeting, April 1962: Bull. Am. Phys. Soc. 7, 341 (1962).

## 6. THE LOW ENERGY STATES IN YTTRIUM-90(*)

Yeong E. Kim

Recently an isomeric state in the odd-odd nucleus $Y^{90}$ has been found,[1] and it is interesting to see if this isomeric state can be explained in terms of the j-j coupling shell model. Furthermore, as several other low energy states were reported previously,[2] it is worth while to perform a theoretical calculation of these observed low energy states, with the hope that it may provide us with useful information on the nature of the effective interaction between protons and neutrons in the nucleus.

We use the central and tensor parts of the nuclear force, neglecting the spin-orbit force entirely. This practice is probably reasonable, as it appears that the existence of the spin-orbit force in the nuclear force is still questionable. The residual interaction of nucleons outside closed shells is not well known, and there seem to be no a priori reasons for retaining the same strength parameters of the free two-nucleon problem for the residual interaction. However, owing to our ignorance of the exact form of the residual interaction, we rely upon the free two-nucleon force parameters in estimating the strengths of our force, which we hope simulates the residual interaction.

It is assumed that 38 protons and 50 neutrons form closed-shell cores. This assumption simplifies the calculation, since there will be only one proton and one neutron outside this doubly closed shell core in $Y^{90}$. The wave function is then the j-j coupled new basis vector, which is a simple vector-coupled product of the wave functions of nonidentical nucleon 1 and 2 (proton and neutron):

$$|a\rangle = R_1(r_1)R_2(r_2)\,|j_1 j_2 JM\rangle =$$

$$\sum_{m_1, m_2} (j_1 m_1 j_2 m_2 | JM) R_1(r_1) |j_1 m_1\rangle\, R_2(r_2)\,|j_2 m_2\rangle \,.$$

Now we assume that the Hamiltonian describing this nucleus at low energy may be written as

$$H = H_1 + H_2 + V_{12},$$

where $H_1$ and $H_2$ are the single-particle shell-model Hamiltonian for particles 1 and 2, respectively, and $V_{12}$ is the two-body interaction between particle 1 and 2. This implies

$$H_i\,|a\rangle = \epsilon_0^i\,|a\rangle\,, \quad i = 1, 2\,,$$

---

*Short version of paper in preparation for Phys. Rev.

1. Y. E. Kim, D. J. Horen, and J. M. Hollander, Nucl. Phys. 31, 451 (1962) (see this paper for references).

2. B. A. Bartholomew, P. J. Campion, J. W. Knowles, and G. Manning, Nuclear Phys. 10, 590 (1959).

where $\epsilon_0^i$ is the single-particle level for particle i. We treat $V_{12}$ as a perturbation on the central field $H_i$ of the shell-model core, and evaluate the first-order perturbation term. The total energy for the state of a given J is then given approximately by

$$E \approx \epsilon_0^i + \epsilon_1, \qquad i = 1, 2,$$

where the higher terms are neglected. The values of $\epsilon_1$, and consequently of E, are obtained from the eigenvalue equation

$$\sum_{a'} \left[ \left\langle a \middle| V_{12} \middle| a' \right\rangle - (E - \epsilon_{0_{a'}}) \delta aa' \right] \left\langle a' \middle| aJM \right\rangle = 0.$$

The residual two-body interaction $V_{12}$ is chosen as

$$V_{12} = V^C(r_{12}) + V^T(r_{12}) S_{12},$$

where the first term is the central force, and the second term is the tensor force. The explicit forms of these forces are

$$\begin{aligned} V^C(r_{12}) = \Big[ & V^C_{TE} P_{TE} \exp(-\beta^C_{TE} r^2) \\ & + V^C_{SE} P_{SE} \exp(-\beta^C_{SE} r^2) \\ & + V^C_{TO} P_{TO} \exp(-\beta^C_{TO} r^2) \\ & + V^C_{SO} P_{SO} \exp(-\beta^C_{SO} r^2) \Big] \end{aligned}$$

and

$$\begin{aligned} V^T(r_{12}) = \Big[ & V^T_{TE} P_{TE} \exp(-\beta^T_{TE} r^2) \\ & + V^T_{TO} P_{TO} \exp(-\beta^T_{TO} r^2) \Big], \end{aligned}$$

where $P_{TE}$, $P_{SE}$, $P_{TO}$, and $P_{SO}$ are the projection operators for the triplet-even, singlet-even, triplet-odd, and singlet-odd states respectively, and V's are the corresponding strength parameters. $S_{12}$ is the tensor operator defined as

$$S_{12} = \frac{3(\vec{\sigma}_1 \cdot \vec{r}_{12})(\vec{\sigma}_2 \cdot \vec{r}_{12})}{r_{12}^2} - \vec{\sigma}_1 \cdot \vec{\sigma}_2.$$

The central-force matrix element can be expressed as

$$\langle a | V^C(r_{12}) | a' \rangle = \frac{1}{2}\left\{\left[(V^C_{TE} + V^C_{TO}) + (V^C_{TE} - V^C_{TO})(-1)^{j_1' + j_2' + J} P'_{12}\right]\right.$$

$$\langle a | U^C(r_{12}) | a' \rangle + \left[(-V^C_{TE} + V_{SE} - V^C_{TO} + V^C_{SO})\right.$$

$$\left.\left. + )-V^C_{TE} - V^C_{SE} + V^C_{TO} + V^C_{SO})(-1)^{j'1 + j'2 + J}\right]\langle a | U^C(r_{12}) P_S | a' \rangle\right\},$$

where $P_S$ is the singlet projection operator, and the operator $P'_{12}$ is defined as $P'_{12} | j_1' \; j_2' \; J \rangle = | j_2' \; j_1' \; J \rangle$. The matrix elements $\langle a | U^C(r_{12}) | a' \rangle$ and $\langle a | U^C(r_{12}) P_S | a' \rangle$ are given by

$$\langle a | U^C(r_{12}) | a' \rangle = (-1)^{j_2' + j_2 + J} \sqrt{[j_1][j_2][j_1'][j_2']}$$

$$\times \sum_k F_k(j_1' \; \tfrac{1}{2} \; j_1 \; -\tfrac{1}{2} \; | \; k0)(j_2' \; \tfrac{1}{2} \; j_2 \; -\tfrac{1}{2} \; | \; k0) W(j_1 \; j_1' \; j_2 \; j_2'; kJ),$$

with the restriction that $k + \ell_1 + \ell_1'$ and $k + \ell_2 + \ell_2'$ are both even, and the symbol $[a]$ stands for $[2a + 1]$;

$$\langle a | U^C(r_{12}) P_S | a' \rangle = (-1)^{j_2' + j_2 + J - 1} \sqrt{[j_1][j_2][j_1'][j_2']} \sqrt{[\ell_1][\ell_2][\ell_1'][\ell_2']}$$

$$\times W(\ell_1 \; j_1 \; \ell_2 \; j_2; \tfrac{1}{2} \; J) \; W(\ell_1' \; j_1' \; \ell_2' \; j_2'; \tfrac{1}{2} \; J)$$

$$\times \sum_k F_k(\ell_1 \; 0 \ell_1' \; 0 \; | \; k0) \; (\ell_2 \; 0 \; \ell_2' \; | \; k \; 0) \; W(\ell_1 \; \ell_1' \; \ell_2 \; \ell_2'; \; kJ).$$

The slater integral $F_k$ is defined as

$$F_k = \iint R^*_{n_1 \ell_1}(r_1) \, R^*_{n_2 \ell_2}(r_2) \, R_{n_1' \ell_1'}(r_1) R_{n_2' \ell_2'}(r_2) \, r_1^2 \, r_2^2 \, dr_1 dr_2$$

$$\times \int d\left(\frac{\cos\theta_{12}}{2}\right) P(\cos\theta_{12}) U^C(r_{12})$$

where $U^C(r_{12})$ takes the Gaussian form $\exp(-\beta r^2)$ with different values of $\beta$ for the corresponding states.

For the tensor force, the matrix element is expressed as

$$\langle a | V^T(r_{12}) | a' \rangle$$

$$= \frac{1}{2}\left[(V^T_{TE} + V^T_{TO}) + (V^T_{TE} - V^T_{TO})(-1)^{j'_1 + j'_2 + J} P'_{12}\right] \langle a | U^T(r_{12}) S_{12} | a' \rangle ,$$

and

$$\langle a | U^T(r_{12}) S_{12} | a' \rangle = 3 \sum_{k,x,y} \langle a | F_{xy} | a' \rangle W(1x1y; K2)$$

$$\times \langle j_1 j_2 JM | \bar{T}_1^{(1x)K} \cdot \bar{T}_2^{(1y)K} | j'_1 j'_2 J' M' \rangle ,$$

where

$$\langle a | F_{xy} | a' \rangle = -5 \sum_{kij} \langle a | r_i r_j | a' \rangle \; X_{ij};\; i, j = 1, 2$$

$$X_{11} = \sqrt{\frac{2}{15}} \sqrt{[x]} (20\, k0 \mid x0),$$

$$X_{22} = \sqrt{\frac{2}{15}} \sqrt{[y]} (20\, k0 \mid y0),$$

$$X_{12} = \sqrt{[x][y]} (10\, k0 \mid x0)(10\, k0 \mid y0)$$

$$\times W(11xy; 2k),$$

and

$$\langle a | r_i r_j | a' \rangle = (2k+1) \int_0^\infty dr_1 r_1^2 R_1 R'_1 \int_0^\infty dr_2 r_2^2 R_2 R'_2 \, r_i r_j$$

$$\times \int_{-1}^{1} d\left(\frac{\cos\theta_{12}}{2}\right) P_k(\cos\theta_{12}) \frac{U^T(r_{12})}{r_{12}^2} .$$

Here the radial function $U^T(r_{12})$ takes the forms

$$U^T(r_{12}) = \exp(-\beta^T_{TE} r^2) \text{ for the triplet-even}$$

$$= \exp(-\beta^T_{TO} r^2) \text{ for the triplet-odd.}$$

The angular part in terms of 3-, 6-, and 9-j symbols is

$$\left\langle j_1 j_2 JM \left| \bar{T}_1^{(1x)K} \cdot \bar{T}_2^{(1y)K} \right| j_1' j_2' J' M' \right\rangle$$

$$= (-1)^{j_1' + j_2 + J + \ell_1 + \ell_2} 6\, \delta_{JJ'}\, \delta_{MM'} \begin{Bmatrix} J & j_2 & j_1 \\ K & j_1' & j_2' \end{Bmatrix}$$

$$\times \sqrt{[j_1][j_2][j_1'][j_2']}\ \sqrt{[\ell_1][\ell_2][\ell_1'][\ell_2']}$$

$$\times \begin{pmatrix} \ell_1 & x & \ell_1' \\ 0 & 0 & 0 \end{pmatrix} \begin{pmatrix} \ell_2 & y & \ell_2' \\ 0 & 0 & 0 \end{pmatrix} \begin{Bmatrix} \frac{1}{2} & \frac{1}{2} & 1 \\ \ell_1' & \ell_1 & x \\ j_1' & j_1 & k \end{Bmatrix} \begin{Bmatrix} \frac{1}{2} & \frac{1}{2} & 1 \\ \ell_2' & \ell_2 & y \\ j_2' & j_2 & k \end{Bmatrix} .$$

Before the tensor force is introduced, the numerical calculations are carried out extensively with various central-force mixtures including Serber, Ferrell-Visscher, and Rosenfeld forces, and with various ranges. These calculations have indicated that we must introduce a fairly strong attractive odd force to fit the experimental data. A calculation with one set of central-force parameters with rather strong attractive odd force, which is chosen so as to fit both the doublet spacings of J = 2-, 3- and J = 2+, 7+, is shown in Fig. A.6-1. Although the agreement with the experiment is good, there is no justification for assuming the central force mixture of strong attractive odd-force. Furthermore, this is not the only set of parameters that gives rise to a good fit with the experiment, since there are other sets of the parameters that yield equally good fits. From the free-two-nucleon potential, it is known that the triplet-odd force is weak, and the singlet-odd is even repulsive.

In order to include the tensor force in the residual interaction, we must decide the strength of the tensor force. Since the relative weight of the central force with respect to the tensor force is not well known in the residual force, we try to use the free two-nucleon potential in estimating

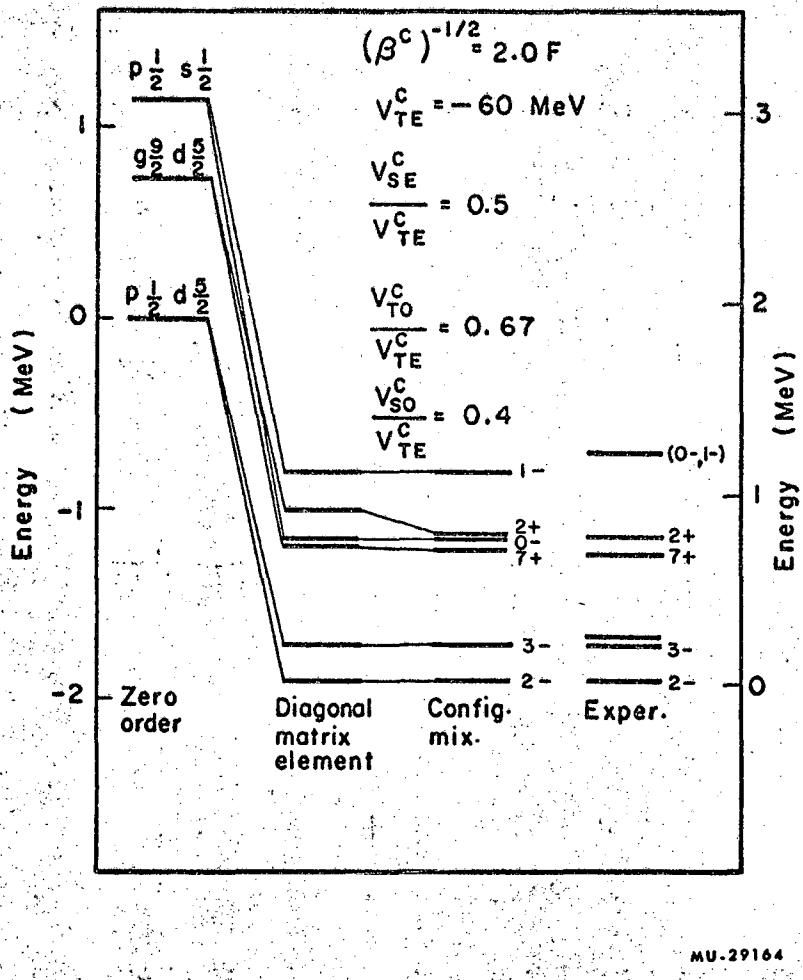


Fig. A.6-1. Calculated results of $Y^{90}$ spectrum with the central force alone. The central-force parameters are adjusted to fit both the doublet spacings of J = 2-, 3- and J = 2+, 7+.

the tensor-force parameters. Recent success of $O^{18}$ calculations by Dawson, Talmi, and Walecka[3] encourages us to try the Brueckner-Gammel-Thaler potential (BGT).[4] Because of the computational complexity involved, we take a slightly different form of the potential from the BGT. We modify the Yukawa radial dependence with a hard core of the BGT potential by replacing it with the Gaussian radial function without the hard core, and treat the hard-core effect as a repulsive short-range force.[5] The parameters of the simulated BGT potential adopted in this manner are listed in Table I. The diagonal tensor-force matrix elements

$$\frac{1}{3}\langle a|P_{TE}U^{T}(r_{12})S_{12}|a\rangle \text{ and } \frac{1}{3}\langle a|P_{TO}U^{T}(r_{12})S_{12}|a\rangle$$

are plotted as a function of the range in Figs. A.6-2, A.6-3, and A.6-4. As we can see from these figures, the tensor-force matrix elements are not always a monotonically increasing function of the range. This is to be contrasted with the fact that the central-force matrix elements are positive and monotonically increasing functions with increasing range. The results of the calculation with the simulated BGT potential are shown schematically in Fig. A.6-5.

Although the experimental spectrum is not sufficiently resolved for us to conclude that our choice of the residual force is a good one, there is a remarkable agreement between the calculated spectrum and experiment if one notes that several shell-model approximations have been made and the force parameters are not all adjusted arbitrarily. A slight increase of the repulsive central singlet-odd force is sufficient to obtain the level sequence of the experiment as shown in Fig. A.6-5, or we may increase the tensor-force strength slightly to fit the experiment. The better fitting of the spectrum by increasing the central-odd or tensor force can be qualitatively understood by considering the hard-core effect as a repulsive short-range potential. The repulsive delta-function force affects only the central-even force contribution because both the central-odd and tensor forces vanish in the zero range limit. This effect may be considered as increases in the strengths of the central-odd and tensor force relative to the central-even force. Furthermore, the introduction of the tensor force makes it possible to eliminate the unrealistic attractive central-odd forces. Concurrently, the simulated BGT potential is used for $Bi^{210}$,[6] where the most of the ground-state multiplet (total of nine levels out of possible ten) are resolved by the high-resolution (d, p) reaction on $Bi^{209}$ at MIT.[7] The analysis of those multiplets in $Bi^{210}$ also indicates that the simulated BGT potential is a rather good approximation for the residual interaction.

---

3. J. F. Dawson, I. Talmi, and J. D. Walecki, Ann. Phys. 18, 339 (1962).

4. K. A. Brueckner and J. L. Gammel, Phys. Rev. 109, 1023 (1958).

5. M. Bauer and M. Moshinsky, Nucl. Phys. 4, 615 (1957); L. Silverberg, Arkiv Fysik 20, 355 (1961).

6. Y. E. Kim and J. O. Rasmussen, Energy Levels of $Bi^{210}$ and the Shell-Model Residual Force, in preparation for submission to Nucl. Phys.

7. J. R. Erskine, W. W. Buechner, , and H. A. Enge, Phys. Rev. 128, 720 (1962).

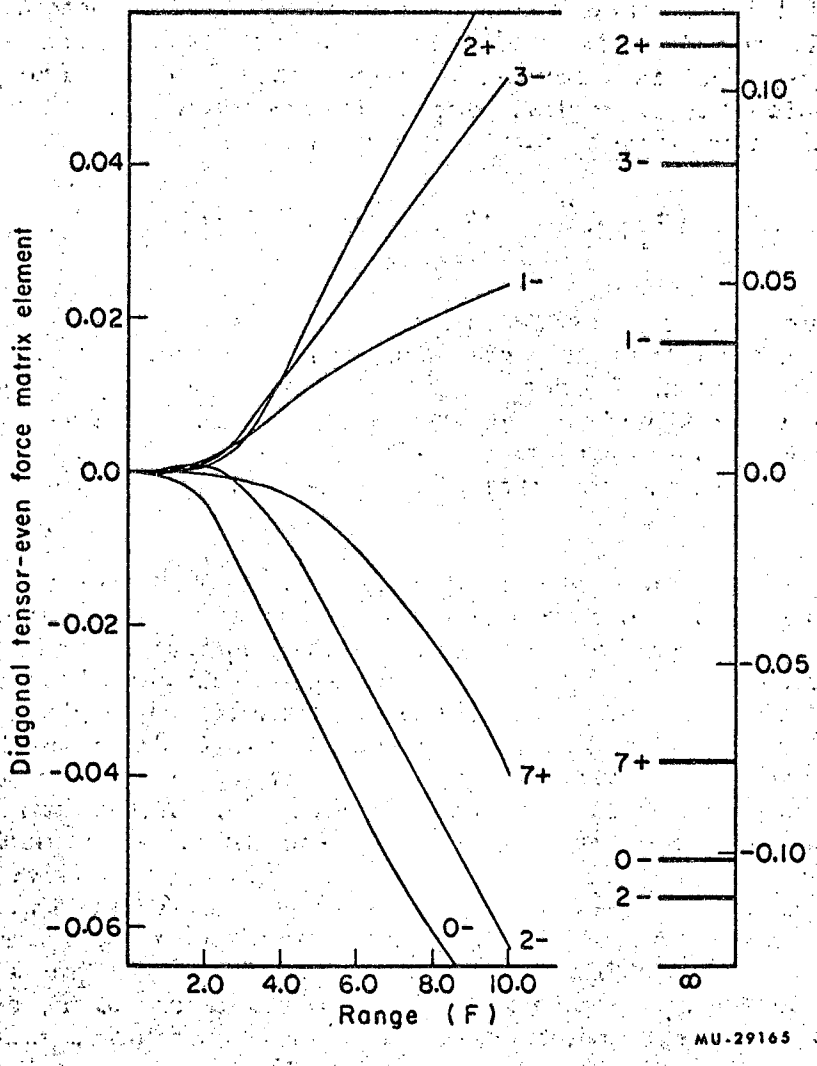


Fig. A.6-2. Diagonal tensor-even force matrix elements for several observed states in $Y^{90}$ as a function of the range parameters.

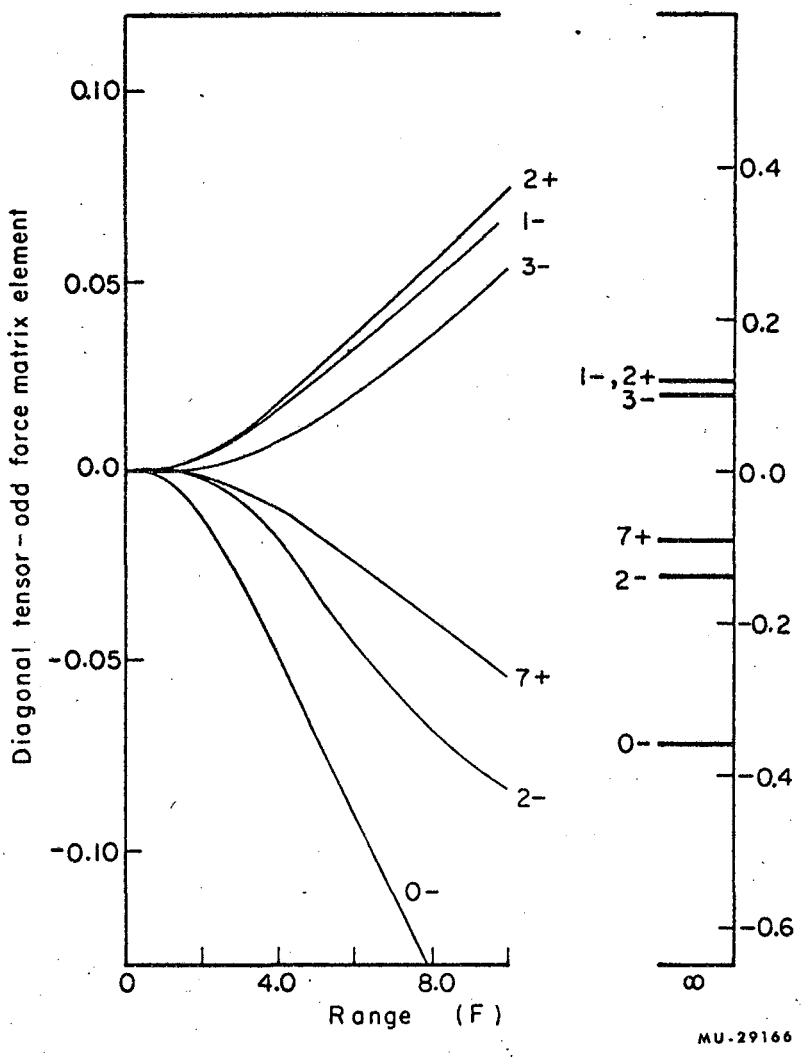


Fig. A.6-3. Diagonal tensor-odd force matrix elements for several observed states in $Y^{90}$ as a function of the range parameters.

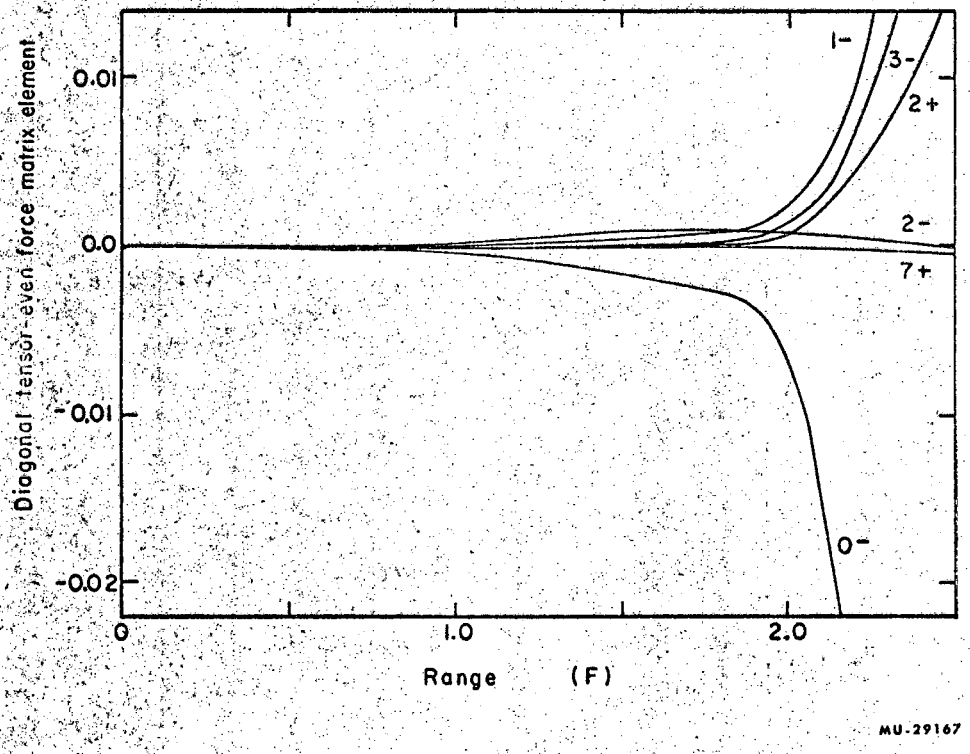


Fig. A.6-4. Diagonal tensor-even force matrix elements for the observed states in $Y^{90}$ as a function of the range at the shorter ranges.

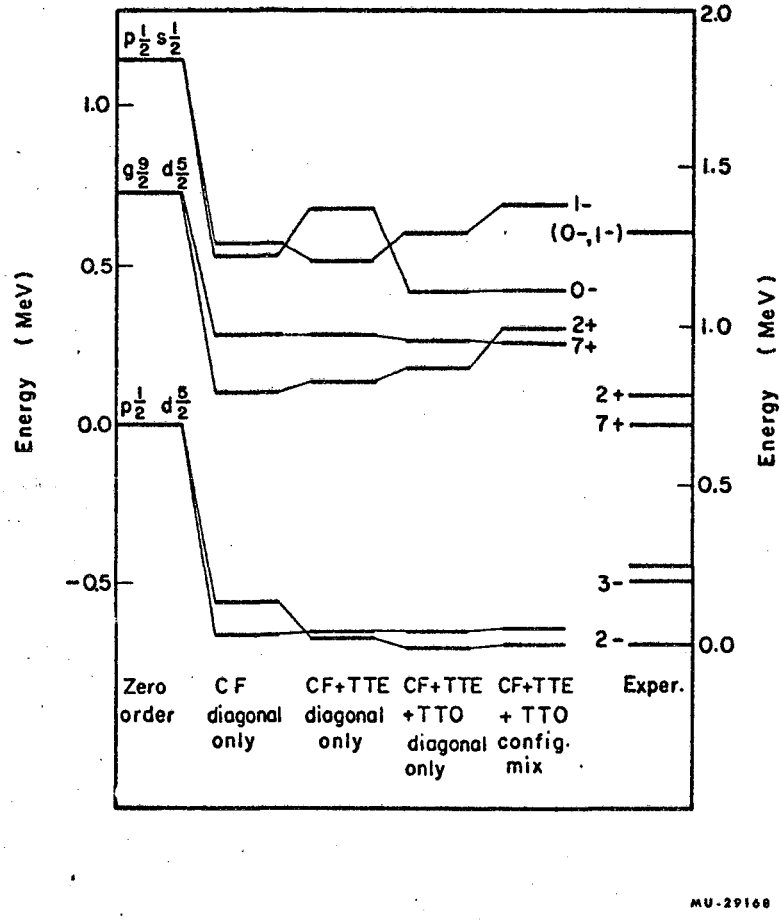


Fig. A.6-5. Comparison of the experiment and the calculated spectra of $Y^{90}$ with the simulated BGT potential. The symbols CF, TTE, and TTO stand for the central, tensor-odd forces respectively. In the fifth column are shown the results when the singlet-odd central force is slightly increased (by a factor of 1.9). In diagonalizing the matrix, the off-diagonal tensor force matrix elements are neglected.

Table I. The parameters for the simulated BGT potential.

| States | Strengths (MeV) | Ranges (F) |
|---|---|---|
| Central triplet-even | -877.39 | 0.47828 |
| Central singlet-even | -434.0 | 0.68965 |
| Central triplet-odd | - 14.0 | 1.0 |
| Central singlet-odd | +130.0 | 1.0 |
| Tensor triplet-even | -159.40 | 0.95292 |
| Tensor triplet-odd | + 22.0 | 1.25 |

Finally a remark should be made on the shell-model residual interaction. From the analysis of various shell-model calculations, the central force alone (that is, without the tensor force) seems to approximate the residual force very well in most cases. This is probably because the tensor force in the residual interaction is rather small. However, the tensor-force contributions are not always negligible, and must be taken seriously in some cases, such as in $Y^{90}$ presented here. The characteristic of the tensor-force matrix element is that it may be either positive or negative, so that in some cases the tensor-force effects can not be exactly simulated by a linear combination of four central-force components.

A concurrent work on $Po^{210}$ has indicated that the singlet-even part of the simulated BGT potential yields matrix elements that are rather too large for the ground-state multiplet of $Po^{210}$, and new calculations are presently being made with a somewhat weaker potential which fits the ground-state multiplets of $Bi^{210}$ and $Po^{210}$.

## 7. THE MÖSSBAUER EFFECT IN TELLURIUM-125; QUADRUPOLE SPLITTING IN TELLURIUM METAL

P. H. Barrett, R. B. Frankel, and D. A. Shirley

Tellurium-125 has two unstable isomeric states, a 58-day state at 145 keV and a 1.6-nsec state at 35.5 keV (Fig. A. 7-1). The latter, which decays by an M1 transition to the ground state, is a good candidate for the Mössbauer effect. This effect has been reported in two experiments.[1, 2] In neither was the $\gamma$ ray clearly resolved nor was hyperfine structure seen. We have observed the 35.5-keV transition directly, resolving the $\gamma$ ray with a proportional counter.[3, 4] The photon spectrum is shown in Fig. A. 7-2.

A Mössbauer absorption of up to 25% was found at low termperatures using a source of neutron-irradiated $Te^{124}$ metal and an absorber of $Te^{125}$ metal, both electroplated onto platinum backings. Quadrupole hyperfine structure was clearly resolved. A characteristic 1:2:1 spectrum typical of a doublet source and doublet absorber is shown in Fig. A. 7-3. The splitting is 0.77 cm/sec, or $9.1 \times 10^{-7}$ ev at 4.2°K. The excited state is confirmed to have spin 3/2, and the half-life, deduced from the line width, is $1.54 \pm 0.20$ nsec. A plot of absorption vs temperature is shown in Fig. a. 7-4. Finally in Fig. A. 7-5 is shown a spectrum taken with a source of SnTe. This compound is cubic (therefore the field gradient and consequent quadrupole coupling vanish by LaPlace's equation), and produces a single-line source. As expected, two lines of equal intensity are seen, split by 0.77 cm/sec, in good agreement with the Te:Te data.

---

1. N. Shikazono, T. Shoki, H. Takekoshi, and P. K. Tseng, J. Phys, Soc. Japan 17, 1205 (1962).

2. P. Z. Hien, V. C. Shapiro, and V. S. Shpinel, Soviet Phys. JETP (English Transl.) 15, 489 (1962).

3. G. Friedlander and W. C. Orr, Phys. Rev. 84, 484 (1951).

4. J. C. Bowe and P. Axel, Phys. Rev. 85, 858 (1952).

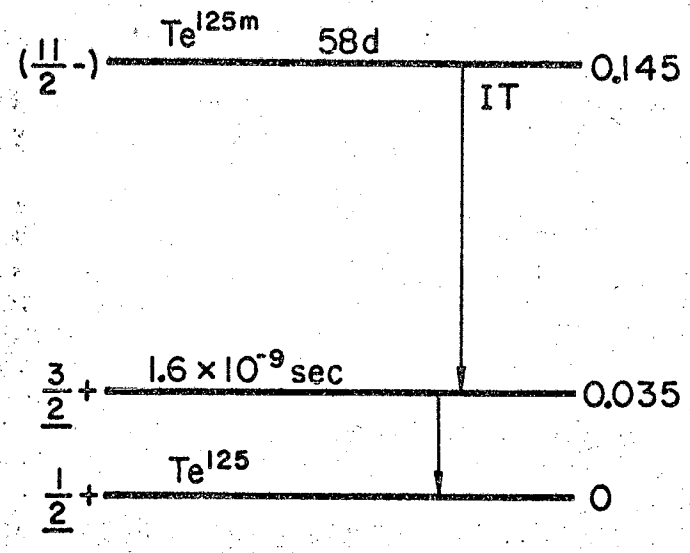


Fig. A.7-1. $Te^{125}$ energy level diagram.

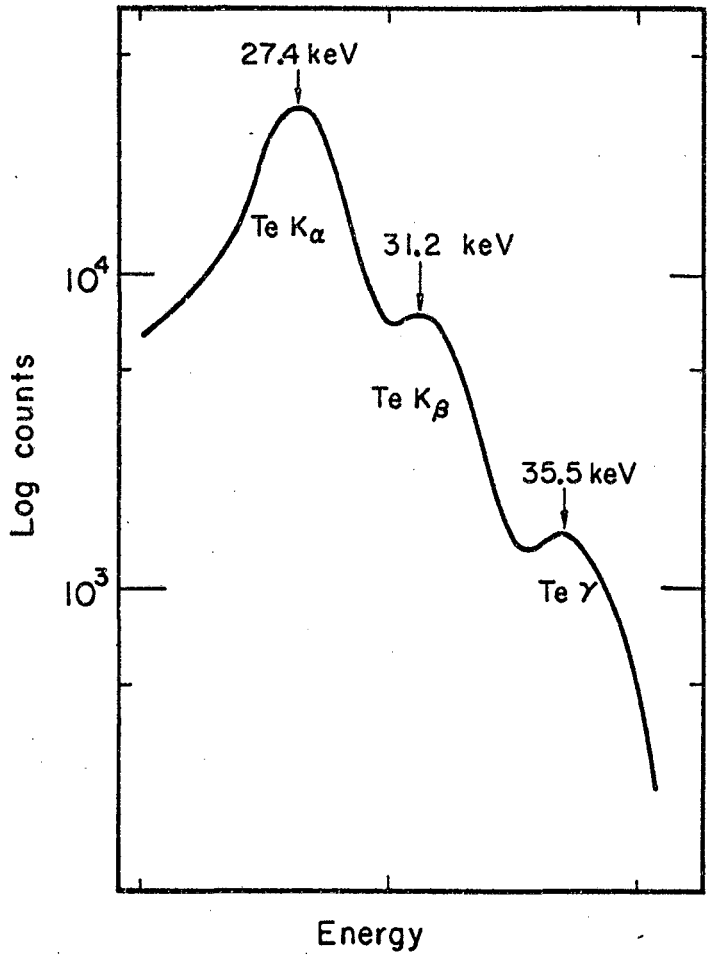


Fig. A.7-2. Photon spectrum of $Te^{125}$ taken with a proportional counter.

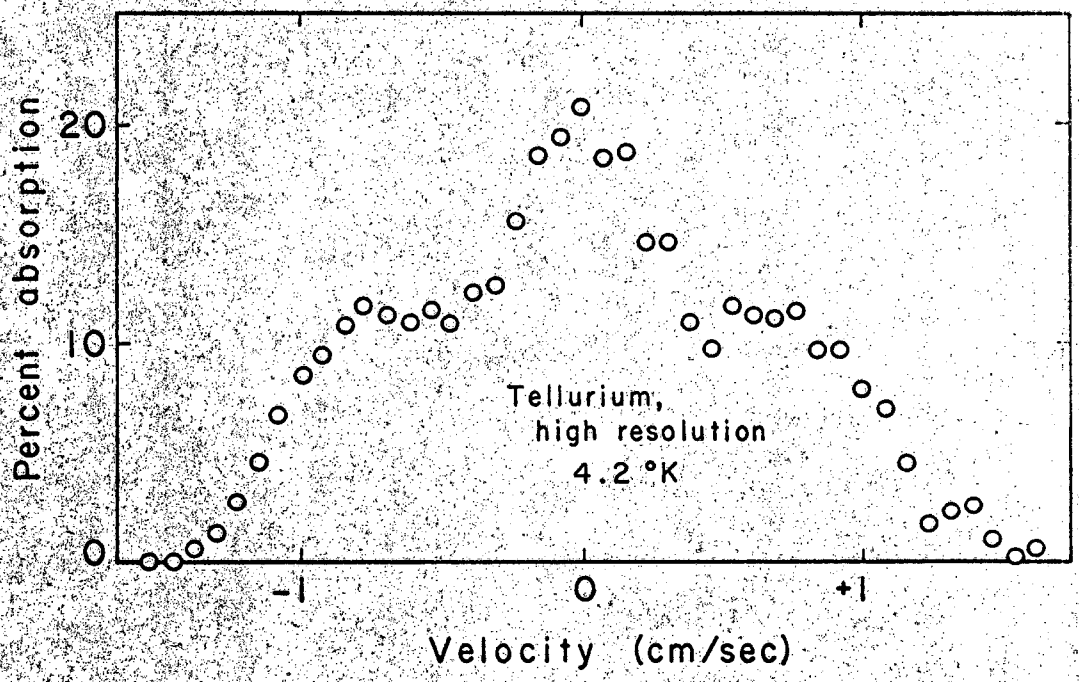


Fig. A.7-3. Absorption spectrum of tellurium metal, taken by using a tellurium metal source and absorber.

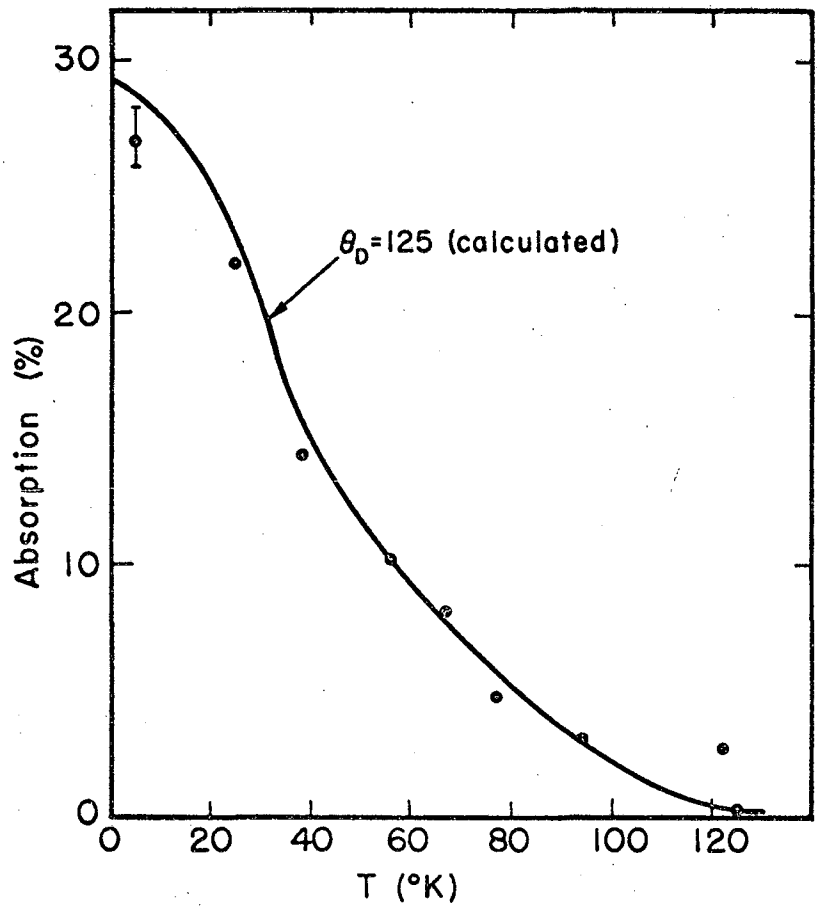


Fig. A.7-4. Absorption (%) vs temperature, for a Te source and Te absorber.

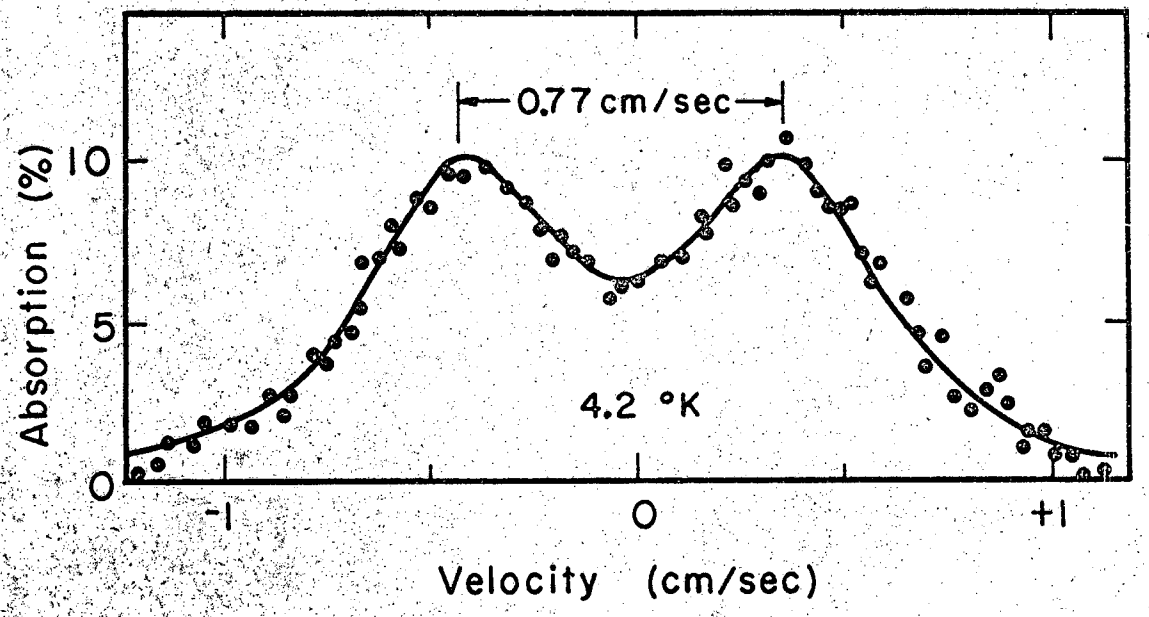


MU-29346

Fig. A.7-5. Absorption spectrum taken by using a source of SnTe and a Te absorber.

# 8. CONVERSION-ELECTRON MEASUREMENTS IN THE DECAY OF 11.5-d BARIUM-131(*)

William H. Kelly† and Daniel J. Horen

The internal-conversion electron spectrum of 11.5-d $Ba^{131}$ was measured with 180° permanent-magnet photographic-recording spectrographs, having field strengths of 50, 100, 150, and 340 gauss, with momentum resolution of approximately 0.1%. [1] In most cases, relative intensities of the conversion lines were determined with a 25-cm double-focusing iron-core spectrometer (DFIC), operated at a resolution of about 0.5%. Some measurements were performed with the new Berkeley iron-free spectrometer (IF) with the baffles set to operate at a resolution of about 0.17%. Since these measurements were made prior to the completion of the spectrometer cooling system, they were restricted to energies of less than 200 keV.

The photon spectrum of $Ba^{131}$ was measured with a 7.6-cm-diam NaI(Tl) crystal, 7.6 cm thick, at a source-to-crystal distance of 20 cm. Analysis of these data yielded the relative photon intensities given in Table I. For comparison, the results of August et al. are also presented. [2] To determine the relative K x-ray intensity, a separate experiment was performed in which a barium source was chemically purified and the photon spectrum was measured with a $3.8 \times 2.5$-cm crystal that had a thin beryllium cover. The relative K x-ray intensity so obtained has been corrected for the small amount of xenon K x-ray from the decay of the daughter $Cs^{131}$ which had grown in prior to the measurement. In correcting the K x-ray intensity, account was also taken of the escape peak caused by the $K_\beta$ x rays whose energy is greater than the K binding energy in iodine.

The multipolarities of a number of transitions in $Cs^{131}$ have been inferred from comparisons of the K/L ratios, L-subshell ratios, and internal-conversion coefficients with the theoretical values as computed by Rose, [3] and the results are given in Table II. Except where noted, the conversion coefficients have been obtained by normalizing the data for internal-conversion electron and photon intensity to a theoretical K-conversion coefficient of 0.02 for the 372.8-keV transition (50% E2 + 50% M1).

In their measurement of the half-life of the 123.7-keV state (see Fig. A.8-1) Bodenstedt et al. found that the 500-keV–124 keV coincidence delay curve consisted of two components, i.e., $3.77 \pm 0.05$ nsec and $13.3 \pm 0.5$ nsec. [4] These authors showed that the 3.77-nsec component was attributable to the

---

*Brief version of paper to be submitted to Nucl. Phys. (UCRL-10582, Oct. 1962).

†Permanent address: Department of Physics and Astronomy, Michigan State University, East Lansing, Michigan.

1. W. G. Smith and J. M. Hollander, Phys. Rev. 101, 746 (1956).

2. L. S. August, R. W. Campbell and M. Goodrich, Bull. Am. Phys. Soc. 2, 231 (1957); L. S. August, Thesis, Louisiana State University (1957); and R. W. Campbell, Thesis, Louisiana State University (1957).

3. M. E. Rose, "Internal Conversion Coefficients" (North-Holland Publishing Co., Amsterdam, 1958).

4. E. Bodenstedt, H. J. Körner, C. Günter, D. Hovestadt, and J. Radeloff, Nuclear Phys. 20, 557 (1960).

Table I. Relative photon intensities in the decay of $Ba^{131}$.

| Photon energy[a] (keV) | Relative intensity[b] This work | Relative intensity[b] Campbell (from Ref. 2) |
|---|---|---|
| K x-ray | 4730 | |
| 123.7, 133.5, 137.1 | 1660 | 2080 |
| 156.9 | 51.4[c] | 105 |
| 215.8 | 1120 | 1570 |
| 239.2, 246.3, 248.8 | 356 | 595 |
| 372.8 | 775 | 1030 |
| 403.8 | 121 | 154 |
| 480.4, 486.4, 496.1 | 2850 | 2850 |
| 573.1, 584.8 | 110 | 101 |
| 619.6 | 83[d] | 100 |
| 674.2, 696.5 | 52 | 24 |
| 830.9 | 15 | 22 |
| 922.9 | 46.3 | 54 |
| 1046.5 | 80 | 87 |

[a] When applicable, the photon energies are those determined in the conversion-electron measurements.

[b] These intensities are normalized at the 372.8-keV photon in the manner adopted in Table III.

[c] This intensity has been corrected for solid angle addition of 123.7-keV photons and K x-rays (≈ 12%).

[d] This intensity has been corrected for solid angle addition of 496.1- and 123.7-keV photons (≈ 10%).

Table III. Total transition intensities in the decay of $Ba^{131}$.

| Transition energy (keV) | Relative electron intensity (arbitrary units) K | Relative electron intensity (arbitrary units) ΣL, M... | Relative photon intensity | | Total transition intensity (% EC decays) |
|---|---|---|---|---|---|
| K-X | | | | 4730 | |
| 55.0 | (34.2)[a] | 55.7 | | (5.4)[a] | 1.68 |
| 78.6 | 55.7 | 8.5 | | (37)[b] | 1.97 |
| 82.4 | 1.8 | | | (1)[c] | 0.05 |
| 92.3 | 27.8 | > 0.45 | | (27.8)[b] | 1.0 |
| 123.7 | 975 | 406 | 1550[d] | | 52.0 |
| 133.5 | 43 | 9.0 | 116[e] | 1660 | 2.98 |
| 137.1 | 1.0 | | 2.2[f] | | 0.06 |
| 156.9 | (2.6)[g] | 0.3 | | 51.4 | 0.96 |
| 215.8 | 100 | 18.0 | | 1120 | 21.9 |
| 239.2 | 9.2 | 1.66 | 146[i] | | 2.78 |
| 246.3 | (3.5)[h] | 0.53 | 69 | 356 | 1.3 |
| 248.8 | 8.8 | 1.76 | 141 | | 2.69 |
| 294.0 | 0.34 | | | (8.5)[j] | 0.16 |
| 323.9 | 0.06 | | | (2.3)[c] | 0.04 |
| 350.3 | 0.12 | | | (5.2)[c] | 0.09 |
| 372.8 | 15.5 | 3.6 | | [775][k] | 14.1 |
| 403.9 | (1.95)[c] | 0.14 | | 121 | 2.18 |
| 426.7 | 0.06 | | | (4.4)[c] | 0.08 |
| 452.0 | 0.3 | | | (25)[c] | 0.45 |
| 461.1 | 0.05 | | | (4.5)[c] | 0.08 |
| 480.4 | 0.32 | 0.04 | 33[l] | | 0.59 |
| 486.4 | 1.04 | 0.11 | 109 | 2850 | 1.95 |
| 496.1 | 25.9 | 4.28 | 2710 | | 48.6 |
| 573.1 | 0.06 | | 14[l] | 110 | 0.25 |
| 584.8 | 0.42 | 0.06 | 96 | | 1.7 |
| 619.6 | 0.32 | 0.03 | | 83 | 1.48 |
| 674.2 | 0.05 | | 29[m] | 52 | .52 |
| 696.5 | 0.04 | | 23 | | .41 |
| 830.9 | 0.04 | | | 15 | .27 |
| 914.1 | ≈ 0.005 | | | 46.2 | |
| 922.9 | 0.09 | 0.009 | 46 | | .82 |
| 1046.5 | 0.12 | 0.014 | | 80 | 1.42 |

[a] Calculated by assuming theoretical K/L ratio (0.834) and L-conversion coefficient for an E2 transition (see Table II).

[b] Calculated by assuming theoretical K-conversion coefficient for an M1 transition (see Table II).

[c] Calculated by assuming theoretical K-conversion coefficient for a 50% M1 + 50% E2 transition.

[d] Calculated by assuming theoretical K-conversion coefficient for an E2 transition (see Table II).

[e] Calculated assuming theoretical K-conversion coefficient for a 80% M1 + 20% E2 transition (see Table II)

[f] Calculated assuming theoretical K-conversion coefficient for an E2 transition.

[g] Calculated assuming theoretical K/L ratio for an M1 transition (see Table III).

[h] Calculated assuming theoretical K/L ratio for a 50% M1 + 50% E2 transition.

[i] Photon intensity distributed on the basis of K and L electron intensities of the 239.2-, 246.3-, and 248.8-keV conversion lines.

[j] Calculated assuming theoretical K-conversion coefficient, $\alpha_K = 0.04$.

[k] Photon relative intensity scale normalized to the theoretical 50% M1 + 50% E2 conversion coefficient of the 372.8-keV transition, $\alpha_K = 0.02$.

[l] Photon intensity distributed according to K-conversion electron intensities.

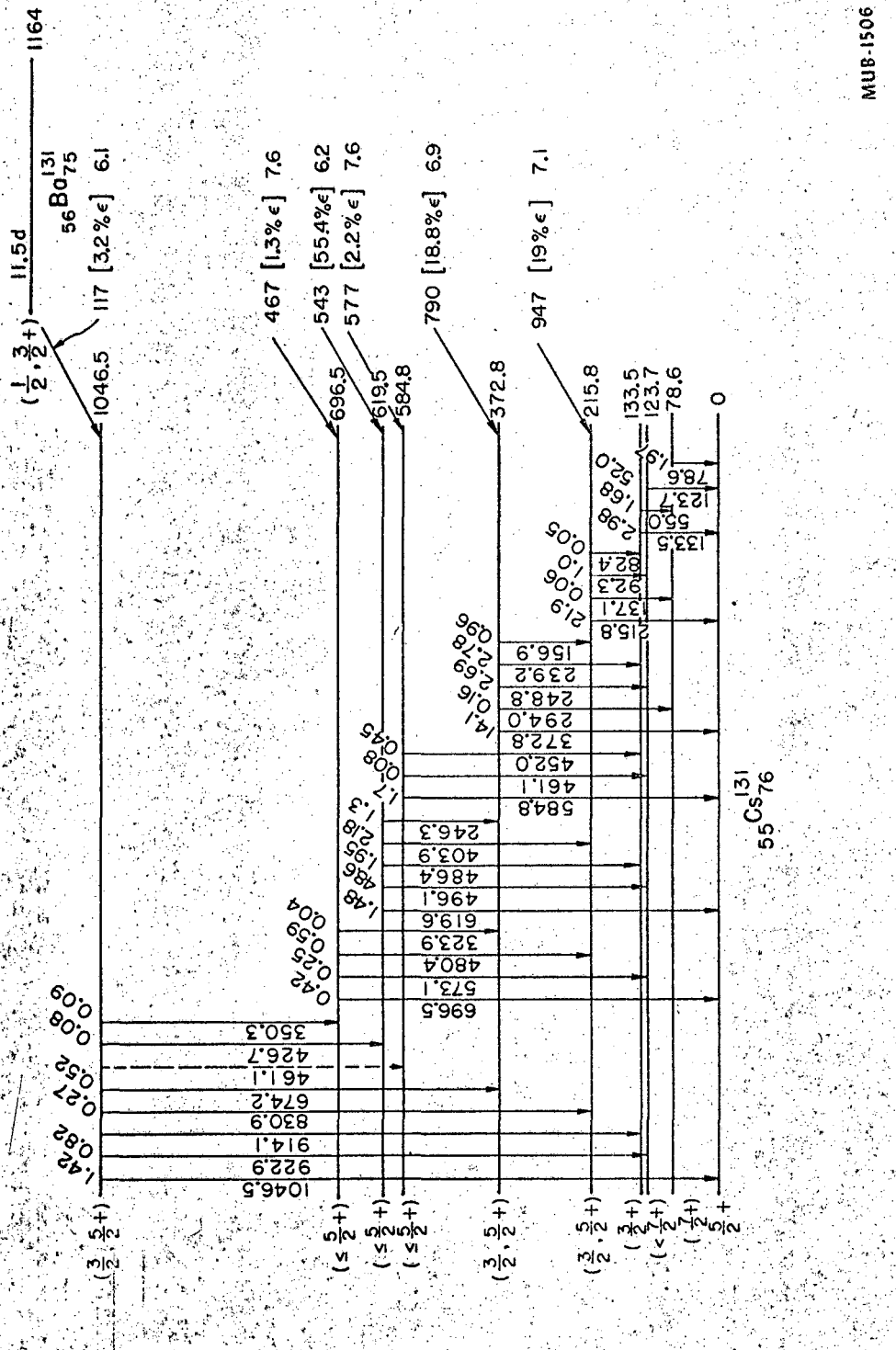


Fig. A. 8-1 Tentative decay scheme for 11.5-d $Ba^{131}$.

half-life of the 123.7-keV state, and the 13.3-nsec component to the 133.5-keV state. We have remeasured the 500–124-keV delay curve and have also found that it consisted of two components corresponding to half-lives of $3.49 \pm 0.31$ nsec and $12.7 \pm 1.0$ nsec, in good agreement with the data of Bodenstedt et al.[4]

Energy and intensity sums have been used to construct the decay scheme of 11.5-d $Ba^{131}$ as shown in Fig. A. 8-1. That the 78.6-keV transition originates from a level at this energy is definitely established by the observance of the 137.1- and 294.0-keV transitions between the 78.6-keV level and the 215.8- and 372.8-keV levels, respectively. The level at 696.5 keV, first suggested by August et al.[2] on the basis of coincidences between photons of energies 216 and 500 keV (480.4 keV in this work), is verified by the detection of transitions leading from this level to the ground, 123.7-, and 372.8-keV states. The level at 584.8 keV has not been proposed previously.

Table III shows the transition intensities in percent electron-capture decays as calculated for the decay scheme shown in Fig. A. 8-1. The number of K x rays expected on the basis of this decay scheme is equal within experimental error to the measured value given in Table I. Hence there appears to be no capture to the first four states in $Cs^{131}$. Also shown in Fig. A. 8-1 are the percent electron-capture branches and log ft values for them. The log ft values were calculated on the assumption of a total decay energy of 1164 keV.[5]

As a result of this work we note:

(a) A consistent decay scheme for 11.5-d $Ba^{131}$ has been constructed which clarifies most of the known experimental data.

(b) Acceptance of the presently available experimental data per se does not yet allow definite spin assignments to all known levels in $Cs^{131}$. (For further enlightenment concerning this comment, reference should be made to the UCRL report pertaining to this work, issued as UCRL-10582, Dec. 1962.)

(c) Our tentative spin assignment of 3/2+ for the 133.5-keV level does not allow a comparison of these results with the theoretical calculations of Person and Rasmussen.[6] (The latter authors based their calculations on spins of 1/2+ and 7/2+, respectively, for the 123.7- and 133.5-keV levels.)

---

5. B. L. Robinson, Bull. Am. Phys. Soc. 7, 541 (1962).

6. L. W. Person and J. O. Rasmussen, Nuclear Phys. 36, 666 (1962).

Table II. Summary of data pertaining to multipole order assignments of transitions in the decay of $Ba^{131}$.

| Transition energy (keV) | K/L | $L_I/L_{II}/L_{III}$ | $a_K$ | Multipole order |
|---|---|---|---|---|
| 55.0 | | 1/7.4/9.5[a, b] | | E2 |
| 78.6 | 8.7 ± 0.9 | 1/0.12/<0.06[a] | | M1 or 98% M1 + < 2% E2 |
| 92.3 | | 1/.../...[a] | | M1 |
| 123.7 | 3.0 ± 0.2 | 1/1.25/1.35[b] | 0.23 ± 0.04[c, d] | E2 or E2 + < 10% M1 |
| 133.5 | 6.3 ± 0.7 | 1/0.25/0.25[a, b] | | 80% M1 + 20% E2 |
| 156.9 | | 1/.../...[a] | 0.006[c] | M1 |
| 215.8 | >6.7 | 1/0.16/...[a, e] | 0.093 ± 0.010[d] | M1 or M1 + E2 |
| 239.2 | 8.3 ± 1.2 | | 0.063 | M1 or M1 + E2 |
| 248.8 | 7.2 ± 1.5 | | 0.062 | E2 or M1 + E2 |
| 372.8 | >5.0[f] | | 0.026 ± 0.006[d] | M1 or M1 + E2 |
| 403.9 | | | 0.0012[c] | |
| 480.4 | 7.5 ± 1.9 | | 0.0097 | M1 + E2 |
| 486.4 | 9.1 ± 1.8 | | 0.0096 | M1 or M1 + E2 |
| 496.1 | 7.3 ± 0.8 | | 0.012 ± 0.002[d] | M1 or M1 + E2 |
| 573.1 | | | 0.0043 | |
| 584.8 | 7.2 ± 1.5 | | 0.0042 | E2 |
| 619.5 | 10 ± 3[g] | | 0.0039 | E2 or M1 + E2 |
| 674.2 | | | 0.0017 | |
| 696.5 | | | 0.0017 | |
| 830.9 | | | 0.0027 | M1 + E2 |
| 922.9 | 9 ± 3[g] | | 0.0020 | M1 + E2 |
| 1046.5 | 8.4 ± 1.6[g] | | 0.0015 | M1 + E2 |

[a] Determined visually from photographic plates of permanent-magnet spectrometers.

[b] Measured with iron-free spectrometer.

[c] This value is for the L-conversion coefficient.

[d] Measured by the internal-external conversion method (IEC).

[e] The K 246.3 line is composite with the L 215.8 line, and its contribution to the latter has not been removed, hence the low K/L ratio. (See text for further comment.)

[f] The K 403.9 line is composite with the L 372.8 line, and its contribution to the latter has not been removed, hence the low K/L ratio.

[g] For these transitions the ratio is K/LM.

## 9. CHARACTERISTICS OF THE DECAY OF BARIUM-131m(*)

Daniel J. Horen, William H. Kelly,† and L. Yaffe‡

Sources of $Ba^{131m}$ were produced by bombarding sodium iodide with about 38-MeV $Li^7$ ions in the Hilac. After chemical purification, the decay of $Ba^{131m}$ was studied by scintillation techniques. The singles photon spectrum measured with a 2.5-cm-diam × 3-mm-thick NaI(Tl) crystal is shown in Fig. A. 9-1 (curve A). The entire photon spectrum could be attributed to $Ba^{131m}$ and the ground state of $Ba^{131}$ (weak, and not shown in Fig. A. 9-1). The half-life of $Ba^{131m}$ was determined by following the decay of the 107-keV photon for 8 hours. The 107-keV photon intensity decayed with a half-life of 14.6 ± 0.2 minutes over a period of eight half-lives.

The singles photon spectrum was found to consist of K x-ray, 78 ± 5-keV photon, and 107 ± 3-keV photon peaks, with relative intensities of 88 ± 16, 2.4 ± 1.2, and 100, respectively. Coincidence measurements ($2\tau \approx 10^{-7}$ sec) showed that the 107-keV photon was in coincidence with L x rays, K x rays, and the 78-keV photon (Fig. A. 9-1, curve B), with relative intensities of > 8.4, 24 ± 2.2, and 2.4, respectively.

From the coincidence data, the K-conversion coefficient of the 78-keV transition was determined as $\alpha_K^{78} = 12.3 \pm 1.5$. For the total conversion coefficient for their transition we obtained $\alpha^{78} = 96 \pm 19$. That the 78-keV transition has multipolarity E3 is shown by the agreement of these results with the theoretical values as calculated by Rose[1] ($\alpha_K = 12.3$, $\alpha \approx 117$) for an E3 transition.

Knowledge of the K- and total-conversion coefficients of the 78-keV transition allowed the determination of the K-conversion coefficient of the 107-keV transition from the relative intensities of the K x ray and photons. We found $\alpha_K^{107} = 0.90 \pm 0.15$, which lies between the theoretical K-conversion coefficients[1] for an M1 transition [$\alpha_K(M1) = 0.7$] and an E2 transition [$\alpha_K(E2) = 1.0$]. Thus the 107-keV transition appears to have multipolarity M1 + E2.

Unfortunately, the ground-state spin of $Ba^{131}$ has not yet been measured, although it is expected to be 1/2 + or 3/2 +. In view of this uncertainty, we offer the following three possible interpretations of our data (summarized in Fig. A. 9-2).

---

*Condensed version of paper submitted to Phys. Rev. (UCRL-10413, Aug. 1962).

†Permanent address: Department of Physics and Astronomy, Michigan State University, East Lansing, Michigan.

‡Summer visitor from the Department of Chemistry, McGill University, Montreal, Canada.

1. M. E. Rose, Internal Conversion Coefficients (North-Holland Publishing Company, Amsterdam, 1958).

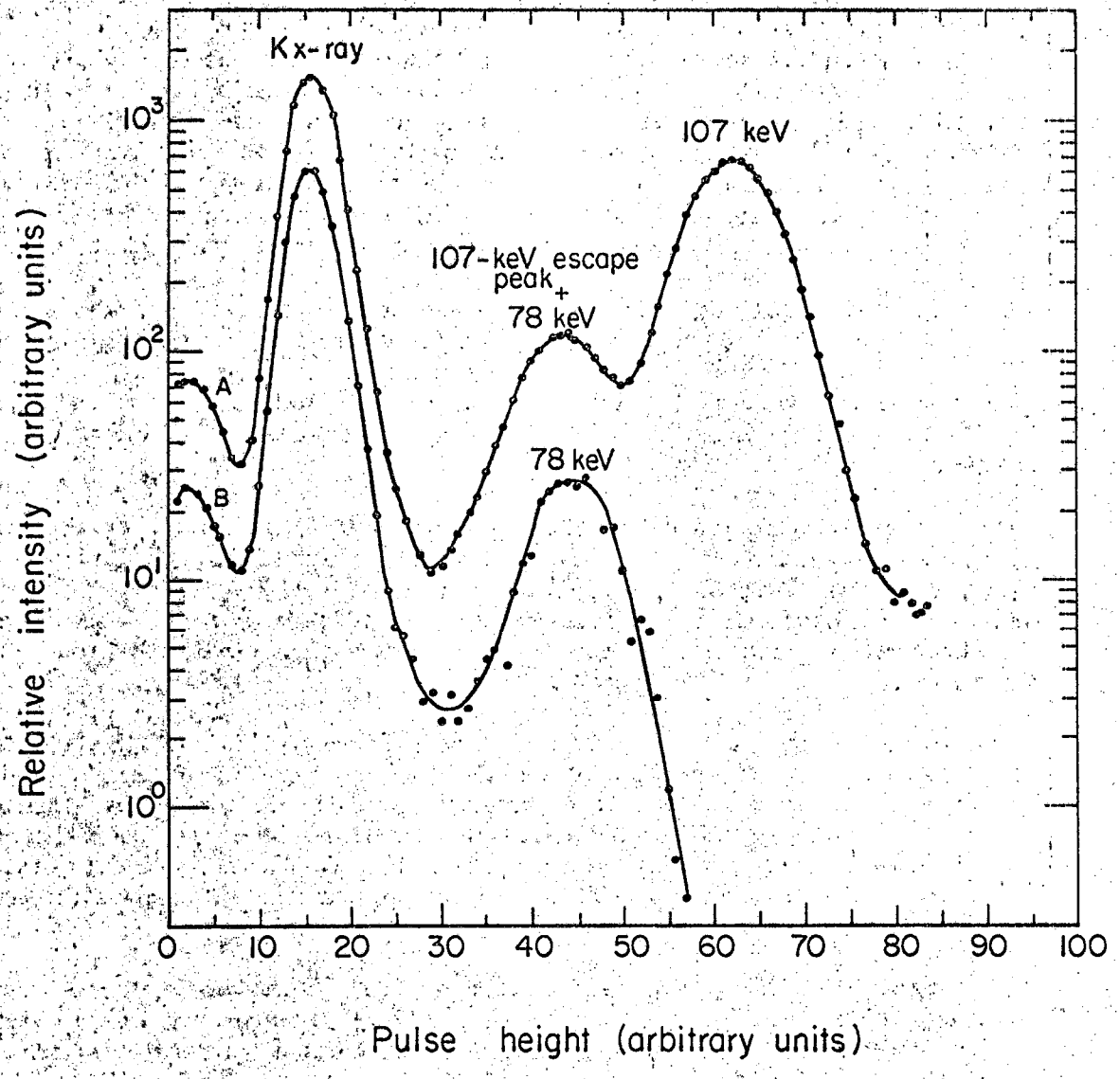


Fig. A. 9-1. Photon spectra in the decay of $Ba^{131m}$ taken with a 1-in.-diam × 3-mm-thick NaI (Tl) crystal: singles spectrum, spectrum in coincidence with the 107-keV photon.

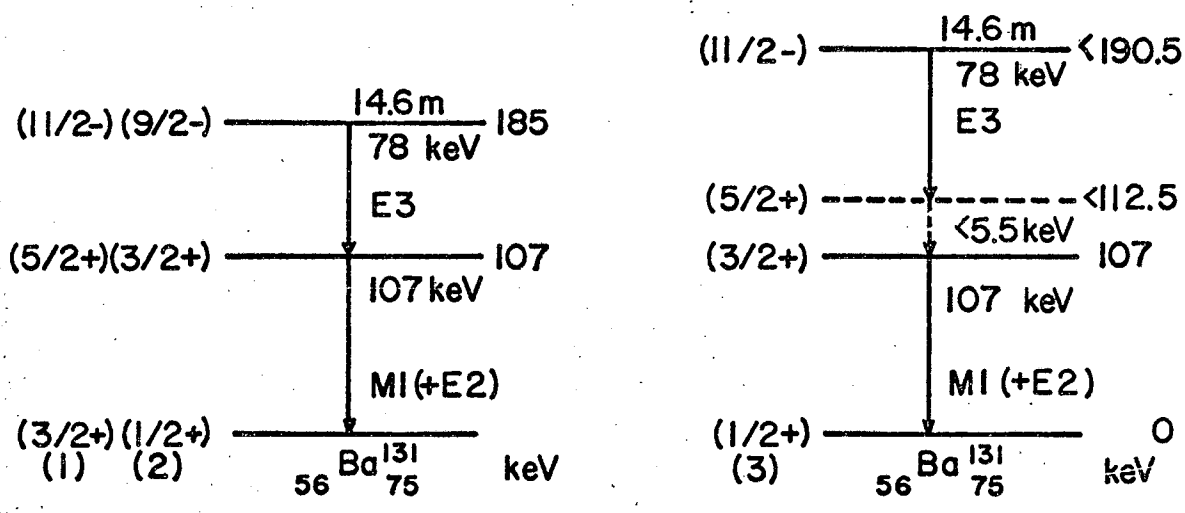


Fig. A. 9-2. Alternative decay scheme for $Ba^{131m}$ (see text for discussion).

The decay of $Ba^{131m}$ proceeds as

$$\frac{11}{2}- \xrightarrow{E3} \frac{5}{2}+ \xrightarrow{M1+E2} \frac{3}{2}+, \quad (1)$$

$$\frac{9}{2}- \xrightarrow{E3} \frac{3}{2} \xrightarrow{M1+E2} \frac{1}{2}+, \quad (2)$$

or

$$\frac{11}{2}- \xrightarrow{E3} \frac{5}{2}+ \longrightarrow \frac{3}{2}+ \xrightarrow{M1+E2} \frac{1}{2}+. \quad (3)$$

## 10. THE NUCLEAR SPIN OF NEODYMIUM-141(*)

Seymour S. Alpert, Burton Budick, Edgar Lipworth, and Richard Marrus

The spin of 2.5-h neodymium-141 was measured by the method of atomic beams and found to be 3/2. Six resolved "flop-in" resonances were observed at various values of the magnetic field. The observed transitions are of the types ($F = 11/2$, $M_F = -1/2 \leftrightarrow F = 11/2$, $M_F = -5/2$) and ($F = 9/2$, $M_F = 1/2 \leftrightarrow F = 9/2$, $M_F = -3/2$). The radioactive isotope was produced in the Berkeley 60-inch cyclotron by the reaction $Pr^{141}(p, n)Nd^{141}$. Beam was detected by collection on freshly flamed platinum foils, which were counted in continuous-flow beta counters.

---

*Abstract for meeting of the American Physical Society, Bull. Am. Phys. Soc. 7, 239 (1962).

## 11. THE g FACTOR OF THE 2.083-MeV STATE OF CERIUM-140(*)

R. M. Levy and D. A. Shirley

One of the major advances in low-energy nuclear physics in recent years has been the development of theoretical methods for studying even-even spherical nuclei. Much of the theory of superconductivity has been carried over to treat such nuclei, with considerable success. A fairly detailed treatment has been applied to nuclei with a single closed shell (SCS) of neutrons or protons.[1] Cerium-140, with a closed shell of 82 neutrons as

---

*Brief version of paper submitted to Phys. Letters (UCRL-10454, Sept. 1962).

1. L. S. Kisslinger and R. A. Sorenson, Kgl. Danske Videnskab. Selskab Mat.-Fys. Medd. 32, No. 9 (1960).

well as a closed subshell of 58 protons, is thus one of the SCS nuclei accessible to this theory. The 2.083-MeV level of $Ce^{140}$ has a lifetime of 4.97 nsec,[2] and is thus sufficiently long-lived for an experimental study of its g factor, a parameter that affords a sensitive test of the wave functions proposed for nucleon states. In this case three possible descriptions of the 2.083-MeV 4+ state are available. We list them, along with their g factors:

(a) $|(g_{7/2})^2\rangle_4$ ; $g = +0.49$,

(b) $|g_{7/2}\, d_{5/2}\rangle_4$; $g = +0.95$,

(c) $|(d_{5/2})^2\rangle_4$; $g = +1.92$.

The Schmidt limits were used to obtain these values. We have determined the g factor experimentally as $g = +1.08 \pm 0.10$ by observing the rotation of the 329-keV–487-keV $\gamma$-$\gamma$ angular correlation pattern in an external magnetic field perpendicular to the correlation plane.[3] The correlation patterns are shown in Fig. A. 11-1.

This result may be interpreted in two ways: (a) The state is nearly pure $|g_{7/2}\, d_{5/2}\rangle_4$, or (b) the state is a very strong admixture of the three possibilities above. It is clear that neither of the pure quasi-particle states, $|(d_{5/2})^2\rangle_4$ or $|(g_{7/2})^2\rangle_4$, is allowed by the data. It is interesting that if one uses the empirical g factor of +0.79 for the spin-7/2 ground state of isotonic $La^{139}$ and +1.94 [4] for the spin-5/2 ground state of isotonic $Pr^{141}$, it is possible to couple to a 4+ state with $g \approx +1.16$, within the limits of error of the experimental value. This may be a more valid procedure than using the Schmidt limits, as we have done above.

---

2. W. M. Currie, Nucl. Phys. 32, 574 (1962).

3. An erroneous result was reported in Phys. Letters 3, 46 (1962). Correction of a computational error leads to the g factor reported here.

4. This is the average of two values. There is considerable uncertainty in this number.

## 12. PSEUDO-QUADRUPOLE COUPLING IN PROMETHIUM ISOTOPES(*)

R. W. Grant and D. A. Shirley

Pseudo-quadrupole coupling is a magnetic effect arising in second-order perturbation theory. A low-lying singlet is connected with a higher doublet in such a way as to produce hyperfine splitting of a quadrupolar form in the singlet state. The coupling constant depends on the nuclear magnetic moment and spin,

---

*Brief version of paper submitted to Phys. Rev. (UCRL-10472, Sept. 1962).

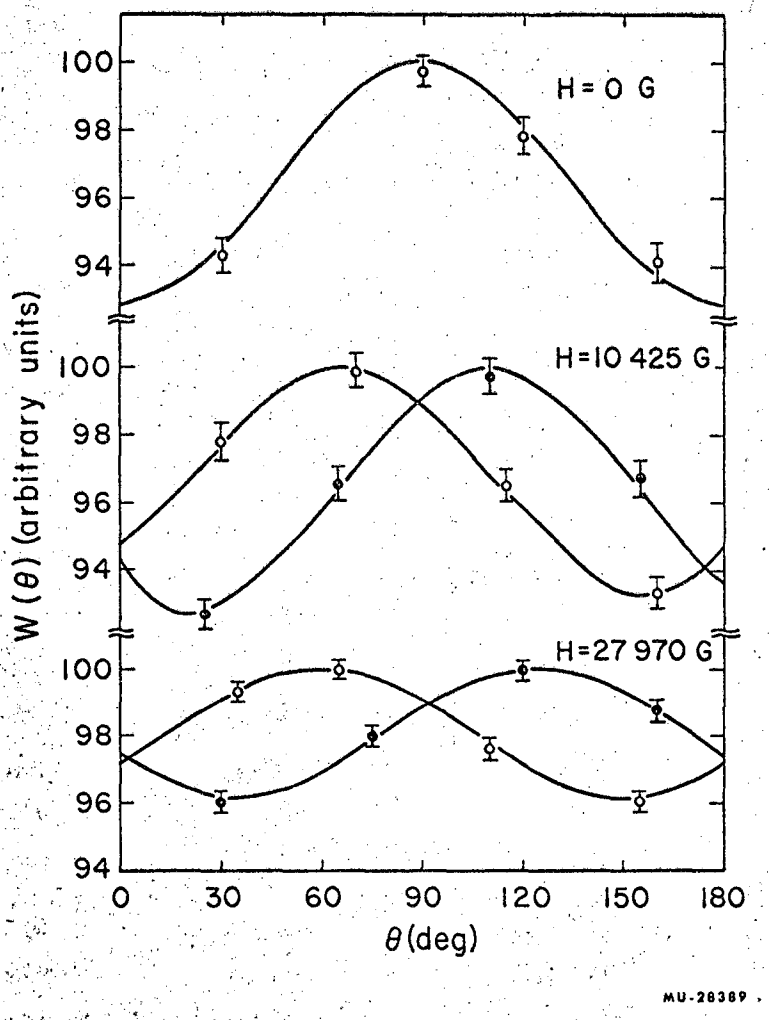


Fig. A. 11-1. Angular correlation of $Ce^{140}$ in zero external field, 10425-gauss field, and 27970-gauss field. o, field direction up; •, field direction down.

$$P' = C' \mu^2/I^2. \quad (1)$$

Here C' is a constant. In the conventional electric quadrupole case the coupling constant depends on the nuclear quadrupole moment and spin,

$$P = CQ/4I(2I-1). \quad (2)$$

In practice only the sum $P'' = P' + P$ can be measured. Usually P dominates. It is an old problem in atomic spectroscopy to separate the two interactions.[1]

In recent nuclear orientation experiments a pseudo-quadrupole effect was observed for $Pm^{+3}$ ions in cerium magnesium nitrate.[2] We have extended this work to several Pm isotopes and evaluated the constant C' in Eq. (1). We find

$$C' = (+1.01 \pm 0.17) \times 10^{-3} \text{ cm}^{-1}(\text{nm})^{-2}.$$

The validity of the pseudo-quadrupolar form for this interaction was established by comparison of the theoretical temperature dependence of nuclear orientation with experimental results on $Pm^{144}$ and $Pm^{143}$ (Figs. A. 12-1 and A. 12-2).

Theoretical electronic wave functions for $Pm^{+3}$ in cerium magnesium nitrate are given in Table I. The experimental value of C' given above requires that the lowest singlet and doublet be separated by only about 1 $cm^{-1}$. Coupling constants for the Pm isotopes in this crystal as well as in neodymium ethylsulfate are given in Table II. From these constants nuclear moments may be derived:

$$\mu_{148(5.4d)} = 1.82 \pm 0.19,$$

$$\mu_{148(41d)} = 1.80 \pm 0.18,$$

$$\mu_{149} = 3.3 \pm 0.5.$$

The last value was derived from the data of Chapman et al. Finally, by combining these data with decay-scheme work,[3,4] we can establish the spins of all the levels in $Pm^{148}$ and $Sm^{148}$, shown in Fig. A. 12-3.

---

1. C. H. Townes, Handbuch der Physik, Vol. 38/1, p. 402.

2. C. J. S. Chapman, M. A. Grace, J. M. Gregory, and C. V. Sowter, Proc. Roy. Soc. (London) A259, 377 (1960).

3. C. F. Schwerdtfeger, E. G. Funk, Jr., and J. W. Nihelich, Phys. Rev. 125, 1641 (1962).

4. C. W. Reich, R. P. Schuman, J. R. Berreth, M. K. Brice, and R. L. Heath, Phys. Rev. 127, 192 (1962).

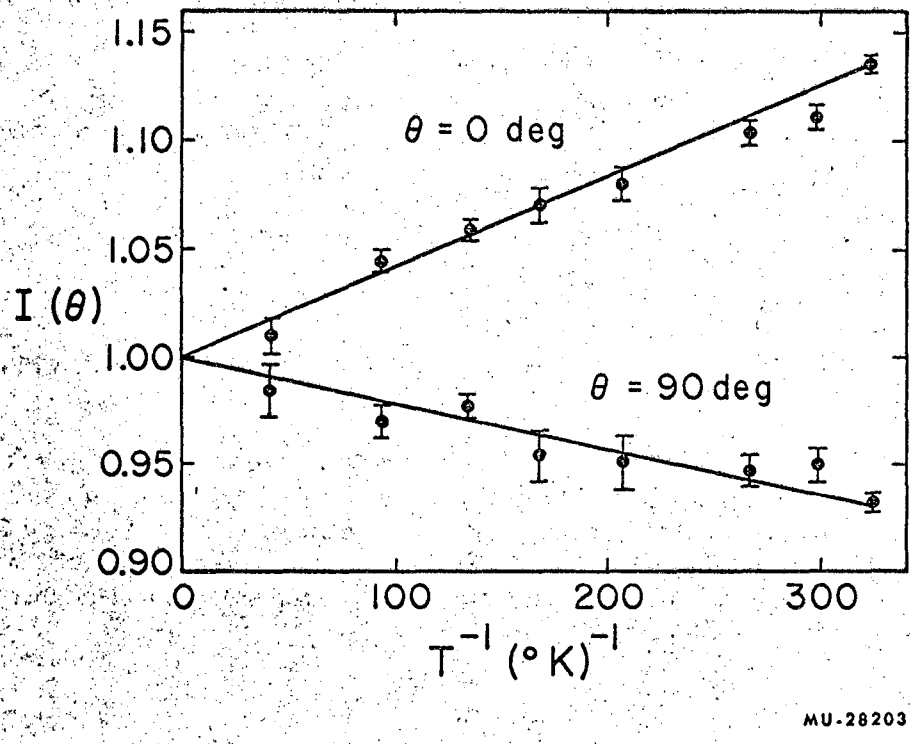


Fig. A. 12-1. Temperature dependence of $I(\theta)$ for the 695-keV $\gamma$ ray in the decay of aligned $Pm^{144}$ taken at 0° and 90° from the crystalline C axis in CMN. Normalized theoretical curves are shown.

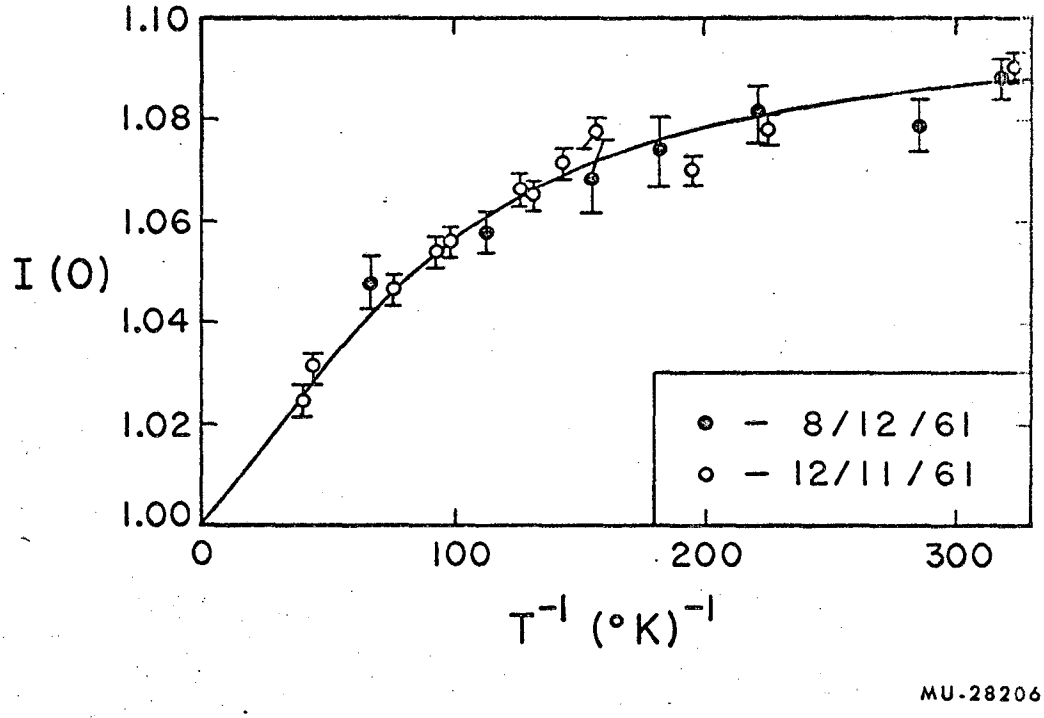


Fig. A. 12-2. Temperature dependence of I(0) for the 740-keV γ ray in the decay of $Pm^{143}$ in CMN. Data of August 12, 1961 and December 11, 1961 are shown with normalized theoretical curve.

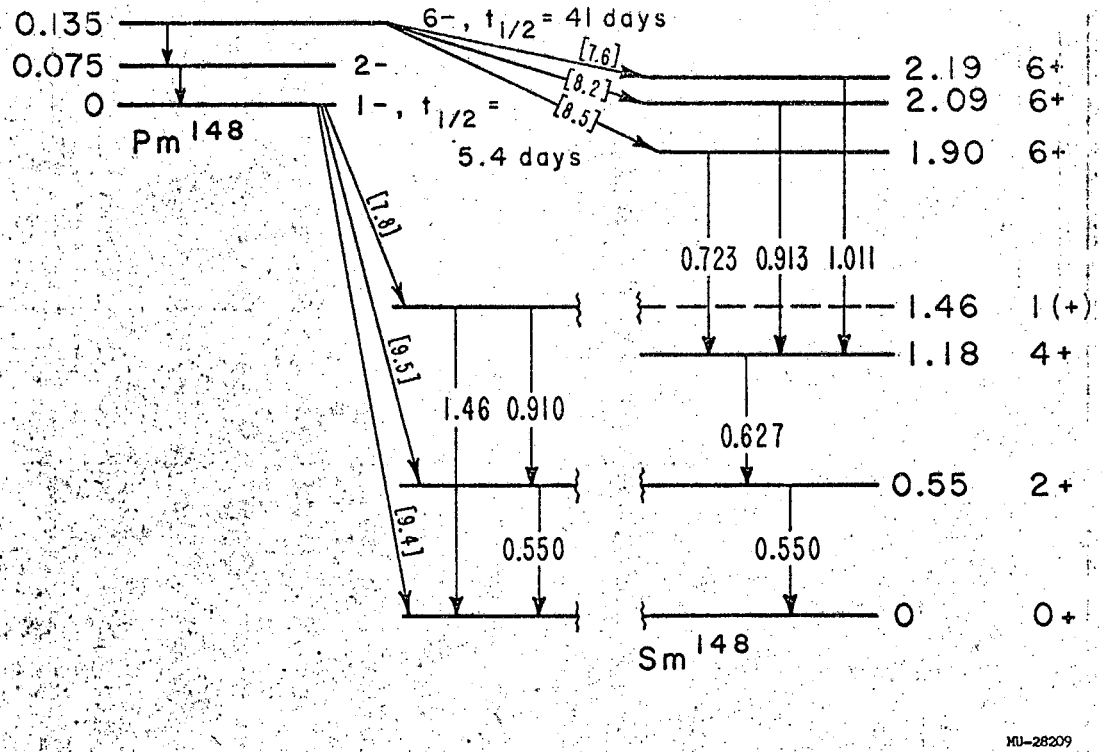


Fig. A. 12-3. Partial decay scheme of the $Pm^{148}$ isomers relevant to this work.

Table I. Energies and wave functions of the eigenstates of $^5I_4$ $Pm^{+3}$ in CMN, calculated from crystal field theory.

| Energies ($cm^{-1}$) | Degeneracy | Wave functions in $J_z$ notation |
|---|---|---|
| -181.66 | 1 | $+0.56\|+3\rangle + 0.61\|0\rangle - 0.56\|-3\rangle$ |
| -162.82 | 2 | $+0.66\|+4\rangle \mp 0.73\|\pm 1\rangle + 0.21\|\mp 2\rangle$ |
| -123.51 | 2 | $\pm 0.475\|\pm 4\rangle + 0.18\|\pm 1\rangle \mp 0.86\|\mp 2\rangle$ |
| 172.53 | 1 | $+0.71\|+3\rangle + 0.71\|-3\rangle$ |
| 193.91 | 2 | $+0.59\|\pm 4\rangle \pm 0.66\|\pm 1\rangle + 0.46\|\mp 2\rangle$ |
| 194.00 | 1 | $-0.43\|+3\rangle + 0.79\|0\rangle + 0.43\|-3\rangle$ |

Table II. Hyperfine-structure coupling constants, A, and total quadrupole coupling constants, P'', for several Pm isotopes in NES and CMN, respectively. Errors are given parenthetically.

| Isotope | I-spin | $A(10^{-3}\ cm^{-1})$ | $P''(10^{-3}\ cm^{-1})$ |
|---|---|---|---|
| $Pm^{143}$ | 5/2 | 29 (3) | 2.2 (.3) |
| | 7/2 | 22 (2) | 1.25 (.20) |
| $Pm^{144}$ | 5 | 6.5 (.5) | 0.11 (.1) |
| | 6 | 5.6 (.5) | 0.073 (.004) |
| (5.4-day) $Pm^{148}$ | 1 | 35 (4) | 3.3 (.7) |
| (41-day) $Pm^{148}$ | 6 | 5.8 (.3) | -------- |
| $Pm^{149}$ | 7/2 | ------- | 0.88 (.2) |

## 13. NUCLEAR SPINS OF NEODYMIUM-149, PRASEODYMIUM-143, AND ERBIUM-165(*)

Burton Budick, Walter M. Doyle, Richard Marrus, and William A. Nierenberg

The spins of three radioactive rare earth isotopes have been measured by the method of atomic-beam magnetic resonance. They are found to be $Nd^{149}$(I=5/2), $Pr^{143}$(I=7/2) and $Er^{165}$(I=5/2). The radioactive neodymium and praseodymium are produced by pile irradiation. The erbium is produced in the Berkeley 60-inch cyclotron by bombarding holmium with protons. All three isotopes are collected on platinum foils and their decay rates measured. The isotopes can be positively identified by the method of production, the measured $g_J$ values, and the measured half-lives.

*Abstract for meeting of American Physical Society, Bull. Am. Phys. Soc. 7, 476 (1962).

## 14. ANOMALOUS QUADRUPOLE COUPLING IN EUROPIUM ETHYLSULFATE(*)

B. R. Judd, C. A. Lovejoy, and D. A. Shirley

One of the significant trends in chemical and atomic physics in the past few years has been the increasing awareness, both experimental and theoretical, of small hyperfine-structure effects that cannot be explained by the very simplest models involving only valence electrons in pure, non-interacting hydrogenlike orbitals. These effects are observed, for example, in some internal magnetic fields, in antishielding, and in the influence on hyperfine structure of higher-order crystal-field interactions and deviations from Russell-Saunders coupling.

Elliott has shown[1] that $Eu^{+3}$, nominally in a $^7F_0$ state and therefore devoid of hyperfine structure, should exhibit a small quadrupole effect in certain crystals, such as rare earth ethylsulfates, arising from interaction, in second-order perturbation theory, between the ground singlet and a higher doublet characterized by $|J = 2, J_2 = 0\rangle$. The interaction takes place via the $Y_2^0$ component of the crystalline field.

In attempting to observe this second-order effect in nuclear orientation experiments on $Eu^{152}$ and $Eu^{154}$ in neodymium ethylsulfate we found an effect, but of twice the expected magnitude and opposite sign. The difference is attributed to antishielding. A leading term in the antishielding correction-

*Brief version of published paper, Phys. Rev. 128, 1733 (1962).

1. R. J. Elliott, Proc. Phys. Soc. (London) 70B, 119 (1957).

the admixing of the $5p^5 6p\ ^1D_2$ state into the closed-shell state $5p^6\ ^1S_0$, via the crystal-field potential – was calculated and found to account for over 1/3 of the discrepancy.

The spins of 2- states at 1531 keV in $Sm^{152}$ and at 1400 and 1723 keV in $Gd^{154}$, as well as the pure electric dipole multipolarity of radiations depopulating these states, were established. The quadrupole moment of $Eu^{154}$ was found to be $3.29 \pm 0.37$ barns. It is interesting to calculate the intrinsic, or deformation-dependent, quadrupole moments of the four europium isotopes with neutron numbers 88 through 91. The intrinsic quadrupole moment $Q_0$ may be calculated from the spectroscopic quadrupole moment Q, in these cases, using the relationship[2]

$$Q_0 = Q[(I + 1)/I]\ [(2I + 3)/(2I - 1)].$$

Intrinsic moments calculated in this way are given in Table I. In Fig. A. 14-1 we have plotted $Q_0$ against neutron number. It is evident that the onset of nuclear deformation occurs rather abruptly at 88 neutrons.

Table I. Quadrupole moments of europium.

| Isotope | Q | $Q_0$ | Reference |
|---|---|---|---|
| $Eu^{151}$ | +0.95 (10)[a] | +2.66 (28) | 3 |
| $Eu^{152}$ | 2.61 (20) | 6.26 (50) | 4 |
| $Eu^{153}$ | +2.42 (20) | +6.78 (56) | 3 |
| $Eu^{154}$ | 3.24 (37) | 7.78 (.88) | this work |

a. Standard deviations are given in parentheses. We are responsible for assigning standard deviations to derived quantities.

2. A. Bohr and B. R. Mottelson, Kgl. Danske Videnskab. Selskab Mat. -Fys. Medd. 27, No. 16 (1953).

3. K. Krebs and R. Winkler, Naturwiss. 47, 490 (1960).

4. Seymour S. Alpert (Lawrence Radiation Laboratory, Berkeley), private communication; also Seymour S. Alpert, The Moments, Spins, and Hyperfine Structures of the Radioactive Isotopes $I^{133}$(21-h), $Nd^{141}$ (2.5-h), $Eu^{152}$(13-yr), and $Bi^{210}$ (5-day) (Thesis), UCRL-9850, Sept. 1961.

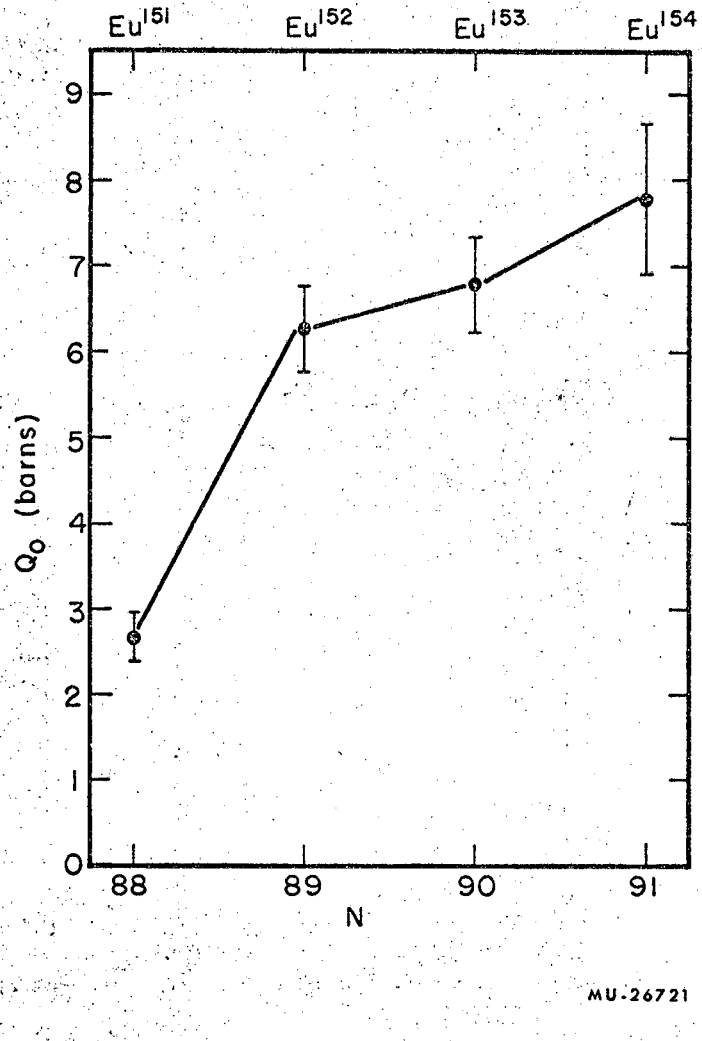


Fig. A. 14-1. Intrinsic quadrupole moments vs neutron number for the europium isotopes. Only in $Eu^{151}$ and $Eu^{153}$ are the signs of the $Q_0$'s known; for the even isotopes the $Q_0$'s are assumed to be positive. $(Q_0)_{152}$ and $(Q_0)_{154}$ are known to have the same sign. The total possible error is indicated in each case; the relative magnitudes are known more precisely.

## 15. EUROPIUM-151: A NEW MÖSSBAUER NUCLEUS(*)

D. A. Shirley, Morton Kaplan, R. W. Grant, and D. A. Keller

A serious limitation on application of the Mössbauer effect has been the scarcity of nuclei for which it is applicable. In fact only $Fe^{57}$ and $Sn^{119}$ have had wide application to date. It seemed useful to find a rare earth isotope which could exhibit the effect at high temperatures and with which it was possible to produce a single-line source. These two criteria eliminate nearly all the possibilities; indeed only trivalent $Eu^{151}$ and divalent $Sm^{149}$ pass both tests. Both have low-energy (22-keV) $\gamma$ transitions, so an appreciable effect could be expected even at room temperature. In addition both have the configuration $4f^6$. Thus the level $^7F_0$ is the lowest electronic state. This level has zero angular momentum, thus (to first order) no hyperfine structure, and a single-line source could be expected.

We have observed and studied the Mössbauer effect in $Eu^{151}$, using a source and absorber of $Eu_2O_3$. Self-absorption in the source was minimized by using enriched $Eu^{153}$. A typical room-temperature velocity spectrum is shown in Fig. A.15-1. In Fig. A.15-2 is shown an absorption curve taken at 77°K. These data were best fitted with a characteristic Debye temperature of $\theta = 125$°K, while at room temperature a Debye temperature of $\theta = 185$°K gave the best fit. This increase of the apparent Debye temperature with increasing ambient temperature is evidence for the presence of optical branches in the phonon spectrum of the $Eu_2O_3$ lattice.

Some nuclear information was also obtained. From the observed linewidth of 0.23 m/sec and the observed magnitude of absorption, a value of $\tau = 12 \pm 3$ nsec may be set for the mean life of the 21.7-keV level of $Eu^{151}$.

---

*Brief version of published paper, Phys. Rev. 127, 2097 (1962).

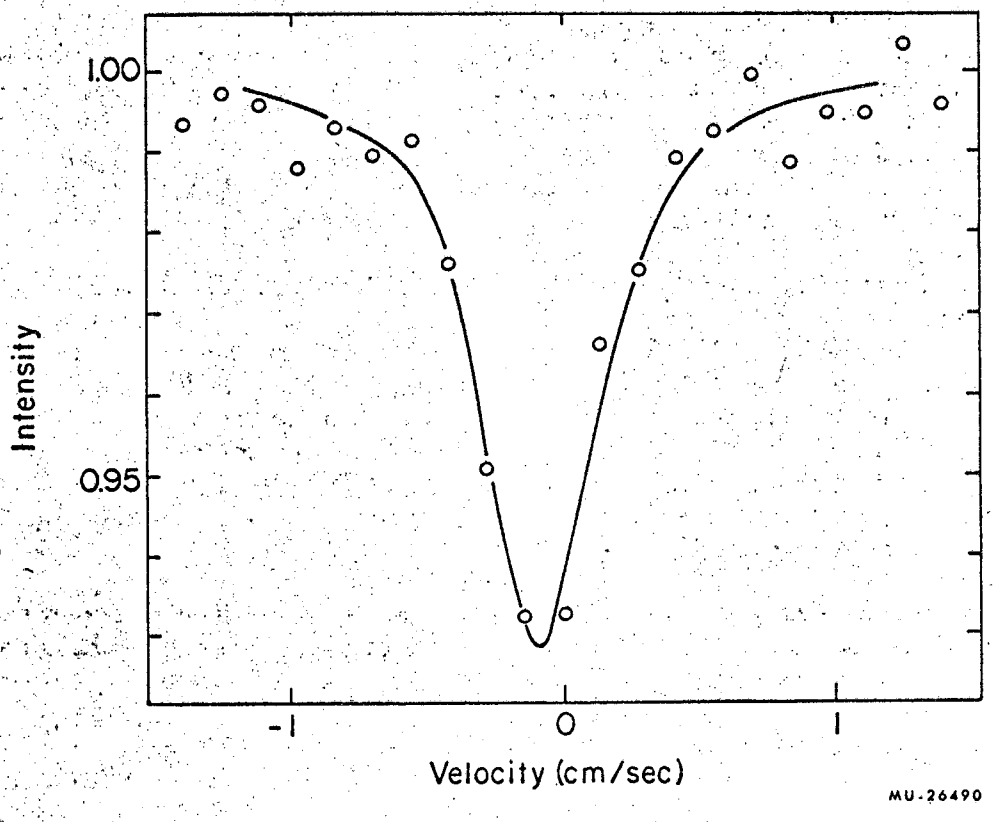


Fig. 15-1. Room-temperature velocity spectrum of the 21.7-keV γ ray in $Eu^{151}$, uncorrected for background, obtained by using a thin sodium iodide scintillation counter. Source is natural $Nd_2O_3$, absorber is 9.6 mg $cm^{-2}$ natural $Eu_2O_3$.

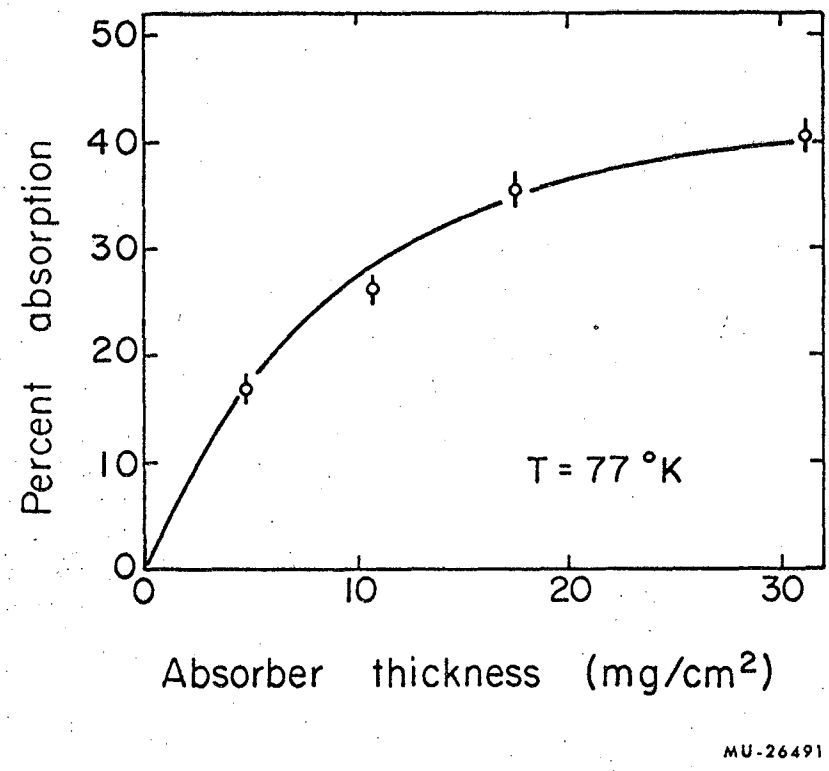


Fig. 15-2. Absorption vs absorber thickness for a source of $Gd^{151}$ in $Eu_2O_3$ enriched in $Eu^{153}$, and an absorber of natural $Eu_2O_3$, both at 77°K. The theoretical curve is for a Debye $\theta$ of 125°K, an excited state spin of 7/2, and a total conversion coefficient of 32.

# 16. LIFETIME OF THE 21.7-keV STATE IN EUROPIUM-151(*)

Daniel J. Horen, H. H. Bolotin† and W. H. Kelly‡

Recently, Shirley et al. observed the Mössbauer effect of the 21.7-keV transition in $Eu^{151}$ and were able to place a lower limit of 6.8 nsec on its half-life. [1] Early attempts to measure this half-life by delayed coincidence techniques proved inconclusive. [2] During the course of this work, Berlovich et al. reported its value as 3.4 ± 0.2 nsec. [3] In their investigation, the latter authors used thin stilbene crystals to detect coincidences between the K-conversion electrons from the 175-keV transition and L, M, and N electrons from the 21.7-keV transition.

For this study, $Gd^{151}$ was produced by a (p, n) reaction on $Eu_2O_3$ (enriched in $Eu^{151}$), from which it was separated by the usual ion-exchange techniques. [4]

The decay of 140-d $Gd^{151}$ populates the 21.7-keV level of $Eu^{151}$. Although many workers have investigated this decay, [3, 5-8] a final decay scheme has not yet been presented. However, from a summarization of the previous work, it appears as though the scheme shown in Fig. A. 16-1 is the best available at this time. Some qualitative coincidence experiments on our part were in agreement with this proposed scheme. For our purposes, we were mainly concerned with the manner in which the 21.7-keV level is populated. The excess intensity of the K x-ray and 21.7-keV transitions relative to the other transitions suggested that the 21.7-keV level is predominantly fed by electron capture. By photon-photon coincidence experiments, we have shown this to be so.

---

*Paper to be submitted to Nucl. Phys.

†Summer visitor, 1962; present address: Argonne National Laboratory, Argonne, Illinois.

‡Permanent address: Department of Physics and Astronomy, Michigan State University, East Lansing, Michigan.

1. D. A. Shirley, M. Kaplan, R. W. Grant, and D. A. Keller, Phys. Rev. 127, 2097 (1962).

2. V. S. Shirley and J. O. Rasmussen, Phys. Rev. 109, 2092 (1958); see reference 20 in this paper as well as text on p. 2094.

3. E. Ye. Berlovich, Yu. K. Gusev, V. V. Ilyin, V. V. Nikitin, and M. K. Nikitin, Nucl. Phys. 37, 469 (1962).

4. The sources were kindly provided by Dr. D. A. Shirley of this Laboratory.

5. A. Bisi, E. Germagnoli, and L. Zappa, Nucl. Phys. 3, 671 (1957).

6. N. M. Anton'eva, A. A. Bashilov, B. S. Dzhelepov, and B. K. Preobrazhenskii, Bull. Acad. Sci. U.S.S.R. (translation) 22, 134 (1958).

7. G. M. Gorodinskii, A. N. Murin, V. N. Pokrovski, and B. R. Preobrazhenskii, Bull. Acad. Sci. U.S.S.R. (translation) 21, 1611 (1957).

8. B. S. Dzhelepov and V. A. Sergienko, Bull. Acad. Sci. U.S.S.R. (translation) 23, 203 (1959).

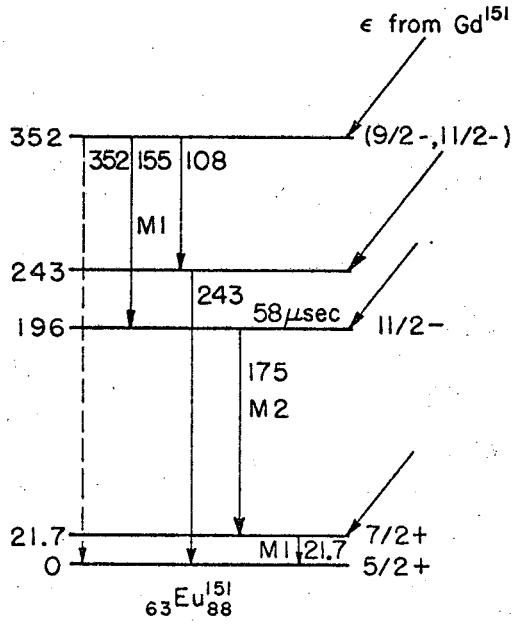


Fig. A. 16-1. Tentative decay scheme of $Gd^{151}$.

For the half-life measurements, the 21.7-keV photon was detected in a 2.54-cm-diam × 0.3-cm-thick NaI(Tl) crystal with a 0.13-mm beryllium cover. A similar crystal was used to detect the K x-rays. A 5.1-cm-diam × 5.1-cm-thick NaI(Tl) crystal was used to gate on the 175- and 155-keV photons. The electronics consisted of a typical fast-slow coincidence system, utilizing a time-to-height converter and a RIDL 400-channel analyzer. Measurements were performed in both 90° and 180° geometry with identical results.

155-, 175-keV – 21.7-keV Coincidences

One method of measuring the half-life of the 21.7-keV state was as follows: The pulses from the 5.1 × 5.1-cm scintillation spectrometer were fed into two single-channel analyzers, one set to pass pulses with heights corresponding to the lower third of the 155- to 175-keV composite photon peak and the other set to pass pulses from the upper third. The outputs of these analyzers were put in slow coincidence with the output of a third single-channel analyzer, which gated on pulses with heights corresponding to the upper half of the 21.7-keV photon peak detected in the thin NaI crystal. The 400-channel analyzer was gated by the output of the slow coincidence circuit, and programmed to record the delay curve arising from the lower third of the 155 + 175-keV peak (henceforth designated as 155-keV delay curve) in the first half of the memory, and from the upper third (henceforth designated as 175-keV delay curve) in the second half of the memory. The results are shown in Fig. A. 16-2.

The 155-keV delay curve arises predominantly from prompt coincidences between the 155-keV photon and K-x-ray-initiated events which result in pulse heights that gate the single-channel analyzer set to pass the upper half of the 21.7-keV photon. If one considers this curve as representing the "prompt" curve, then the half-life of the 21.7-keV state can be determined from the slope of the 175-keV delay curve. The latter yields a value $T_{1/2}$ = 10.4 nsec. It should be noted that the 155-keV delay curve has not been corrected for contributions from other cascades. Analysis has shown that the 175-keV delay curve contains less than about 20% prompt coincidences, assuming the 155-keV delay curve represents the "prompt" spectrum.

In view of the large discrepancy between our value for the half-life of the 21.7-keV state in $Eu^{151}$ and that reported by Berlovich et al.,[3] we have analyzed the data shown in Fig. A. 16-2 by the centroid shift method.[9] Since we have not "purified" either the 155-keV "prompt" curve nor the 175-keV delay curve, we consider such an analysis valid only to determine a lower limit for the half-life of the 21.7-keV state in $Eu^{151}$. Of course, this also includes the assumption that the lifetime of the 352-keV level is short enough so that it in itself does not influence the results of such an analysis. The value so obtained was $T_{1/2} \geq 6.8$ nsec.

K-x-Ray – 21.7-keV Coincidences

Two thin NaI crystals were used to measure the delay curve arising from coincidences between K x-rays and 21.7-keV photons. The single-channel

9. Z. Bay, Phys. Rev. 77, 419 (1950).

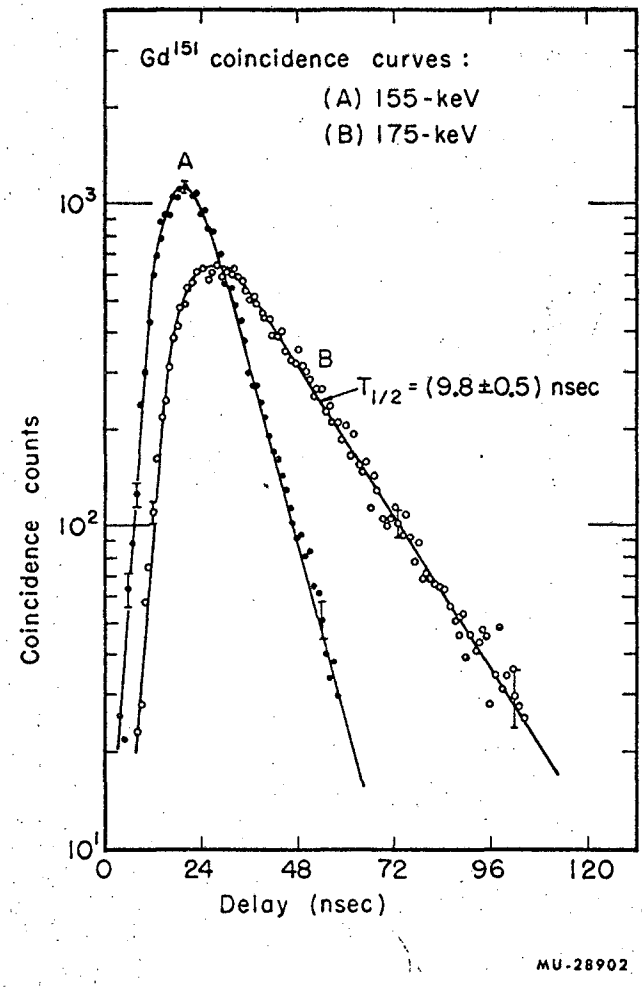


Fig. A.16-2. $Gd^{151}$ coincidences:
A: "prompt" spectrum, 155 and 21.7 keV;
B: delay spectrum, 175 and 21.7 keV.

analyzers were set to gate on the upper halves of the K-x-ray and 21.7-keV photon peaks, respectively. Curve A in Fig. A. 16-3 shows the K-x-ray–21.7-keV delay curve so obtained. Curve B in this figure represents the "prompt" curve obtained by inserting a 0.038-mm gold absorber between the source and the detector used to select the 21.7-keV photon. From the slope of the K-x-ray–21.7-keV delay curve we obtain $T_{1/2} = 9.5$ nsec for the half-life of the 21.7-keV state. Treatment of the data shown in Fig. A. 16-3 by the centroid shift method yielded $T_{1/2} \geq 6.8$ nsec.

The discrepancy between the half-life determinations by the slope method and centroid shift method was believed to be caused by the presence of prompt coincidences in the K-x-ray – 21.7-keV delay curve. To investigate this possibility, as well as to check that the circuitry was functioning properly, we narrowed the window of the analyzer used to detect the 21.7-keV photon and recorded a number of delay curves with the threshold varied over an energy range from 10 to 35 keV. With the threshold set at 35 keV, the delay curve was similar to that shown by curve B in Fig. A. 16-3. When the threshold was lowered so as to gate on 21.7-keV photons, the result was similar to curve A in Fig. A. 16-3. As the threshold was further reduced, the slope of the delay curve corresponded to 9.7 nsec, but the peak began to show the type of structure expected to result from a composite prompt and delay curve. When the threshold was set at 10 keV, the delay curve again resembled the "prompt" curve (curve B in Fig. A. 16-3), except that the slopes were slightly lower (i. e., longer fall-off).

We conclude from these results that our measured delay curves contain a component due to prompt coincidences, and that the half-life of the 21.7-keV state in $Eu^{151}$ can be determined from their slopes. From a number of least-square fits to the curves, our best value for this half-life is $T_{1/2} = 9.7 \pm 0.5$ nsec.

The large discrepancy between our value ($T_{1/2} = 9.7 \pm 0.5$ nsec) and that reported by Berlovich et al.[3] ($T_{1/2} = 3.4 \pm 0.2$ nsec) for the half-life of the 21.7-keV state in $Eu^{151}$ is not understood. However, our results are in good agreement with the lower limit of 6.8 nsec set by Shirley et al.[1] on the basis of their Mössbauer scattering experiments.

The half-life determined in this work and the total conversion coefficient ($\alpha_T = 29.1$) for the 21.7-keV transition[10] allows one to calculate its absolute transition probability as $T_{exp} = 2.42 \times 10^6$ sec$^{-1}$. A comparison with that calculated by the Moskowski single-particle formula[11] shows that this $\ell$-forbidden M1 transition is hindered by a factor of 118. Utilizing the data given in Table I of the paper by Berlovich et al.[3] for the analogous $\ell$-forbidden M1 transitions in $Eu^{147}$ (229.5 keV) and $Eu^{149}$ (150 keV), and recalculating their hindrance factors, we obtain values of 107 and 71, respectively. That the hindrance factor for the transition in $Eu^{151}$ is larger than those for the transitions in $Eu^{147}$ and $Eu^{149}$ appears to invalidate the conclusion drawn by Berlovich et al.[3] that the hindrance factor for these M1 transitions decreases monotonically when approaching the deformation region (i. e., $N > 88$).

10. W. T. Achor, W. E. Phillips, J. I. Hopkins, and S. K. Haynes, Phys. Rev. 114, 137 (1959).

11. S. A. Moszkowski, in Beta and Gamma-Ray Spectroscopy, edited by K. Siegbahn (North-Holland Publishing Co., Amsterdam, 1955), Chap. 13.

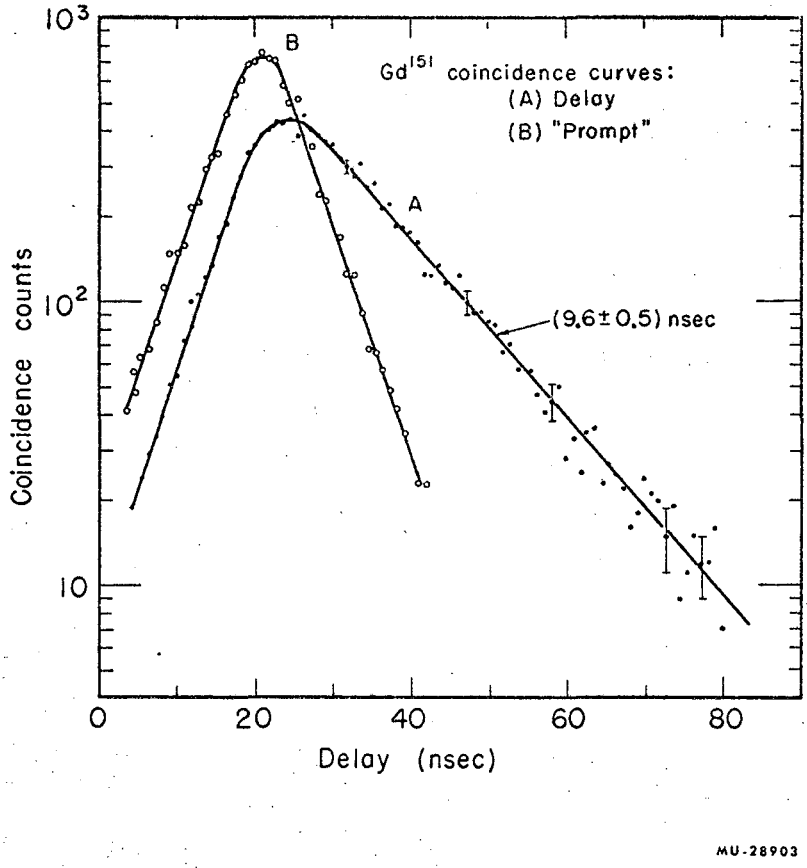


Fig. A. 16-3. $Gd^{151}$ coincidences.
A: K x ray–21-keV delay spectrum;
B: "prompt" spectrum obtained by inserting 0.38 mm gold absorber.

## 17. NUCLEAR SPIN OF $Tb^{161}$ (*)

Isaac Maleh and Richard Marrus

The nuclear spin of 7-day $Tb^{161}$ has been measured by means of an atomic-beam magnetic-resonance flop-in experiment. A spin of 3/2 was determined in the J = 13/2 and 11/2 levels of the configuration $(4f)^8 5d$. The atoms were collected on flamed platinum foils and detected in continuous-flow β counters. Identification was ascertained by measuring the half-life. The radioactive isotope was produced from stable Gd metal in the reaction

$$Gd^{160}(n, \gamma)Gd^{161} \xrightarrow{3.7 \text{ min}} Tb^{161}.$$

The spin of 3/2 can be explained by a state assignment of $2d_{3/2}$ for the 65 protons or by the Nilsson state $[411]\frac{3}{2}+$.

---

*Abstract for meeting of American Physical Society, Bull. Am. Phys. Soc. 7, 477 (1962).

## 18. COULOMB EXCITATION OF TERBIUM-159, HOLMIUM-165, AND THULIUM-169 WITH OXYGEN-16 IONS (*)

Richard M. Diamond and F. S. Stephens

The Coulomb excitation of $Tb^{159}$, $Ho^{165}$, and $Tm^{169}$ has been studied using 60-MeV $O^{16}$ ions produced at the Hilac. Both γ-ray and electron spectra were taken. The data are not reproduced in detail here (see full report*), but the level schemes deduced are shown in Figs. A. 18-1, A. 18-2, and A. 18-3.

Three types of levels have been excited. Firstly, intrinsic (or single particle) levels were seen in $Tb^{159}$ at 971 and 348 keV and probably in $Tm^{169}$ at ~ 900 keV. All of these are thought to be reached by E2 excitation from the ground state. The 361 keV intrinsic state in $Ho^{165}$ is probably populated mainly by E1 decay from the 514 keV band and hence is not a direct excitation from the ground state. In each case, assignment could be made to an expected Nilsson[1] orbital, and the only further comment we will make is that the E2 strengths to these levels, 0.3-1.0 single particle unit, are rather large and most likely due to Coriolis admixtures of these states into their respective ground states. Such mixing, even though small, can introduce large E2 transition probabilities because of the very large collective quadrupole moments of nuclei in this region. The other two types of level seen are both collective in nature. As expected, the most prominent excitations were those

---

*Brief version of paper submitted to Nucl. Phys. (UCRL-10557).

1. S. G. Nilsson, Kgl. Danske Videnskab. Selskab Mat.-Fys. Medd. 29, No. 16 (1955).

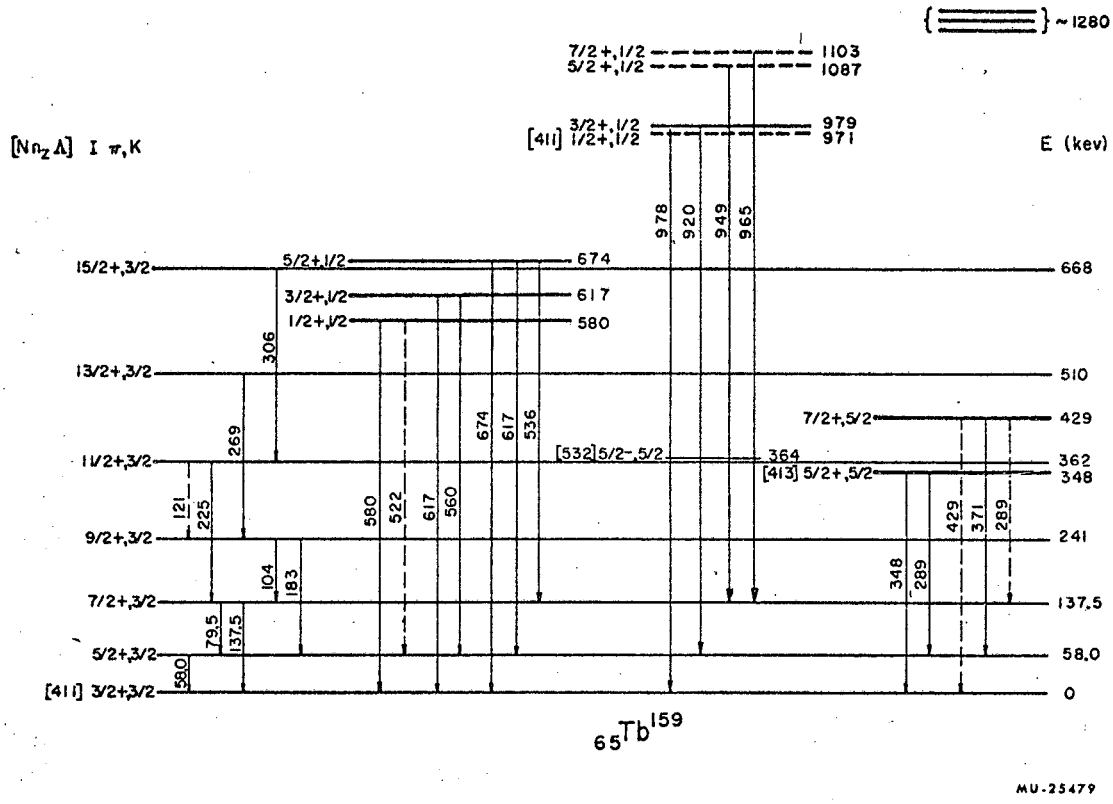


Fig. A. 18-1. Level scheme of $Tb^{159}$. The quantum numbers, $[Nn_z\Lambda]$, refer to the Nilsson description (ref. 1), and I, $\pi$, and K are spin, parity, and projection of the spin along the symmetry axis, respectively. The levels designated by heavy lines are those excited in the present work.

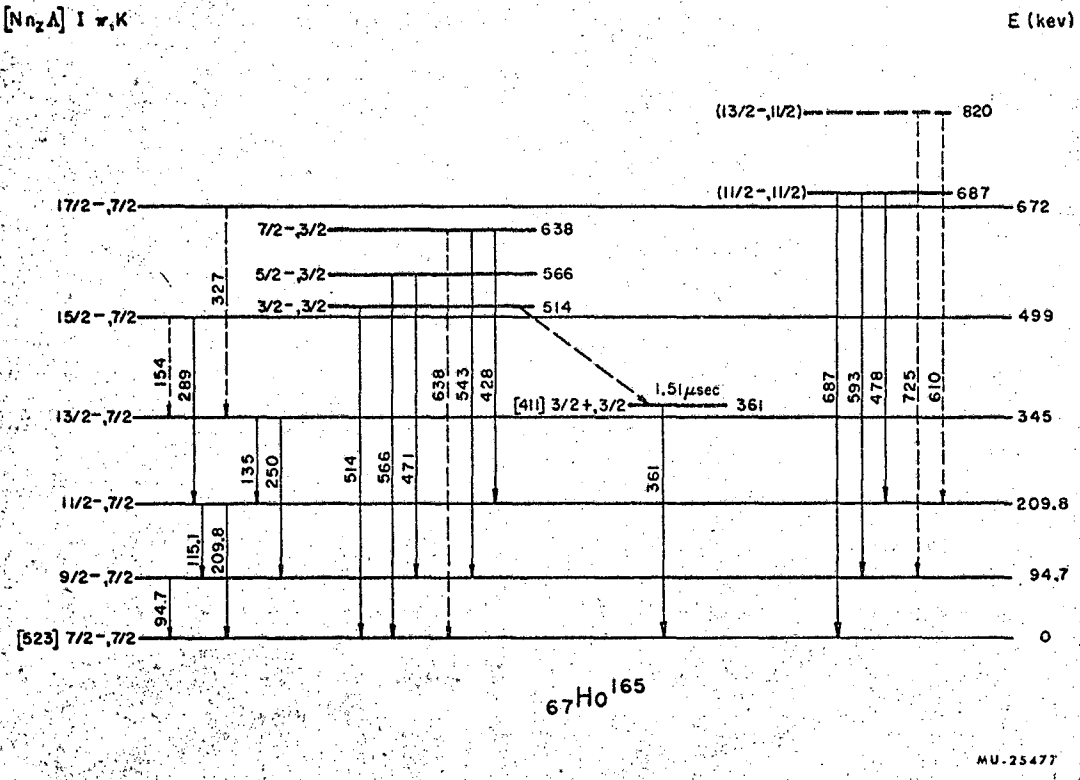


Fig. A.18-2. Level scheme of $Ho^{165}$.

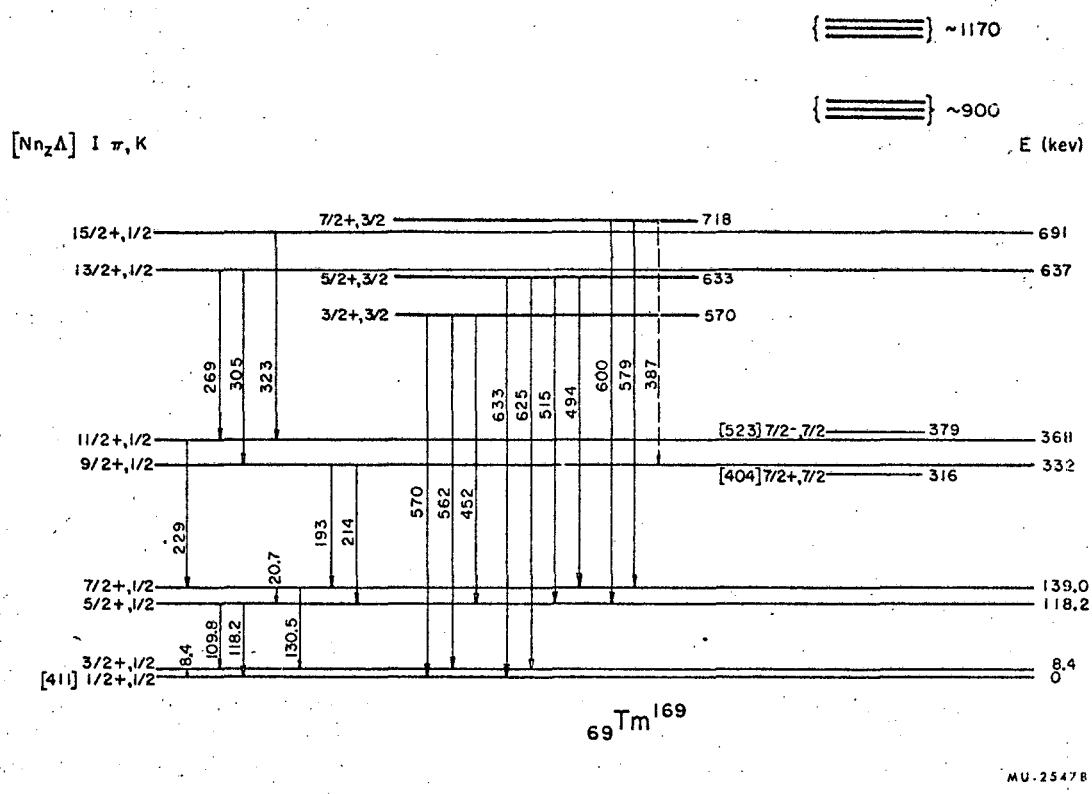


Fig. A. 18-3. Level scheme of $Tm^{169}$.

in the ground state rotational band. The large E2 strengths made it possible, through the multiple excitation process, to excite as many as eight members of the band. The other type of collective excitation produced bands which seem to be related to the ground state by $K = K_0 \pm 2$. We are calling these states "gamma-vibrational states" following the terminology of Bohr and Mottelson[2] although it must be recognized that the results of our measurements do not give any obvious means of distinguishing between different models which provide collective excitations with change of K by two units. Some of the systematic properties observed in the two types of collective levels will be summarized in the following paragraphs.

The $K_0-2$ gamma vibrational band is seen in $Ho^{165}$ (514 keV band), in $Tb^{159}$ (580 keV band), and probably in $Tm^{169}$ (570 keV band). The $K_0+2$ gamma band is seen in $Ho^{165}$ (687 keV band) and possibly in the other two nuclei (~ 1280 and ~ 1170 keV in $Tb^{159}$ and $Tm^{169}$, respectively). In all three cases the $K_0-2$ band lies lower in energy; by 170 keV in $Ho^{165}$, and probably by 600 or 700 keV in the other cases. It is interesting to note that in $Re^{187}$, the only other odd mass nuclei where gamma bands have been reasonably well established,[3] it is the $K_0-2$ bands alone that are seen. A reasonable implication is that these bands lie lower in energy than the $K_0+2$ bands. As far as we know there has been no theoretical treatment of the relative energies expected for such bands. While it seems quite reasonable to us that the $K_0-2$ band should be lower, the magnitude of the splitting in $Tb^{159}$ and $Tm^{169}$ is surprising. Even if our tentative $K_0+2$ assignments are not correct in these cases, the failure of this band to show up at lower energies still implies a large splitting. The difference between these cases and that of $Ho^{165}$, which has a considerably smaller splitting, is not clear.

The E2 transition probabilities (for a vector addition coefficient of unity) between these vibrational states and their respective ground states is in all cases between one and two single particle units. Furthermore, the indication is that in a given nucleus the E2 strengths to the $K_0+2$ and $K_0-2$ bands from the ground state are nearly equal. The relative E2 transition probabilities for de-excitation of these bands in $Ho^{165}$ (in $Tb^{159}$ and $Tm^{169}$ they de-excite principally by M1 radiation) followed the predictions of the vector addition coefficients with a slight modification for mixing of the ground and vibrational states, as has been observed by O. B. Nielsen[4] in even-even nuclei. The evidence is fairly strong that this mixing correction is necessary. The relative E2 transition probabilities for Coulomb exciting the members of these bands in all three nuclei seemed also to follow the modified vector addition coefficients, but are subject to additional corrections which are not well known and may be large, due to the effects of multiple Coulomb excitation and intraband rotational de-excitations.

---

2. A. Bohr and B. R. Mottelson, Kgl. Danske Videnskab. Selskab Mat.-Fys. Medd. 27, No. 16 (1953); A. Bohr, Kgl. Danske Videnskab. Selskab Mat.-Fys. Medd. 26, No. 14 (1952).

3. C. J. Gallagher, W. F. Edwards, and G. Manning, Nucl. Phys. 19, 18 (1960).

4. O. B. Nielsen, in Proceedings of the Rutherford Jubilee International Conference, (Heywood and Company Ltd., London 1961), p. 317; P. Gregers-Hansen, O. B. Nielsen, and R. K. Sheline, Nucl. Phys. 12, 413 (1959).

A surprising result was that when $|K_{vib}| = |K_{gnd}| \pm 1$, as is the case for the $K_0$-2 bands of both $Tb^{159}$ and $Tm^{169}$, the de-exciting transitions were predominantly M1 rather than E2. For these particular cases, M1 transitions are not K-forbidden. In fact, the appropriate vector addition coefficients should be those for $|K_{vib}| \rightarrow |K_{gnd}|$, and the data followed these within our limits of error. Such transitions, however, are not expected in a pure vibrational model. On this model we also would not have expected the relatively fast E1 transition(s) observed to occur in $Ho^{165}$ between the $K_0$-2 gamma band and a nearby intrinsic state (361 keV).

The occurrence of such transitions does not argue against the collective nature of these states, which seems to us to be rather strongly suggested. Even a lack of K-purity in these states is not indicated. The disagreement is with the detailed vibrational description, and particularly in the case of the E1 transitions, it is not clear to us that reasonable admixtures of nearby states can account for the observed transition moments. In this regard it would be interesting to see calculations based on the Davydov-Filippov model.[5] In this model such transitions are not in general forbidden. On the other hand Davydov's calculation for $j = \Omega = 1/2$ is also in very poor quantitative agreement with our data on $Tm^{169}$ where $\Omega = 1/2$. It remains to be seen if relaxing the requirement, $j = 1/2$, can bring this calculation into agreement with the experimental data.

The feature most interesting to us in the ground state rotational bands was the term in the energy formula of the form: $+C(-)^{I+1}(I-1/2)(I+1/2)(I+3/2)$. This term occurred in both $Tb^{159}$ and $Tm^{169}$. Such a term was predicted, and is the result of mixing between $K = 3/2$ and anomalously-spaced ($a \neq 0$) $K=1/2$ bands. We have tentatively ascribed almost all the effect in $Tb^{159}$, and about one-half of the effect in $Tm^{169}$ to Coriolis mixing between these two particular levels. As far as we can tell, all the data are consistent with this analysis; the only unexpected result is a Coriolis matrix element between these two states which is about three times larger than that calculated from the Nilsson wave functions.

---

5. A. S. Davydov and G. F. Filippov, Zh. Eksptl. i Teor. Fiz. 35, 440 (1958); A. S. Davydov, Zh. Eksptl. i Teor. Fiz. 36, 1555 (1959); A. S. Davydov, Nucl. Phys. 16, 597 (1960); and others.

## 19. HYPERFINE STRUCTURE OF ERBIUM-169(*)

Walter M. Doyle and Richard Marrus

The hyperfine structure of radioactive $Er^{169}$ ($T_{1/2}$ = 9.4 days) has been studied in the $^3H_6$ electronic ground state by the atomic-beam magnetic-resonance method. The apparatus used was of sufficient accuracy to measure the nuclear dipole moment directly through its interaction with the external magnetic field. The results are A = 725.46(31) Mc, $g_J$ = -1.16381(5), and $g_I = 5.55(27) \times 10^{-4}$, where A is the dipole interaction constant, and the electronic and nuclear g factors, $g_J$ and $g_I$, are given in units of Bohr magnetons. The nuclear magnetic moment inferred from $g_I$ and corrected for diamagnetic shielding is $\mu_I$ = 0.513(25) nm. This value of $\mu_I$ is consistent with that obtained from A by using the $\langle 1/r^3 \rangle$ value given by Lindgren.

---

*Abstract of UCRL-10484, Nov. 1962.

## 20. HYPERFINE STRUCTURES AND NUCLEAR MOMENTS

The reader seeking further information on such nuclear and atomic properties may be interested in a recent report of related work:

Matthew B. White, Hyperfine Structures and Nuclear Moments of $Lu^{176m}$, $Br^{80}$, $Br^{80m}$, and $I^{132}$ (thesis), UCRL-10321, Sept. 1962.

The paper describes determinations (by the method of atomic-beam radiofrequency spectroscopy) of magnetic dipole interaction constants and electric quadrupole interaction constants for the isotopes listed, also nuclear spin I and the electronic $g_J$ factor for $Lu^{176m}$.

In addition, Isaac Maleh is computing results (which will be reported soon) of measuring the magnetic dipole interaction constant and the electric quadrupole constant for $Er^{171}$ by means of an atomic-beam magnetic resonance flop-in technique using radioactive detection.

## 21. NUCLEAR SPIN OF TUNGSTEN-187(*)

Walter M. Doyle and Richard Marrus

The nuclear spin of 24-h tungsten has been measured by the atomic-beam magnetic-resonance method and found to be 3/2. The beam was produced by electron bombardment of a 0.010-in. -diam tungsten wire, and detection was by collection on platinum foils and subsequent β-counting. Decay plots of resonance foils served to identify the isotope. The results are consistent with a collective-model assignment of the state 3/2-[512] for the 113th neutron.

*Abstract for meeting of American Physical Society, Bull. Am. Phys. Soc. 7, 476 (1962).

## 22. HYPERFINE STRUCTURE OF $_{69}Tm^{171}$(*)

Isaac Maleh

The hfs of $_{69}Tm^{171}$ (I = 1/2) has been measured by the atomic-beam magnetic-resonance flop-in technique. The results are

$$|a| = 372(9) \text{ Mc},$$

$$g_J = -1.14116(10).$$

When the approximate wave functions of Judd and Lindgren[1] are used to evaluate $\langle 1/r^3 \rangle$, the magnetic moment obtained is

$$|\mu_I| = 0.242(15) \text{ nm}.$$

Based on unpublished results of G. Ritter on $Tm^{169}$ and the Fermi-Segrè relationship,

$$\mu_I = 0.225(10).$$

The isotope was produced according to the reaction

$$E_r{}^{170}(n)E_r{}^{171} \xrightarrow[(7.5\ h)]{\beta^-} Tm^{171}(1.9\ yr).$$

*Abstract for meeting of American Physical Society, Bull. Am. Phys. Soc. 7, 606 (1962).

1. B. R. Judd and I. Lindgren, Phys. Rev. 122, 1802 (1962).

# 23. ISOMERIC LEVELS IN THE LIGHT THALLIUM ISOTOPES

Richard M. Diamond and F. S. Stephens

This paper reports the beginning of a series of investigations of short-lived activities and of gamma-ray cascades occurring as the last step of a nuclear reaction. By irradiating suitable targets at the Hilac with heavy ions ranging from $_2He^4$ to $_{10}Ne^{20}$, excited thallium nuclei from mass number 200 to mass 191 have been produced according to the type reaction,

$$_{81-z}X^a + {}_zY^b \rightarrow {}_{81}Tl^{a+b-x} + xn.$$

Those transitions following the decay of metastable states having half-lives in the range of milliseconds to minutes can then be observed very cleanly in the intervals between the 3-msec-long Hilac beam bursts (65 to 165 msec, depending upon the repetition rate used), by either a $\gamma$-ray or (most often in this study) an electron spectrometer.

From the electron spectra, the energies and intensities of the various lines could be determined. Mass assignments of these lines could be made from the nature (projectile, target, and energy) of the irradiation and, in many cases, the lines could be identified with previously known transitions. Irradiations at two slightly different projectile energies helped with the mass assignments and showed which transitions belonged to the same cascade. Measurement of the half-lives of the principal electron lines observed also showed which transitions were associated with a particular metastable state, as well as determining the half-life of that state. From the experimental K/L electron ratios, multipole assignments were made by use of the theoretical conversion coefficients of Sliv and Band.

The results are summarized in the level schemes for the even-mass and odd-mass isotopes shown in Figs. A. 23-1 and A. 23-2, respectively. Among the even-mass nuclei, the sequence of E3 transitions previously known[1] in $Tl^{204}$ and $Tl^{202}$ was extended to $Tl^{200}$ with the observation of a 37-msec 213-keV E3 transition. A 539-keV E2 of the same half-life and of the same total transition intensity was the only other radiation observed for mass 200, and with a known ground-state spin of 2- suggests the simple 7+(E3)4-(E2)2- cascade shown in Fig. A. 23-1, in complete analogy with $Tl^{202, 204}$.

With the odd-mass nuclei, the two previously known E3 transitions in $Tl^{197}$ and $Tl^{195}$ were observed,[2] and the corresponding transitions in $Tl^{199}$ and $Tl^{193}$ were found. The energies and half-lives of the new transitions fit in very well with the previously known ones. But in all four cases it was found that the E3 transition went to the 3/2+ first excited state, and not to the 5/2+ state as had been suggested for $Tl^{197, 195}$.[2] The evidence for this is quite substantial. In $Tl^{193}$, $Tl^{195}$, and $Tl^{197}$ the 5/2+ → 3/2+ transition

---

1. J. A. McDonell, R. Stockendal, C. S. Herrlander, and I. Bergström, Nucl. Phys. 3, 513 (1957).

2. G. Andersson, E. Arbman, and B. Jung, Arkiv Fysik 11, 297 (1957); G. Andersson, P. A. Tove, B. Jung, and I. B. Svensson, Nucl. Phys. 3, 493 (1957).

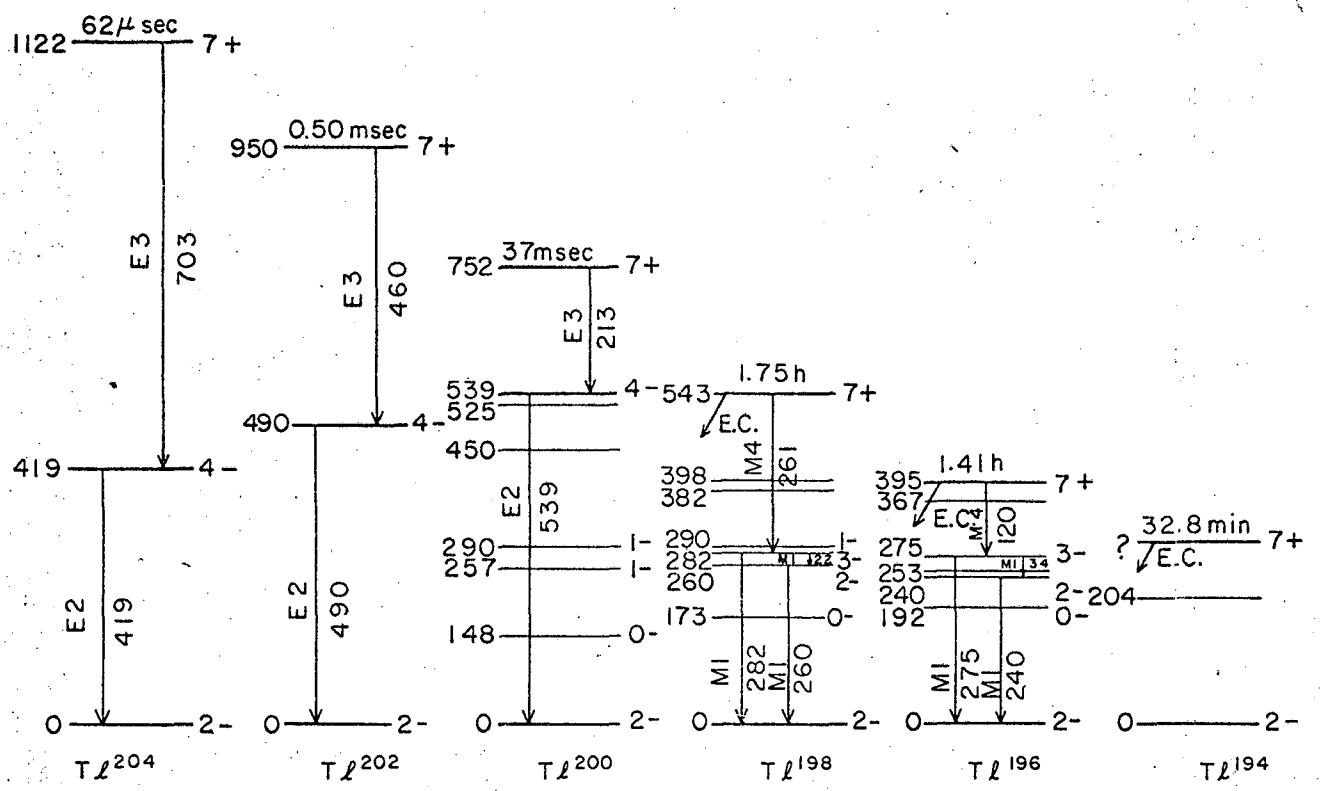


MUB-1515

Fig. A. 23-1. Level schemes of the even-mass thallium isotopes. Only the transitions from the decay of the metastable 7+ states are shown.

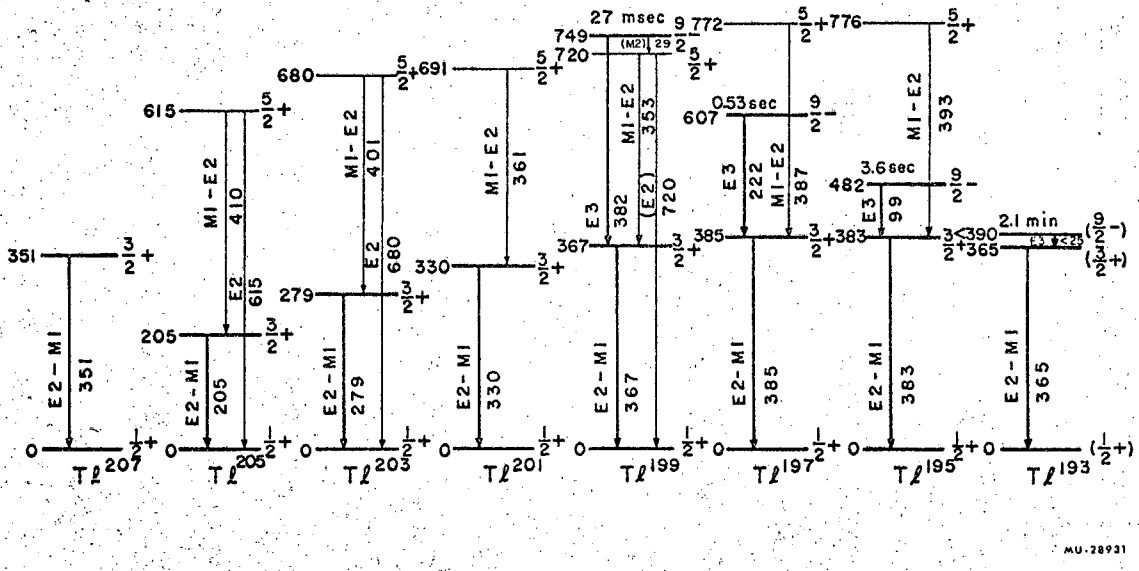


Fig. A. 23-2. Level schemes of the odd-mass thallium isotopes.

is completely missing from the cascade following the isomeric level, and in $Tl^{199}$ it occurs to only a few percent of the E3 intensity, being fed by a 29-keV M2 transition as shown in Fig. A. 23-2. (It was not possible to prove the M2 nature of this transition, however.) Furthermore, the angular distribution of the 367- and 382-keV photons of $Tl^{199m}$ is consistent with the 9/2-(E3)3/2+ (M1-E2)1/2+ cascade required by such a scheme.

One of the main results of this work, then, is the assignment of the isomeric levels in $Tl^{199}$ and $Tl^{193}$ as 9/2- states, as well as the corresponding ones in $Tl^{197}$ and $Tl^{195}$, previously assigned as $h_{11/2}$ single-particle states.[2,3] Since there are no 9/2- levels readily available in this region from a strict single-particle model approach (the $h_{9/2}$ orbital from the next shell lies considerably higher in energy), the observed levels must be largely collective in nature. One way of producing such a 9/2- level is to couple the $h_{11/2}$ proton hole explicitly to two (or more) unpaired neutrons or neutron holes. Another less detailed way is to couple the $h_{11/2}$ proton hole to a collective 2+ excitation (vibration) of the residual even-even core. These are not different models, but correspond to two different levels of analysis of the same type of (collective) state.

Although the 9/2- level lies lowest, the 11/2- or 13/2- level (or both) of such a series of collective states must not lie very much higher in $Tl^{197}$ and $Tl^{195}$. The half-lives for the electron-capture decay of $Pb^{197m}$ and $Pb^{195m}$ rule out the possibility of direct electron capture from the $i_{13/2}$ isomeric states in lead to the 9/2- states in thallium; such first-forbidden unique decays would require impossibly large decay energies to yield the observed half-lives. Thus, the decays most likely proceed via the 11/2- or 13/2- level in the odd-mass thalliums. The discovery and identification of the latter levels in some thallium isotopes would certainly shed additional light on the nature of these states, and such an investigation is in progress. (This work is reported as UCRL-10603, and is to be submitted to Nucl. Phys.)

---

3. I. Bergström and G. Andersson, Arkiv Fysik, 12, 415 (1957).

## 24. ENERGY LEVELS OF BISMUTH-210 AND THE SHELL-MODEL RESIDUAL FORCE(*)

Yeong E. Kim and John O. Rasmussen

The low-lying energy level spectrum of $Bi^{210}$ has been the object of several shell-model theoretical studies. The nucleus has one proton and one neutron beyond the doubly closed shell nucleus $Pb^{208}$, and the lowest proton orbital is $h_{9/2}$ and the lowest neutron orbital $g_{9/2}$. One thus expects a low-lying multiplet of ten levels with spins from 0 to 9 for $Bi^{210}$. With the experimental determination eight years ago of a ground-state spin of 1 a difficult problem was posed for shell-model theory, for almost any reasonable

---

*Brief version of paper in preparation for Nuclear Physics.

attractive central-force mixture acting between the neutron and proton brings spin 0 lower than spin 1, whereas experimentally the spin 0 lies 47 keV higher. Newby and Konopinski made qualitative arguments that an attractive tensor force would operate in the sense needed to explain the discrepancy.[1]

Later, alpha-spectroscopic studies with the long-lived $Bi^{210}$ showed it to be at 250 keV, and it is now generally assumed to be the 9-member of the multiplet. With this experimental information Kharitonov, Sliv, and Sogomanova began shell-model theoretical work anew.[2] They used a phenomenological Gaussian central force with triplet and singlet strengths adjustable but with no space-exchange components; that is, they used a force with Wigner and Bartlett components only. They resolved the difficult problem of the spin-1 ground state in the following manner: By increasing the strength of the singlet force the spin-1 member of the higher $h_{9/2}$-$i_{11/2}$ multiplet is strongly lowered, without any effect on the spin-0 state, which is purely triplet. By also lowering somewhat the $g_{9/2}$-to-$i_{11/2}$ neutron orbital spacing from that observed in $Pb^{209}$, they finally bring the spin-1 state from the upper multiplet down to be the ground state, and the wave functions of their Table 3 show the ground state to be 88% $h_{9/2}\, i_{11/2}$.

Now the low-energy, high-resolution (d, p) reaction studies by Erskine et al. on $Bi^{209}$ have presented a wealth of new information on the $h_{9/2}\, g_{9/2}$ multiplet,[3] and necessitate a thorough reexamination of the shell-model theory. They resolve nine of the expected ten levels of the $h_{9/2}\, g_{9/2}$ multiplet and make tentative spin assignments on the basis that the reaction cross sections are proportional to 2I+1, with the assumption that the configuration is pure. Furthermore, they see higher multiplets attributable to capture of the neutrons into $d_{5/2}$ and $s_{1/2}$ excited orbitals. The multiplets arising from capture into $i_{11/2}$ or $j_{15/2}$ orbitals are weak and not resolved completely, presumably because the high orbital angular-momentum transfers are strongly discriminated against in the (d, p) reaction.

Figure A. 24-1 shows Erskine's spectrum with indicated level numbers. The spins are assigned in sequence of J = 1, 0, 9, 2, 3, 5 and 8 (or 5 and 7), 4, 6, and 7 (or 8), with corresponding level numbers 0, 1, 2, 3, 4, 5, 6, 7, and 8. These results strongly indicate that the ground state involves mainly the $g_{9/2}$ neutron orbital and not the $i_{11/2}$. Erskine made shell-model calculations with a finite Gaussian Serber force (central-even components only) as a function of range.[4] He took a singlet-to-triplet strength ratio of 0.66, reasonable from free-space two-body scattering and from other shell-model work. At a force range of 2.7 F he finds a fairly good fit for all except the spin 0 and 1 levels, which are inverted from their experimental order.

---

1. N. Newby, Jr., and E. J. Konopinski, Phys. Rev. 115, 434 (1959).

2. Yu. I. Kharitonov, L. A. Sliv, and G. A. Sogomonova, Nuclear Phys. 28, 210 (1961).

3. J. R. Erskine, W. W. Bueckner, and H. A. Enge, Phys. Rev. 128, 720 (1962).

4. J. R. Erskine (Massachussetts Institute of Technology), private communication.

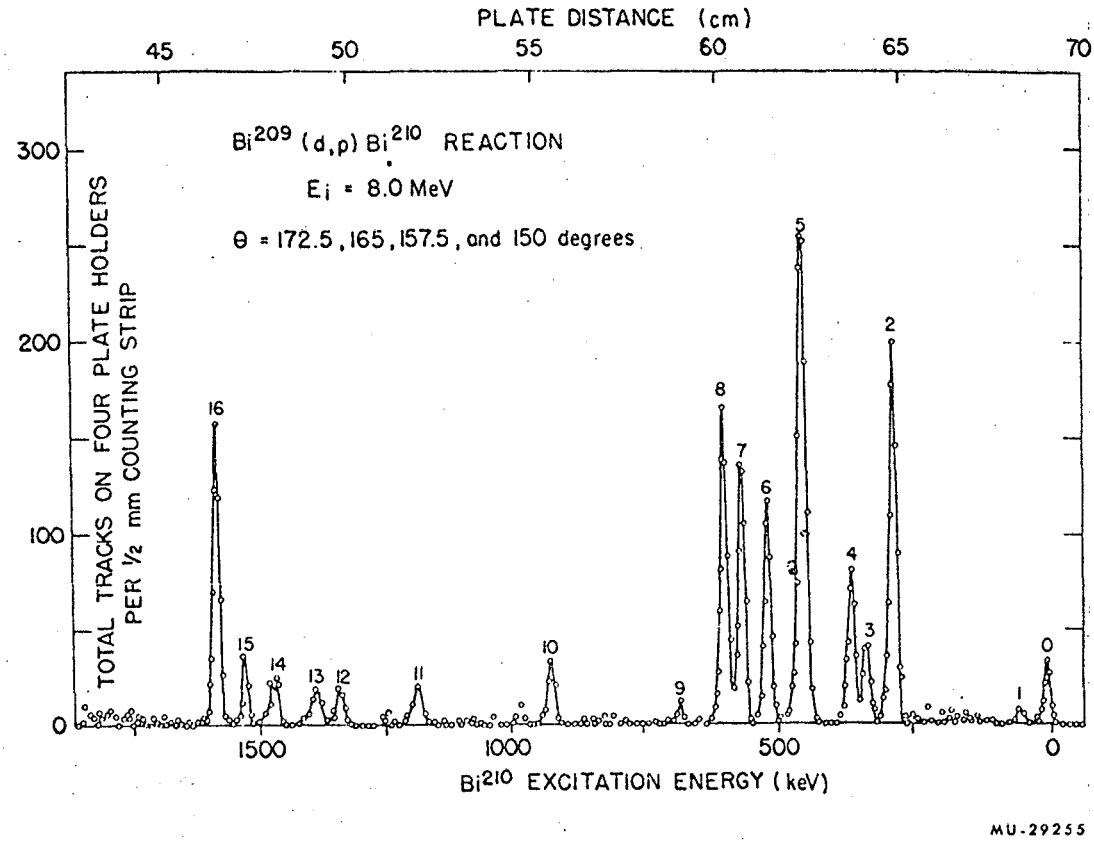


Fig. A. 24-1. Spectrum of protons from the (d, p) reaction on $Bi^{209}$ as observed by Erskine et al. (reference 3).

At this point we felt it most important to make a quantitative evaluation of the tensor-force matrix element with a realistic radial dependence.

The tensor force can be written with the use of projection operators as

$$V^T(r_{12}) = \left[ V^T_{TE} P_{TE} U^T_{TE}(r_{12}) + V^T_{TO} P_{TO} U^T_{TO}(r_{12}) \right] S_{12},$$

where $P_{TE}$ and $P_{TO}$ are the projection operators for the triplet-even and triplet-odd states with the corresponding strengths $V^T_{TE}$ and $V^T_{TO}$, and $S_{12}$ is the tensor operator of the form

$$S_{12} = \frac{3(\vec{\sigma}_1 \cdot \vec{r}_{12})(\vec{\sigma}_2 \cdot \vec{r}_{12})}{r^2_{12}} - \vec{\sigma}_1 \cdot \vec{\sigma}_2 .$$

For the radial dependence, we assume the Gaussian form

$$U^T_{TE} = \exp(-\beta^T_{TE} r^2); \; U^T_{TO} = \exp(-\beta^T_{TO} r^2).$$

The matrix element of the tensor force $V^T(r_{12})$ may be written as

$$\begin{aligned}
&\langle a\, j_1\, j_2\, J\, M | V^T(r_{12}) | a'\, j'_1\, j'_2\, J'\, M' \rangle \\
&= \frac{1}{2} V^T_{TE} \Big[ \langle a\, j_1\, j_2\, J\, M | U^T_{TE}(r_{12})\, S_{12} | a'\, j'_1\, j'_2\, J'\, M' \rangle \\
&+ (-1)^{j'_1 + j'_2 + J} \langle a\, j_1\, j_2\, J\, M | U^T_{TE}(r_{12})\, S_{12} | a'\, j'_2\, j'_1\, J'\, M' \rangle \Big] \\
&+ \frac{1}{2} V^T_{TO} \Big[ \langle a\, j_1\, j_2\, J\, M | U^T_{TO}(r_{12}) S_{12} | a'\, j'_1\, j'_2\, J'\, M' \rangle \\
&+ (-1)^{j'_1 + j'_2 + J} \langle a\, j_1\, j_2\, J\, M | U^T_{TO}(r_{12}) S_{12} | a'\, j'_2\, j'_1\, J'\, M' \rangle \Big]
\end{aligned}$$

and

$$\begin{aligned}
&\langle a\, j_1\, j_2\, J\, M | U^T(r_{12}) S_{12} | a'\, j'_1\, j'_2\, J'\, M' \rangle \\
&= 3 \sum_{K,x,y} \langle a | F_{xy} | a' \rangle \; W(1x1y; K\, 2) \\
&\times \langle j_1\, j_2\, J\, M | \bar{T}_1^{(1x)K} \cdot \bar{T}_2^{(1y)K} | j'_1\, j'_2\, J'\, M' \rangle ,
\end{aligned}$$

where

$$\langle \alpha | F_{xy} | \alpha' \rangle = -5 \sum_{kij} \langle \alpha | r_i r_j | \alpha' \rangle X_{ij}, \quad \text{for } i, j = 1, 2;$$

$$X_{11} = \sqrt{\frac{2}{15}} \sqrt{2x+1} \; (2\ 0\ k\ 0 \,|\, x\ 0),$$

$$X_{22} = \sqrt{\frac{2}{15}} \sqrt{2y+1} \; (2\ 0\ k\ 0 \,|\, y\ 0),$$

$$X_{12} = \sqrt{(2x+1)(2y+1)} \; (1\ 0\ k\ 0 \,|\, x\ 0)\ (1\ 0\ k\ 0 \,|\, y\ 0)$$

$$\times\ W(1\ 1\ x\ y;\ 2k),$$

and

$$\langle \alpha | r_i r_j | \alpha' \rangle = (2k+1) \int_0^\infty dr_1\, r_1^2\, R_1 R_1' \int_0^\infty dr_2\, r_2^2\, R_2 R_2'\, r_i r_j$$

$$\times \int_{-1}^{1} d\left(\frac{\cos\theta_{12}}{2}\right) P_k(\cos\theta_{12}) \; \frac{U^T(r_{12})}{r_{12}^2} \; .$$

The angular part in terms of 3, 6, and 9-j symbols is

$$\langle j_1\ j_2\ J\ M \,|\, \bar{T}_1^{(1x)K} \cdot \bar{T}_2^{(1y)K} \,|\, j_1'\ j_2'\ J'\ M' \rangle$$

$$= (-1)^{j_1' + j_2 + \ell_1 + \ell_2 + J}\ 6\ \delta_{JJ'}\ \delta_{MM'} \begin{Bmatrix} J & j_2 & j_1 \\ K & j_1' & j_2' \end{Bmatrix}$$

$$\times \sqrt{[j_1][j_2][j_1'][j_2']} \quad \sqrt{[\ell_1][\ell_2][\ell_1'][\ell_2']}$$

$$\times \begin{pmatrix} \ell_1 & x & \ell_1' \\ 0 & 0 & 0 \end{pmatrix} \begin{pmatrix} \ell_2 & y & \ell_2' \\ 0 & 0 & 0 \end{pmatrix} \begin{Bmatrix} \frac{1}{2} & \frac{1}{2} & 1 \\ \ell_1' & \ell_1 & x \\ j_1' & j_1 & K \end{Bmatrix} \begin{Bmatrix} \frac{1}{2} & \frac{1}{2} & 1 \\ \ell_2' & \ell_2 & y \\ j_2' & j_2 & K \end{Bmatrix} ,$$

where the symbol [a] stands for [2a+1].

Figures A. 24-2 through A. 24-5 present the results for the diagonal contribution of the tensor-even and tensor-odd forces on the $h_{9/2}$ $g_{9/2}$ multiplet as a function of the range parameter. The results confirm the qualitative predictions of Newby and Konopinski, for an attractive tensor force, both even and odd components, is quite repulsive for the spin-0 state. At ranges comparable to the free-space ranges of Gammel and Thaler the tensor force affects the spin-1 in an opposite sense to the spin-0, and it has only a rather small effect on the states of spin-2 or higher.

Since so few shell-model calculations have been made with a realistic range tensor force, we turn to a comparison with the Brueckner-Gammel-Thaler[5] force for the two nucleons in free space. That this comparison is a useful guideline is reinforced by the success of the calculations by Dawson, Talmi, and Walecka[6] on the $O^{18}$ spectrum, using the free-space of Brueckner, Gammel, and Thaler including tensor force and the hard core with Yukawa radial dependence.

To obtain an idea of the $Bi^{210}$ spectrum if the Brueckner-Gammel-Thaler potential were used, we try to fit the medium distances of the Yukawa potentials by (a) taking the same range parameters of the Yukawa potential for the Gaussian, and matching the two potentials at the radial distance equal to the same ranges, and (b) taking the Gaussian range (1/e point) equal to twice the Yukawa range parameter ($e^{-2}/2$ point), and matching the values of the potentials at this point. Two sets of the Gaussian parameters thus obtained are shown in Table I.

Table I. The parameters for the simulated BGT potentials. For each force, the strengths are given in the upper row, and the ranges in the lower row. The radial dependence is the Yukawa form with a hard core (core radius 0.4 F) for the BGT, and the Gaussian without the hard core for the simulated BGT.

| Potential | Central force | | | | Tensor force | |
|---|---|---|---|---|---|---|
| | TE | SE | TO | SO | TE | TO |
| Simulated BGT(I) | -877.39 (MeV) | -434.0 | -14.0 | +130.0 | -159.40 | +22.0 |
| | 0.47828(F) | 0.68965 | 1.0 | 1.0 | 0.95292 | 1.25 |
| Simulated BGT(II) | -161.39 (MeV) | -79.83 | -2.57 | +23.91 | -29.32 | + 4.05 |
| | 0.95656(F) | 1.37930 | 2.0 | 2.0 | 1.90584 | 2.5 |

5. K. A. Brueckner and J. L. Gammel, Phys. Rev. 109, 1023 (1958).

6. J. F. Dawson, I. Talmi, and J. D. Walecka, Ann. Phys. (N. Y.) 18, 339 (1962).

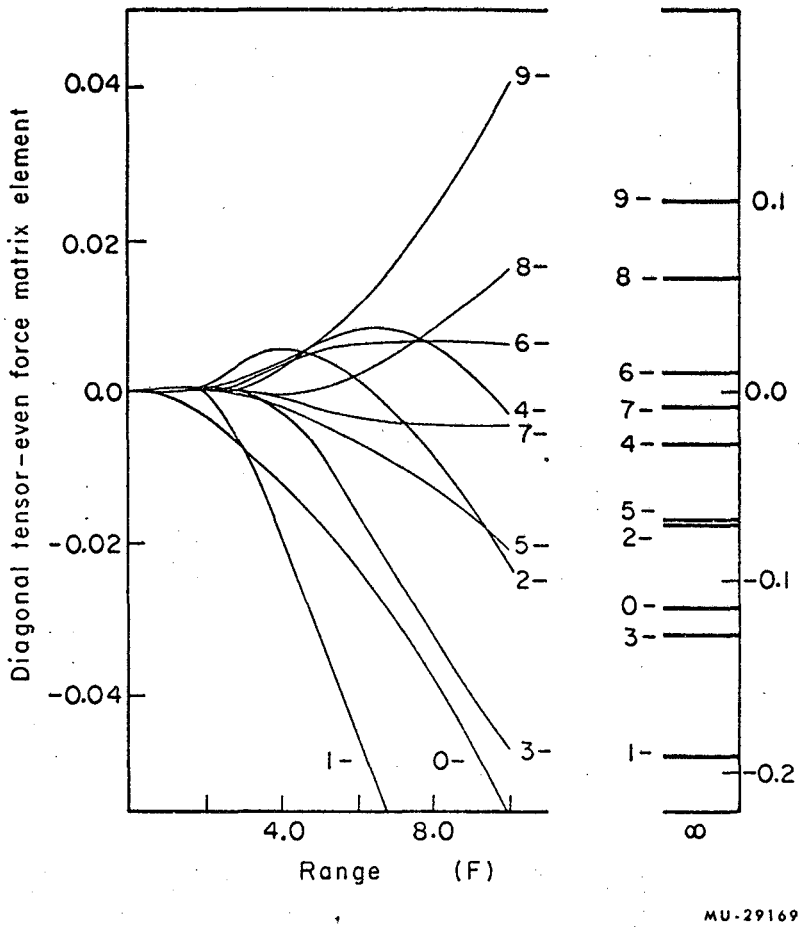


Fig. A. 24-2. Diagonal matrix elements of the tensor-even force $1/3\ P_{TE}\ U^{T}_{TE}(r_{12})\ S_{12}$ for the multiplet $h_{9/2}\ g_{9/2}$ in $Bi^{210}$ as a function of the range parameter $(\beta^{T}_{TE})^{-1/2}$.

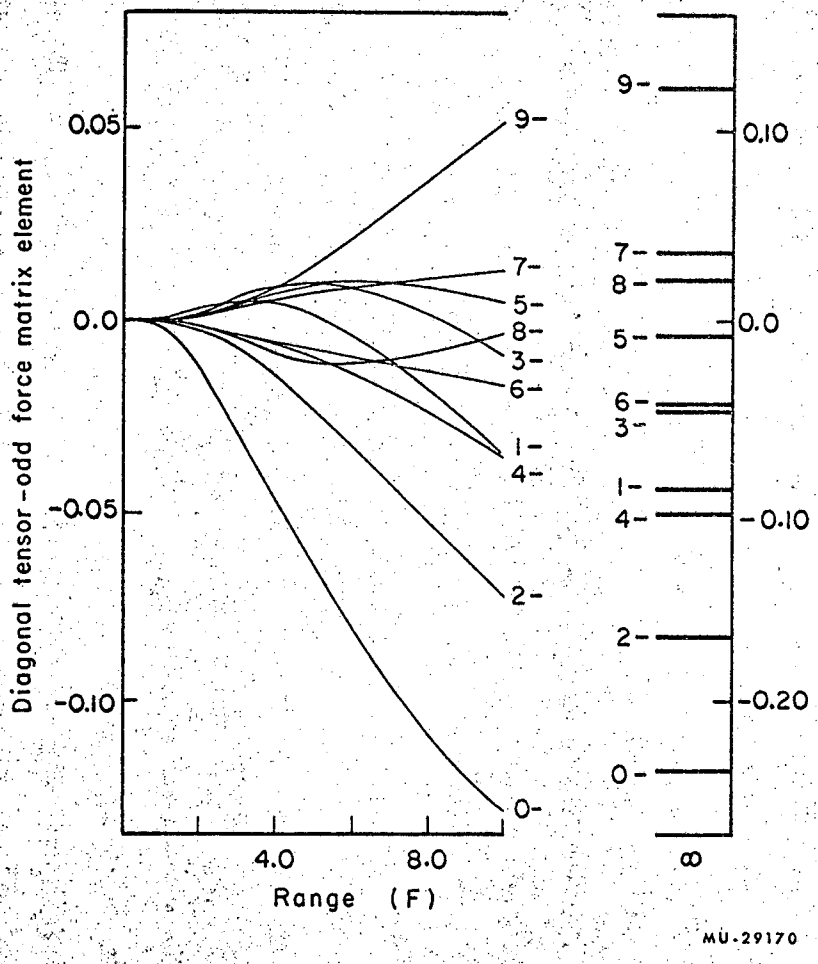


Fig. A.24-3. Diagonal matrix elements of the tensor-odd force $1/3\ P_{TO}\ U^{T}_{TO}\ (r_{12})\ S_{12}$ for the multiplet $h_{9/2}\ g_{9/2}$ in $Bi^{210}$ as a function of the range parameter $(\beta^{T}_{TO})^{-1/2}$.

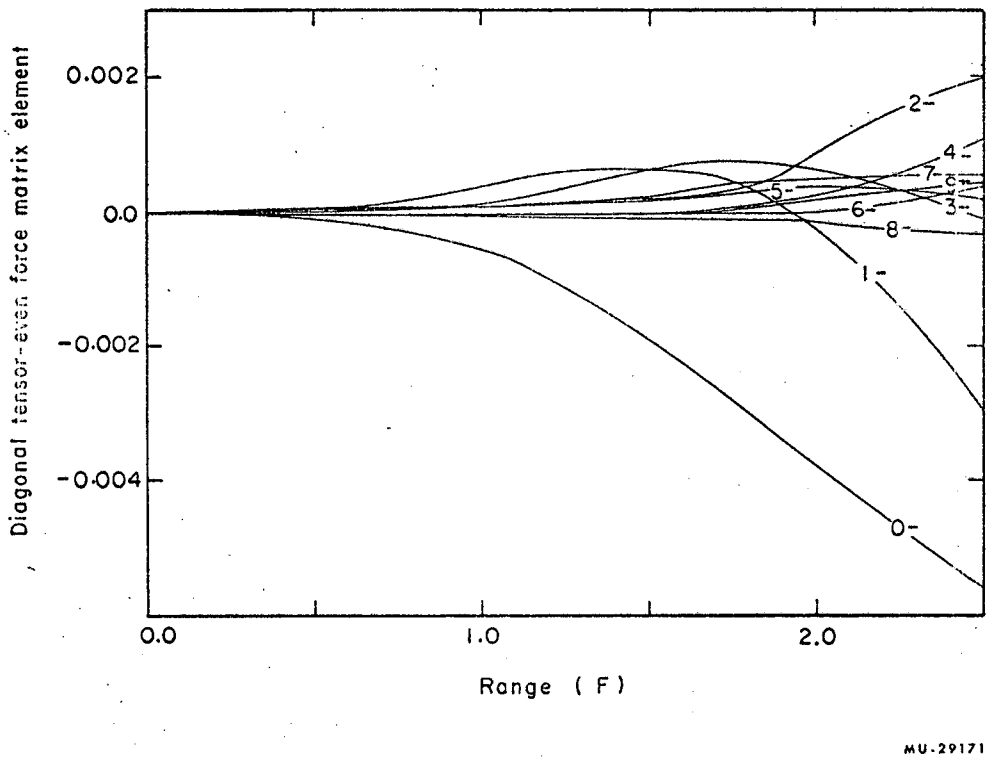


Fig. A. 24-4. Diagonal matrix elements of the tensor-even force for the multiplet $h_{9/2}\, g_{9/2}$ in $Bi^{210}$ as a function of the range at the shorter ranges.

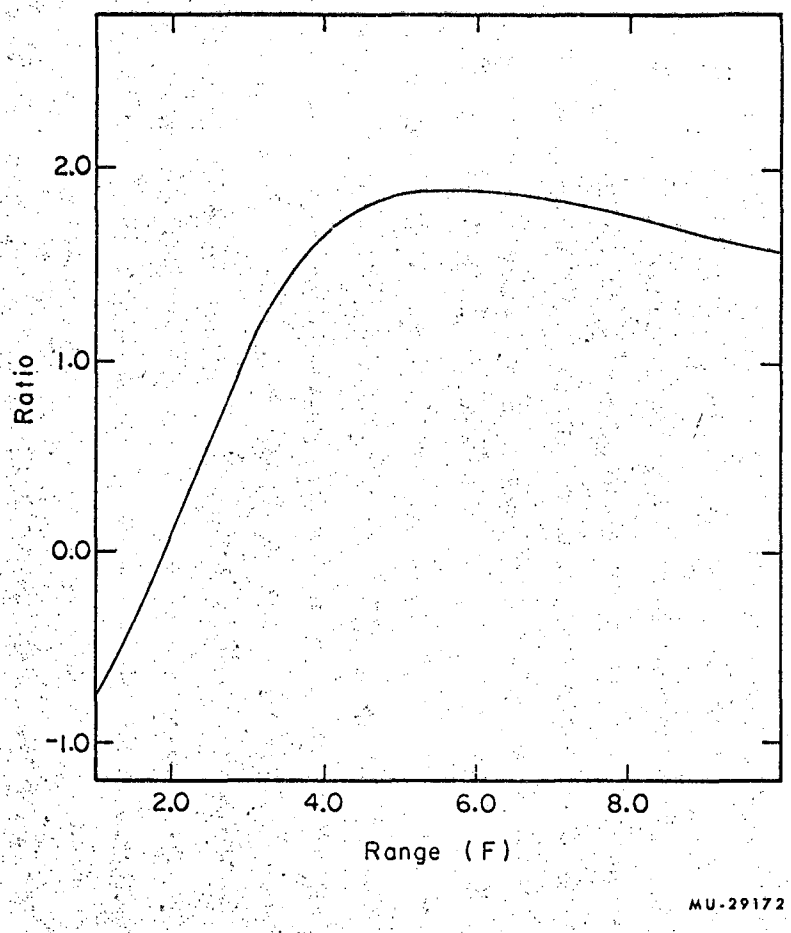


Fig. A. 24-5. Ratio of the diagonal tensor-even force matrix element for the spin 1 state to the spin 0 state of the configuration $h_{9/2}\, g_{9/2}$ as a function of the range.

In Figs. A. 24-6 and A. 24-7 we plot the effect on the $h_{9/2}\ g_{9/2}$ multiplet of adding successive components of the simulated Gammel-Thaler force. The $h_{9/2}\ d_{5/2}$ and $h_{9/2}\ s_{1/2}$ multiplets seen in the (d, p) reaction are also plotted.

In the Gammel-Thaler force an attractive tensor-even and a repulsive tensor-odd force (with odd force weaker but longer-range) are prescribed. In order to get a satisfactory fit in either case, it is necessary only to somewhat weaken the repulsive tensor-odd force component which seems too much to attenuate the effect of the attractive tensor-even in reverting spin-0 and 1 states. In the first case, we find that it is sufficient to shorten the range of tensor-odd to that of tensor-even, while increasing the depth of its potential slightly. In the doubled-range case a good fit is obtained by omitting the tensor-odd force altogether.

The tensor force indeed seems to correct the order and spacing of the troublesome spin-0 and 1 levels. At the short ranges employed, the tensor force acts so specifically on these two levels that it is not possible to simulate it by a linear combination of the four central-force components.

We see that the fitting of the calculated spectrum with the experiment is quite good, realizing that the spin assignments by the 2J+1 rule may be uncertain as to interchange of adjacent spin values.

A recent calculation of $Po^{210}$ spectra indicated that the singlet-even part of the simulated BGT potentials is somewhat too strong, and a new calculation is now being made with a modified potential which is consistent with the ground-state and low-energy properties of the deuteron.

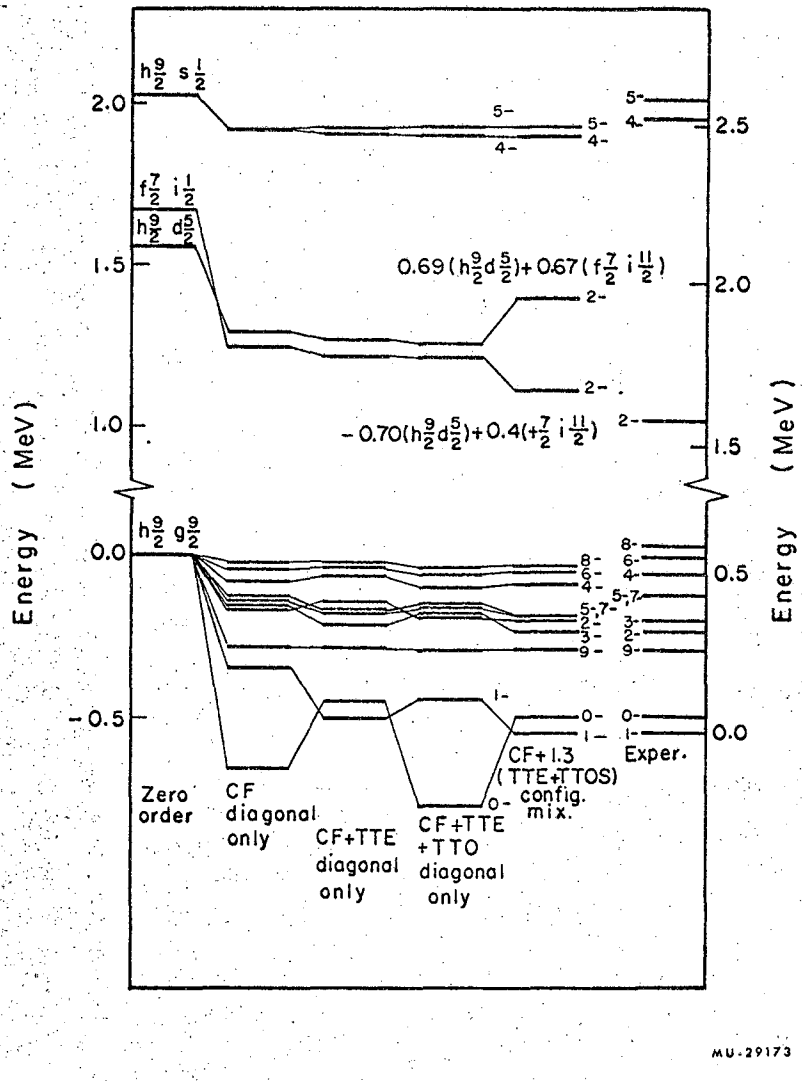


Fig. A.24-6. Comparison of the experiment and the calculated spectra of the $Bi^{210}$ ground-state multiplet with the stimulated BGT(I) force. The symbols CF, TTE, and TTO refer to the central, tensor-even, and tensor-odd forces, respectively. In the fifth column, the tensor-odd force is shortened to the same range as the tensor-even (abbreviated as TTOS), and the strengths for both the tensor-even and tensor-odd forces are slightly increased by a factor of 1.3.

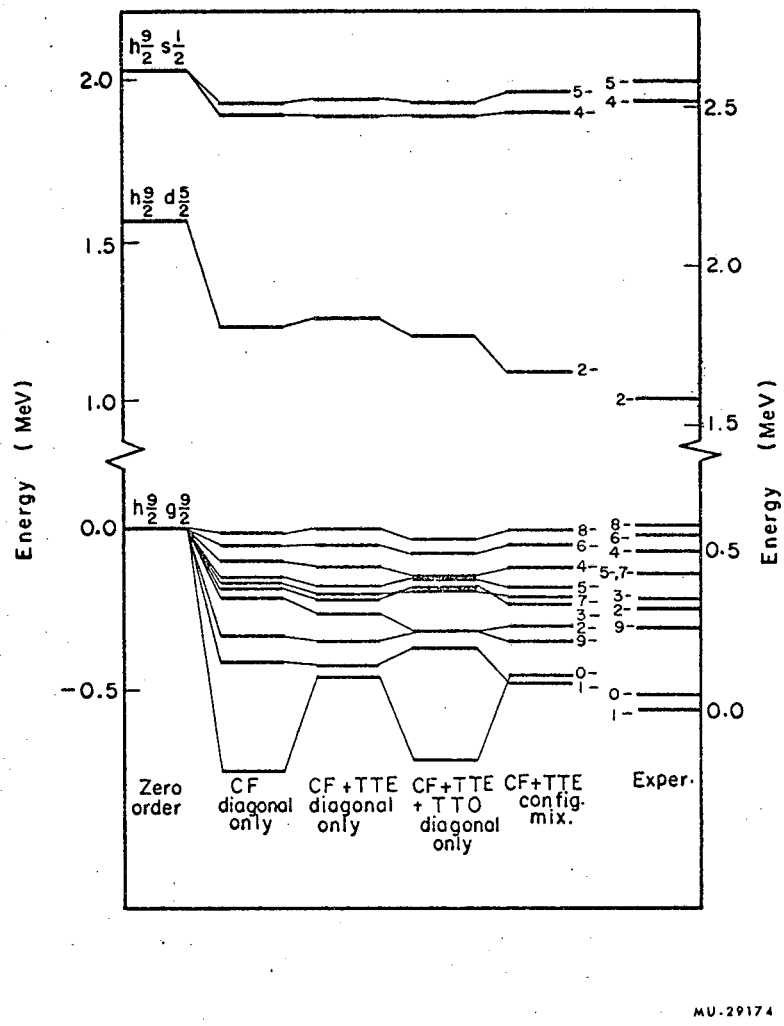


Fig. A. 24-7. Comparison of the experimental and the calculated spectra of the $Bi^{210}$ multiplet with the simulated BGT(II). The abbreviations CF, TTE, and TTO refer to the central, tensor-even, and tensor-odd forces, respectively.

## 25. ISOMERS OF ASTATINE-204 AND ASTATINE-206

P. E. Thoresen, Frank Asaro, and I. Perlman

Previous bombardments of bismuth with high-energy α particles from the 184-inch cyclotron have produced a 25-min electron-capture isotope, which was assigned to $At^{204}$, and a 2.7-hour electron-capture isotope assigned to $At^{206}$.[1] The $At^{206}$ assignment has been confirmed by Stoner.[2] More recent bombardments of gold with carbon ions have produced a 9-min alpha-emitting and electron-capturing isomer assigned to $At^{204}$ and a 25-min alpha emitter assigned to $At^{206}$.[3] In the carbon ion bombardments no trace was observed of the 30-min $At^{204}$, although a special effort was made to detect it.[3,4]

One of the objects of this work is to determine if the 9-min $At^{204}$ and 30-min $At^{206}$ are made in an α-particle bombardment of bismuth, and to confirm if possible the 25-min $At^{204}$ and 3.7-hour $At^{206}$ isotopes. We bombarded a fused $Bi_2O_3$ target with 330-MeV α particles from the 184-inch cyclotron. The target was 2.5 cm high and 0.2 cm wide perpendicular to the beam, and about 1 cm long parallel to the beam. The resulting energies of the α particles within the target varied from about 330 to 100 MeV.

After bombardment the $Bi_2O_3$ target, which was wrapped in platinum foil containing a narrow slit, was heated by high-frequency induction. The $Bi_2O_3$ melted, and the At vaporized onto a cold plate above the slit. This plate then served as a source for "recoil milking" of the polonium isotopes produced by electron capture of the astatine.

In the recoil milking process, a negative potential of 300 volts is applied to a collector plate with respect to the plate containing the astatine isotopes, about 1/8 in. away. When the At isotopes electron-capture, the resulting charged polonium isotopes are ejected onto the collector plate.

Some astatine is also collected because it is ionized by the radioactivity of the source, but this was removed by flaming the platinum collector plates at the end of collection.

The flamed plates were placed in alpha grid chambers, where the $Po^{204}$ and $Po^{206}$ content could be measured by the alpha spectra. The resulting decay curves for the At parents determined by successive recoil milkings are shown in Figs. A. 25-1 and A. 25-2. It is seen that 9-min $At^{204}$ and 30-min $At^{206}$ are indeed produced in the alpha bombardments of Bi. The amount of the longer-lived isomers of $At^{204}$ and $At^{206}$ produced in our bombardments was less than 5% of the mass of the shorter-lived isomers.

---

1. G. W. Barton, A. Ghiorso, and I. Perlman, Phys. Rev. 82, 13 (1951).

2. A. W. Stoner, Nuclear Properties of Some Neutron-Deficient Isotopes of Emanation, Polonium, and Astatine (Thesis), UCRL-3471, June 1956.

3. R. W. Hoff, F. Asaro, and I. Perlman, Bull. Am. Phys. Soc. II4, 293 (1959).

4. Robert M. Latimer, Glen E. Gordon, and T. Darrah Thomas, Alpha-Particle Branching Ratio for Neutron-Deficient Astatine Isotopes, UCRL-9217, June 1960.

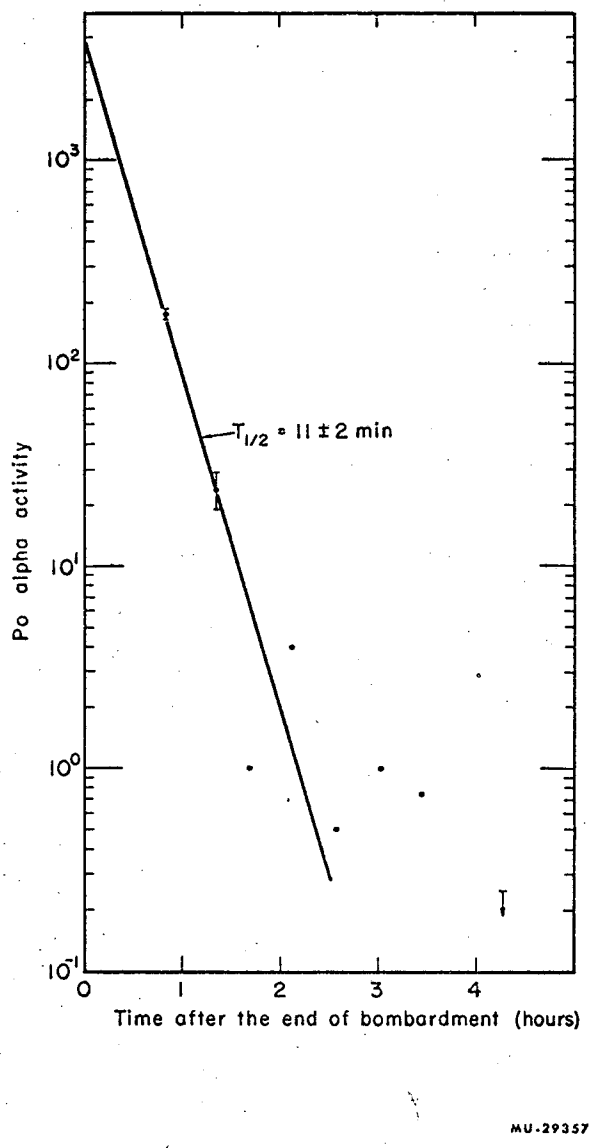


Fig. A. 25-1. $At^{204}$ decay as measured by recoil-collected $Po^{204}$.

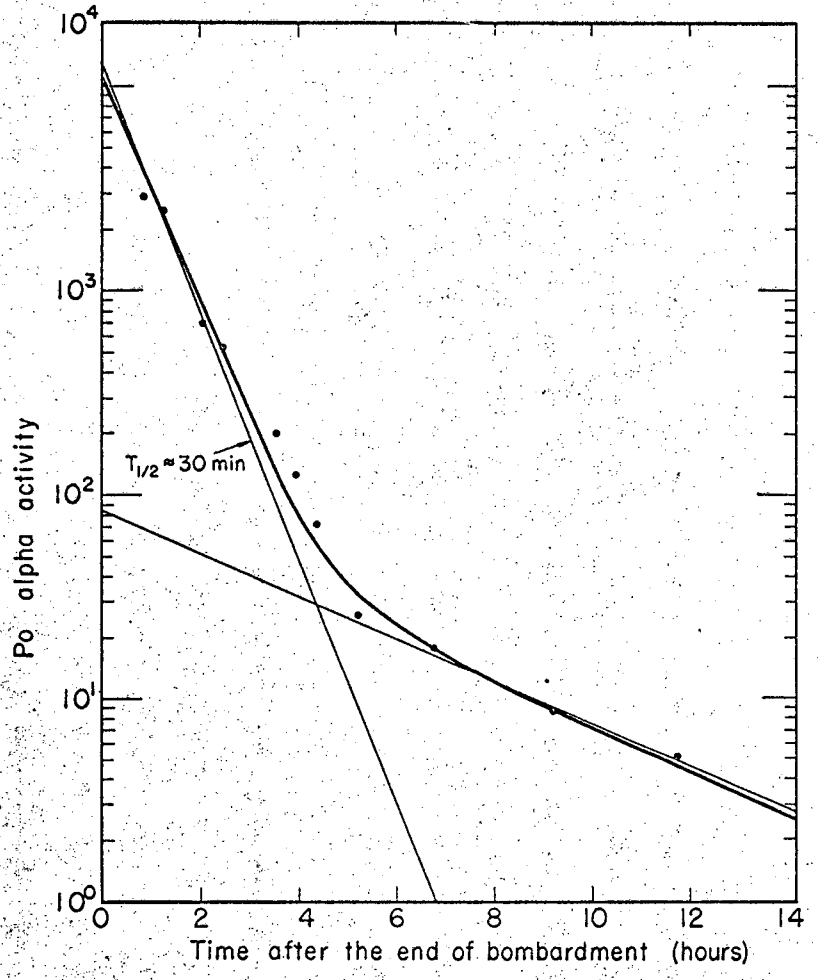


Fig. A. 25-2. $At^{206}$ decay as measured by recoil-collected $Po^{206}$.

Reprinted from THE PHYSICAL REVIEW, Vol. 127, No. 3, 917-922, August 1, 1962
Printed in U. S. A.

26.

## Isomeric State of $Po^{212}$†

I. PERLMAN, F. ASARO, A. GHIORSO, A. LARSH, AND R. LATIMER
*Lawrence Radiation Laboratory, University of California, Berkeley, California*

(Received March 16, 1962)

An isomer of $Po^{212}$ with a half-life of (45.1±0.6) sec and an excitation energy of 2.93 MeV has been positively identified by chemical and nuclear spectroscopic techniques. The isomer decays to known states of $Pb^{208}$ by the emission of alpha particles with energies and intensities of (11.65±0.02)MeV–97%, (9.08±0.015)MeV–(1.00±0.04)%, and (8.52±0.015)MeV–(2.05±0.09)%. In coincidence with $Po^{212m}$ alpha particles we found gamma rays with energies and intensities of (2.61±0.02)MeV–(2.6±0.3)% and (0.57±0.015)MeV–~2%. An immense alpha-decay hindrance factor for the 11.65-MeV group of $4\times10^{13}$ is explained by spin and parity assignments of 18+ for $Po^{212m}$ in conjunction with a theoretical shell-model analysis made by Glendenning.

The alpha-particle energies and intensities of previously known alpha groups of $Po^{211m}$ [(25.5±0.3)sec] were measured yielding values of (8.87±0.01)MeV–(7.04±0.14)%, (7.99±0.015)MeV–(1.66±0.03)%, and (7.27±0.015)MeV–91%. A new alpha group was found with an energy and intensity of (8.30±0.015) MeV–(0.25±0.02)%. In coincidence with $Po^{211m}$ alpha particles was a gamma ray of (0.90±0.015)MeV–(1.65±0.11)%. These $Po^{211m}$ radiations are all consistent with the known energy level scheme of $Pb^{207}$.

## 27. THE ALPHA DECAY OF PROTACTINIUM-227

V. Subrahmanyam, Duane F. Mosier, Frank Asaro,
and I. Perlman

A decay scheme has been arrived at for the alpha decay of $Pa^{227}$ based principally upon α-particle γ-ray coincidence measurements. The ground state was shown to be populated by a previously known 6.46-MeV alpha group. A higher-energy group at 6.52 MeV has been shown to belong to the decay of $Ac^{223}$.

$Pa^{227}$ was prepared by bombarding a thick target of $Th^{232}$ with 150-MeV deuterons. Alpha-particle γ-ray coincidence measurements were made by using the double-focusing spectrograph for alpha analysis and a 3×3-in. NaI(Tl) crystal for gamma detection. The details of the equipment have been described elsewhere.[1] The resolving time of the coincidence circuit was 1 μsec.

Neither photons nor x rays from internal conversion were observed in coincidence with 6.46-MeV α particles, reported earlier to populate an excited state.[2] Attempts to establish the existence of an isomeric state which would not have been observed in the coincidence experiments also proved negative.

---

1. D. F. Mosier, in Chemistry Division Annual Report, 1961, UCRL-10023, Jan. 1962, p. 224.

2. Max Hill, Ph. D. Thesis, University of California, Berkeley, 1958.

The multipolarity assignments indicated in the decay scheme were based on the intensities of photons or conversion x rays (or both) observed in coincidence with each group.

Although it was by no means certain that nuclei in this region are sufficiently deformed to permit description in terms of Nilsson's asymptotic quantum numbers, the evidence obtained here and in earlier work[2] on $Pa^{227}$ and $Pa^{229}$ indicate that such assignments may be proper. The nine energy levels shown in Fig. A. 27-1 can be placed into two rotational bands of opposite parity which have one important distinction. The alpha-decay hindrance factors to both bands place all in the category of "favored transitions," a feature associated with transitions in which the initial and final states have the same intrinsic configuration. It is tempting to say (as was done for $Pa^{229}$)[2] that both bands have the odd proton in the same $K = 5/2$ state and that the change of parity involves a collective octupole excitation analogous to the odd-parity bands seen at low excitation energies in the even-even nuclei in this region. The fact that the E1 transitions are fast (they compete with the enhanced intra-band E2 transitions) is taken as supporting evidence for this conclusion.

## 28. MAGNETIC FIELD DEPENDENCE OF AMERICIUM-243 α-γ ANGULAR CORRELATIONS(*)

K. Siegbahn† and Frank Asaro

### Introduction

Strong perturbations, attributed to a magnetic interaction, have been shown to occur in α-γ angular correlations of $Am^{243}$ and $Cm^{243}$ when the α-decay recoils are allowed to enter a vacuum or a Mylar environment.[1] In the experiments presented here the anisotropy of the $Am^{243}$ α-γ angular correlation (with recoils traveling into vacuum or into Ag) was investigated as a function of an applied magnetic field.

### Unperturbed Angular Correlation

A partial decay scheme of $Am^{243}$ is shown in Fig. A. 28-1. The α-γ correlation of interest is that between the most intense α group and the 75-keV γ ray. The theoretical unperturbed anisotropy is -45.6%. Considerations of the effect of quadrupole coupling[2] could change this value to -50.5%. The anisotropies for the $\alpha_{75}$ - $\gamma_{75}$ correlation will be reduced somewhat by the $\alpha_{118}$ - $\gamma_{75}$ triple correlation. The resulting theoretical unperturbed anisotropies for the combined $(\alpha_{75} + \alpha_{118})$ - $\gamma_{75}$ correlation are shown in Fig. A. 28-2.

---

*Shortened version of published paper, Phys. Letters 2, 323 (1962).

†Present address: Institute of Physics, University of Uppsala, Uppsala, Sweden.

1. E. Flamm and F. Asaro, Phys. Rev., to be published (1962); E. Flamm, (Ph.D. Thesis), Lawrence Radiation Laboratory Report UCRL-9325, Aug. 1960.

2. R. R. Chasman and J. O. Rasmussen, Phys. Rev. 115, 1260 (1959).

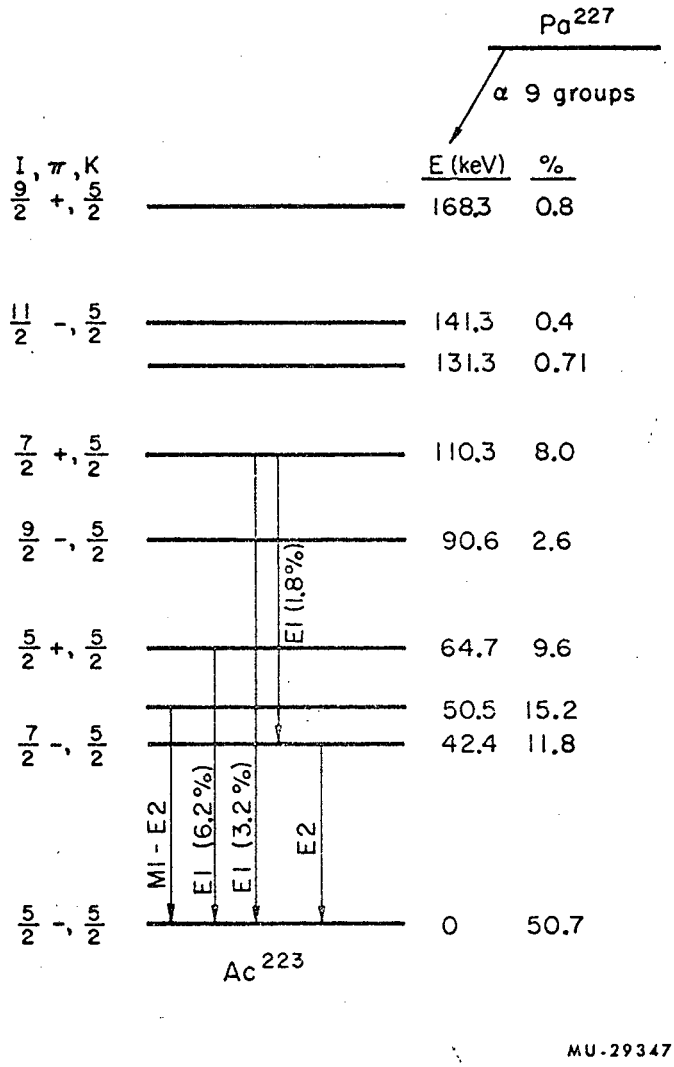


Fig. A. 27-1. Decay scheme of $Pa^{227}$.

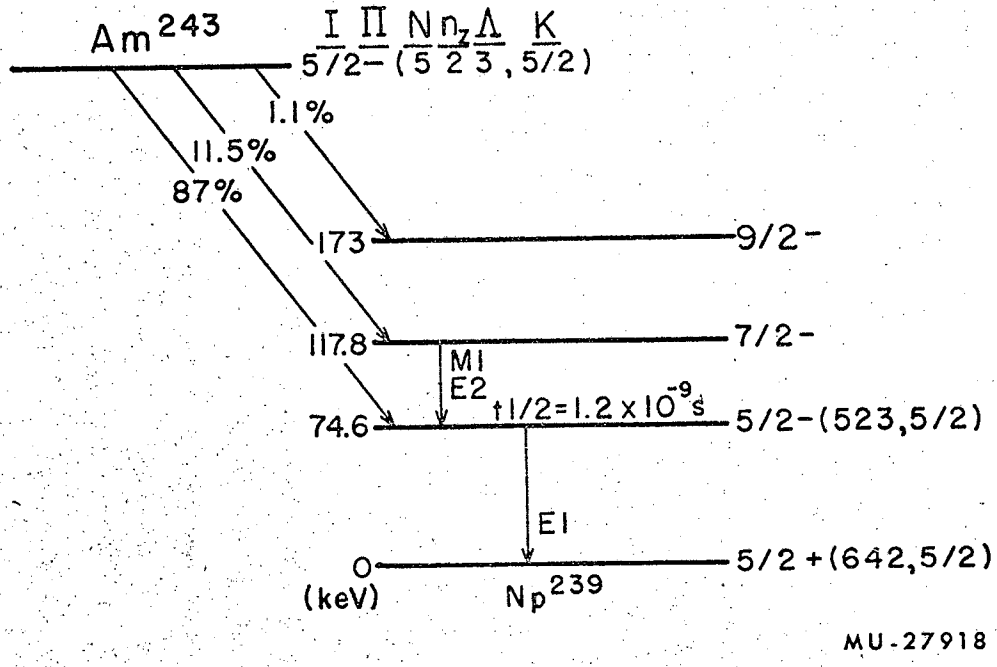


Fig. A.28-1. Partial decay scheme of $Am^{243}$. This figure was taken from reference 1.

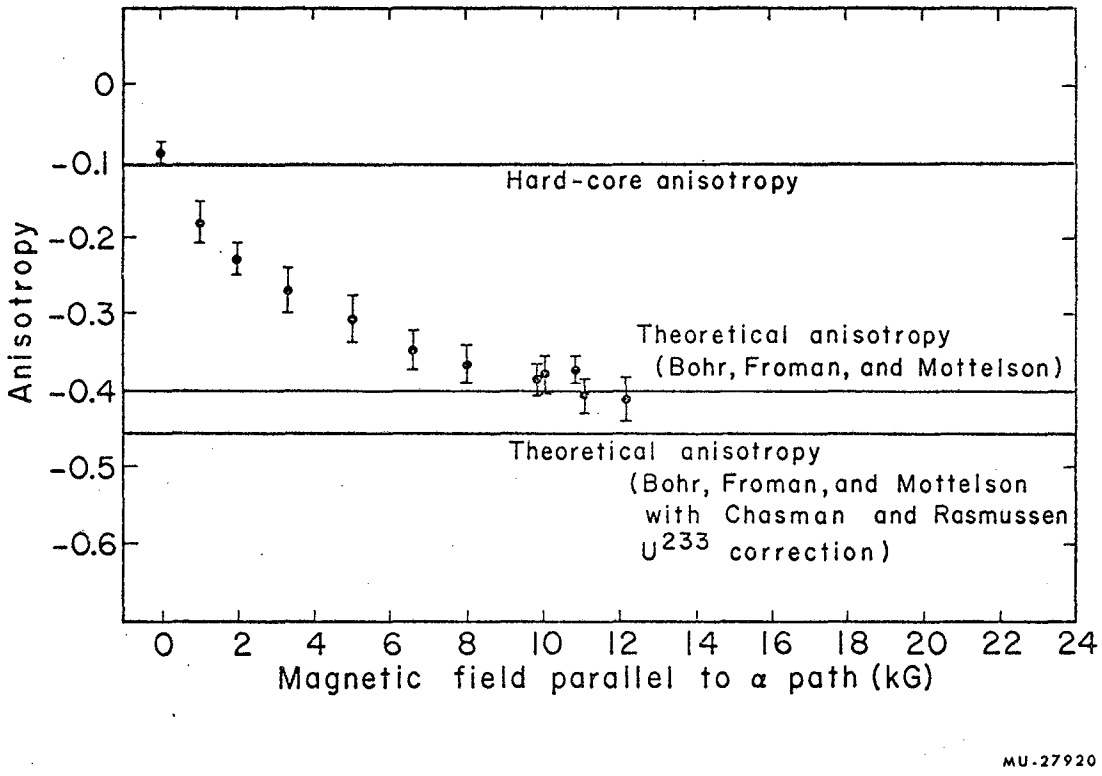


Fig. A.28-2. $Am^{243}$ $(\alpha_{75} + \alpha_{118}) - \gamma_{75}$ angular correlation as a function of an applied magnetic field. The recoiling nuclei are in a vacuum environment.

## Results

The experimental anisotropies for the combined $(a_{75} + a_{118}) - \gamma_{75}$ angular correlation, with recoils going into vacuum, are shown in Fig. A. 28-2 as a function of an applied magnetic field. The values have been corrected for the finite size of the source and detectors. With no applied magnetic field our anisotropy is consistent with the hard-core value for a static interaction, $G_2 \approx 0.20$ for the combined correlation. It is also, however, reasonably close to the previous value,[1] which was definitely below the hard-core value (Fig. A. 28-3). Our experiment differed principally from the previous one in that our source was thicker by about an order of magnitude.

As seen in Fig. A. 28-2, the anisotropies become more pronounced with increasing magnetic field parallel to the a path. This is the type of behavior expected for a hyperfine-structure interaction.[3] Thus our results confirm the earlier diagnosis[1] as to the cause of the perturbations observed in vacuum.

Our results are presently not adequate to determine the validity of the corrections of Chasman and Rasmussen. In Fig. A. 28-3 we have assumed these corrections to be valid and have plotted the attenuation factor, $G_2$, as a function of the applied magnetic field. With the exception of the point at 0 field the remaining points, which have relatively large standard deviations, appear to exhibit an exponential dependence on the magnetic field. The shape of this curve could be analyzed theoretically from the equations of Goertzel.[3]

With the recoils going into the Ag backing material the anisotropy for the $a_{75} - \gamma_{75}$ angular correlations with no applied magnetic field is $-0.30 \pm 0.02$, in good agreement with the earlier value of -0.28.[1] Our value corresponds to $G_2$ (with the Chasman and Rasmussen correction) of $0.54 \pm 0.05$. With an applied magnetic field of 1.1 kilogauss, the anisotropy is $-0.29 \pm 0.03$, corresponding to a $G_2$ of $0.52 \pm 0.05$. Thus the attenuation is not reduced by the application of a magnetic field; hence, the observed perturbations, with recoils going into Ag, are caused by field gradients external to the recoiling atom.

---

3. C. Goertzel, Phys. Rev. 70, 897 (1946).

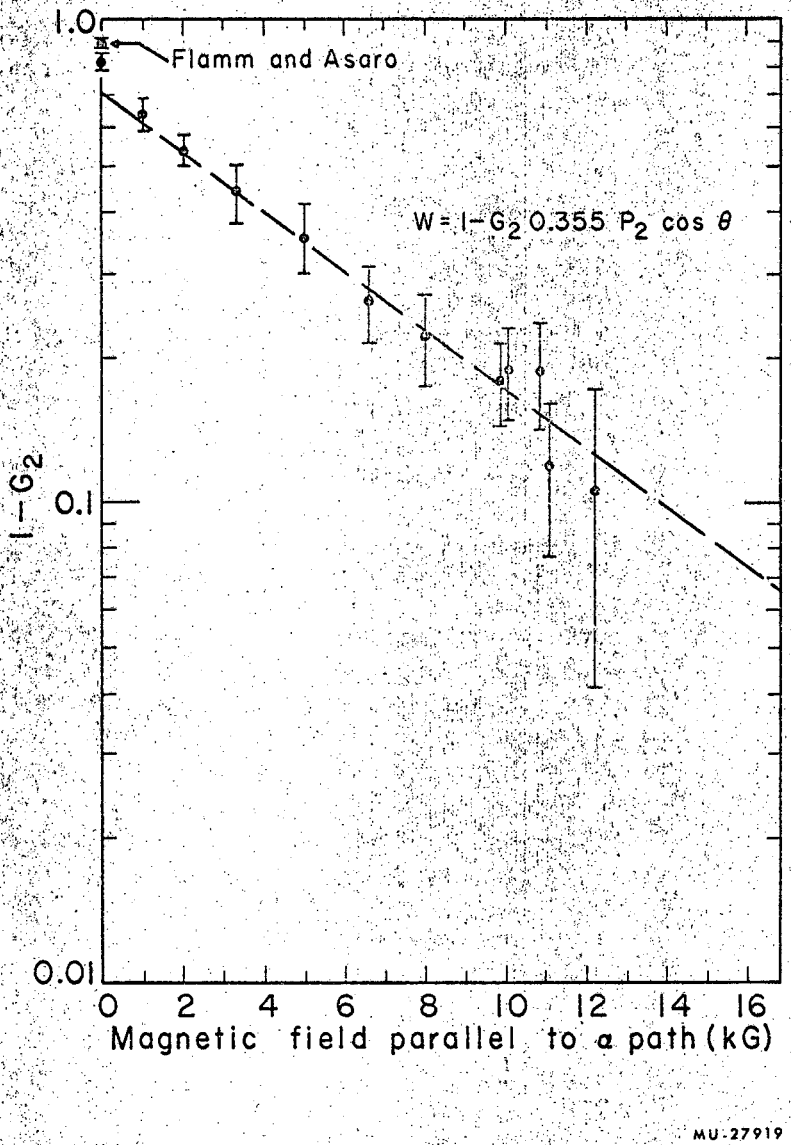


Fig. A.28-3. The attenuation factor, $G_2$, for the $Am^{243}$ $(a_{75} + a_{118}) - \gamma_{75}$ correlation in a vacuum environment as a function of an applied magnetic field. The theoretical anisotropy was calculated with the correction of Chasman and Rasmussen. The dashed line, which is the best representation of the data from 1 → 12 kilogauss, can be expressed by the equation $1 - G_2 = 0.7 \times 10^{-0.06 H}$.

ARKIV FÖR FYSIK Band 23 nr 2

Read 11 April 1962

29.

# Some properties of the levels of $_{100}Fm^{254}$

By J. M. Hollander, C. L. Nordling, and K. Siegbahn

ABSTRACT

Measurements have been made of the energies and intensities of the $E2$ transitions which de-excite the gamma ($K=2$) vibrational band in $_{100}Fm^{254}$ following the beta decay of 38.5 hour $_{99}E^{254}$. The measured relative intensities are interpreted within the framework of the Bohr–Mottelson nuclear model, including the effect of mixing of the $K=2$ and $K=0$ ground bands. It is found that the rotation–vibration constant of the ground state band is very small [$B=(-0.4\pm 1.8)\cdot 10^{-3}$ keV] and can be accounted for completely by the ($K=2$) mixing amplitude calculated from the intensity data.

## 30. A NEW SEMIEMPIRICAL MASS FORMULA

Sven A. E. Johansson

A semiempirical mass formula, which has given considerably improved mass values, has been derived. It has the form

$$E_B = a_1 A + a_2 A^{2/3} + a_3 \frac{Z^2}{A^{1/3}} + a_4 \left(1 - \frac{c}{A^{1/3}}\right) \left[\frac{(N-Z)^2 + 4(N-Z)}{4A}\right] + E_{def} + E_{shell}.$$

The first part is similar to the standard type of Weizsäcker mass formula. It was found, however, that it is necessary to use a somewhat more complicated symmetry-energy term in order to get a good fit to the line of beta stability. A term that gives a symmetry correction to the surface energy and also a term that is linear in the neutron excess have therefore been included. The most important change, however, is the addition of the deformation energy $E_{def}$. It accounts for the change in energy when the nuclear deformation varies, and is written as

$$E_{def} = -C_1 \beta + C_2 \beta^2 + C_3 \beta^3,$$

where $\beta$ is the deformation parameter. The first term represents the tendency to deform the nucleus caused by certain levels in the single-particle level diagram. The constant $C_1$ can be obtained in two ways. It can be calculated directly from the level diagram. Another possibility, which gives

about the same results, is to adjust $C_1$ so that it reproduces the experimental $\beta$ values as well as possible. The last two terms are the first part of the expansion of the surface and Coulomb energies, and are obtained from the liquid-drop model.

The deformation energy is so sensitive to variations in $\beta$ that a schematic representation of $\beta$ (for example, by sinus functions) leads to considerable errors. If a high accuracy is wanted it is necessary to use experimental $\beta$ values or theoretical values with a reasonably good accuracy. This is, of course, a certain limitation, but good experimental values are now available for many nuclei and they can be used as starting points for a theoretical extrapolation, that gives fairly accurate values for most nuclei of interest.

The shell correction term $E_{shell}$ is estimated from shell-model theory. The present mass formula is included to be used for nuclei not too close to magic numbers, and the shell correction term is therefore not so important. It has been found that it is possible to represent the shell correction term by the expression

$$E_{shell} = \kappa(\beta_0 - \beta),$$

where $\kappa$ is a constant and $\beta_0$ is the maximum deformation within a shell. This form of the correction term, which is purely empirical, gives a very convenient and fairly accurate expression for the shell correction energy.

The constants in the mass formula are determined in the following way. The constant $a_2$ is chosen so that it reproduces the experimentally determined Coulomb energies as well as possible. The constants $a_4$ and c together with $a_3$ determine the line of beta stability, and $a_4$ and c are chosen so that they give a good fit to the experimental line. The remaining two constants, $a_1$ and $a_2$, are determined from a least-squares fit to the masses of a great number of nuclei in the region of strong nuclear deformations.

By use of this mass formula, masses have been calculated for a great number of nuclei from A = 60 to A = 270. The best possibilities for testing the formula are offered by the rare earth region and the actinide region. There the masses as well as the deformations are well known. The difference between calculated and experimental masses is about 0.2 MeV. This error can be accounted for almost completely by the uncertainties in the experimental values for mass and deformation. The remaining part of the error can probably be attributed to single-particle effects. The variations in level spacing in the single-particle level diagram must produce deviations from the values obtained from a mass formula, which essentially is based on a statistical model assuming a great number of nucleons. An estimate of the single-particle effect shows that it is of the right order of magnitude to explain the deviations. An interesting fact is that there appear to be no systematic errors in the mass formula.

An application of the mass formula is the calculation of the masses of very heavy nuclei. As an illustration, Fig. A. 30-1 shows a comparison between calculated and experimental $\alpha$ energies. The mean error is about 0.15 MeV. It is interesting to note that the fine structure in the $\alpha$ energies is to some extent reproduced by the mass formula. Since the formula fits the known masses so well it should be fairly reliable for an extrapolation to unknown nuclei. Figure A. 30-1 shows part of such an extrapolation.

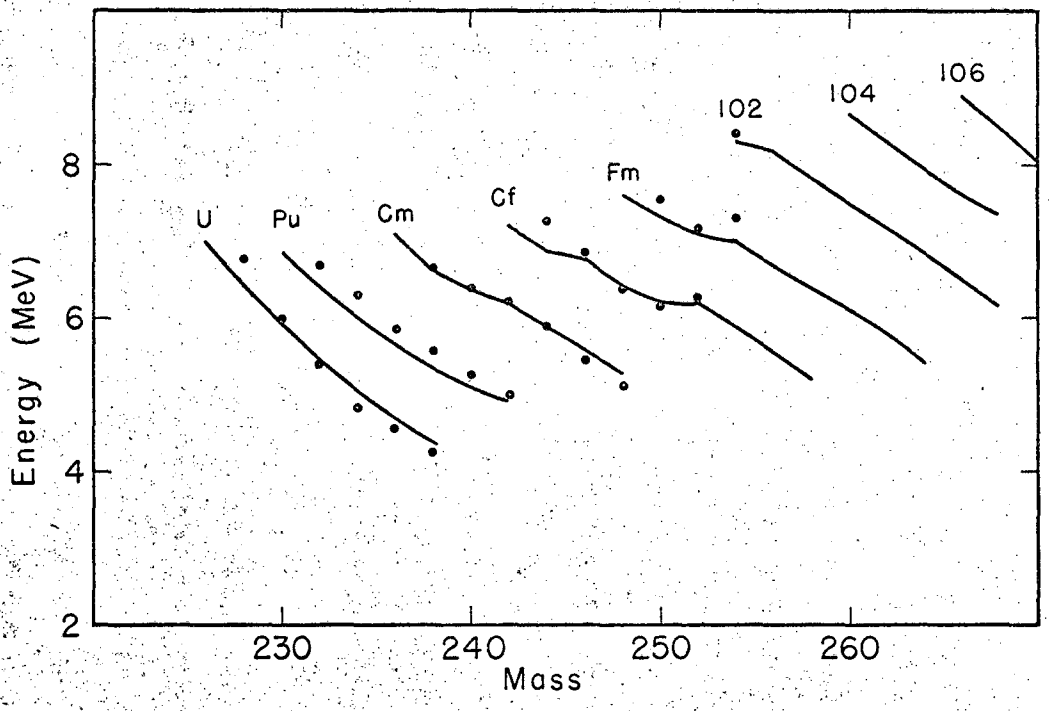


Fig. A. 30-1. Comparison between calculated and experimental α energies.

● experimental
—— theoretical

# 31. REFINED PAIRING-FORCE CALCULATIONS FOR DEFORMED NUCLEI

John O. Rasmussen, Hans-Joerg Mang, Kenneth Poggenburg, Jean Pradal, and Vincent Gillet*

The fundamental equations for treating the pairing-force effects in deformed nuclei were given by Belyaev:[1]

$$\Delta_\nu = \frac{1}{2} \sum_{\nu'} \frac{\nu\nu' | G | \nu'\nu'}{\sqrt{(\tilde{\epsilon}_{\nu'} - \lambda)^2 + \Delta_{\nu'}^2}} \Delta_{\nu'} , \qquad \text{(B. 27)}$$

$$N = \sum_{\nu} \left( 1 - \frac{\tilde{\epsilon}_\nu - \lambda}{\sqrt{(\tilde{\epsilon}_\nu - \lambda)^2 + \Delta_\nu^2}} \right) , \qquad \text{(B. 43)}$$

$$\tilde{\epsilon}_\nu = \epsilon_\nu - \sum_{\nu_1} \langle \nu\nu_1 | \bar{G} | \nu_1\nu \rangle \frac{1}{2} \left( 1 - \frac{\tilde{\epsilon}_{\nu_1} - \lambda}{\sqrt{(\tilde{\epsilon}_{\nu_1} - \lambda)^2 + \Delta_{\nu_1}}} \right) ,$$

where the $\epsilon_\nu$ are the energies of the Nilsson orbitals,[2] N is the number of nucleons, $\lambda$ is the chemical potential, and the $\Delta_\nu$ are the pairing-correlation energy parameters for the orbitals. The $G_{\nu\nu'}$ matrix elements are a measure of the pairing-force scattering of a pair of nucleons in time-reversed orbits $\nu$ into orbits $\nu'$. The $\bar{G}_{\nu\nu_1}$ are the pairing-force diagonal contributions to the self-consistent potential experienced by the pair in the $\nu$th orbital when the $\nu_1$th orbital is occupied by a pair.

There have been several studies[3] of nuclear properties, based on solution of these equations for Nilsson orbital energies -- always, so far as

*Present address: Department of Physics, Carnegie Institute of Technology, Pittsburgh, Pa.

1. S. T. Belyaev, Kgl. Danske Videnskab. Selskab Mat.-Fys. Medd. 31, No. 11 (1959).

2. S. G. Nilsson, Kgl. Danske Videnskab. Selskab Mat.-Fys. Medd. 29, No. 16 (1955); B. R. Mottelson and S. G. Nilsson, Kgl. Danske Videnskab. Selskab Mat.-Fys. Skr. 1, No. 8 (1959).

3. J. J. Griffin and M. Rich, Phys. Rev. 118, 850 (1960); S. G. Nilsson and O. Prior, Kgl. Danske Videnskab. Selskab Mat.-Fys. Medd. 32, No. 16 (1961); V. G. Soloviev, Kgl. Danske Videnskab. Selskab Mat.-Fys. Medd. 1 No. 11 (1961); C. J. Gallagher, Jr. and V. G. Soloviev, Kgl. Danske Videnskab. Selskab Mat.-Fys. Medd. 2, No. 2 (1962); Z. Szymański, Nucl. Phys. 28, 63 (1961); D. R. Bès and Z. Szymański, Nucl. Phys. 28, 42 (1961).

we know, with the simplifying assumptions that all matrix elements $\bar{G}_{\nu\nu'}$ be considered equal and that the $\tilde{\epsilon}_\nu = \epsilon_\nu$. The former assumption simplifies Eq. (B. 27), and there results only a single $\Delta$ value, applying to all orbitals. It occurred to us that the assumption of constant $G_{\nu\nu'}$ might be questionable.

We had at hand the rather complicated computer program used earlier by Mang and Rasmussen for alpha-decay rate calculations,[4] and we realized that it could easily be adapted to calculation of pairing-force matrix elements for a singlet delta force. Furthermore, it can be shown that for a singlet delta force one has

$$\langle \nu\nu \,|\, G \,|\, \nu'\nu' \rangle = \langle \nu\nu' \,|\, \bar{G} \,|\, \nu'\nu \rangle ,$$

so we could readily obtain both kinds of matrix elements and solve the set of Belyaev's equations, thereby improving on the usual approximations.

Our most extensive study so far has been with a set of 25 Nilsson orbitals appropriate for protons in the actinide region. We have the possibility of comparing our results against the constant-G calculations of Voros, Soloviev, and Siklos (hereafter referred to as VSS).[5] Nilsson wave functions at deformation $\eta = 6$ were used for delta-force matrix element calculations. The energies $\epsilon_\nu$ are those interpolated values used by Nilsson and Prior[3] at $\eta = 5$ deformation, except that we shifted the N = 6 orbitals up by one unit in $\kappa \hbar\mathring{\omega}_0$ (= $0.05 \times 41\ A^{1/3} \approx 330$ keV) relative to the N = 5, and the N = 4 down by one unit. These shifts improve the agreement of calculations with the observed ground-state spins of odd-proton actinide nuclei. The orbitals used are listed in Table I along with their $\epsilon_i$ values.

In the hope of finding a basis for systematic discussion of results we attempted to find a way for dividing orbitals into two classes, with off-diagonal elements smaller between than within classes. Examination of the 300 off-diagonal elements showed that a classification according to slope is not very significant, as some of the larger elements occur between classes. Other bases of classification, such as evenness or oddness of $n_z$, number of cylindrical nodes in the asymptotic wave function, and so on, were examined without satisfying us. Certainly there is a wide variation in size of matrix elements, but there is no apparent classification that has no large matrix elements between classes. The one systematic feature that can be singled out is that the diagonal elements are larger than off-diagonal by factors of 2 to 4. In Table I we list for each orbital its diagonal element and the average of its off-diagonal elements, as well as the maximum and minimum off-diagonal elements. We shall not take the space here to list all 325 matrix elements. Also given are the Nilsson energy values $\epsilon_\nu$ in units of $\kappa \hbar\mathring{\omega}_0$.

---

4. H. J. Mang and J. O. Rasmussen, Kgl. Danske Videnskab. Selskab Mat. -Fys. Medd. 2, No. 3 (1962).

5. T. Voros, V. G. Soloviev, and T. Siklos, "An Investigation of Properties of Transuranic Elements," Report No. E932 of Joint Institute of Nuclear Studies, Dubna, U. S. S. R., 1962 (unpublished).

Table I. Matrix elements.

| Orbital $\Omega\pi(N n_z \Lambda)$ | $\epsilon_i$ (in $\kappa \hbar \omega_0$) | $G_{\nu\nu}$ | $G_{\nu\nu'}$ (av) | $G_{\nu\nu'}$ (max) | $G_{\nu\nu'}$ (min) |
|---|---|---|---|---|---|
| $\frac{1}{2}$ - (541) | -23.37 | 0.2643 | 0.0784 | 0.2363 | 0.0327 |
| $\frac{3}{2}$ - (532) | -20.82 | 0.1897 | 0.0826 | 0.1597 | 0.0421 |
| $\frac{1}{2}$ + (660) | -20.17 | 0.2801 | 0.0710 | 0.2363 | 0.0361 |
| $\frac{11}{2}$ - (505) | -20.00 | 0.2461 | 0.0965 | 0.2399 | 0.0417 |
| $\frac{3}{2}$ + (402) | -19.94 | 0.2458 | 0.1040 | 0.1938 | 0.0464 |
| $\frac{1}{2}$ + (400) | -19.76 | 0.3692 | 0.1029 | 0.1881 | 0.0407 |
| $\frac{3}{2}$ + (651) | -18.83 | 0.1980 | 0.0750 | 0.1959 | 0.0349 |
| $\frac{1}{2}$ - (530) | -18.82 | 0.2925 | 0.0797 | 0.1576 | 0.0381 |
| $\frac{5}{2}$ - (523) | -17.01 | 0.1818 | 0.0852 | 0.1567 | 0.0464 |
| $\frac{5}{2}$ + (642) | -16.70 | 0.1731 | 0.0772 | 0.1597 | 0.0361 |
| $\frac{3}{2}$ - (521) | -14.75 | 0.1970 | 0.0846 | 0.1918 | 0.0493 |
| $\frac{7}{2}$ + (633) | -13.41 | 0.1643 | 0.0790 | 0.1447 | 0.0398 |
| $\frac{7}{2}$ - (514) | -12.33 | 0.1908 | 0.0883 | 0.1736 | 0.0507 |
| $\frac{1}{2}$ - (521) | -10.98 | 0.1963 | 0.0844 | 0.1918 | 0.0452 |
| $\frac{9}{2}$ + (624) | - 9.680 | 0.1657 | 0.0810 | 0.1567 | 0.0476 |
| $\frac{5}{2}$ - (512) | - 9.545 | 0.1868 | 0.0874 | 0.1829 | 0.0495 |
| $\frac{13}{2}$ + (606) | - 7.540 | 0.2256 | 0.0901 | 0.2256 | 0.0327 |
| $\frac{9}{2}$ - (505) | - 6.986 | 0.2342 | 0.0965 | 0.2399 | 0.0421 |
| $\frac{11}{2}$ + (615) | - 5.421 | 0.1795 | 0.0837 | 0.1736 | 0.0416 |
| $\frac{3}{2}$ - (512) | - 4.249 | 0.1816 | 0.0872 | 0.1829 | 0.0497 |
| $\frac{7}{2}$ - (502) | - 3.658 | 0.2200 | 0.0937 | 0.2165 | 0.0424 |
| $\frac{1}{2}$ - (510) | - 3.330 | 0.2778 | 0.0837 | 0.1881 | 0.0435 |
| $\frac{5}{2}$ - (503) | 2.838 | 0.2133 | 0.0938 | 0.2165 | 0.0426 |
| $\frac{3}{2}$ - (501) | 4.507 | 0.2503 | 0.0879 | 0.2488 | 0.0349 |
| $\frac{1}{2}$ - (501) | 6.721 | 0.2475 | 0.0880 | 0.2488 | 0.0349 |

The matrix elements were multiplied by an adjustable normalization factor V, so that the solutions give about the same binding-energy differences between odd-Z and even-Z neighboring nuclei as are observed experimentally. Rather than simply identifying an average Δ value with the odd-even mass difference, we have followed the more careful procedure of Soloviev[3] and made blocking calculations, where the orbital occupied by the odd nucleon is excluded in solving the pairing equations. A V value of about 5.0 gave good agreement with experimental pairing energies and the calculations of VSS. The experimental decrease of pairing energy with increasing Z is reproduced by VSS and our calculations.

Table II gives the $\Delta_\nu$ values developed for a few representative calculations. The Δ value of the orbital closest the Fermi surface is underlined. Our force-normalization constant of V = 5.0 was used for the values of Table II.

From Table II we see that some differences in $\Delta\nu$ values for different levels do develop, but the difference among the half dozen orbitals nearest the Fermi surface are usually less than 20%. From Table II we may note the qualitative corrections that these refined calculations make to energy spectra. The orbitals with the larger Δ values are systematically somewhat higher in odd-Z nuclei than in constant-G calculations, and such orbitals may fail even to become ground states. Such is the case with the upcoming 1/2 + (400) orbital, which never appears as a nuclear ground state. Also the 1/2 - (530) never quite becomes a ground state in our calculations, although it is in fact at ground for Z = 91. In a later section, where we discuss projection out of a fixed-particle number, this deficiency is corrected. Conversely, orbitals with low Δ values may appear systematically lower in spectra and may occur as a ground state for two successive odd-Z nuclei.

From Table II one can discern another systematic trend: that is, the Δ value of a given orbital reaches its maximum when its orbital energy is nearest the Fermi surface. This behavior arises mainly from the fact that the diagonal G matrix elements are larger than off-diagonal. The fall-off of Δ values for more and more distant orbitals should continue, owing to a fall-off of the G-matrix elements to far distant orbitals; thus, the problem of the logarithmic divergence of the BCS solutions with number of orbitals should no longer arise. It was merely an artifact of the assumption of constant G-matrix elements.

Table III presents a comparison with values of Table IV of VSS. They give the factor by which Δ (C in their notation) is reduced for odd Z by blocking the ground-state orbital. In our case we average the Δ values for all levels except the blocked one and take the ratio.

We find somewhat greater reductions in pairing correlation when one level is blocked than do VSS. This effect is mainly due to the great difference in magnitude between diagonal and off-diagonal matrix elements in G.

The effects due to inclusion of the $\bar{G}$ matrix elements in modifying $\epsilon_\nu$ to $\tilde{\epsilon}_\nu$ are not especially large. In going from Z = 88 to Z = 102 there is some systematic drift of some orbital energies and a few crossovers. These trends can be traced on Fig. A. 31-1, where we plot $\tilde{\epsilon}_i$ vs number of protons.

Table II. Correlation-function (Δ) values for several cases

| Orbital | Unblocked | | Δ | |
|---|---|---|---|---|
| $\Omega\pi(N n_z \Lambda)$ | Z = 90 | Z = 100 | Z = 91 | Z = 99 |
| $\frac{1}{2}$ - (541) | 2.975 | 1.667 | 2.417 | 0.993 |
| $\frac{3}{2}$ - (532) | 2.939 | 1.964 | 2.332 | 1.068 |
| $\frac{1}{2}$ + (660) | 2.735 | 1.559 | 2.240 | 0.895 |
| $\frac{11}{2}$ - (505) | 2.793 | 1.982 | 2.399 | 1.132 |
| $\frac{3}{2}$ + (402) | 2.904 | 2.047 | 2.540 | 1.245 |
| $\frac{1}{2}$ + (400) | 3.067 | 2.006 | 2.704 | 1.216 |
| $\frac{3}{2}$ - (651) | 2.773 | 1.659 | 2.229 | 0.939 |
| $\frac{1}{2}$ - (530) | 2.971 | 1.945 | 2.488 | 1.158 |
| $\frac{5}{2}$ - (523) | 2.742 | 2.177 | 2.251 | 1.214 |
| $\frac{5}{2}$ + (642) | 2.752 | 1.826 | Blocked | 1.009 |
| $\frac{3}{2}$ - (521) | 2.596 | 2.160 | 2.207 | 1.333 |
| $\frac{7}{2}$ + (633) | 2.622 | 2.026 | 2.128 | Blocked |
| $\frac{7}{2}$ - (514) | 2.532 | 2.126 | 2.114 | 1.207 |
| $\frac{1}{2}$ - (521) | 2.657 | 2.133 | 2.258 | 1.315 |
| $\frac{9}{2}$ + (624) | 2.426 | 2.065 | 2.019 | 1.174 |
| $\frac{5}{2}$ - (512) | 2.338 | 1.941 | 2.006 | 1.176 |
| $\frac{9}{2}$ - (505) | 2.779 | 1.989 | 2.384 | 1.136 |
| $\frac{11}{2}$ + (615) | 2.796 | 1.934 | 1.936 | 1.103 |
| $\frac{3}{2}$ - (512) | 2.344 | 1.958 | 2.012 | 1.192 |
| $\frac{7}{2}$ - (503) | 2.500 | 1.730 | 2.180 | 1.039 |
| $\frac{1}{2}$ - (510) | 2.352 | 1.834 | 2.036 | 1.109 |
| $\frac{13}{2}$ + (606) | 2.540 | 1.800 | 2.195 | 1.034 |
| $\frac{5}{2}$ - (503) | 2.493 | 1.736 | 2.173 | 1.043 |
| $\frac{3}{2}$ - (501) | 2.283 | 1.581 | 2.001 | 0.959 |
| $\frac{1}{2}$ - (501) | 2.284 | 1.583 | 2.001 | 0.960 |

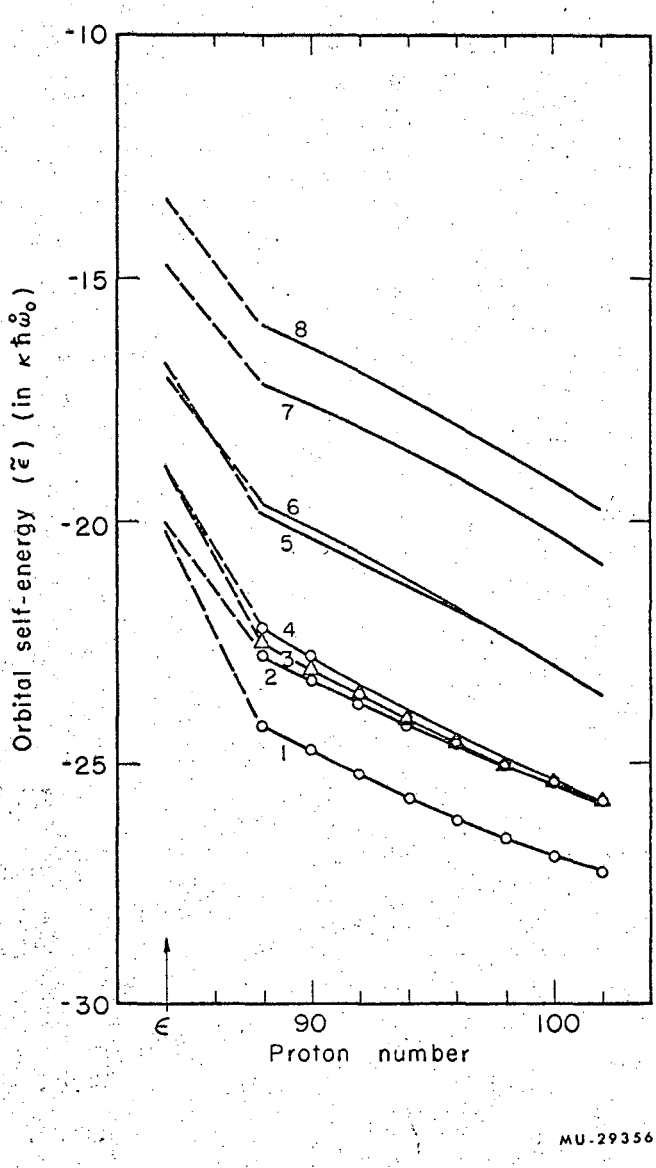


Fig. A.31-1. A plot of the orbital self energies $\tilde{\epsilon}_\nu$ for various proton numbers. The unmodified Nilsson orbital energies $\tilde{\epsilon}_\nu$ are connected at the extreme left by dashed lines. The calculation is for 25 proton orbitals with a force constant of 5.0. The orbitals plotted, in the notation $K\pi(N_1 n_z \Lambda)$, are

1. $\frac{1}{2}+(660)$
2. $\frac{11}{2}-(505)$
3. $\frac{3}{2}+(651)$
4. $\frac{1}{2}-(530)$
5. $\frac{5}{2}-(523)$
6. $\frac{5}{2}+(642)$
7. $\frac{3}{2}-(521)$
8. $\frac{7}{2}+(633)$

Table III. Ratios $\Delta_{odd}/\Delta_{even}$.

| | $Z_{odd}/Z_{even}$ | | | |
|---|---|---|---|---|
| | 93/94 | 95/96 | 97/98 | 99/100 |
| Blocked orbital | $\frac{5}{2}$ + (642) | $\frac{5}{2}$ - (523) | $\frac{3}{2}$ - (521) | $\frac{7}{2}$ + (633) |
| VSS ratio | 0.83 | 0.74 | 0.71 | 0.71 |
| Our ratio V = 5.0 (average) | 0.81 | 0.56 | 0.46 | 0.59 |

We have further studied what changes are brought about when we work with wave functions that are eigenfunctions of the number operator. Following a proposal of Kerman, Lawson, and Macfarlane,[6] we project out of the BCS wave function that part which contains a fixed number of nucleons equal to the average nucleon number of the BCS theory. The most convenient way to deal with such a problem is to introduce a contour integral in the complex plane and use Caudey's Theorem.[7] We write the wave function as

$$\psi_n = \frac{\mathcal{N}}{2\pi i} \oint \frac{d\zeta}{\zeta^{n+1}} \prod_{\nu=1}^{N} (U_\nu + \zeta V_\nu a_\nu^+ a_\nu^+) \,|\, 0\rangle, \qquad (1)$$

$\mathcal{N}$ being a normalization constant, and n half the number of nucleons. The quantities $U_\nu$ and $V_\nu$ are considered as known from a solution of the BCS equations:

$$U_\nu^2 = \frac{1}{2}\left(1 + \frac{\tilde{\epsilon}_\nu - \lambda}{\sqrt{(\tilde{\epsilon}_\nu - \lambda)^2 + \Delta_\nu^2}}\right); \quad U_\nu = +\sqrt{U_\nu^2},$$

$$V_\nu^2 = \frac{1}{2}\left(1 - \frac{\tilde{\epsilon}_\nu - \lambda}{\sqrt{(\tilde{\epsilon}_\nu - \lambda)^2 + \Delta_\nu^2}}\right); \quad V_\nu = +\sqrt{V_\nu^2}. \qquad (2)$$

6. A. K. Kerman, R. D. Lawson, and M. H. Macfarlane, Phys. Rev. 124, 162 (1961).

7. B. F. Bayman, Nucl. Phys. 15, 33 (1960).

To calculate the energy $E_n$,

$$E_n = \langle \psi_n | H | \psi_n \rangle ,$$

we have evaluated the expression

$$E_n = \frac{\mathcal{N}^2}{(2\pi i)^2} \oint \frac{d\zeta}{\zeta^{n+1}} \oint \frac{d\eta}{\eta^{n+1}}$$

$$\left\langle 0 \left| \prod_{\nu} \left( U_\nu + \zeta V_\nu \, a_{-\nu} \, a_\nu \right) \right. \times H \prod_{\nu'} \left( U_{\nu'} + \eta \, V_{\nu'} \, a_{\nu'}^{+} \, a_{-\nu'}^{+} \right) \left| 0 \right\rangle$$

$$= \frac{\mathcal{N}^2}{2\pi i} \oint dZ \sum_{\nu} \left\{ \left( 2\epsilon_\nu + \langle \nu\nu | \bar{G} | \nu\nu \rangle \right) V_\nu^2 \right.$$

$$\times \frac{1}{Z^n} \prod_{\nu' \neq \nu} \left( U_{\nu'}^2 + V_{\nu'}^2 Z \right) \Bigg\} + \sum_{\substack{\nu_1 \nu \\ \nu_1 \neq \nu}} \left\{ U_{\nu_1} V_\nu \right.$$

$$\times U_\nu V_{\nu_1} \langle \nu\nu | G | \nu_1 \nu_1 \rangle \frac{1}{Z^n} + V_{\nu_1}^2 V_\nu^2 \langle \nu \nu_1 | \bar{G} | \nu_1 \nu \rangle \frac{1}{Z^{n-1}} \Bigg\}$$

$$\times \prod_{\nu' \neq \nu_1 \nu} \left( U_{\nu'}^2 + V_{\nu'}^2 Z \right) .$$

The results of the fixed-particle-number calculation are given in Table IV and compared with the results of our ordinary BCS calculation and with the independent particle binding energy with no pairing forces. The energies $BE_n$ are only slightly greater than the BCS binding energy, about 200 to 400 keV, in good agreement with the results of Kerman et al. for spherical nuclei.[6] The pairing force gives about 1 MeV per proton extra binding.

In Fig. A. 31-2 the even-odd mass difference,

$$S(Z) = \frac{1}{2}\left[E(Z-1) + E(Z+1) - 2E(Z)\right],$$

has been plotted versus proton numbers. A force constant V = 5.0 gives values of S(Z) consistent with experimental values and in good agreement with VSS. The values for S(Z) obtained with fixed particle number are somewhat below the BCS values.

Figure A. 31-3 gives the energy levels as we predict them for odd-Z nuclei. For Z = 91 and Z = 95 the BCS theory and the refined calculation predict different states to be the ground state. At Z = 91 the BCS calculation disagrees with experiment, whereas at Z = 95 the refined calculation with a fixed nucleon number predicts a wrong ground-state spin.

Table IV. Theoretical total binding energies of valence protons (in MeV).

| Z (proton number) | 88 | 90 | 92 | 94 | 96 | 98 | 100 | 102 |
|---|---|---|---|---|---|---|---|---|
| no. of pairs treated | 6 | 7 | 8 | 9 | 10 | 11 | 12 | 13 |
| BE (no pairing force) | 82.03 | 85.55 | 106.92 | 118.17 | 129.21 | 138.96 | 147.83 | 155.98 |
| $BE_6$ (ordinary BCS) | 91.31 | 105.83 | 120.13 | 134.10 | 147.65 | 160.60 | 172.99 | 184.84 |
| $BE_n$ (fixed particle number) | 91.56 | 106.15 | 120.50 | 134.48 | 148.13 | 161.00 | 173.40 | 185.21 |

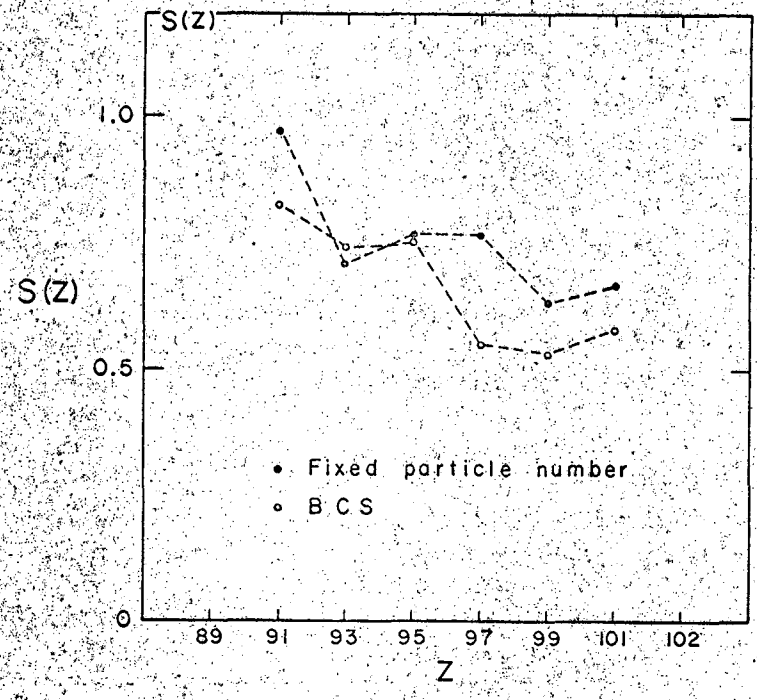


Fig. A.31-2. Plot of the theoretical odd-even mass difference (MeV) by the ordinary blocking calculation (solid dots) and by the projection of a fixed particle number from the BCS wave functions of even (unblocked) and odd (open circles). The simple formula taking the mass difference of the odd system and the average of the adjacent even systems was used:

$$S(Z) = \frac{1}{2}[E(Z-1) + E(Z+1) - 2E(Z)].$$

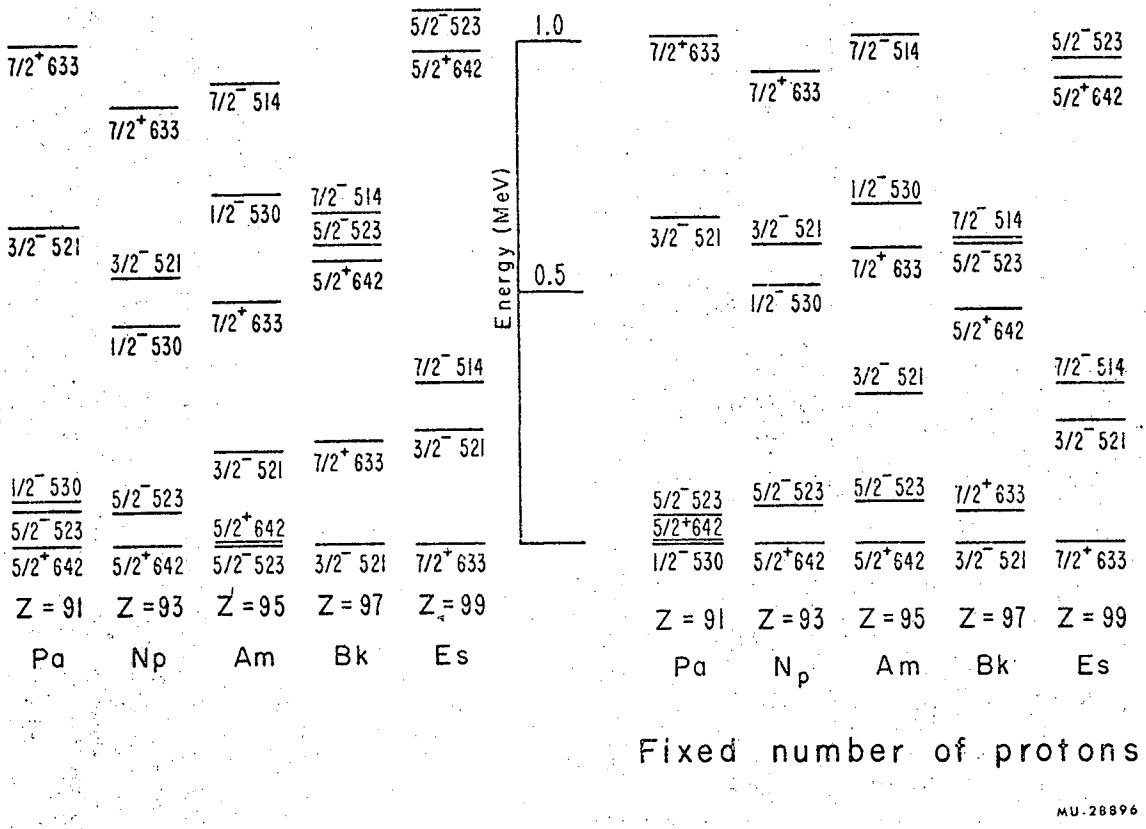


Fig. A. 31-3. Theoretical band-head energies in the spectra of several odd-proton nuclei. For the spectra on the right half of the figure a fixed particle number has been projected from the blocking BCS wave functions. For the spectra on the left the projection of fixed particle number has not been made.

## B. FISSION

### 1. MASS-SPECTROMETRIC STUDY OF MASS AND CHARGE DISTRIBUTION IN THE FISSION OF URANIUM-233, URANIUM-235, AND URANIUM-238 INDUCED BY INTERMEDIATE-ENERGY HELIUM IONS (*)

Nadia M. Souka† and Maynard C. Michel

In an attempt to extend the precision and -- we hope -- the accuracy of mass spectrometry to the measurement of the intermediate-energy fission yields, we have applied this technique to the fission of $U^{233}$, $U^{235}$, and $U^{238}$ induced by helium ions in the energy range from 23 MeV to 44 MeV. (The reader is referred to the full report of this work for a discussion of experimental details.*) In general, the techniques used were similar to those described by Chu,[1] with modifications to reduce the effects of contamination of the target by stable isotopes of the fission-product elements being investigated.

The experimental measurements were relative chain yields for the heavy-mass wing of the yield-mass curve ($U^{233}$ fission) and various independent yields of shielded or semishielded nuclides in the mass region 130 to 155 (for all three uranium isotopes). In addition, much of the yield-mass work of Chu[1] was confirmed.

As described by McHugh in Paper B. 2 in this report, it is possible in the case of the mass-135 chain, to measure three essentially independent yields in the same isobaric chain, thus conclusively demonstrating the shape of the charge-distribution function. This has been done for $U^{235}$ and $U^{238}$ at several different energies, with results in agreement with the data of McHugh on the fission of $Th^{232}$.

The mass-135 chain measurements have shown that the charge-distribution function can best be fitted with a Gaussian of the form

$$Pz = \frac{1}{\sqrt{\pi c}} \exp\left[-(Z-Z_p)^2/c\right],$$

where $Z$ and $Z_p$ are the nuclear charge of the fragment and most probable nuclear charge for the isobaric chain, respectively. The constant $c$ is

---

*Brief version of a report to be issued as UCRL-10555.

†Present address: United Arab Atomic Energy Establishment, Chemistry Division, Dakki, Cairo, U. A. R.

1. Yung Yee Chu, Charged-Particle-Induced Fission: A Mass-Spectrometric Yield Study (Thesis), UCRL-8926, Nov. 1959.

approximately equal to unity. As noted by McHugh, this is essentially the same charge distribution as observed by Wahl et al.[2] for the thermal-neutron fission of $U^{235}$. We have also found that this shape and width are independent of target isotope and excitation energy over the range studied.

For other independent yields measured in this work only one yield is available per mass number, so the variation of charge distribution with A could not be investigated. In view of Wahl's results, and assuming one universal shape independent of A, it is possible to determine an empirical $Z_p$-vs-A function. However, because of the success of Blann[3] and McHugh, an attempt was made to predict the $Z_p$ function by the use of the minimum-potential-energy (MPE) treatment by Swiatecki,[4] which is in turn a modification of the earlier work of Present.[5] In essence this treatment assumes an approach to electrostatic equilibrium during the rapid deformations preceding scission such that there is at least partial minimization of the electrostatic potential. This should result in a light fragment's receiving a higher proton-to-neutron ratio than a heavy fragment, as is indeed observed.

Making use of Swiatecki's work and using the most-stable-charge function ($Z_a$) of Green,[6] it is found possible to make reasonable predictions of the course of the $Z_p$-vs-A function. It must be noted that in this case the number ($\bar{\nu}$) and distribution of neutrons between the two fragments are undetermined quantities which seriously affect comparison of the results with experimental data. Also important, but more easily handled, are the neutrons emitted before fission, if any. The value of $\bar{\nu}$ has not yet been measured for fission at intermediate energies, although one can estimate an approximate number rather easily (see, for example, Thomas[7]). Our approach has been to use the data of Vandenbosch on prefission neutrons,[8] and treat $\bar{\nu}$ and the distribution of neutrons between heavy and light fragments ($\nu_H/\nu_L$) as parameters to be varied in seeking a good fit of the MPE rule with our experimental data. The restrictions placed on these parameters are

---

2. Arthur C. Wahl, Robert L. Ferguson, David R. Nethaway, David E. Troutner, and Kent Wolfsberg, Phys. Rev. 126, 1112 (1962).

3. H. M. Blann, Fission of Gold with 112-MeV $C^{12}$ Ions: Mass and Charge Distribution Characteristics, Phys. Rev. 123, 1356 (1961).

4. Wladyslaw Swiatecki (Lawrence Radiation Laboratory), private communication.

5. R. D. Present, Phys. Rev. 72, 7 (1947).

6. A. E. S. Green, Phys. Rev. 95, 1006 (1954).

7. T. Darrah Thomas, Spallation-Fission Competition from the Compound System $U^{233}$ and $He^4$ (Thesis), UCRL-3791, July 1957.

8. Vandenbosch, Thomas, Vandenbosch, Glass, and Seborg, Spallation Fission Competition in Heaviest Elements: Helium-Ion-Induced Reactions in Uranium Isotopes, UCRL-8032, Nov. 1957.

(a) $\bar{\nu}$ must be consistent with the excitation energy,

(b) $\frac{d\nu}{dEex}$ must be consistent with neutron binding energies,

(c) for a given target and energy, all measured independent yields must be fitted by the same value of $\bar{\nu}$ (although no restriction is placed on $\nu_H/\nu_L$, this ratio also seems to be approximately independent of A for a given situation).

The results of this treatment are shown in Figs. B. 1-1, B. 1-2, and B. 1-3 for $U^{235}$, $U^{233}$, and $U^{238}$ respectively. It is seen that the agreement of the various independent yields with the smooth Gaussian is rather good, but far from perfect. For some of the higher yields, in particular, the deviations seem to be outside the experimental errors. Both the constant-charge-to-mass ratio (CCR) and equal-charge-displacement rules fail rather conclusively to fit all the present data without unreasonable assumptions about $\bar{\nu}$ or $\nu_H/\nu_L$. In particular the CCR rule seems incapable of explaining the data under any circumstances.

We have also compared other available data, primarily those of Chu[1] (mass spectrometer) and of Colby and Cobble (radiochemical).[9] Within the experimental errors, all data except the $Pr^{142}$ yields of Colby and Cobble seem to agree with the Gaussian charge distribution of Figs. B. 1-1, B. 1-2, and B. 1-3.

The observation by Chu[1] that in this energy region shell effects seem to be unimportant is again supported by the smooth yield-mass curve for $U^{233}$ fission (Fig. B. 1-4) and the necessity of using a non-shell-affected $Z_A$ function such as Green's in the MPE calculations. Also, of course, the mass-135 independent yields are on the 82-neutron shell edge, and show no serious deviation from a smooth Gaussian.

---

9. J. L. Colby, Jr., and J. W. Cobble, Phys. Rev. 121, 1410 (1961).

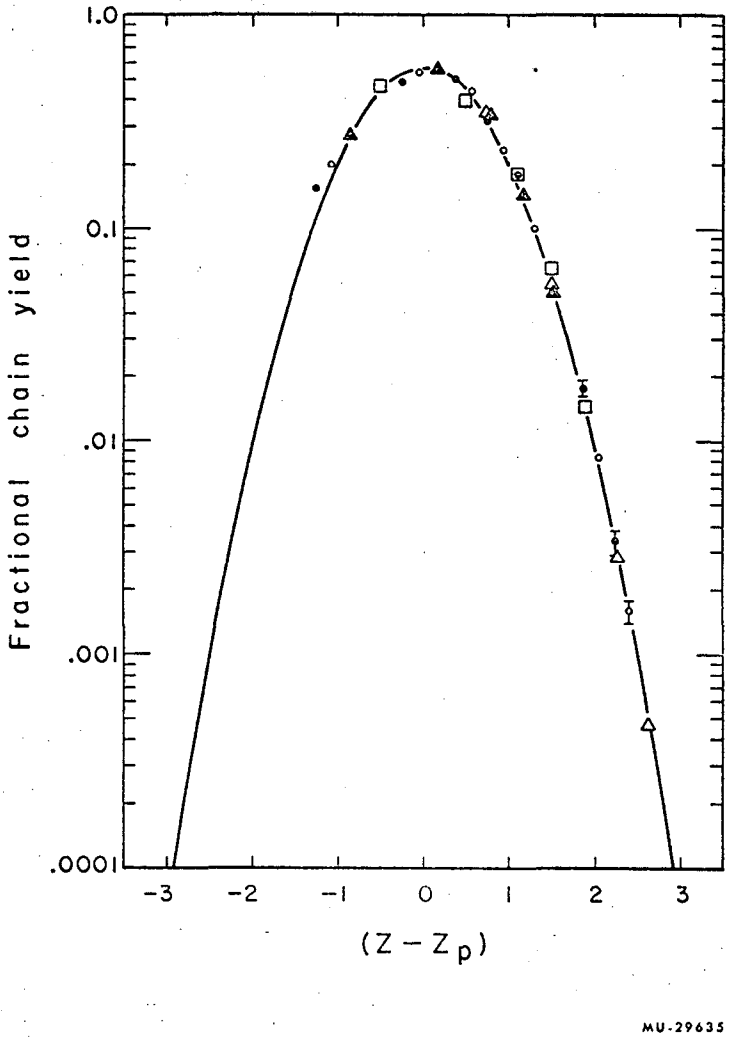


Fig. B. 1-1. Charge distribution for $U^{235}$(a, F) based on MPE rule and Green's masses.

- ● 43.3 MeV
- △ 29.8 MeV
- ○ 35.4 MeV
- □ 22.2 MeV
- ▲ 28.8 MeV

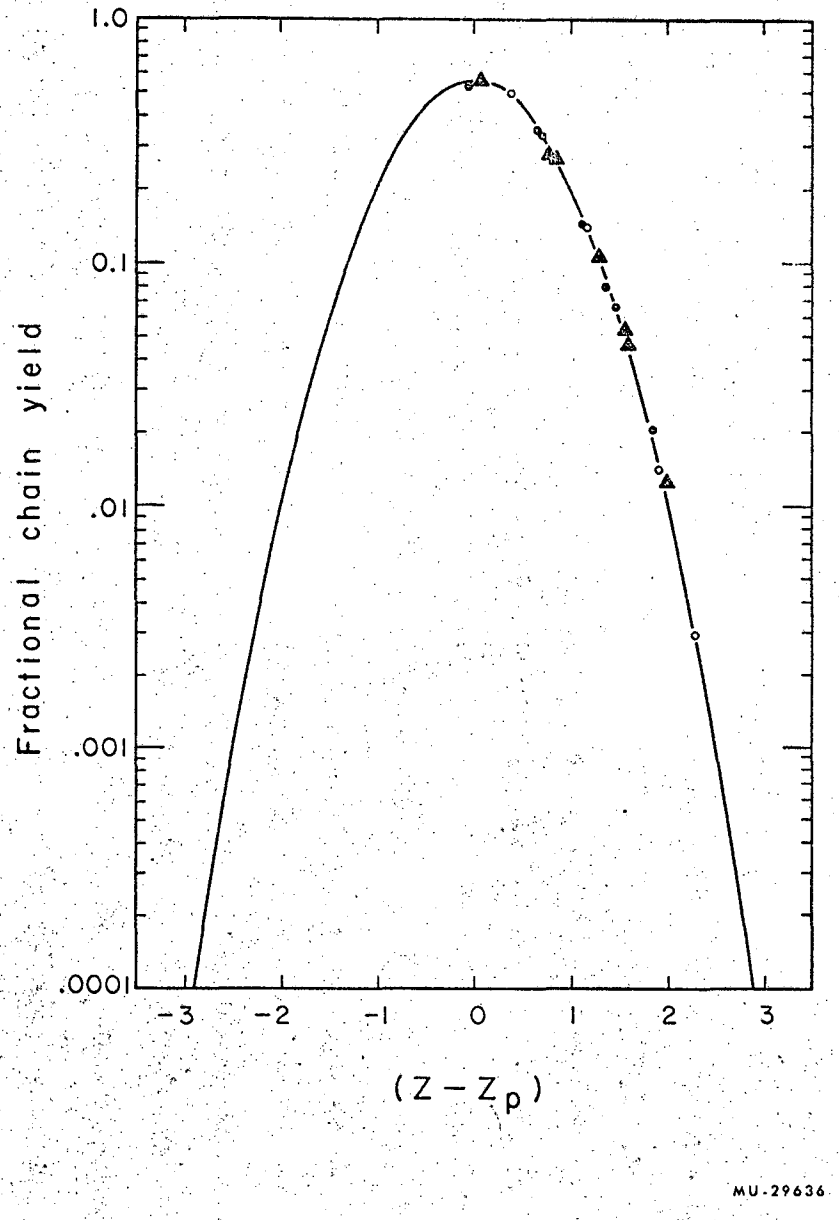


Fig. B. 1-2. Charge distribution for $U^{233}(\alpha, F)$ based on MPE rule and Green's masses.
○ 25.5 MeV
▲ 34.1 MeV
◉ 42.3 MeV

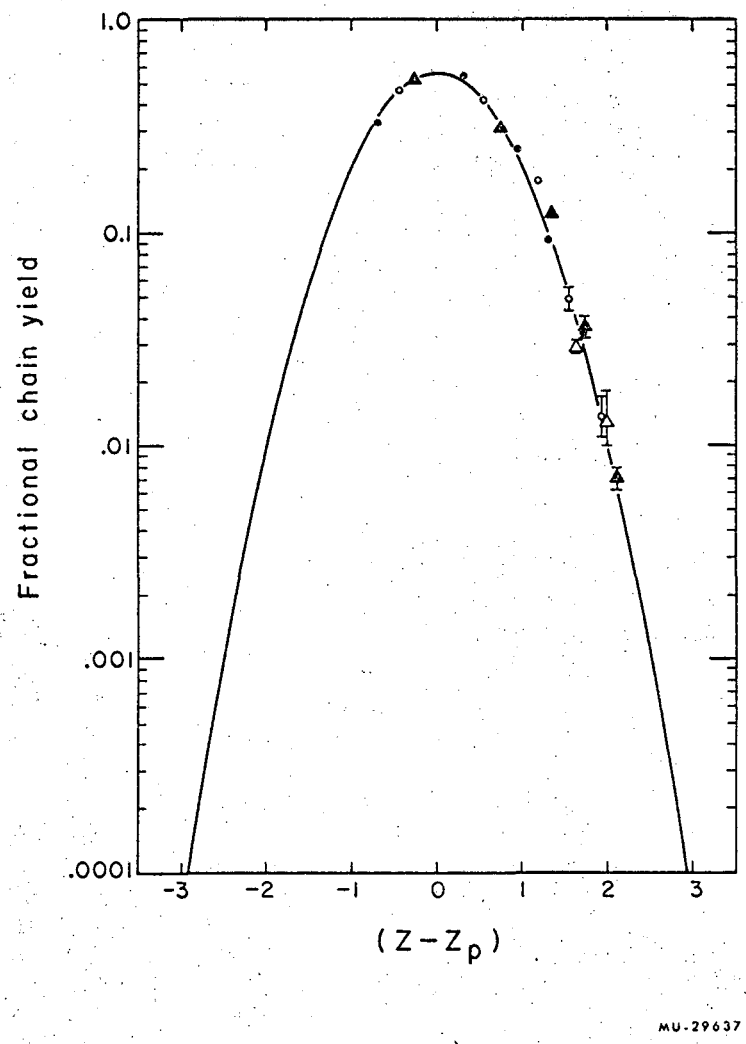


Fig. B. 1-3. Charge distribution for $U^{238}$ (a, F) based on MPE rule and Green's masses.

◉ 44.2 MeV ▲ 30.9 MeV

○ 36.8 MeV △ 25.6 MeV

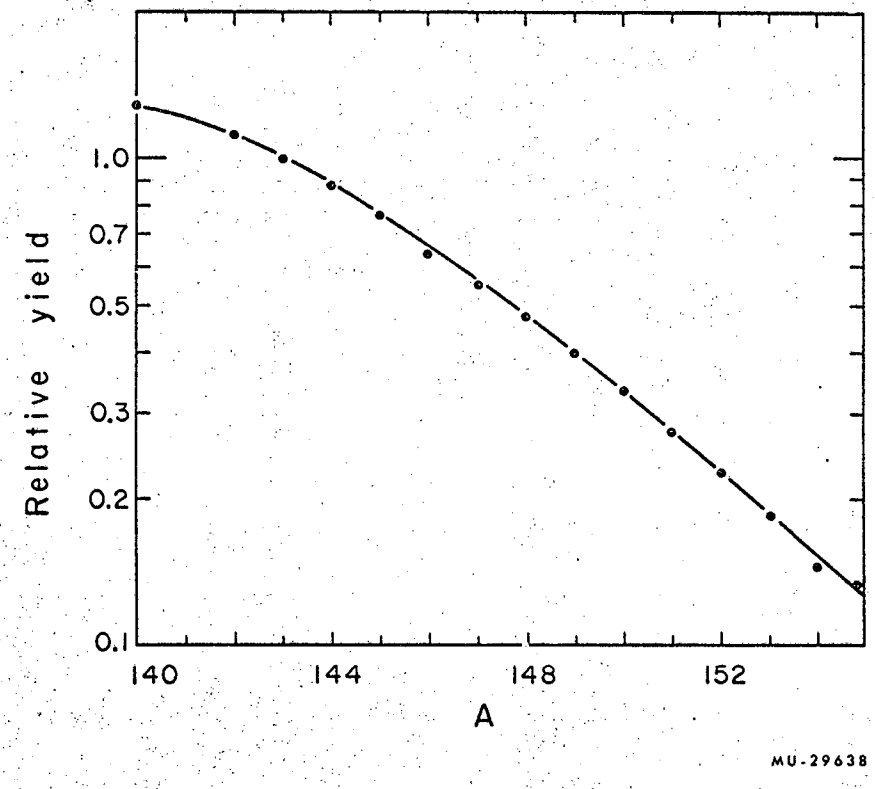


Fig. B. 1-4. Yield-mass curve for fission of $U^{233}$ induced by 42-MeV helium ions.

## 2. NUCLEAR CHARGE DISTRIBUTION FOR FISSION OF THE MODERATELY EXCITED $U^{236*}$ COMPOUND NUCLEUS

James A. McHugh and Maynard C. Michel

One of the interesting and important problems in nuclear fission concerns the division of nuclear charge between the primary fragments, or the way in which the most probable charge for a given mass ($Z_p$) varies with fragment mass. The measurement of a primary fission yield after prompt-neutron emission and the knowledge of the primary yield distribution in the isobaric chain fixes $Z_p$ for that mass. The thermal-neutron fission of $U^{235}$ ($U^{236*}$) has been studied extensively to determine its charge distribution and $Z_p$ functions. For this reason, it was of interest to study the charge distribution resulting from fission of a more highly excited $U^{236*}$. A study was undertaken on the $Th^{232} + He^4$ ($U^{236*}$) system for excitations from 18 MeV to 39 MeV, utilizing high-sensitivity mass-spectrometric techniques for the yield measurements.[1]

To derive useful $Z_p$ information from our fractional-chain-yield data,[2] we must know the charge-distribution function. The distribution has been measured in one isobaric chain (mass 135) for a number of exciation energies.

Fractional chain yields for two or more members of the same chain are required in order to obtain direct information concerning the charge-distribution shape. By observing the growth rate of the long-lived $Cs^{135}$, it was possible, from the accurate knowledge of the half-lives and the equations of radioactive transformation, to calculate the major primary yields in the 135 chain.[1] The growth was observed by chemically separating $Cs^{135}$ from its precursors at known times after irradiation, and measuring the accumulated $Cs^{135}$ relative to $Cs^{137}$ ($Cs^{137}$ precursors have in all cases completely decayed prior to chemistry). For each energy the $Cs^{135}$:$Cs^{137}$ ratio was measured for three decay periods. The three measurements are sufficient to determine the fractional chain yields of $Cs^{135}$ and $Xe^{135}$, and the fractional cumulative yield of $I^{135}$. The fraction of $Xe^{135}$ produced independently as $Xe^{135m}$ was assumed to be 0.5. This assumption has little effect on the $I^{135}$ and $Xe^{135}$ yields. However, it does affect the small $Cs^{135}$ yield. For this reason, the yield calculations were performed for the complete range of possible $Xe^{135m}/Xe^{135}$ values so that the uncertainty in the $Cs^{135}$ yield could be assessed. A summary of the results is given in Table I and Fig. B. 2-1.

The fractional-yield data for the 135 chain are consistent with a Gaussian curve

$$y_i = (c\pi)^{-1/2} \exp\left[-(Z - Z_p)^2/c\right],$$

---

1. For a more detailed discussion refer to Ph. D. thesis of James A. McHugh, in preparation as UCRL-10673.

2. Fractional chain yield is the ratio of a primary yield of a mass chain to the total chain yield.

Table I. Fractional chain yields of 135 isobars for fission of $U^{236*}$

| Excitation energy (MeV) | $Cs^{135}$ | $Xe^{135}$ | $I^{135}$ [a] | $Z_p$ [b] |
|---|---|---|---|---|
| 39.3 | 0.098 ± 0.006 | 0.523 ± 0.010 | 0.376 ± 0.009 | 53.72 |
| 26.8 | 0.032 ± 0.004 | 0.381 ± 0.009 | 0.586 ± 0.012 | 53.38 |
| 23.0 | 0.014 ± 0.004 | 0.333 ± 0.009 | 0.653 ± 0.015 | 53.28 |
| 15-18. | (<0.009) | 0.22 ± 0.01 | 0.78 ± 0.02 | 53.05 |

a. Fractional cumulative yield

b. $Z_p$ obtained from the maximum in the Gaussian distribution, which was fitted to the fractional-yield data (fractional yield vs Z)

where $y_i$ is the fractional independent yield of a chain member having atomic number Z, and c is the normalization or width constant of the distribution. The value of c that best fits all energies is 0.95 ± 0.05.

Wahl and co-workers have measured fractional yields for two or more members of several decay chains in the thermal-neutron fission of $U^{235}$.[3] The value of c obtained from a weighted average of the several chains was 0.94 ± 0.15.

These results indicate that a single charge-distribution function is maintained through a wide range of excitations (6.5 to 39 MeV). Swiatecki and Blann[4] have pointed out that if the charge fluctuations for a system in thermodynamic equilibrium with harmonic restoring forces can be attributed to statistical and quantum fluctuations, a Gaussian charge-distribution function results. A quantum statistical relationship between the charge-distribution width constant c and the nuclear temperature was derived that is valid for all nuclear temperatures. Their relationship indicates that the width constant should be independent of temperature within the range of excitations that have been reported here (as is observed). The results of other researchers[5,6] also support these observations.

Because of the close proximity of the 82-neutron shell to the 135 isobars, one might expect possible perturbations in the primary yield distribution. No deviations from a smooth Gaussian function were observed for excitations from 18 MeV to 39 MeV.

The fractional chain yield of $Cs^{136}$ and the cumulative yield of $Xe^{136}$ have been recently determined and also found to be consistent with a Gaussian charge-distribution function identical to that found for the 135 chain.

3. A. C. Wahl, R. L. Ferguson, D. R. Nethaway, D. E. Troutner, and K. Wolfsberg, Phys. Rev. 126, 1112 (1962).

4. W. J. Swiatecki (Lawrence Radiation Laboratory), private communication.

5. B. D. Pate, J. S. Foster, and L. Yaffe, Can. J. Chem. 36, 1691 (1958).

6. H. M. Blann, Phys. Rev. 123, 1356 (1961).

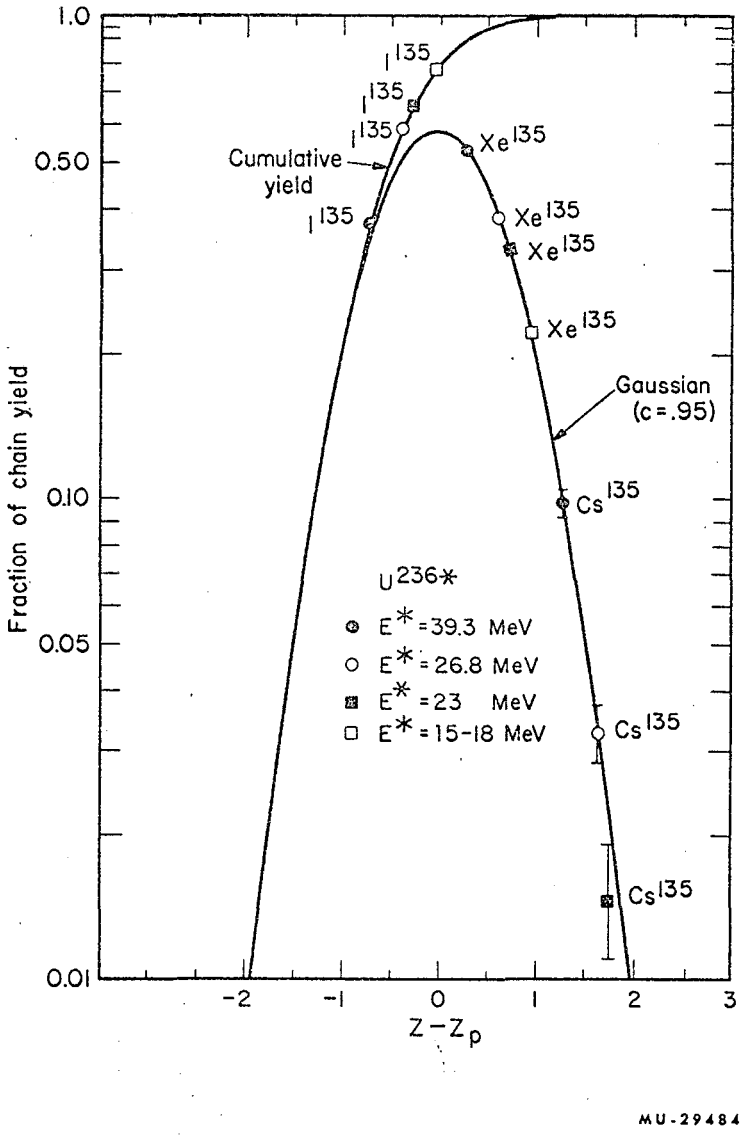


Fig. B. 2-1. Fractional yields for the 135 chain plotted vs $(Z-Z_p)$. Iodine yields are cumulative and thus fall on the integrated portion of the distribution curve. The error bars on the $Cs^{135}$ are associated with the uncertainty in $Xe^{135m}/Xe^{135}$.

## 3. MOMENTUM TRANSFER IN HEAVY-ION-INDUCED FISSION. II

Torbjørn Sikkeland and Victor E. Viola, Jr.

We report results from a series of experiments designed to study reactions between various ions and targets. The method consisted of measuring the angular correlation between coincident pairs of fission fragments. $U^{238}$, $Au^{197}$, and $Ho^{165}$ were chosen as targets. The ions used were $He^4$, $C^{12}$, $O^{16}$, and $Ne^{20}$.

The experiments were performed at the Hilac. The fragments were counted with two Au-Si surface barrier detectors D-1 and D-2. Detector D-2 was fixed at 90° to the beam (x) axis in the horizontal (xy) plane. The position $(\xi,\psi)$ of D-1 was varied; $\xi$ is the angle D-1 forms with the xy plane; $\psi$ is the angle between D-1 and the x axis in the xy plane.

The electronics applied were the standard fast-slow circuitry used in coincidence experiments.

With the ions $C^{12}$, $O^{16}$, and $Ne^{20}$ at 10.4 MeV per nucleon incident on $U^{238}$ the correlation functions $W(\xi,\psi)$ show two maxima at $W(0,\overline{\psi}_{CN})$ and $W(0,\overline{\psi}_{NCN})$. As a typical example, $W(\xi,\psi)$ for the system $U^{238} + O^{16}$ is shown in a contour diagram in Fig. B. 3-1. The highest and sharpest peak around $W(0,\overline{\psi}_{CN})$ can be shown to be due to fragments coming from nuclei which have forward momenta equal the ions and no sidewise momentum. The spreads are due to neutron evaporation and to spreads in the fragments' mass and momentum. The functions for the lighter targets and for the system $U^{238} + He^4$ all show only this CN peak. By use of a simple formula the average number of neutrons N emitted and their energy 2T can be evaluated from the experimental spreads. The results are given in Table I.

The other peak is due to a non-compound-nucleus (NCN) reaction with incomplete momentum transfer by the ion to the nucleus. The large spreads in the function for these types of reactions can be explained only by the fissioning nuclei's having momenta at an angle to the beam axis. From the experimental data we can obtain values for $\langle P_N^2 \rangle / P_I^2$, where $P_N$ and $P_I$ are the laboratory-system momenta of the fissioning nucleus and the heavy ion. Similarly, values for $\langle \tan^2 \theta_N \rangle$, where $\theta_N$ is the angle between $\vec{P}_N$ and $\vec{P}_I$, can be evaluated. These values are given in Table I.

By a momentum analysis we can find approximate values for $\langle P_S \rangle / P_I$ and $\langle \theta_S \rangle$, where $P_S$ is the momentum taken off by the stripped ion and $\theta_S$ the angle between $\vec{P}_S$ and $\vec{P}_I$. By assuming the stripped ion to have the same velocity as the incoming heavy ion, the number of nucleons transferred $N_T$ to the nucleus can be evaluated. Values for $\langle P_S \rangle / P_I$, $\langle \theta_S \rangle$, and $N_T$ are given in Table I.

We see that $\langle \theta_S \rangle$ and $N_T$ are practically independent of type of ion.

The ratios between the two reactions are given in the table. These are approximately in agreement with results from other types of experiments.

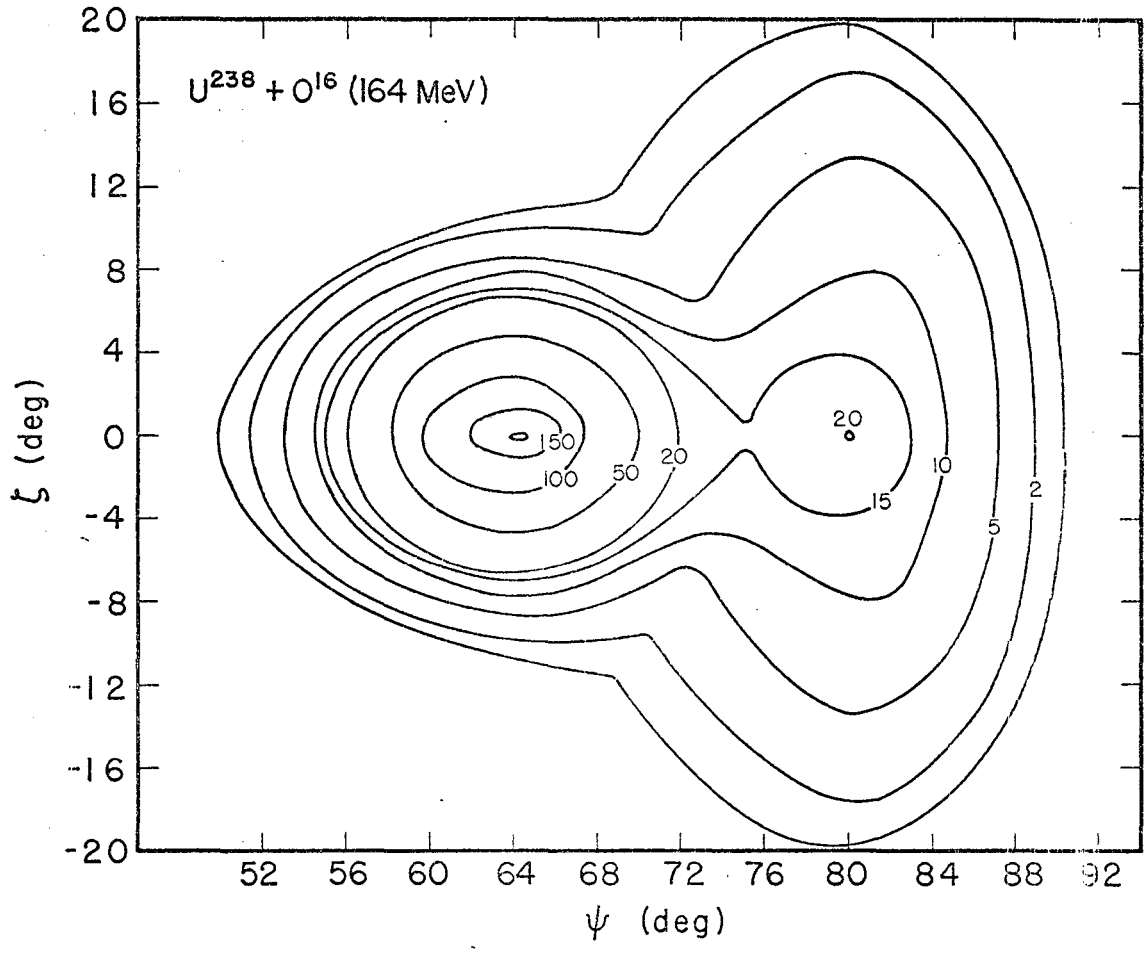


Fig. B. 3-1. Contour diagram of the angular correlation function $W(\eta\,\psi)$ for fragment pairs in $O^{16}$-induced fission of $U^{238}$. ($O^{16}$ energy = 164 MeV.)

Table I. Data from fragment-fragment angular studies.

| System | $\overline{\psi}_{CN}$ | $\overline{N}$ | $2\overline{T}$ | $\overline{\psi}_{NCN}$ | $\frac{\langle P_N^2 \rangle}{P_I^2}$ | $\langle \tan^2 \theta_N \rangle$ | $\frac{\langle P_S \rangle}{P_I}$ | $\langle \theta_S \rangle$ | $N_T$ | $\sigma_{NCN}/\sigma_{CN}$ |
|---|---|---|---|---|---|---|---|---|---|---|
| $He^4 + U^{238}$ | 82.5 | 5 | 4.6 | | 1.0 | | | | | |
| $C^{12} + U^{238}$ | 70.0 | 12 | 4.0 | 82.0 | 0.31 | 0.60 | 0.66 | 33 | 4.1 | 0.18 |
| $O^{16} + U^{238}$ | 64.0 | 14 | 4.4 | 80.0 | 0.32 | 1.40 | 0.77 | 35 | 3.7 | 0.33 |
| $Ne^{20} + U^{238}$ | 59.0 | 16 | 4.4 | 78.5 | 0.34 | 2.07 | 0.82 | 36 | 3.5 | 0.33 |
| $O^{16} + Au^{197}$ | 59.4 | 10 | 4.6 | | 1.0 | | | | | |
| $O^{16} + Ho^{165}$ | 54.0 | 8.5 | 4.4 | | 1.0 | | | | | |

At lower velocities of the ions we find that $\overline{\psi}_{NCN}$ approaches $\overline{\psi}_{CN}$, which means the stripped ion is emitted at higher angles. For this reason the cross sections for the different reactions become increasingly difficult to evaluate. Qualitatively, however, we can state that NCN reactions are appreciable over the energy range from the Coulomb barrier up to the maximum energy of 10.4 MeV/nucleon.

The NCN reactions observed here definitely belong to surface reactions and can be interpreted with the so-called grazing model.[1]

---

1. R. Kaufmann and R. Wolfgang, Phys. Rev. 121, 192 (1961).

## 4. FRAGMENT KINETIC ENERGY RELEASE IN FISSION INDUCED BY HEAVY IONS(*)

Victor E. Viola, Jr., and Torbjørn Sikkeland

The most probable kinetic energy release, $\bar{E}_K$, in fission induced by 125-MeV $C^{12}$ ions and 166-MeV $O^{16}$ ions has been measured for a wide range of fissioning nuclei. Targets of $Pr^{141}$, $Tb^{159}$, $Ho^{165}$, $Tm^{169}$, $Lu^{175}$, $Au^{197}$, $Bi^{209}$, $Th^{232}$, $U^{238}$, and $Pu^{240}$ have been fissioned. The results were obtained from single-fragment spectra by use of silicon-diode surface-barrier detectors. A $Cf^{252}$ spontaneous fission source served as the absolute energy calibration. Corrections were made to the data for the effects of target thickness, center-of-mass transformation, mass defect in the crystal, and evaporation of neutrons from the fragments after fission.

A least-squares analysis of our data (shown in Fig. B. 4-1) and those compiled by others[1, 2, 3] gave an excellent fit to the function

$$\bar{E}_K(\text{MeV}) = 0.1065\, Z^2/A^{1/3} + 20.1.$$

However, it was not possible to fit all the data with the simple relationship of Terrell, $\bar{E}_K = 0.121\, Z^2/A^{1/3}$, based on a tangent sphere model.

In order to examine a more realistic configuration for the scission shapes, we have compared the data with recent liquid-drop calculations by

---

*Shortened version of a paper submitted to Phys. Rev. (Victor E. Viola, Jr., and Torbjørn Sikkeland, Kinetic Energy Release in Heavy-Ion-Induced Fission Reactions, UCRL-10284, Oct. 1962.)

1. J. Terrell, Phys. Rev. 113, 527 (1959).

2. H. C. Britt, H. E. Wegner, and J. Gursky, Phys. Rev. Letters 8, 98 (1962); and H. C. Britt, private communication.

3. R. Brandt (Lawrence Radiation Laboratory), private communication.

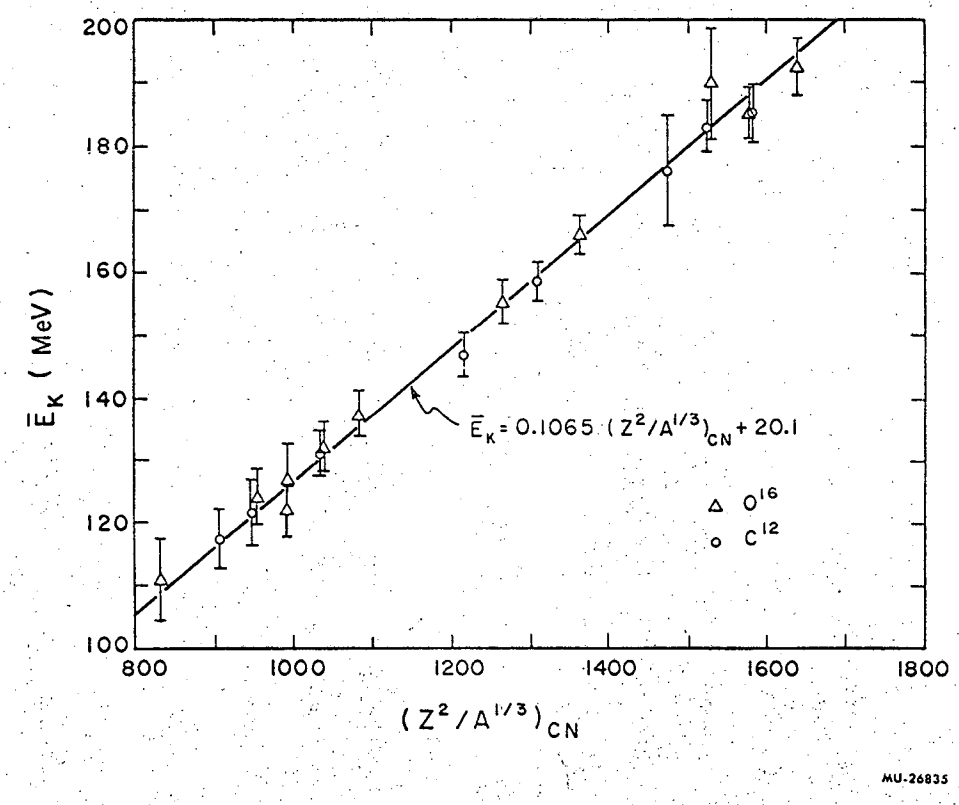


Fig. B.4-1. Plot of $\bar{E}_K$ versus $Z^2/A^{1/3}$ for the fissioning nuclei studied in this work.

Cohen and Swiatecki.[4, 5] They have calculated the electrostatic energy of two spheroids whose optimum ratio of major to minor axes C/A minimizes the total energy for a nucleus of a given fissionability. Assuming equal volumes for the fragments in all cases, and the C/A ratios calculated by Cohen and Swiatecki, we compared with four models:

(a) Tangent spheroids, assuming the nuclear vibration is slow with respect to separation, i. e., C/A is constant;

(b) tangent spheroids that vibrate according to the classical laws of motion;[6]

(c) spheroids separated by a distance characterized by a parameter D, where

$$\frac{\text{separation distance}}{R_0} = \left(\frac{4\pi}{3}\right)^{1/3} D$$

and D = 0.2, assuming a constant C/A; and

(d) the spheroids with D = 0.2 separating as in (b).

Good agreement with the data is found with either model (b), (c) or (d). This leads us to conclude that the kinetic energy release in fission reactions arises from Coulomb repulsion of fragments whose deformations vary as a function of x.

We have also measured the kinetic energy release as a function of excitation energy of the fissioning nucleus and have found $\bar{E}_K$ to be nearly independent of the excitation energy. It is also observed that the spread in the kinetic energy distribution (full width at half maximum of the fragments) is relatively constant below $\chi$ values of about 0.70 for the fissioning nucleus, but increases rapidly above this value. We correlate this finding with the calculations by Cohen and Swiatecki.[4, 5] They predict that below x = 0.7 the saddle and scission shapes are nearly identical, permitting a restricted spread in the properties of the fragments. Above x = 0.7 substantial deformation occurs between the saddle and the scission points, allowing a wider distribution in the product properties. The width of the $\bar{E}_K$ distribution also is observed to increase with increasing excitation energy. This we attribute to vibrational effects in the nucleus.

---

4. S. Cohen and W. J. Swiatecki, Ann. Phys. 19, 67 (1962).

5. Stanley Cohen and Wladyslaw J. Swiatecki, The Deformation Energy of a Charged Drop: Part V: Results of Electronic Computer Studies, UCRL-10450, Aug. 30, 1962.

6. J. R. Nix (Lawrence Radiation Laboratory), private communication.

# 5. TOTAL CROSS SECTIONS FOR FISSION OF URANIUM-238 INDUCED BY HELIUM-4 AND HEAVY IONS(*)

Victor E. Viola, Jr., and Torbjørn Sikkeland

The total fission cross sections have been measured for bombardment of $U^{238}$ with $He^4$, $B^{11}$, $C^{12}$, $N^{14}$, $O^{16}$, and $Ne^{20}$ ions at energies up to 10.4 MeV per nucleon. The experimental technique -- involving the use of silicon diode surface-barrier detectors -- was described in the preceding annual report, as also were the methods involved in determining the final data.

Because of the high fissionability of these systems, it is assumed that the fission cross section is equal to the total reaction cross section for heavy-ion reactions. For $He^4$-initiated reactions, measured spallation cross sections were added to the fission cross sections. Good agreement with previous results was found.[1]

The data have been compared with the theoretical reaction cross-section calculations by Thomas, assuming (a) a square-well nuclear potential, and (b) a parabolic approximation to the real part of the optical potential.[2] At energies well above the Coulomb barrier, the data are well represented by use of a square-well potential and $r_0 = 1.50$ F. Near the barrier, however, the agreement is poor.

With the parabolic approximation, the entire excitation function can be generally reproduced except in the case of $Ne^{20}$. The experimental results and the theoretical calculations are shown on Fig. B. 5-1. Values for the parameters of the parabolic approximation are given in Table I. These include the well depth $V_0$, the nuclear radius parameter $r_0$, and a surface diffuseness parameter d. We find that as the mass of the bombarding particle increases, $r_0$ increases and d decreases.

The parameters derived from fitting the experimental data for the various heavy ions should be useful in calculating total reaction cross sections and average angular momenta $\langle \ell \rangle$ for heavy-ion bombardment of other heavy targets. However, it should be stressed that any quantitative interpretation of heavy-ion reactions must take into account the perturbations created by nuclear surface reactions.[3]

For example, it is known that, in 166-MeV $O^{16}$ bombardment of $U^{238}$, about 25% of the fission reactions occur by a direct-interaction mechanism.[4] If one presumes that these are surface reactions that occur in the highest orbital angular momentum states, then for $\langle \ell \rangle$ is lowered from 57.4 to 49.4 for the compound-nucleus reactions. The overall $\langle \ell \rangle$ will be even lower because the fission resulting from direct interaction will be from nuclei of low angular momentum.

---

*Shortened version of published paper, Phys. Rev. 128, 767 (1962).

1. J. R. Huizenga, R. Vandenbosh, and H. Warhanek, Phys. Rev. 124, 1964 (1961).

2. T. D. Thomas, Phys. Rev. 116,703 (1959).

3. T. Sikkeland, E. L. Haines, and V. E. Viola, Jr., Phys. Rev. 125, 1350 (1962).

4. Torbjørn Sikkeland and Victor E. Viola, Jr., Paper B. 3 (this report).

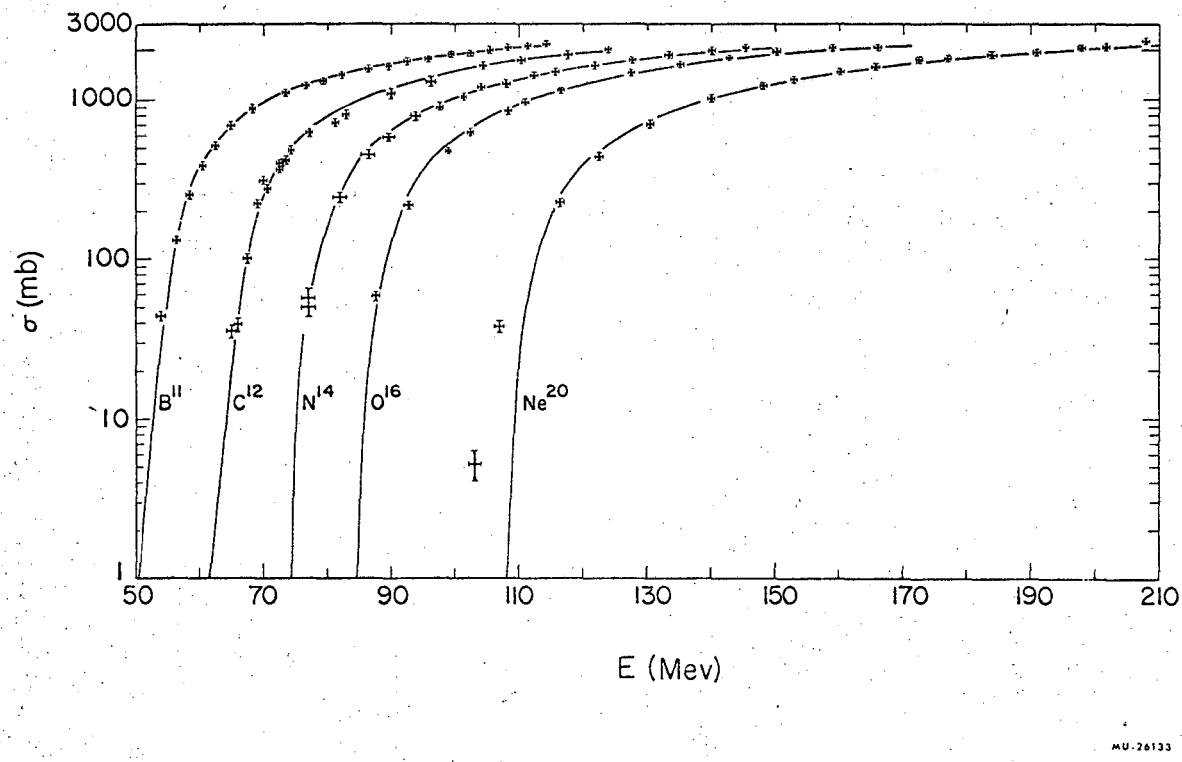


Fig. B. 5-1. Best fits for the parabolic approximation to the real part of the optical potential (solid line) to the excitation functions for fission of $U^{238}$ with $B^{11}$, $C^{12}$, $N^{14}$, $O^{16}$, and $Ne^{20}$. (Parameters for calculation are given in Table I.)

Table I. Parameters for parabolic approximation to the real part of the optical potential giving best fit to the experimental results.

| Ion | $He^4$ | $B^{11}$ | $C^{12}$ | $N^{14}$ | $O^{16}$ | $Ne^{20}$ |
|---|---|---|---|---|---|---|
| $r_0$(F) | 1.17 | 1.23<br>1.24 | 1.24 | 1.24 | 1.25 | 1.26 |
| $V_0$(MeV) | -66.6 | -70 | -70 | -70 | -70 | -70 |
| d(F) | 0.574 | 0.50<br>0.48 | 0.48 | 0.48 | 0.48 | 0.44 |

## 6. ANGULAR DISTRIBUTIONS OF FRAGMENTS FROM FISSION INDUCED BY HEAVY IONS IN GOLD AND BISMUTH(*)

Victor E. Viola, Jr., T. Darrah Thomas, and Glenn T. Seaborg

The qualitative results of measurements of the angular distribution of fission fragments produced by irradiation of $Au^{197}$ and $Bi^{209}$ with various heavy ions have been reported in previous annual reports. The projectiles $B^{11}$, $C^{12}$, $N^{14}$, and $O^{16}$ had energies from a few MeV above the Coulomb barrier to 10.4 MeV per nucleon.

The gross features of these results can be explained by use of a model and parameters[1,2] that have been used by others to account for angular distributions of fission fragments from $He^4$ bombardments.[3,4,5] The anisotropy predicted by this model is characterized by the parameter

$$p = \frac{\hbar^2 I_{max}^2}{\Im_{eff}^2 T} ,$$

*Shortened version of paper submitted to Phys. Rev. (UCRL-10248, May 1962).

1. I. Halpern and V. Strutinski, in Proceedings of the Second United Nations International Conference on the Peaceful Uses of Atomic Energy, Vol. 15 (United Nations, Geneva, 1958), p. 408.

2. J. J. Griffin, Phys. Rev. 116, 107 (1959).

3. I. Halpern and C. T. Coffin, Phys. Rev. 112, 536 (1958).

4. R. Vandenbosch, H. Warhanek, and J. R. Huizenga, Phys. Rev. 124, 846 (1961).

5. R. Chaudhry, R. Vandenbosch, and J. R. Huizenga, Phys. Rev. 126, 220 (1962).

where $I_{max}$ is the maximum angular momentum of the fissioning nucleus (calculated from other results of one of the authors[6]), $\Im_{eff}$ is the effective moment of inertia,[2] and T is the nuclear temperature. For T we have used

$$T = \sqrt{(E^* - E_{th} - E_{rot})/a} \quad ,$$

where $E^*$, $E_{th}$, and $E_{rot}$ are the excitation energy, fission threshold energy, and rotational energy of the fissioning nucleus respectively, and the level density parameter $a = A/8$.[7]

Measurement of p values gave all the information needed to calculate $\Im_{eff}$ and thereby gain some knowledge of the deformation of the nucleus at the saddle point.[2] In Fig. B.6-1 we have plotted the values of $\Im_{eff}/\Im_0$ versus the fissionability parameter $Z^2/A$. Here $\Im_0$ is the moment of inertia of a sphere. Also shown in this graph are the data of Ref. 3, where $\Im_{eff}$ was found to be independent of excitation energy. A smooth curve connects their five points. Our data confirm the previous results[2] that $\Im_{eff}/\Im_0$ increases with increasing $Z^2/A$. Because $\Im_{eff}/\Im_0$ is an inverse function of the deformation, this result agrees with the prediction by Cohen and Swiatecki that the deformation increases as $Z^2/A$ decreases.[8]

We note that, although the points based on our work bracket this smooth curve, the range of deviation is quite large. However, these deviations are systematic: the points falling above the curve correspond to bombardments at the highest energies, whereas points falling below the curve are at the lowest energies. In particular the three points falling farthest below the curve are from bombardments at energies only a few MeV above the Coulomb barrier.

The most reasonable explanation of this behavior is that we are not predicting the correct value of $I_{max}$, or $\ell$. To investigate this possibility, we have assumed $\Im_{eff}/\Im_0$ is given by the curve in Fig. B.6-1 and have then calculated values of $\langle \ell \rangle$ necessary to give this moment of inertia from the experimental data. Designating this quantity as $\langle \ell \rangle_{expt}$, we plot the ratio of $\langle \ell \rangle_{expt}$ to $\langle \ell \rangle_{calc}$ as a function of energy in Fig. B.6-2. The data for the eight different systems fall roughly on one curve.

This result supports the idea that our estimates for $\langle \ell \rangle$ are in error. At high energies this is readily explained by the occurrence of direct interaction at the nuclear surface.[6, 9] The high fission barriers for these systems require compound-nucleus formation to occur before fission can proceed. Correction of the $I_{max}$ values for this effect gives good agreement with the results of Ref. 2 for $\Im_{eff}/\Im_0$. It appears that our model for calculating $I_{max}$ may be in error at the lowest energies.

---

6. V. E. Viola, Jr., and T. Sikkeland, Phys. Rev. 128, 767 (1962).

7. J. R. Huizenga, R. Chaudhry, and R. Vandenbosch, Phys. Rev. 126, 210 (1962).

8. S. Cohen and W. J. Swiatecki, Ann. Phys. 19, 67 (1962).

9. T. Sikkeland, E. L. Haines, and V. E. Viola, Jr., Phys. Rev. 125, 1350 (1962).

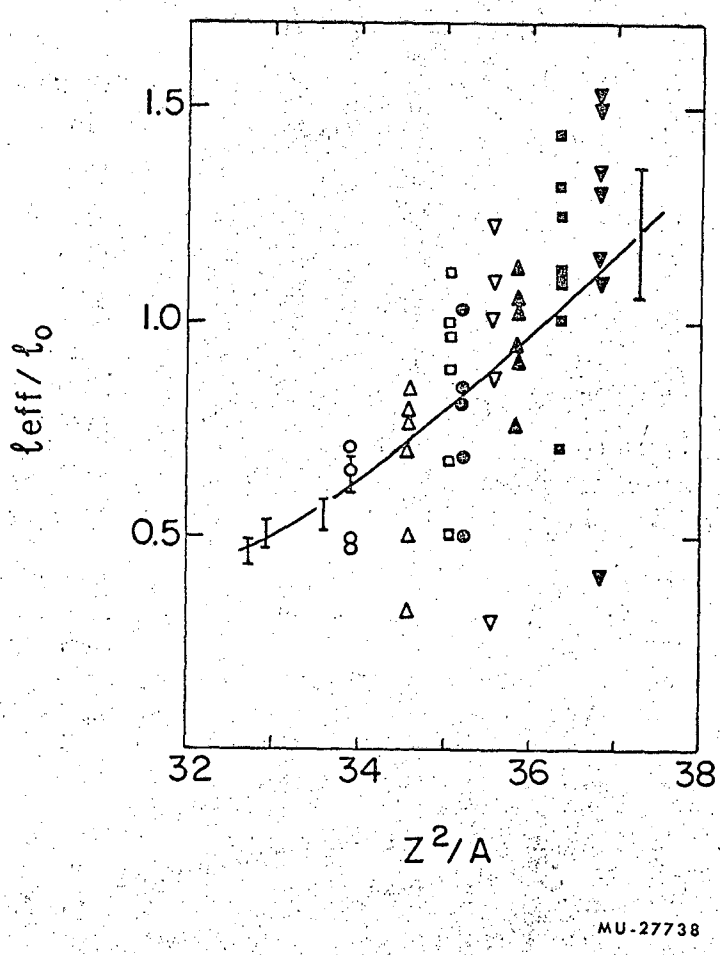


Fig. B.6-1. Ratio of effective moment of inertia at the saddle point, $\mathcal{I}_{eff}$, to the moment of inertia of a rigid sphere, $\mathcal{I}_0$, plotted against $\chi = \frac{Z^2/A}{50.13}$ for various fissioning systems. Open points refer to bombardments of $Au^{197}$, closed to bombardments of $Bi^{209}$. Bombarding projectiles are indicated as follows: ○ ●, $B^{11}$; △ ▲, $C^{12}$; □ ■, $N^{14}$; ▽ ▼, $O^{16}$. The vertical lines are from Ref. 3. The line is a smooth curve connecting the points from Ref. 3.

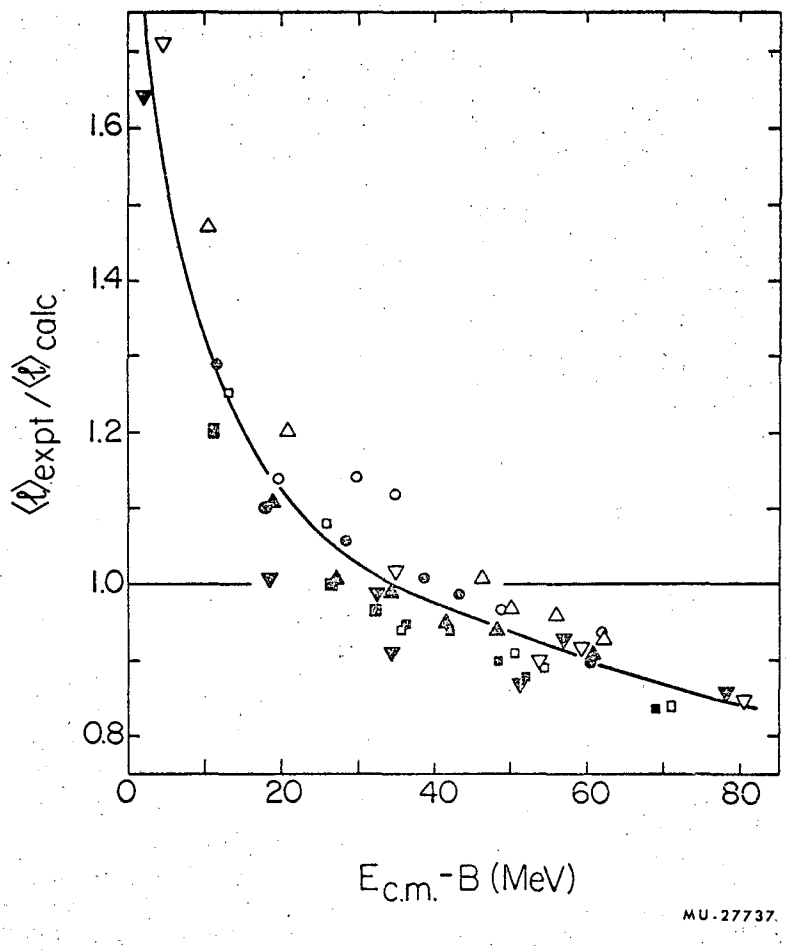


Fig. B.6-2. Ratio of experimental to calculated average angular momentum plotted against center-of-mass kinetic energy of the projectile in excess of the Coulomb barrier. The various symbols have the same significance as in Fig. B.6-1.

# 7. SPONTANEOUS FISSION OF THE HEAVIEST ELEMENTS(*)

Sven A. E. Johansson

The spontaneous-fission rates of nuclei with $Z \geq 98$ have been calculated. Deviations of these fission rates from the general trend predicted by the liquid-drop model are attributed to the fine structure of the single-particle level diagram. Our calculations reproduce the experimental values reasonably well, particularly the rapid drop in half-life with increasing neutron number just about neutron number 152. Contrary to previous predictions, our results show that this drop is a local effect and that the half-lives soon start to increase with increasing neutron number. Heavy, neutron-rich nuclei may therefore have considerable stability against spontaneous fission.

The predicted half-lives indicate that neither prolonged neutron irradiation nor heavy-ion bombardment is a very promising method of producing very heavy nuclei. The most promising method appears to be production by means of nuclear explosives.

The difficulty of predicting spontaneous-fission rates stems from the fact that they vary in a very irregular way, which is contrary to what one expects on the basis of the liquid-drop model. This author recently proposed a theory to account for these fluctuations.[1] They are assumed to be caused by the fine structure of the single-particle level diagram. By using this assumption, it was possible to account for the half-life systematics of the experimentally studied nuclei. The purpose of the investigation reported here was to extend this work to heavier nuclei, to predict half-lives in this region, and to use the predicted values in a discussion of the problems mentioned above.

The principles of the calculation have been described previously.[1] Essentially, the change of energy caused by addition of one or two nucleons to a given nucleus is determined from the single-particle level diagram. The irregular behavior of the spontaneous-fission rates is caused by the large fluctuations in level spacing. For details of the calculations the reader is referred to the previous paper.[1]

Depending on the type of nuclei considered we have several cases. The first is the even-even nuclei. Here we consider the addition of two protons or two neutrons to a given nucleus. As discussed previously, since the two extra nucleons are paired, they can move in the level diagram so that the total energy is minimized.[1] The influence of the extra nucleons on the barrier can then easily be found and the change in penetrability calculated.

In the case of odd nuclei the situation is different. Since the spin and parity of the nucleus has to be conserved, the odd nucleon cannot jump in the level diagram but must stay in its original orbit. For the nuclei of interest here this means that the addition of an odd nucleon increases the

---

*Brief version of UCRL-10474, Sept. 1962.

1. Sven A. E. Johansson, Nucl. Phys. 12, 449 (1959).

barrier height, and hence this can account for odd nuclei having considerably longer half-lives than neighboring even-even nuclei. In odd-proton nuclei, however, the situation is complicated by the Coulomb energy of the extra proton. Since the extra proton stays in the same level all the time, the charge distribution of this proton may be quite different from the total charge distribution of the nucleus.

Finally, there is the case of odd-odd nuclei. Here the odd proton and the odd neutron couple to give the total spin and parity of the nucleus. When the deformation increases there are various possible ways to change the proton-neutron configuration while conserving spin and parity. However, neither the level diagram nor the coupling rules are known well enough to permit a quantitative calculation. One would expect the half-life to fall between the values of neighboring odd-even and even-even nuclei.

The calculations were performed as described in the previous paper. However, since we are now interested in heavier nuclei, we must include more levels in the level diagrams. The neutron diagram is complemented by the levels 9/2+ [615], 1/2+ [880], 3/2+ [871], 5/2+ [862], and 1/2- [990]. In the proton diagram the levels affect slightly the calculations reported in the previous paper, but they do not change the basic features. However, they are essential for the present calculations. Some results of the calculations for even-even nuclei are shown in Fig. B.7-1 and Table I.

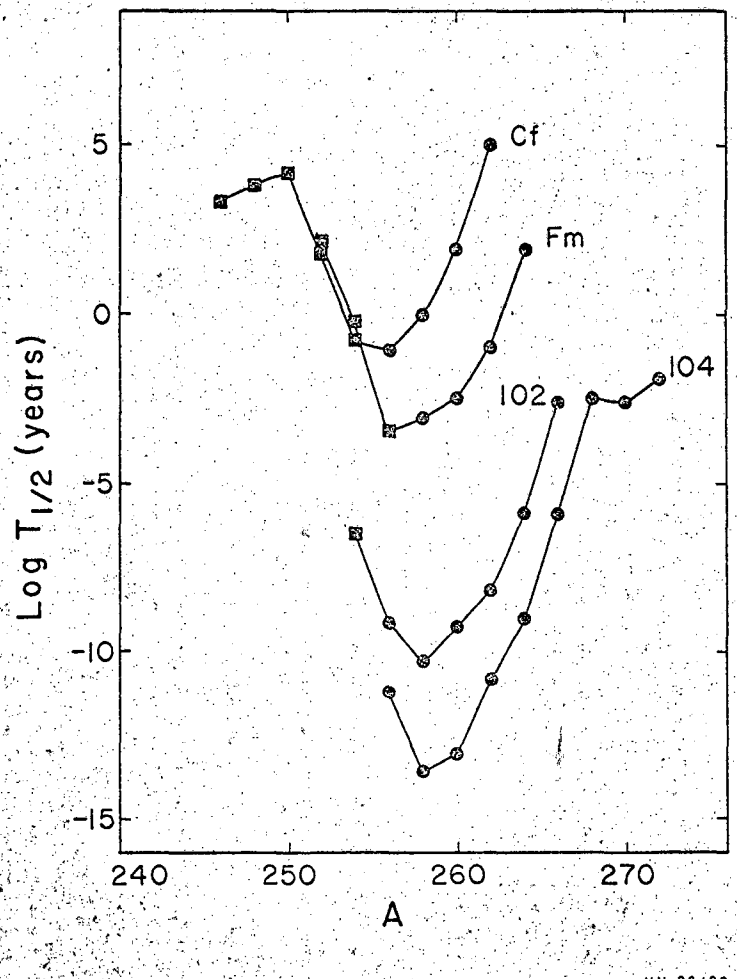


Fig. B. 7-1. Spontaneous-fission half-life of even-even isotopes of the elements Cf, Fm, 102, and 104: squares denote experimental values; circles predicted values.

Table I. Predicted half-lives for some even-even nuclei.

| Nucleus | Log $T_{1/2}$ (years) |
|---|---|
| $Cf^{256}$ | -1.1 |
| $Cf^{258}$ | -0.1 |
| $Cf^{260}$ | 1.9 |
| $Cf^{262}$ | 5.0 |
| $Fm^{258}$ | -3.1 |
| $Fm^{260}$ | -2.5 |
| $Fm^{262}$ | -1.0 |
| $Fm^{264}$ | 1.9 |
| $102^{256}$ | -9.2 |
| $102^{258}$ | -10.3 |
| $102^{260}$ | -9.3 |
| $102^{262}$ | -8.2 |
| $102^{264}$ | -5.9 |
| $102^{266}$ | -2.6 |
| $104^{256}$ | -11.2 |
| $104^{258}$ | -13.6 |
| $104^{260}$ | -13.1 |
| $104^{262}$ | -10.8 |
| $104^{264}$ | -9.0 |
| $104^{266}$ | -5.9 |
| $104^{268}$ | -2.5 |
| $104^{270}$ | -2.6 |
| $104^{272}$ | -1.9 |

# 8. DELAYED GAMMA RADIATION IN FISSION

Sven A. E. Johansson

Most of the gamma radiation accompanying the fission process is emitted within a time shorter than 1 nsec. Some preliminary measurements indicate that the lifetime is of the order of 0.06 nsec. However, it has been found that a portion of the gamma radiation has a considerably longer lifetime, of the order of 25 nsec. The properties of this delayed radiation have been investigated in some detail.

The experimental arrangement consists of an evacuated chamber containing a $Cf^{252}$ source and two solid-state fission detectors. The pulses from the fission detectors are fed to a circuit which divides the two pulses. It is easily shown that the output pulse from this circuit is proportional to the mass ratio of the fragments. The gamma radiation is recorded by means of a sodium iodide spectrometer. Triple coincidences between the two fission counters and the gamma spectrometer were used to gate a multichannel analyzer which recorded either the mass-ratio distribution or the $\gamma$-ray spectrum. When a lead absorber is placed above one of the fission counters the delayed gamma radiation recorded in the experiments comes only from the fragment that is detected in the other fission counter. Hence it is possible to determine not only the mass ratio but also the mass of the fragments emitting delayed gamma radiation.

The time distribution of the gamma radiation was investigated in two ways. First the standard technique of delayed coincidences was used. The delay curves show a tail with an almost pure exponential decay having a half-life of about 25 nsec. In order to get an independent check a time-of-flight method was also used. The $\gamma$-ray counter was shielded in such a way that the fragments had to travel a certain distance before the emitted $\gamma$ rays could reach the counter. This completely eliminated the prompt peak, but the delayed radiation was still observed. This shows that the tail in the delay curve is real and not an instrumental effect. The amount of delayed radiation was found to be about 5% of the total gamma radiation. The lifetime was determined for different mass ratios and was found to vary between 20 and 30 nsec.

The mass distribution of the fission fragments emitting delayed gamma radiation shows a very pronounced structure. Most of the radiation comes from two regions. One is in the light fragment for A = 95 to 110. The other in the heavy fragment for A > 150.

The energy spectra of the delayed radiation was recorded for different masses. Figure B. 8-1 shows energy spectra corresponding to the heavy region (A > 150) and the light region (A = 95 to 110), respectively. It is interesting to note that these spectra are quite different from the spectra of the prompt radiation. They show a pronounced structure with well-defined peaks.

In the interpretation of these delayed $\gamma$ rays one possible assumption is that they are ordinary isomeric transitions. However, this explanation encounters great difficulties. Since the radiation must be emitted from many different nuclei it is difficult to explain the structure in the energy

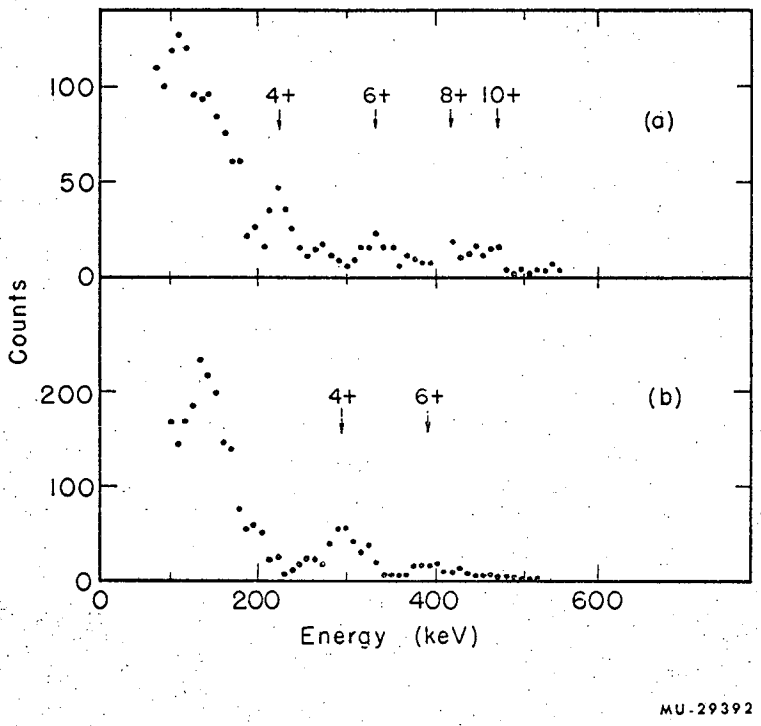


Fig. B.8-1. Delayed γ-ray energy spectrum for (a) heavy-fragment region (A > 150), (b) light-fragment region (A = 95 to 110).

spectra and the well-defined half-life. A possible explanation is suggested by the fact that most of the radiation is associated with deformed fragments. Fragments with A > 150 are certainly deformed. In the region A = 95 to 110 nothing is known experimentally about the nuclear shape, but the fission fragments having these masses are close to a region where one would expect a stable nuclear deformation to occur. Typical transitions in deformed nuclei are the rotational transitions. There is some evidence that fission fragments are formed with a high spin. In such a case it is likely that the gamma de-excitation takes place via the rotational band, for example $10 \rightarrow 8 \rightarrow 6 \rightarrow 4 \rightarrow 2 \rightarrow 0$ in even-even nuclei. It is then very tempting to identify the peaks in Fig. B. 8-1 with rotational de-excitation. In this figure the calculated energies for the transition from different rotational levels have been indicated. As can be seen the agreement is quite good. These data give the first indications of a new region of deformed nuclei with $Z \approx 42$ and $N \approx 62$. They also give information about how the parameters in the expression for the rotational energies vary with mass.

It is rather difficult to say anything with certainty about the mechanism responsible for the delay. It is probably of a general nature, because the half-life is almost independent of mass. A possible explanation, for even-even nuclei, is that the delay is caused by the rearrangement when the nucleus goes from higher excited states to the ground-state rotational band. The experimentally observed radiation agrees with the order of magnitude of theoretical estimates.

## 9. LONG-RANGE α PARTICLES EMITTED IN THE SPONTANEOUS FISSION OF CALIFORNIUM-252

Zeev Fraenkel

A triple-coincidence experiment was performed on the properties of ternary fission of $Cf^{252}$ in which one of the fragments is a high-energy α particle. The experimental arrangement is shown in Fig. B. 9-1. It consisted of a fission chamber, approximately 1 ft in diameter, which contained the source and the solid-state detectors. The source consisted of a 100-$\mu g/cm^2$ Ni foil on which $Cf^{252}$ was transferred by the self-transfer method. The source strength was $1.54 \times 10^7$ fissions per min. The α-particle detector consisted of two Li drifted detectors. A 16-$mg/cm^2$ Au absorber foil was placed in front of the α-particle detectors in order to absorb the 6.1-MeV α particles from the α decay of $Cf^{252}$. The two fission-fragment detectors consisted each of two guard-ring P-diffused solid-state detectors 1 cm in diameter.

These results were analyzed with the aid of a multidimensional analyzer and a computer. The α particles were found to be sharply peaked at approximately 90° with respect to the fission fragments. The most probable alpha energy is approximately 16 MeV. The shape of the alpha spectrum was found to be only slightly dependent on the angle with respect to the fission fragments. The most probable total fission-fragment energy is 172 MeV, as compared with 181 MeV for binary fission of $Cf^{252}$. The total

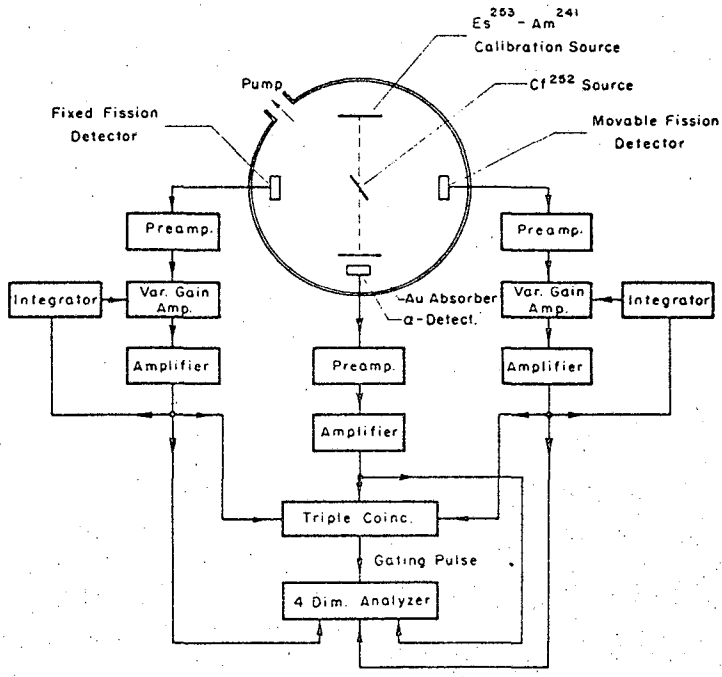


Fig. B. 9-1. Experimental arrangement used in study of $Cf^{252}$ fission.

fission-fragment energy distribution was found to be independent of the alpha energy and the angle of the α particle, and is narrower than the distribution in binary fission. The most probable mass ratio was found to be 1.30, and again the mass-ratio distribution for long-range alpha fission is narrower than the same distribution in binary fission.

All the experimental results can be explained by a simple model which assumes that fission accompanied by the emission of a high-energy α particle does not differ from binary fission up to the point of scission, at which the α particle is emitted and the fission fragments separate. This means that the α particles may be used as an internal "probe" of the configuration of the nucleus at the point of scission.

A complete report of this work is being prepared for publication.

## 10. THE ENERGY AND MASS DISTRIBUTION IN SPONTANEOUS FISSION(*)

Reinhard Brandt, Stanley G. Thompson, Raymond C. Gatti, and Llad Phillips

### Summary

A back-to-back semiconductor counter system was used to study the energy and mass distribution of the fragments in the spontaneous fission of $Fm^{254}$, $E^{253}$, $Cf^{252}$, $Cf^{250}$, and $Cm^{248}$. The results are compared with the spontaneous-fission properties of $Cf^{252}$, which is used as a standard.

All distributions (including those of the odd-mass isotope $E^{253}$) are rather similar to but not identical with the standard. The mean total kinetic energy of the fragments increases with A. The asymmetry of the mass distribution shows only small differences between the isotopes. The variances (widths) of all distributions increase with Z and seem to increase with A.

### Experimental Procedures

The production, isolation, and purification of $Fm^{254}$, $E^{253}$, $Cf^{250}$, and $Cm^{248}$ have been reported previously.[1, 2] The purified samples were electroplated on 5-μin.-thick Ni foils and then placed between two back-to-back phosphorus-diffused silicon solid-state detectors. In this case the

---

*Brief form of report (UCRL-10506, 1962) being prepared for submission to Phys. Rev.

1. R. Brandt, R. C. Gatti, L. Phillips, and S. G. Thompson, in Chemistry Division Annual Report, UCRL-10023, Jan. 1961, p. 66.

2. Reinhardt Brandt, Spontaneous Fission of Some Heavy Isotopes (Ph. D. Thesis), UCRL-10481, Sept. 1962.

energies of both fission fragments from a single fission event could be recorded in coincidence. With standard electronic equipment it was possible to store on paper tape the binary equivalents of the energies of both fragments in a fission event. Later the information was transferred to magnetic tape, and it was possible to calculate with the aid of an IBM 7090 computer the masses of the fission fragments together with the total kinetic energy release. It was thus possible to compute the single-fragment energy distribution, the mass distribution, and the total kinetic energy distribution in the spontaneous fission of the above-mentioned isotopes. The mean value of all distributions, as well as the variance (width) were also computed. The fission fragments of the spontaneous fission in $Cf^{252}$ were used for the energy calibration of the solid-state detectors, since the energy distribution of the fission fragments of $Cf^{252}$ has been determined by time-of-flight measurements.[3]

## Results and Discussion

The essential results of this study can be summarized as follows:

a. The energy and mass distributions are rather similar (but not identical) for all the isotopes investigated here.

b. The mean prompt kinetic energy release of fission fragments increases with Z. This agrees with the findings of Viola and Sikkeland.[4]

c. All mass-yield curves show a strong asymmetric mass distribution. In agreement with previously observed trends, the mean heavy-fragment mass is always around 142 ± 1, whereas the light-fragment mass shows more variation.

d. The behavior of the fission fragments in the spontaneous fission of $E^{253}$ resembles very closely that of the neighboring even-even nuclei. (It should be noted that this is the first work in which the mass and energy distributions in the spontaneous fission of an odd-mass isotope have been investigated.)

In discussing the theoretical interpretation of those experimental results, it seems useful to restrict ourselves here to one semi-emperical correlation. In order to allow the interpretation of the mean prompt total kinetic energy release, $\langle EK \rangle$, on the basis of the liquid-drop model of fission, Swiatecki suggested that the ratio $\langle EK \rangle / E_s^0$ should be shown as a function of X, the well-known fissionability parameter[4, 5] ($E_s^0 = 17.81 \times A^{2/3}$; this is the nuclear surface energy). In Fig. B. 10-1 this correlation is shown. In order to compare the results of this work with other experiments of the same kind, it seemed useful to show also in Fig. B. 10-1 the straight line of Viola et al. They found that this line represents the trend in the variation of $\langle EK \rangle / E_s^0$ with X when all experimentally known cases for total kinetic energy releases are considered.

---

3. J. C. D. Milton and J. S. Fraser, Phys. Rev. 111, 877 (1958).
4. V. E. Viola and T. Sikkeland, UCRL-10284 (Aug. 1962).
5. W. J. Swiatecki (Lawrence Radiation Laboratory), private communication.

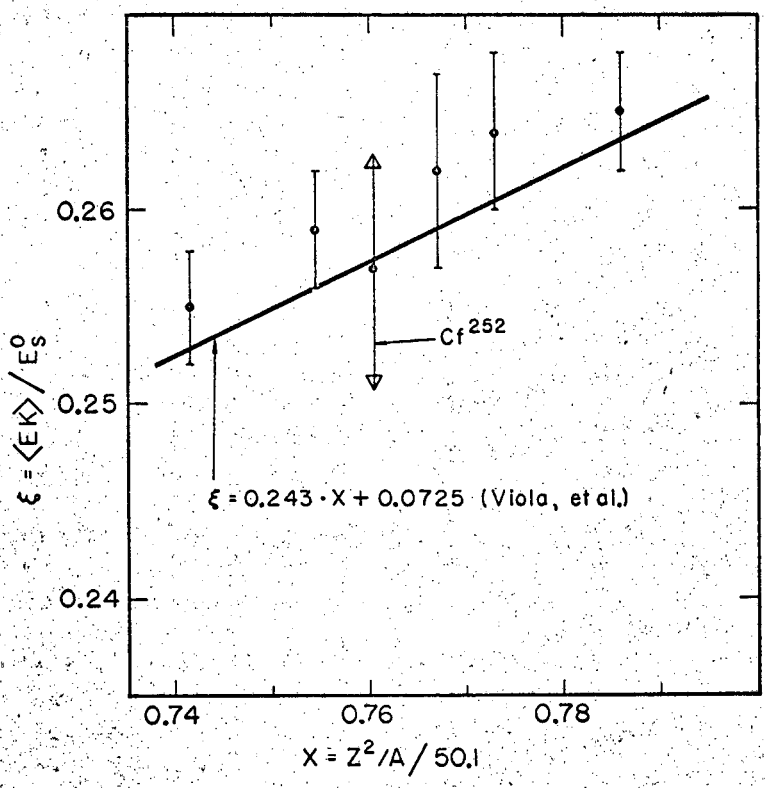


Fig. B.10-1. The mean total prompt energy release $\langle EK \rangle$ is represented by $\xi = \langle EK \rangle / E_s^0$ ($E_s^0 = 17.81 \cdot A^{2/3}$, the nuclear surface energy) and shown as a function of X.

## 11. MASS-ENERGY RELATIONS IN THE FISSION OF HIGHLY EXCITED HEAVY NUCLEI(*)

Eldon L. Haines and Stanley G. Thompson

Mass-energy relations in the fission of the compound $Fm^{254}$ have been studied at excitation energies in the range 58 to 116 MeV. This compound nucleus was produced by bombardments of $Th^{232}$, $U^{238}$, and $Pu^{252}$ with the heavy ions $Ne^{22}$, $O^{16}$, and $C^{12}$, respectively. The kinetic energies of the two fission fragments from each event were measured by use of semi-conductor detectors. From these energies, the masses and total kinetic energies were calculated. The mass distributions were studied as a function of the total kinetic energy. The bell-shaped mass distributions narrowed rapidly as the kinetic energies of the fragments increased. The quantitative behavior of this narrowing suggests that most of the initial excitation energy of the compound nucleus is not available either for conversion into kinetic energy of the fragments or for production of asymmetric mass divisions that are energetically unfavorable.

---

*Abstract of paper based on Haines's thesis, UCRL-10342, June 1962.

## 12. FURTHER STUDIES OF SPONTANEOUS FISSION HALF-LIVES OF SOME CALIFORNIUM AND FERMIUM ISOTOPES

R. C. Gatti, R. Brandt, L. Phillips, and S. G. Thompson

### Summary

Relatively large amounts of short-lived fermium and californium isotopes were made available by the recent chemical processing of curium isotopes re-irradiated at the MTR. In continuation of some work reported previously[1] it was possible to detect a new 11-day fermium activity by its spontaneous-fission decay[2] and to remeasure the spontaneous-fission half-lives of $Cf^{254}$ ($t_{1/2}$ = 60.5 ± 0.2 days) and $Cf^{250}$ ($t_{1/2} = 1.73 \pm 0.6 \times 10^4$ y).[3]

### Experimental Procedures and Results

The production of $Cf^{254}$ is described elsewhere.[1] $Cf^{250}$ was obtained by milking a several-year-old source of $E^{254}$ ($t_{1/2}$ = 480 d). The new 11-day fermium activity was found in the original fermium fraction, which was

---

1. R. Brandt, R. C. Gatti, L. Phillips, and S. G. Thompson, in Chemistry Division Annual Report, 1961, UCRL-10023, Jan. 1962, p. 66.

2. Raymond C. Gatti, Reinhardt Brandt, Llad Phillips, and Stanley G. Thompson, The Discovery of a New Fermium Isotope (UCRL-10456, Sept. 1962), submitted to J. Inorg. Nucl. Chem.

3. Llad Phillips, Raymond C. Gatti, Reinhardt Brandt, and Stanley G. Thompson, Spontaneous-Fission Half-Lives of $Cf^{254}$, $Fm^{255}$, and $Cf^{250}$ (UCRL-10464, Sept. 1962), submitted to J. Inorg. Nucl. Chem.

isolated during the chemical processing of the re-irradiated curium sample. All samples were isolated and purified by the use of standard chemical procedures.[4] The spontaneous-fission half-life of $Cf^{254}$ was redetermined by following its spontaneous-fission decay over a period represented by four half-lives. A least-squares analysis of the $Cf^{254}$ data yields a half-life of 60.5 ± 0.2 days. This result includes a correction for the spontaneous-fission activity due to a small amount of $Cf^{250}$ (1.3%), which was also present in the source. The possible implications of this new spontaneous-fission half-life of $Cf^{254}$ in astrophysical problems are discussed elsewhere.[2, 5]

The redetermined value for the spontaneous fission half-life of $Cf^{250}$ was obtained by measuring the alpha/fission ratio in an isotopically pure $Cf^{250}$ sample with a windowless proportional counter. The measured value for this alpha/fission ratio is (1330 ± 45). Based on a 13-y alpha half-life for $Cf^{250}$,[6] the calculated spontaneous-fission half-life of this isotope is $(1.73 \pm 0.06) \times 10^4$ y.

The new 11-day fermium activity was observed in the original fermium fraction of a curium sample re-irradiated at the MTR. Its spontaneous fission activity was observed (Fig. B. 12-1) with two different counting systems. One was a windowless proportional counter. The other system consisted of a solid-state detector, with which spontaneous fission events could be recorded on a pulse-height analyzer. A least-squares analysis of the spontaneous fission decay yielded a half-life of 10.8 days with a standard deviation of about $^{+2.2}_{-1.8}$ days. An estimated half-life of $11^{+10}_{-6}$ days is reported here on the basis of approximately 50 fission events observed on the fermium sample. The mass of this new 11-day fermium activity is uncertain, but limited to A = 258 or 257.

---

4. S. G. Thompson and L. Muga, Proceedings of the Second International Conference on the Peaceful Uses of Atomic Energy, Geneva, 1958 (United Nations, New York, 1959), Paper P/825.

5. Reinhardt Brandt, Spontaneous Fission of Some Heavy Isotopes (Ph. D. Thesis), UCRL-10481, Sept. 1962.

6. H. Diamond (Argonne National Laboratory), private communication.

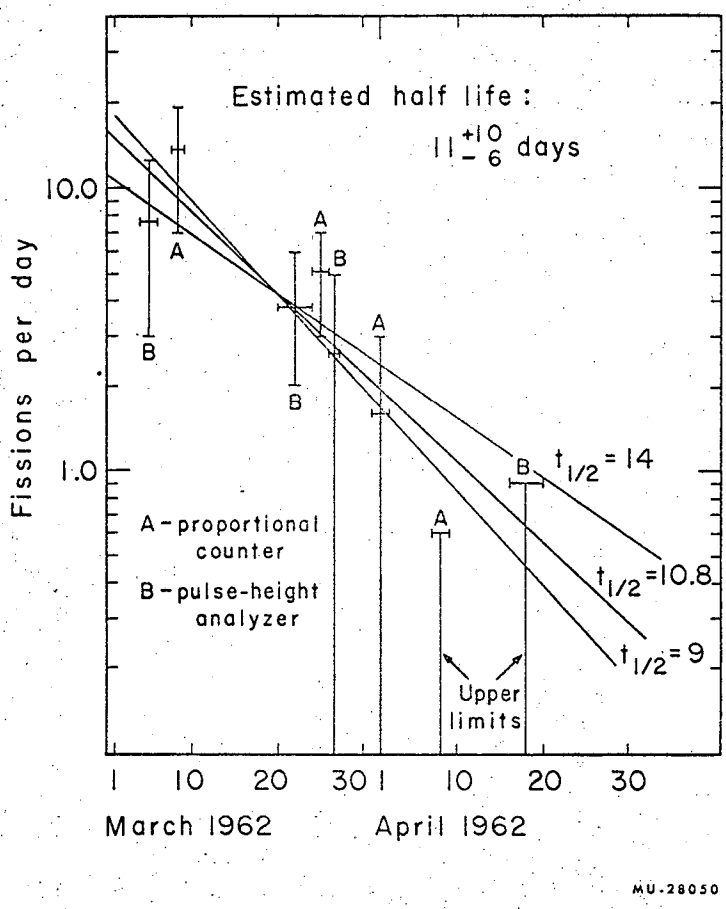


Fig. B. 12-1. Decay of the new Fm isotope. Approximately 50 events have been directly observed. The activity is calculated from the observed events and the geometry factor. Two different sets of counters were used. The background is subtracted.

# 13. FISSION-FRAGMENT KINETIC ENERGY MEASUREMENTS AT MEDIUM EXCITATION ENERGY

Donald S. Burnett and Stanley G. Thompson

Two-dimensional measurements of fission-fragment kinetic energies for $Au^{197}$, $Bi^{209}$, $U^{238}$, and $Th^{232}$ have been made with semiconductor detectors, using the 65-MeV α-particle beam of the 88-inch cyclotron. Preliminary treatment of the data has been carried out by using an energy calibration which assumes a linear pulse-height energy relationship for fission fragments of $Cf^{252}$ in which the coefficients were assumed to be independent of mass. To obtain final values a more sophisticated calibration method will probably be necessary.

The Au and Bi total kinetic energy results were of special interest because they could be compared with the liquid-drop calculations by Nix.[1] In these calculations the fissioning nucleus is approximated as two collinear symmetric spheroids, a system for which the deformation energy can be described by two coordinates. The saddle-point shapes for this model are tangent spheroids and approximate the exact liquid-drop shapes of Cohen and Swiatecki.[2] Consequently the calculations would be expected to hold for the Bi and Au cases, but not necessarily for U and Th.

Two methods of calculating the total kinetic energy release within the framework of the model give good agreement with experiment:

Method A. The spheroids are started from the saddle point and allowed to separate. A dynamical calculation of the shape of the total kinetic energy distribution is made which allows the width of the distribution as well as the most probable value to be calculated. The spheroids are assumed nonviscous; hence the observed fragment kinetic energy is less than the initial Coulomb interaction energy, since some of the interaction energy (approx 10 MeV) goes into oscillation of the separating fragments.

Method B. This is a static calculation in which the spheroids are separated rather than tangent in the initial configuration. The reason for doing this is that, even though the model approximates the exact liquid-drop saddle shapes, it gives a saddle-point energy higher than that of the exact calculations. The separation of the spheroids is thus chosen to correspond to the proper saddle-point energy. If we further assume that the spheroids are viscous, then the final total kinetic energy is just the initial interaction energy. If the spheroids are assumed nonviscous, then the results are 8 to 10 MeV lower than shown here.

The experimental and calculated results for symmetric fission are compared in Table I. The calculated values are labeled according to their above description. The experimental most probable values have been corrected for the mass loss due to the emission of neutrons. Two experimental widths are given. Column 6 gives the observed width after an

---

1. J. R. Nix (Lawrence Radiation Laboratory), private communication.

2. Stanley F. Cohen and Wladyslaw J. Swiatecki, The Deformation Energy of a Charged Drop. Part V. Results of Electronic Computer Studies, UCRL-10450, Aug. 1962.

approximate correction, assuming Gaussian distributions, for the neutron dispersion. There are certainly other dispersions in the data, so the experimental results are expected to be larger than those calculated; however, the calculated widths are 15 to 20% larger. Everything considered, the agreement is quite satisfactory.

The U and Th results are shown for comparison. The agreement between theory and experiment is about the same as in the Bi and Au cases, although the theory was not ecpected to hold in this region. The agreement may not be significant, but this is an unexciting possibility. If one were more speculative, the agreement could be considered to be an indication that, experimentally, symmetric fission in the U-Th region resembles the symmetric fission of the lighter elements. It has been suggested that symmetric fission occurs by a different mechanism than asymmetric fission, with the symmetric mechanism dominant in the lighter elements (the "two-mode" hypothesis). The above results could be analyzed in the same spirit: namely, the calculations are expected to work for the symmetric mode, so if the symmetric fission in the U-Th region is due to the symmetric mode, then the calculations may be appropriate for it also. For this type of analysis, comparison of the U-Th data at various excitation energies would be interesting.

Table I. Experimental and calculated results.

| Target | $Z^2/A$ | Most probable total kinetic energy | | | Full width at half maximum | | |
|---|---|---|---|---|---|---|---|
| | | Exptl. | (A) Tangent nonviscous | (B) Separated viscous | Exptl. | Exptl. (Corr) | (A) Tangent nonviscous |
| $Au^{197}$ | 32.7 | 143 | 143 | 142 | 20 | 17.7 | 19.2 |
| $Bi^{209}$ | 34.0 | 156 | 151 | 151 | 18 | 15.6 | 19.3 |
| $Th^{232}$ | 36.0 | 171 | 166 | 167 | 24 | 22.1 | 23.2 |
| $U^{238}$ | 37.3 | 175 | 170 | 172 | 26 | 23.7 | 23.7 |

## 14. FURTHER STUDIES OF THE PROMPT NEUTRONS FROM THE SPONTANEOUS FISSION OF CALIFORNIUM-252(*)

Harry R. Bowman, J. C. D. Milton,† Stanley G. Thompson, and Wladyslaw J. Swiatecki

The results of previous measurements of the velocity and angular distributions of neutrons associated with light and heavy groups of fission fragments from spontaneous fission of $Cf^{252}$ have been reported.[1] Further calculations using the same data allowed more information to be obtained concerning the details of the fission process in $Cf^{252}$. The energy spectra and angular distributions of neutrons emitted by pairs of fragments of different degrees of asymmetry and different kinetic energies, as recorded in the laboratory system, have been analyzed for consistency with the hypothesis of isotropic emission from fully accelerated fission fragments.

The center-of-mass energy spectra of the neutrons, when these are assumed to be emitted isotropically from moving fragments, have been found to be representable, within fairly narrow limits, by a standard shape. Given this shape, the neutron distribution may be specified by the number $\nu$ of neutrons emitted by a fragment and the average energy $\langle\eta\rangle$. The two quantities $\nu$ and $\langle\eta\rangle$ have been analyzed as functions of the mass number A of a fragment and the kinetic energy $E_K$ as a fragment pair, and the detailed results are presented in a series of tables and graphs. The variation of $\nu$ with A shows the "sawtooth" dependence found in earlier experiments, which may be studied in greater detail on the basis of our results. In contrast, the dependence of $\langle\eta\rangle$ on A does not show a discontinuity in the region of symmetrical mass splits, the values of $\langle\eta\rangle$ being always approximately equal for the two members of a fragment pair.

---

*Brief form of paper (UCRL-10139 Rev, May 1962) submitted to Phys. Rev.

†On leave from Atomic Energy of Canada, Limited, Chalk River, Ontario.

1. Harry R. Bowman, Stanley G. Thompson, J. C. D. Milton, and Wladyslaw J. Swiatecki, Velocity and Angular Distributions of Prompt Neutrons from Spontaneous Fission of $Cf^{252}$, Phys. Rev. 126, 2120 (1962).

## 15. DEFORMATION ENERGY OF A CHARGED ROTATING DROP

Stanley F. Cohen, Franz Plasil, and Wladyslaw J. Swiatecki

The quantitative studies of the properties of saddle-point shapes of a uniformly charged drop possessing a sharp surface[1] have been extended to the case of the rotating drop. The total energy of the drop is now made up of three parts, the rotational energy being considered along with the electrostatic and surface energies. A dimensionless parameter y is used to

---

1. Stanley F. Cohen and Wladyslaw J. Swiatecki, The Deformation Energy of a Charged Drop. Part V. Results of Electronic Computer Studies, UCRL-10450, Aug. 1962.

specify the magnitude of the rotational relative to the surface energy. It is analogous in definition to x, which specifies the magnitude of Coulomb energy relative to surface energy.[1] The expression for $\xi$, the relative deformation energy in units of surface energy of the sphere, $E_s^0$, has been modified to include a term in y and $B_R$. $B_R$ is by analogy to $B_S$ and $B_C$ of reference 1 the rotational energy in units of its value for the spherical configuration. Thus:

$$B_R = \frac{E_R}{E_R^0} = \frac{L^2/2\Im}{L^2/2\Im_0} = \frac{\Im_0}{\Im}$$

and

$$y = \frac{E_R^0}{E_s^0} ,$$

where $\Im$ and $\Im_0$ are the moments of inertia of the distorted drop and the spherical drop respectively.

The only approximation in these calculations is the restriction to axially symmetric shapes, i.e., shapes having two out of three axes equal. The error is believed to be serious only when the shape has three widely different axes. This is expected to take place in a rather narrow region of high x values.

The ground state corresponding to a given saddle configuration is obtained either by rotating the drop about the axis of axial symmetry (referred to as Hiskes shapes) or by rotating it about the axis perpendicular to the axis of symmetry (Beringer-Knox shapes). In the former there is no approximation involved, in the latter the approximation described above holds. The saddle-point shapes, which involve rotation about the axis perpendicular to the axis of symmetry, shall be referred to as Pik-Pichak shapes.

The IBM 7090 FORTRAN program used in reference 1 has been modified for this work. For the Pik-Pichak shapes the calculation is carried out in discrete steps of y for a given x. Values for the y = 0 case from reference 1 were used as starting points in this calculation. The sphere at y = 0 was the starting point for Beringer and Hiskes shapes. A typical result (x = 0.5) is given in Fig. B. 15-1. The ground state for this case takes the form of Hiskes shapes for values of y between 0 and 0.12. Beyond, the Beringer-Knox shape becomes more stable than the Hiskes shape. At y = 0.18 the limit is reached beyond which stable rotating liquid drops cease to exist.

This limit of stability, the relative stability of the Beringer-Knox shapes, and the region of stability to asymmetric deformations (a byproduct of the computer calculations) are of experimental interest.

Figure B. 15-2 shows the above limit of stability in the x-y plane beyond which the centrifugal force would disrupt the nucleus and compound-nucleus formation is not expected to take place. A simple correlation could

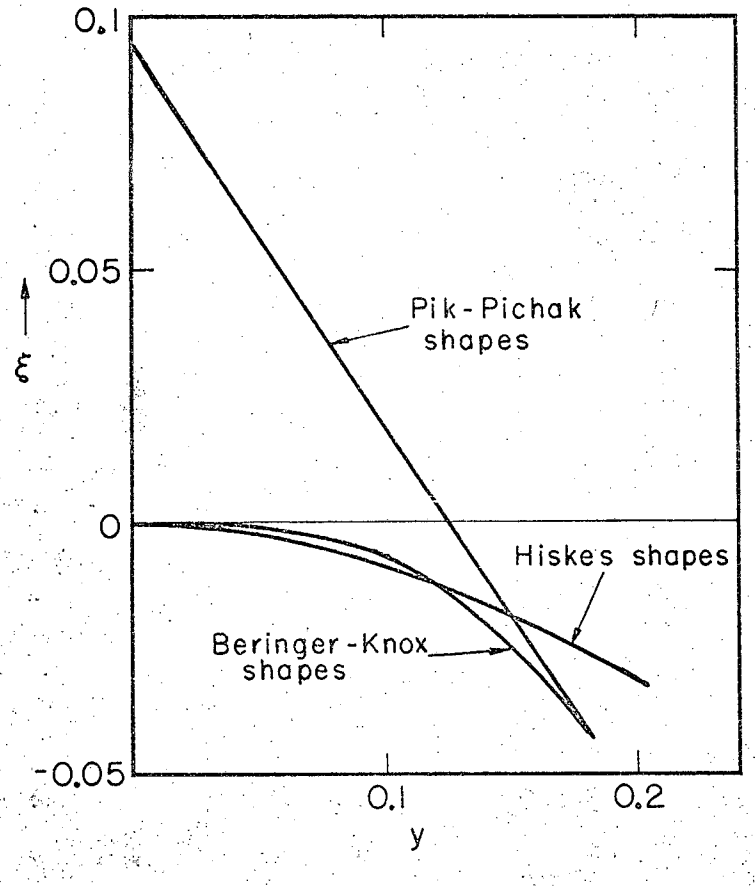


Fig. B. 15-1. Variation of deformation energy with the rotational parameter y for three families of equilibrium shapes.

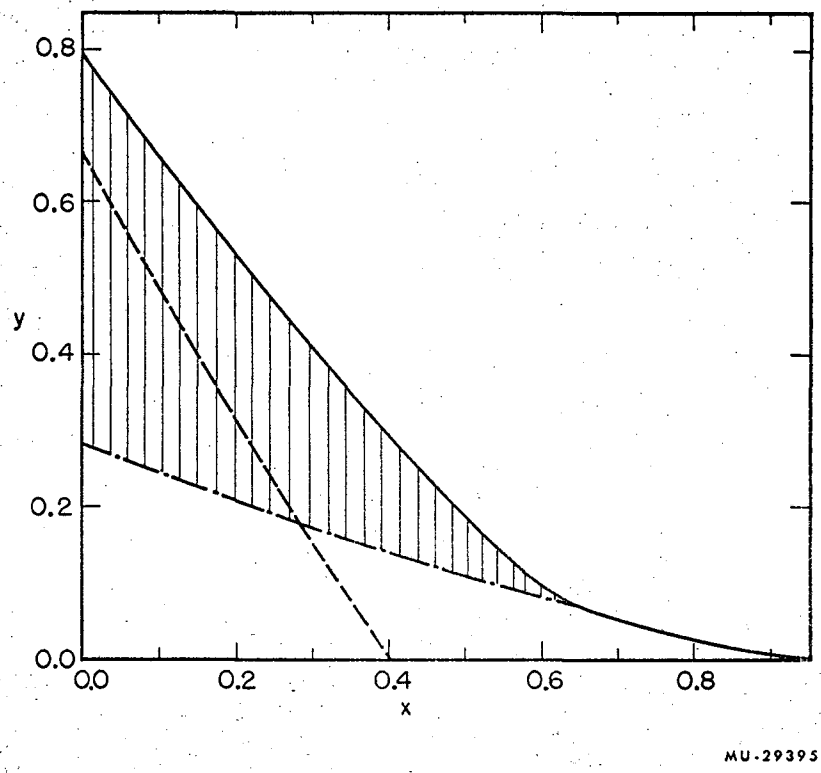


Fig. B. 15-2. Limits of stability beyond which

——— rotating drop is unstable,

—·—·— Beringer-Knox shapes are stable relative to Hiskes shapes,

------- drop is stable to small asymmetric deformations.

Shaded area gives region of stability of elongated Beringer-Knox shapes.

be made between this limit and the extent of incomplete momentum transfer in fission reactions of heavy elements induced by heavy ions.[2]

The shaded area of Fig. B. 15-2 is the region in which stable elongated Beringer-Knox ground states exist. These are stable with respect to fission, and because of their very high moments of inertia, these states could possibly be detected experimentally. This would be a valuable confirmation of liquid-drop theory.

---

2. Momentum Transfer in Heavy-Ion-Induced Fission, T. Sikkeland, E. L. Haines, and V. E. Viola, Jr., Phys. Rev. 125, 1350 (1962).

## C. NUCLEAR REACTIONS

### 1. QUASI-ELASTIC SCATTERING: EXCITATION FUNCTION FOR THE $C^{12}(\pi^-, \pi^-n)C^{11}$ REACTION(*)

Paul L. Reeder and Samuel S. Markowitz

The excitation function for the reaction $C^{12}(\pi^-, \pi^-n)C^{11}$ was measured from 53 to 1610 MeV by bombarding targets of plastic scintillator with pions. The intensity of the pion beam was monitored with a two-counter telescope and 40-Mc scaling system. The scintillator target was mounted on a photo-tube and became the detector for the $C^{11}$ positron activity. Corrections were made for muon contamination in the beam, coincidence losses in the monitor system, $C^{11}$ activity produced by stray background at the accelerator, $C^{11}$ activity produced by secondaries in the target, and the efficiency of the $C^{11}$ detection system.

The $C^{12}(\pi^-, \pi^-n)C^{11}$ cross sections rise to a peak of about 70 mb at 190 MeV, which corresponds to the resonance in free-particle scattering at 190 MeV. Calculations based on a "knock-on" collision mechanism[1] and sharp-cutoff nuclear density reproduce the shape of the experimental excitation function, but the magnitudes of the calculated values are low by a factor of six. The calculation shows that the $C^{12}(\pi^-, \pi^-n)C^{11}$ reaction occurs in the nuclear surface region at all bombarding energies. The contributions to the $(\pi^-, \pi^-n)$ reaction predominate on the front surface of the nucleus in order to give the pion the maximum probability of escaping.

The experimental setup is illustrated in Figs. C. 1-1 and C. 1-2 for those bombardments carried out at the 184-inch cyclotron. The $\beta^+$ spectrum due to the induced $C^{11}$ is shown in Fig. C. 1-3.

The cross sections are presented in Table I and displayed in Fig. C. 1-4.

A calculation based on the assumption that the pion interacts with a single neutron in the $C^{12}$ nucleus was carried out. In Fig. C. 1-5 a schematic representation of a $(\pi^-n)$ collision in $C^{12}$ is shown. By dividing the nuclear volume we are able to calculate that part of the volume which contributes to the $(\pi^-, \pi^-n)$ reaction; the results of the "localization" calculations are shown in Fig. C. 1-6.

---

*Brief version of a report: Paul L. Reeder, Nuclear Reactions Induced by Pions and Protons (Ph. D. thesis), UCRL-10531, Sept. 1962; also Bull. Am. Phys. Soc. 8, 69 (1963); also Paul L. Reeder and Samuel S. Markowitz, Quasi-Elastic Scattering in $C^{12}(\pi^-, \pi^-n)C^{11}$ Excitation Function, UCRL-10548 Abs. Nov. 1962; (full paper submitted to Phys. Rev.)

1. S. S. Markowitz, F. S. Rowland, and G. Friedlander, Phys. Rev. 112, 1295 (1958).

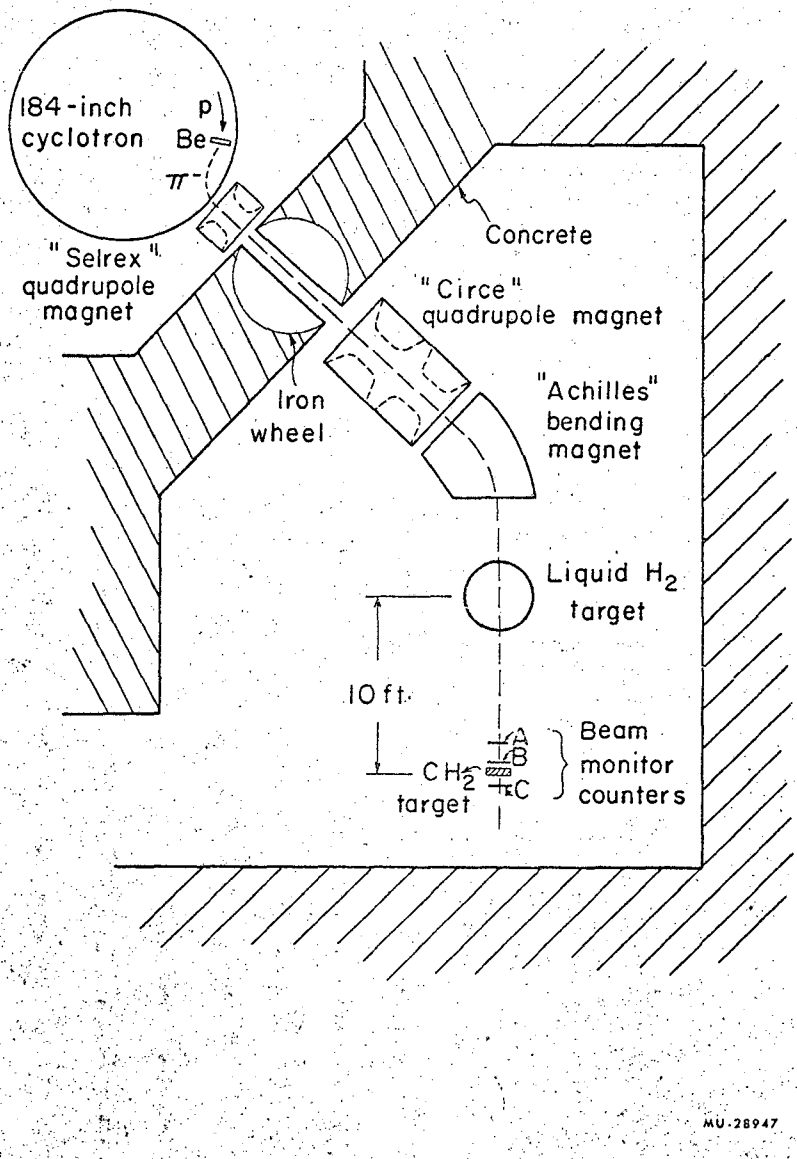


Fig. C. 1-1. Experimental setup at 184-inch cyclotron for 380-MeV $\pi^-$ beam.

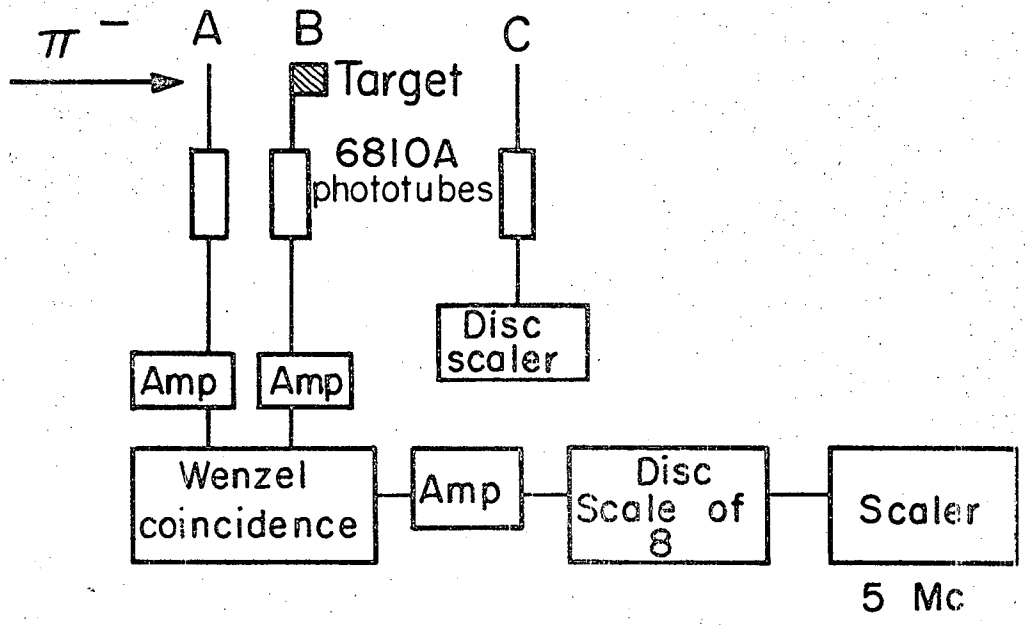


Fig. C. 1-2. Electronics for 40-Mc beam-monitor system.

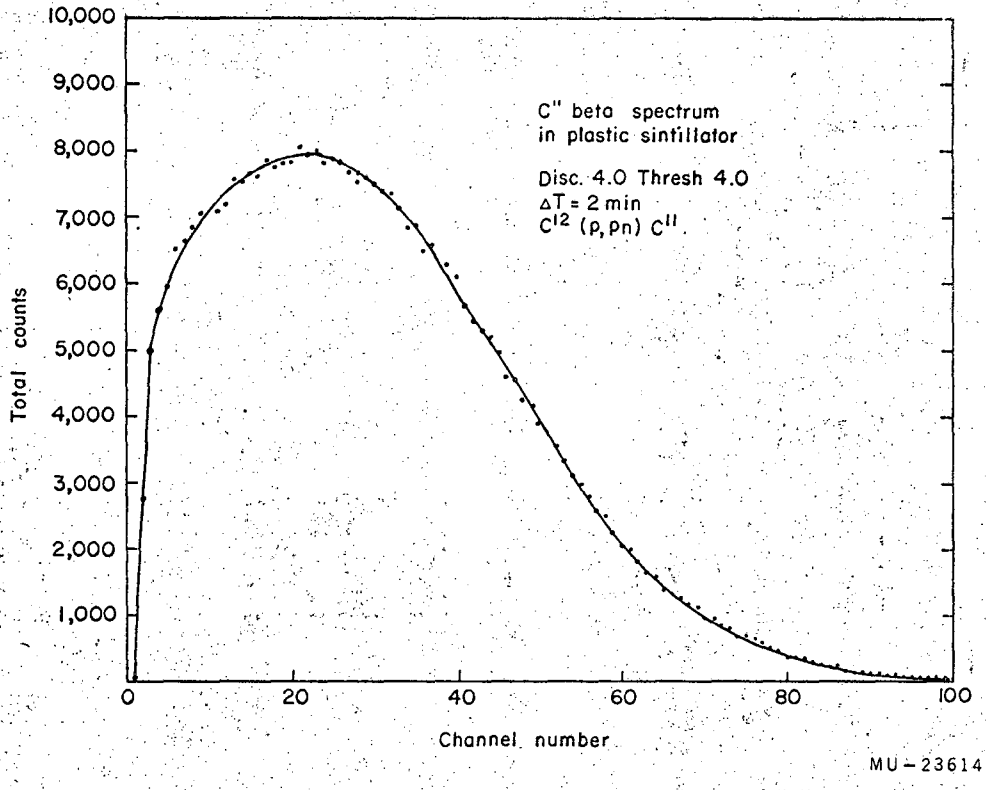


Fig. C. 1-3. $C^{11}$ β spectrum in plastic scintillator. The arrow refers to the discriminator cutoff for the scaler.

Table I. Cross section for the reaction $C^{12}(\pi^-, \pi^-n)C^{11}$

| Incident-pion energy (MeV) | Cross section (mb) | Number of bombardments |
|---|---|---|
| 53 ± 5 | 3 ± 2 | 1 |
| 60 ± 6 | 11 ± 2 | 2 |
| 80 ± 8 | 39 ± 3 | 2 |
| 127 ± 11 | 56 ± 4[a] | 3 |
| 179 ± 10 | 68 ± 6 | 3 |
| 212 ± 10 | 68 ± 6 | 3 |
| 245 ± 10 | 61 ± 6 | 3 |
| 304 ± 9 | 42 ± 4 | 3 |
| 342 ± 10 | 37 ± 4 | 2 |
| 373 ± 10 | 30 ± 3 | 3 |
| 423 ± 10 | 26 ± 8 | 4 |
| 1610 ± 20 | 21 ± 5[b] | 1 |

[a] Pion beam monitored by means of a calibrated ion chamber.

[b] Counter telescope not used for this cross section. Pion intensity calculated from data supplied by Segrè Group experimenters for the pion beam at the Bevatron.

The peak at 190 MeV in the $C^{12}(\pi^-, \pi^-n)C^{11}$ excitation function corresponds to the resonance peak in the free-particle $\pi^-n$ scattering. This is interpreted as additional evidence for the occurrence of quasi-free-particle scattering within nuclear matter.

The full width at half maximum (FWHM) of the $(\pi^-, \pi^-n)$ peak is about 300 MeV, compared with the FWHM of the $\pi^-n$ peak of about 145 MeV. The greater width of the $(\pi^-, \pi^-n)$ peak is probably due to the fact that the struck neutron is moving rapidly within the potential well of the $C^{12}$ nucleus. On the basis of the one-step mechanism, only the $p_{3/2}$ neutrons of $C^{12}$ contribute to the $(\pi^-, \pi^-n)$ reaction because removal of a $s_{1/2}$ neutron leaves the nucleus with too much excitation energy to prevent particle evaporation. If we assume that the $p_{3/2}$ momentum distribution is the same for neutrons and protons, we can use the data of Garron et al. to estimate the resonance broadening due to the neutron momentum distribution.[2] For an average $p_{3/2}$-state momentum of 150 MeV, we estimate that the $\pi^-n$ resonance should be broadened by about 100 MeV to give a FWHM of 245 MeV for the $(\pi^-, \pi^-n)$ peak. The agreement with the experimental width is satisfactory if one considers the uncertainty in both the calculated and experimental widths.

Figure C. 1-7 shows the comparison of the calculated excitation functions for the one-step ("pure knock-on") and two-step ("knock-on followed by evaporation") mechanisms together with the experimental excitation function. The two-step mechanism did not predict the correct

2. J. Garron, J. Jacmart, R. Riou, C. Ruhla, J. Teillac, and K. Strauch, Nucl. Phys. 37, 126 (1962).

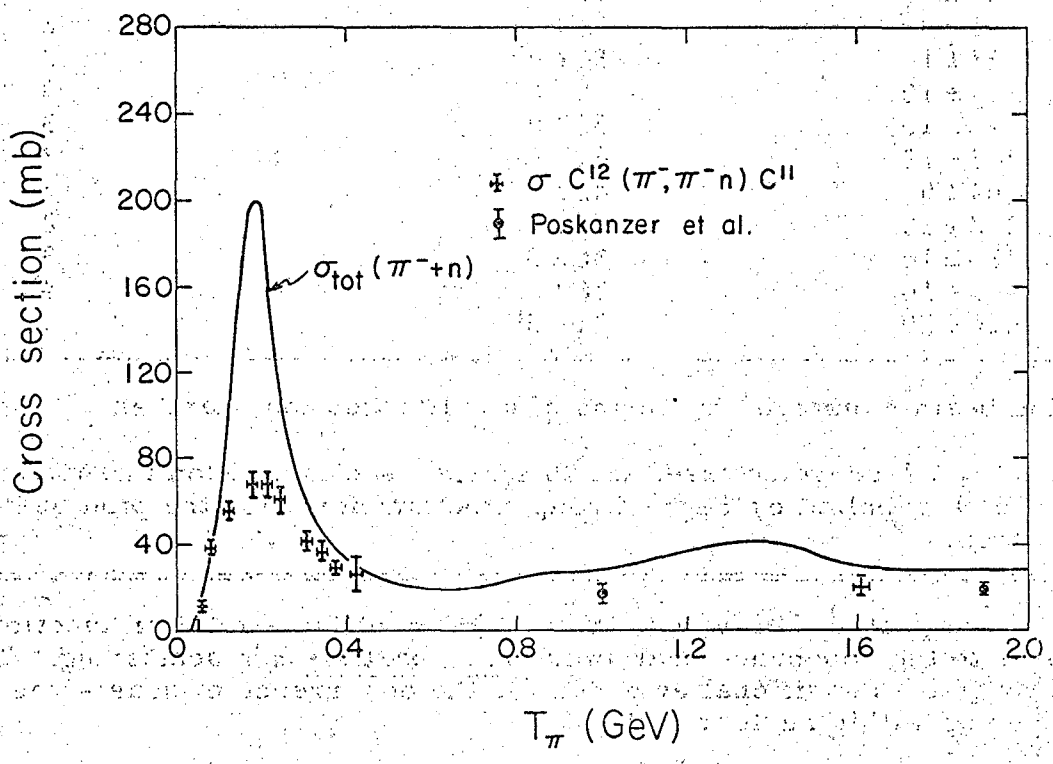


Fig. C. 1-4. Cross section for $C^{12}(\pi^-, \pi^- n)C^{11}$ reaction plotted vs incident pion energy. The smooth curve is the total cross section for $\pi^- n$ free-particle scattering, which is equal to the total cross section for $\pi^+ p$ scattering by charge symmetry.

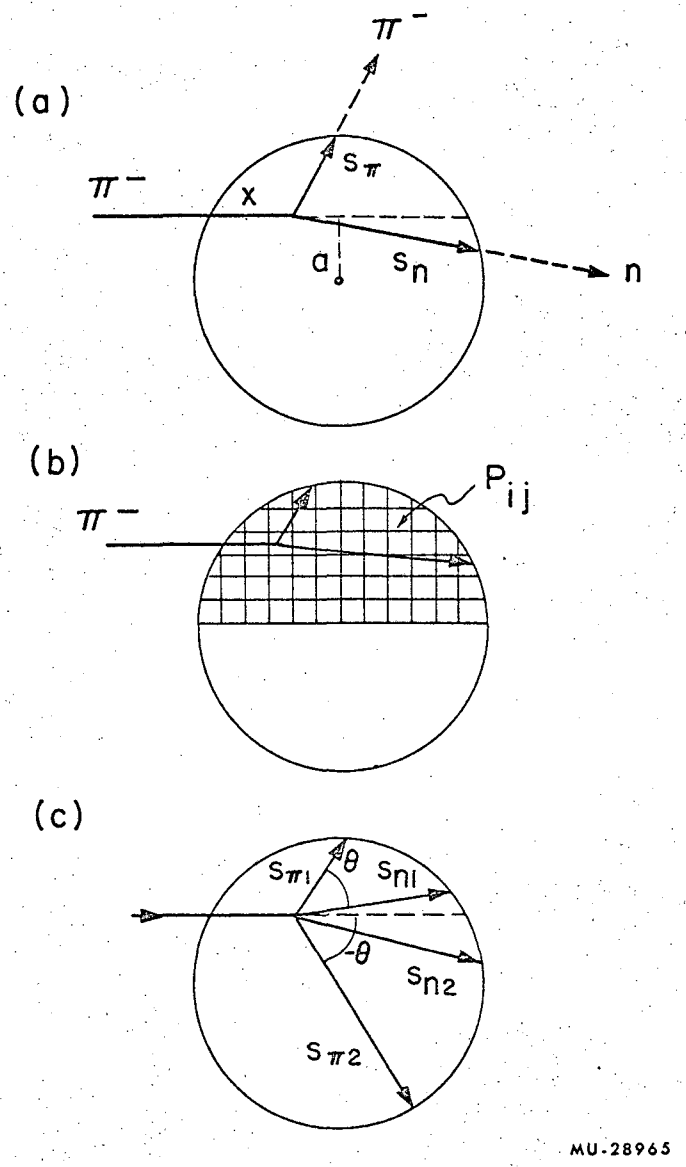


Fig. C. 1-5. (a) Representation of a typical $\pi^-$n collision.
a is the impact parameter of the incident pion.
x is the distance the pion travels in nuclear matter before reaching the point of collision.
$s_n$ is the distance the neutron travels after the collision to reach the nuclear surface.
$s_\pi$ is the distance the pion travels after the collision.
(b) Semicircular matrix $P_{ij}$.
(c) Determination of average exit distances;

$$\langle s_n \rangle = \frac{\langle s_{n1} \rangle + \langle s_{n2} \rangle}{2} \quad \langle s_\pi \rangle = \frac{\langle s_{\pi 1} \rangle + \langle s_{\pi 2} \rangle}{2}$$

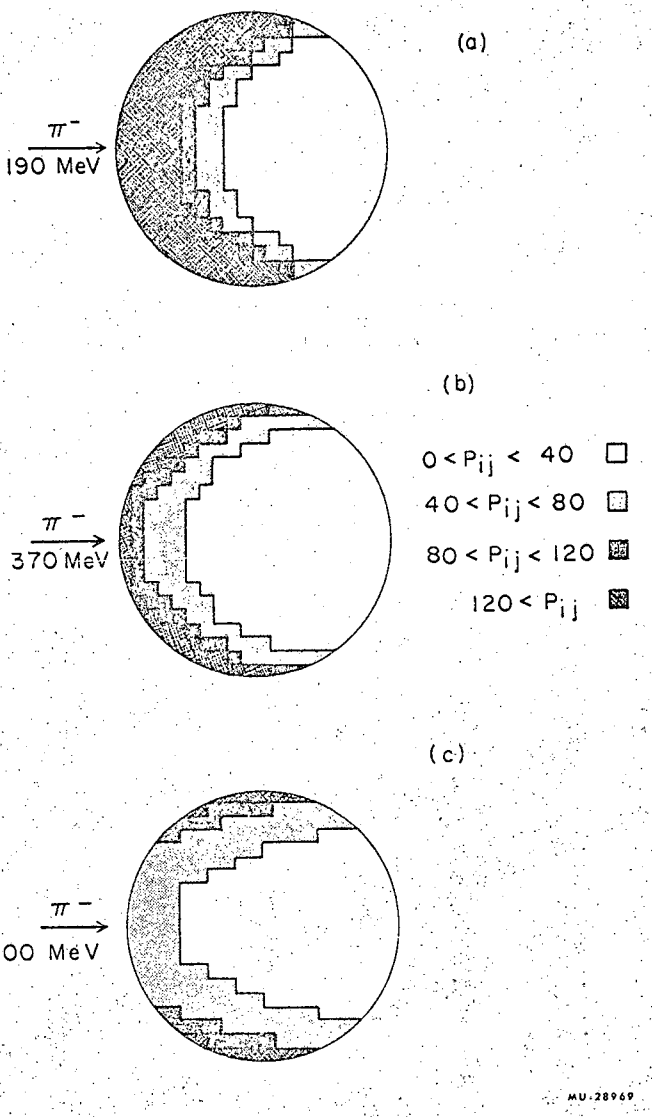


Fig. C. 1-6. Location of $(\pi, \pi n)$ events after integration over scattering angle $\theta$. $P_{ij}$ represents the relative probability of a $(\pi, \pi n)$ event [calculated from $P_{ij} = (P_i P_{coll} P_n P_\pi)$] after weighting by the angular distribution.
(a) Incident pion energy is 190 MeV.
(b) Incident pion energy is 370 MeV.
(c) Incident pion energy is 1600 MeV.

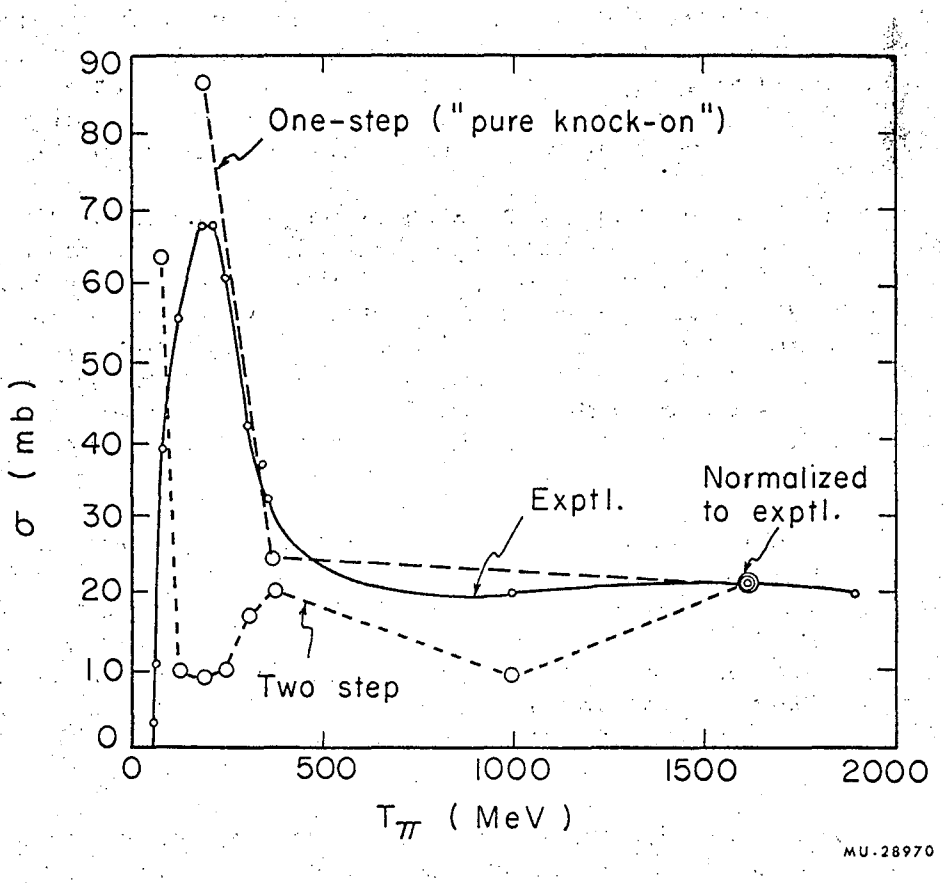


Fig. C. 1-7. Comparison of experimental and calculated $C^{12}(\pi^-, \pi^- n)C^{11}$ excitation functions. Solid curve is experimental. Dashed curve connects the cross sections calculated on the one-step model. The dotted curve connects the points calculated on the two-step model. Both calculated curves have been normalized to the experimental curve at 1610 MeV.

energy dependence of the $C^{12}(\pi^-, \pi^- n)C^{11}$ excitation function in the resonance region, whereas the one-step mechanism does predict the correct shape. It is possible that the two-step mechanism is increasing in importance at energies below the resonance peak although the calculation is not expected to be valid in this region. The one-step calculation was not attempted at energies below the resonance peak because the mean free path of the recoiling neutron was not sufficiently well known for very low recoil energies. However, the strong dependence of the one-step calculation on the free-particle cross section makes it highly probable that the calculated cross sections would decrease in conformity with the free-particle cross sections.

The magnitude of the calculated cross section from the one-step mechanism was lower than the experimental cross sections by a factor of about six. This discrepancy may come from the approximations in the calculation. In particular the use of a square well for the nucleon density may be a major source of error. Monte Carlo calculations with a square well do not predict the correct magnitudes of the (p, pn) reactions. It is probably necessary to do the calculations with a more accurate nucleon-density function because the simple reactions are very sensitive to the shape of the nuclear surface.

An alternative explanation for the discrepancy may lie in the isobar model. If the pion sticks to the struck neutron and both particles travel together through the nucleus with the effective cross sections appropriate to the neutron alone, the calculated cross sections would be raised possibly by a factor of five. This would bring the calculated cross sections into agreement with the experimental cross sections. Refinements of this calculation might provide information on the isobar cross sections in nuclear matter.

Ericson, Selleri, and Van de Walle have recently discussed the use of low-momentum-transfer reactions as a means of obtaining $\pi\pi$ cross sections by radiochemical techniques.[3] The method proposes that peripheral collisions occur within nuclear matter between the incident particle and one nucleon. The $C^{12}(\pi^-, \pi^- n)C^{11}$ excitation function shows that pions do undergo quasi-free-particle collisions within nuclear matter.

---

3. T. Ericson, F. Selleri, and R. Van de Walle, Nucl. Phys. 36, 353 (1962).

## 2. 10-MeV PROTON REACTION CROSS SECTIONS(*)

George Igo and Bruce Wilkins

We have obtained proton nonelastic cross sections at 10 MeV from Be, C, Al, Ti, Mo, Zr, Fe, Ni, Zn, Cu, V, Rh, Nb, Ag, Sn, Ta, Th, Au, and Pb. The most significant feature of the data is the appearance of two strong minima in the elements lighter than Cu. The data are compared with the optical-model predictions by Bjørklund and Fernbach. These calculations predict the right order for the reaction cross section when a surface absorption potential is used which fits existing elastic scattering data. The agreement is quite good above the resonance region although the experimental values are systematically slightly larger than the optical-model predictions. These measurements are compared with other measurements of nonelastic cross sections for 10-MeV protons.

---

*Abstract of paper submitted to Phys. Letters (UCRL-10480, Sept. 1962).

## 3. OPTICAL-MODEL ANALYSIS FOR 10-MeV PROTONS

Bruce D. Wilkins, Richard H. Pehl, and Norman K. Glendenning

An optical-model potential well shape which is consistent with elastic scattering data and reaction cross sections for 10-MeV protons on intermediate-weight elements has been determined. This analysis has been carried out on the IBM 7090 using an automatic parameter search routine.

The optical potential Vf + iWg was used, where

$$f = \frac{1}{1 + \exp[(r - r_0 A^{1/3})/a]}$$

and

$$g = \frac{(1 - \alpha)}{1 + \exp[(r - r_W A^{1/3})/b]} + \alpha \exp[-(r - r_W A^{1/3})/1.45\, b] \quad ;$$

$r_W$ is the radius constant for the imaginary potential. Changing $\alpha$ from 0 to 1 allows the imaginary potential to assume any proportion of volume absorption to surface absorption. Reaction cross sections, recently measured by Wilkins and Igo,[1] have made possible a more precise determination of the shape of the optical potential than was previously possible with elastic scattering and polarization data alone.

---

1. B. D. Wilkins and G. Igo, 10-MeV Proton Reaction Cross Sections for Several Elements, submitted to Phys. Rev.

The elements $Cu^{63}$, Ni, and Ag were chosen for investigation because of the availability of 10-MeV proton elastic-scattering data[2, 3] on these elements. It was also hoped that the sharp minimum in the quantity $\sigma_R - \sigma_{CE}$ ($\sigma_{CE}$ refers to compound elastic scattering) for Ni noted by Wilkins and Igo[1] could be reproduced. Previous attempts at fitting elastic scattering data for Ni had been unsuccessful.[4]

The search routine uses, as a basis for a good fit, $\chi^2$, where

$$\chi^2 = \sum_{\theta} \left( \frac{\sigma(\theta)_{expt} - \sigma(\theta)_{pred}}{\Delta\sigma(\theta)_{expt}} \right)^2 .$$

Besides the well-known $VR^2$ ambiguity, the parameters showed a strong dependence on the imaginary diffuseness parameter b. Sets of parameters giving good fits to elastic scattering data fall along a "b valley" in parameter space. A plot of b vs $r_0$ for volume absorption for 10.20-MeV protons on $Cu^{63}$ is presented in Fig. C. 3-1. Figure C. 3-2 is a similar plot of b vs $r_0$ for a Gaussian surface absorption on the same system. In this case b is related to the width of the Gaussian. An average value of 840 ± 30 mb for $\sigma_R - \sigma_{CE}$ on Cu has been taken from data reported by several groups.[1, 2, 5, 6] Compound elastic scattering is expected to be quite small for 10.20-MeV protons on Cu. Figure C. 3-1 shows that a $\sigma_R$ of 840 mb lies considerably outside the area of good fits for volume absorption.

Volume absorption with $r_W > r_0$ was investigated to see if the reaction cross section could be increased by this means. To obtain areas of low $\chi^2$, however, it was necessary to reduce W. The areas of best fit for $r_W$ up to 1.6 all correspond to values of $\sigma_R$ of about 765 mb. Above $r_W = 1.6$ good fits could not be obtained. In Fig. C. 3-2 the 840-mb line crosses directly through the area of best fit for surface absorption. An analysis was carried out for a combination of equal amounts of volume and surface absorption. Areas of best fit with this well shape correspond to values of $\sigma_R$ of about 790 mb. Figure C. 3-3 shows a fit to the experimental differential elastic scattering data corresponding to the area of minimum $\chi^2$ for 10.20-MeV protons on $Cu^{63}$.

---

2. J. Benveniste, R. Booth, and A. Mitchell, Phys. Rev. 123, 1818 (1961).

3. N. M. Hintz, Phys. Rev. 106, 1201 (1957).

4. A. E. Glassgold, W. B. Cheston, M. L. Stein, S. B. Schuldt, and G. W. Erickson, Phys. Rev. 106, 1207 (1957).

5. V. Meyer and N. M. Hintz, Phys. Rev. Letters 5, 207 (1960).

6. J. Wing and J. R. Huizenga, (p, n) Cross Sections of $V^{51}$, $Cr^{52}$, $Cu^{63}$, $Cu^{65}$, $Ag^{107}$, $Ag^{109}$, $Cd^{111}$, $Cd^{114}$, $La^{139}$ from 5 to 10.5 MeV.

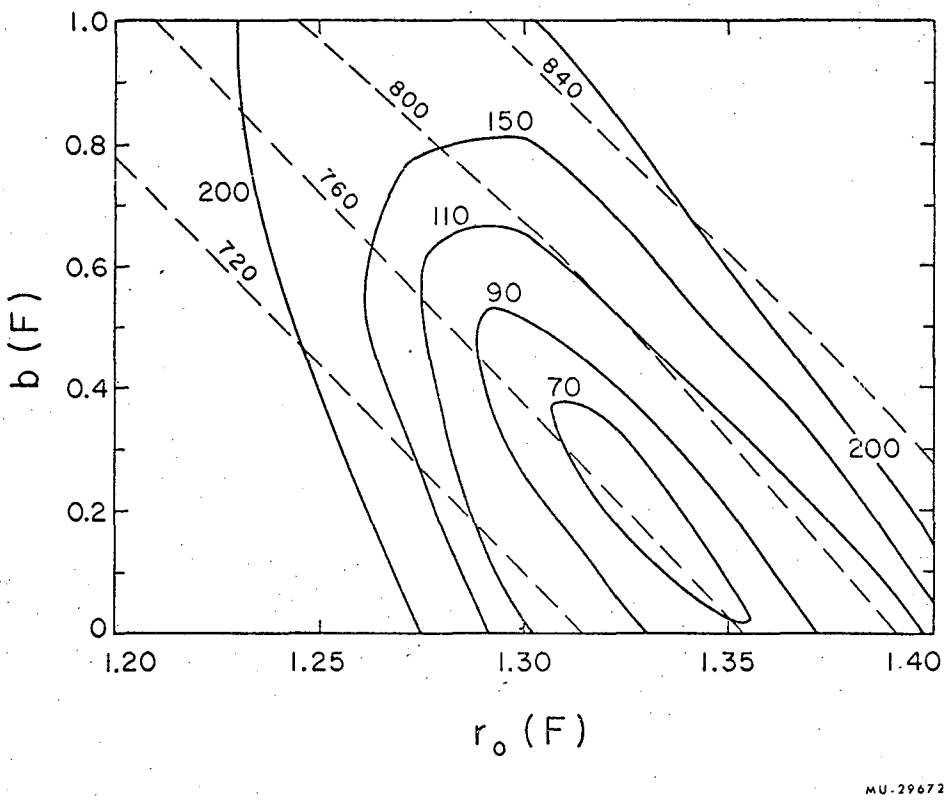


Fig. C. 3-1. Contour map of $\chi^2$ obtained by using volume absorption for 10.20-MeV protons on $Cu^{63}$. The dashed lines are the predicted values of $\sigma_R$. For a given point in the b - $r_0$ grid the other optical-model parameters are adjusted with $r_W = r_0$, so as to minimize $\chi^2$.

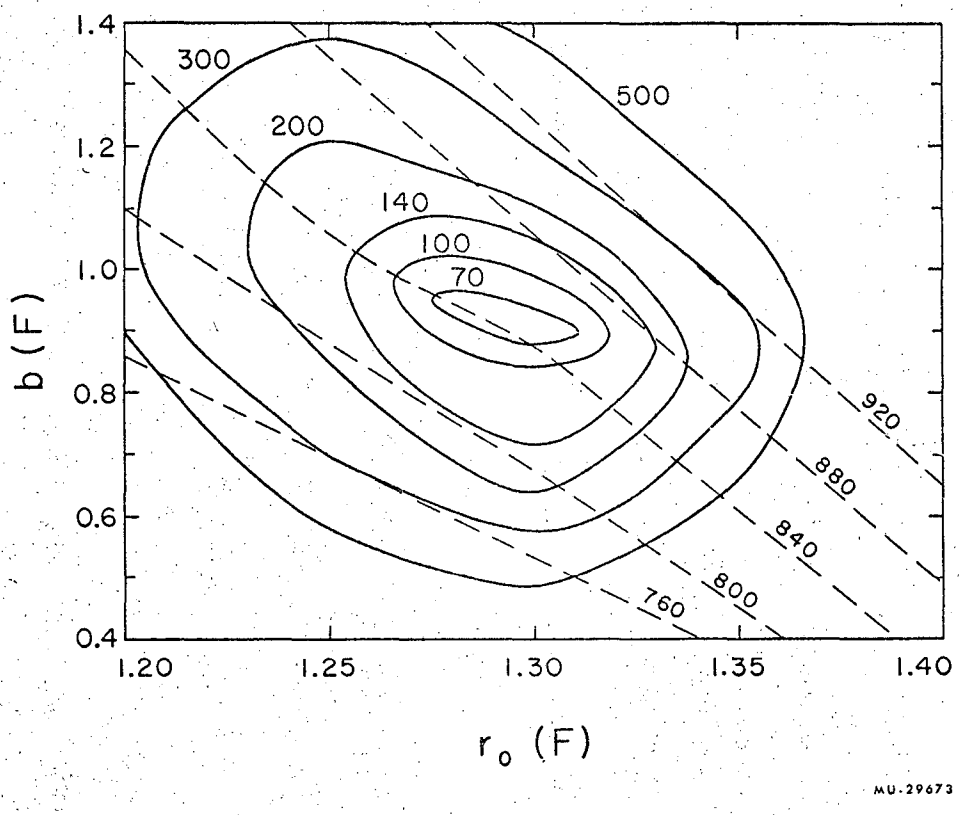


Fig. C. 3-2. Contour map of $\chi^2$, similar to Fig. C. 3-1, obtained by using surface absorption for 10.20-MeV protons on $Cu^{63}$. The dashed lines are the predicted values of $\sigma_R$.

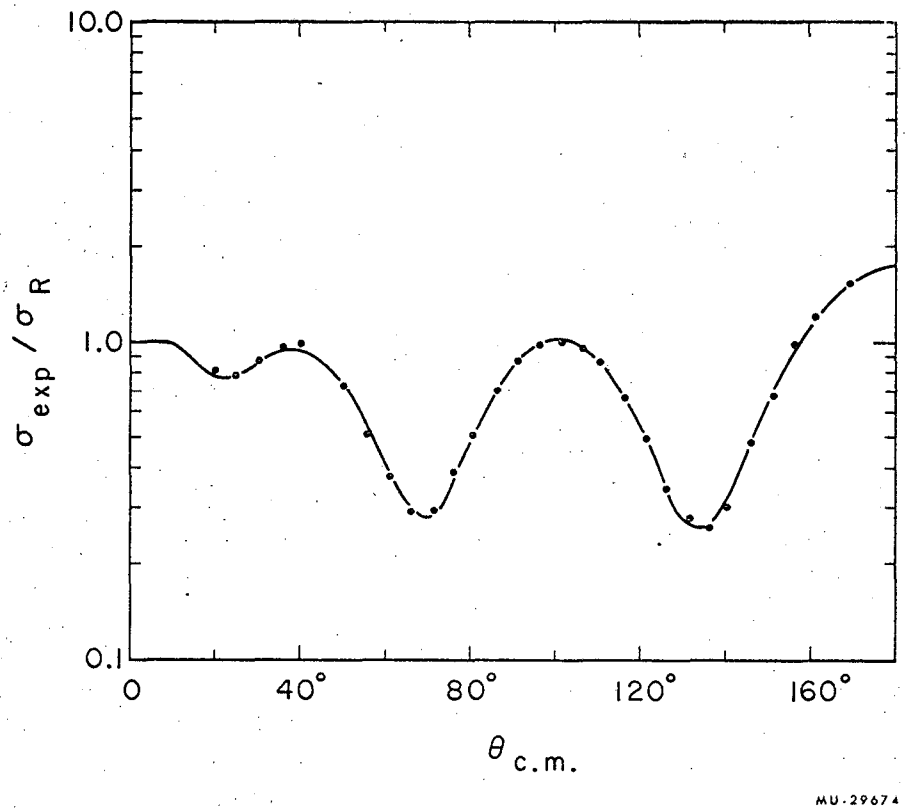


Fig. C. 3-3. Optical-model fit to $\sigma/\sigma_R$ for 10.20-MeV protons on $Cu^{63}$ using surface absorption. The parameters used are V = -48.8, W = -11.5, a = 0.622, b = 0.83, $r_0 = r_W = 1.30$. The smooth curve is the optical-model calculation, the circles the experimental points (reference 2).

When volume absorption was used for the analysis of elastic scattering from natural nickel it was impossible to obtain a good fit. However, very good fits were obtained with surface absorption when a surprisingly small value for b was used (see Fig. C. 3-4). The very thin region on the surface for absorption could be related to the circumstance that Ni is a magic-number nucleus. It is interesting to note that the large difference in $\sigma_R$ between Cu and Ni noticed by Wilkins and Igo is also predicted by our analysis. The experimental value of 680 ± 45 mb for $\sigma_R - \sigma_{CE}$ falls in the area of the best fits to elastic scattering data, as shown in Fig. C. 3-4. A fit to the experimental differential elastic scattering data for 9.85-MeV protons on Ni corresponding to the area of minimum $\chi^2$ is presented in Fig. C. 3-5.

The Ag elastic scattering data[3] are also fitted much better by surface absorption rather than volume absorption. The measured value of $\sigma_R - \sigma_{CE}$ is 700 ± 65 mb.[1] The corresponding predicted value of $\sigma_R$ with surface absorption, although not quite at the minimum in $\chi^2$ space, lies considerably lower in $\chi^2$ space than does a $\sigma_R$ prediction of 700 mb using volume absorption.

In conclusion, a surface-absorption potential gives much better agreement with $\sigma_R$ and elastic scattering data. It should also be noted that, contrary to general opinion, increasing the radius of the imaginary potential does not increase the reaction cross section when one requires equally good fits to elastic-scattering data.

## 4. POLARIZATION OF 22-MeV PROTONS IN p-d ELASTIC SCATTERING

H. E. Conzett, G. Igo, and W. J. Knox†

We have measured significant left-right asymmetries, $\epsilon(\theta)$, in the elastic scattering of 22-MeV polarized protons from deuterons. The measured asymmetry in elastic scattering is given by

$$\epsilon(\theta) = P_1 P_2(\theta),$$

where $P_1$ is the fractional polarization of the proton beam, and $P_2(\theta)$ is the proton polarization that would be induced in the scattering of unpolarized protons by deuterons. The polarized beam with $P_1 \approx 1.0$ was generated by α-p scattering as described before.[1] Thus, the measured asymmetry, $\epsilon(\theta)$, is equal to $P_2(\theta)$. Measurements in p-d elastic scattering below 15 MeV

---

† Physics Department, University of California at Davis.

1. H. E. Conzett, G. Igo, and A. Nir; Proceedings of the International Symposium on Polarization Phenomena of Nucleons, Helv. Physica Acta, Supplementum VI (1961).

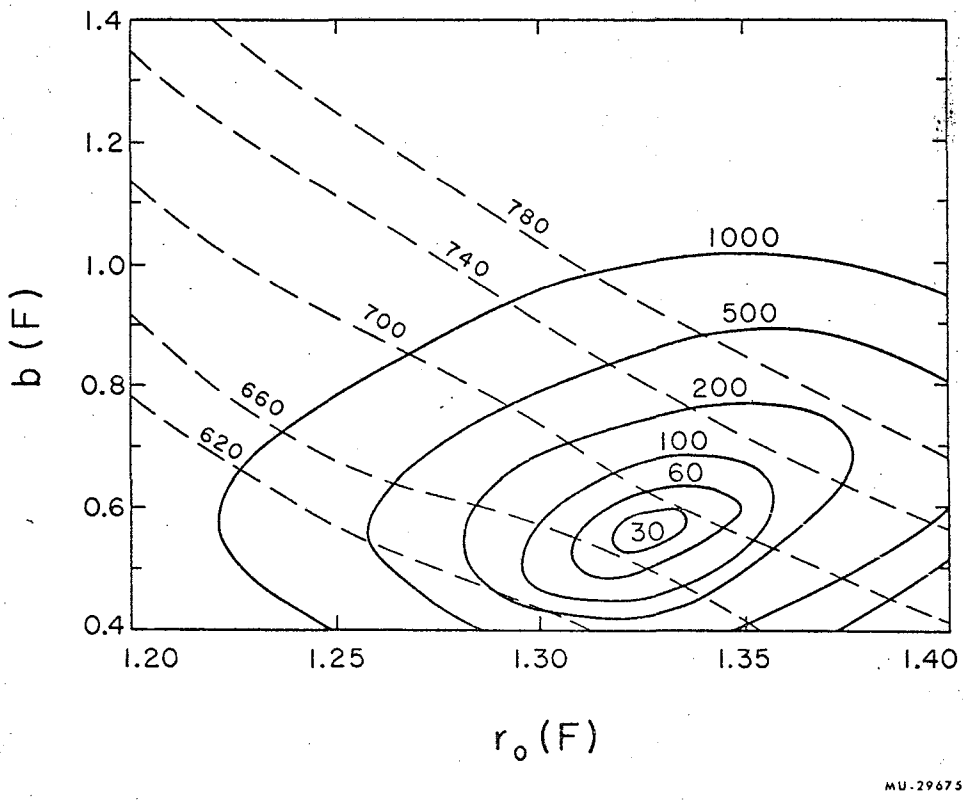


Fig. C. 3-4. Contour map of $\chi^2$ obtained by using surface absorption for 9.85-MeV protons on Ni. The dashed lines are the predicted values of $\sigma_R$.

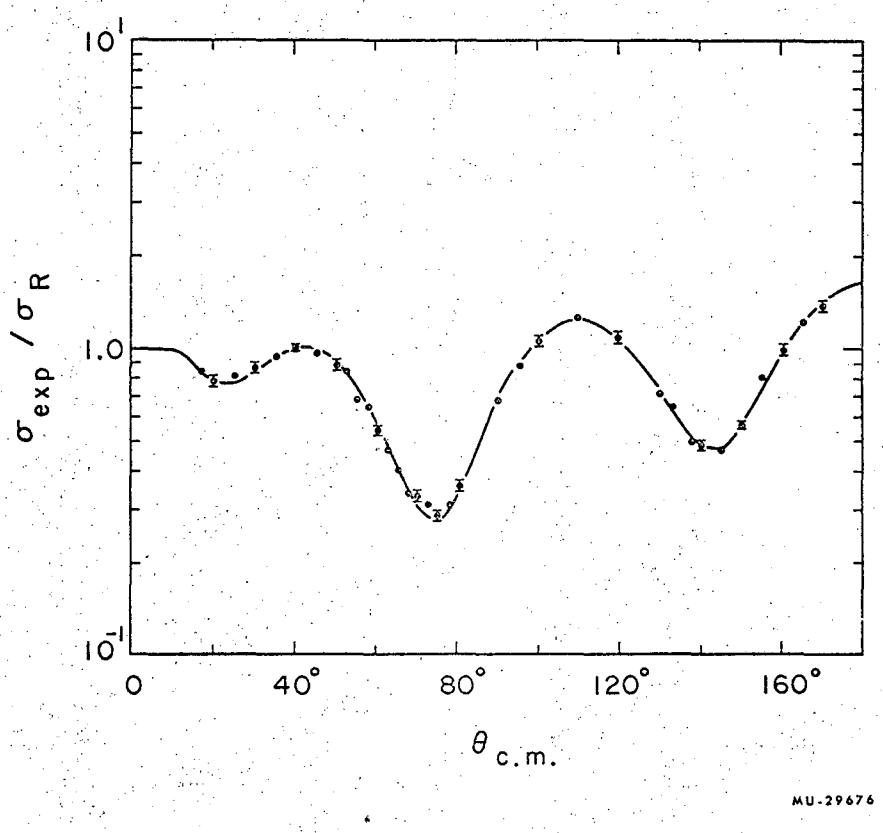


Fig. C. 3-5. Optical-model fit to $\sigma/\sigma_R$ for 9.85-MeV protons on Ni using surface absorption. The parameters used are V = -47.7, W = -16.2, a = 0.580, b = 0.55, $r_0 = r_W = 1.325$. The smooth curve is the optical-model calculation, the circles the experimental points (reference 3).

have been consistent with negligible polarization.[2] Thus, the onset of appreciable polarizations within the next several MeV should be significant with respect to the nature of the nucleon-nucleon force.

Our results are shown in Fig. C. 4-1 and are listed in Table I. In column 3 we indicate that for $\theta_{c.m.} \leq 106^\circ$ the proton asymmetries were measured, whereas those for larger angles were determined from recoil-deuteron asymmetries.

A phase-shift analysis will be made of these data together with the 20.5-MeV p-d elastic differential cross section data.[3] Also, an impulse-approximation calculation[4] has been started to examine, at least qualitatively, the contributions to the p-d polarization from the p-p and p-n interactions.

Table I. Proton polarization in p-d elastic scattering at 22 MeV

| $\theta_{c.m.}$ | $P(\theta)$ | Particle detected |
|---|---|---|
| 31.4 | $+0.030 \pm 0.007$ | p |
| 37.2 | $+0.033 \pm 0.010$ | p |
| 44.5 | $+0.042 \pm 0.011$ | p |
| 58.8 | $+0.039 \pm 0.007$ | p |
| 64.4 | $+0.037 \pm 0.013$ | p |
| 72.5 | $-0.012 \pm 0.011$ | p |
| 79.2 | $-0.027 \pm 0.016$ | p |
| 85.7 | $-0.076 \pm 0.021$ | p |
| 92.0 | $-0.088 \pm 0.010$ | p |
| 98.0 | $-0.096 \pm 0.021$ | p |
| 106.2 | $-0.157 \pm 0.021$ | p |
| 122.0 | $+0.023 \pm 0.022$ | d |
| 128.0 | $+0.271 \pm 0.023$ | d |
| 136.0 | $+0.253 \pm 0.025$ | d |

2. At 14.5 MeV: L. Rosen and W. T. Leland, Phys. Rev. Letters 8, 379 (1962); at 10 MeV: L. Rosen, J. E. Brolley, Jr., and L. Stewart, Phys. Rev. 121, 1423 (1961); near 3.5 MeV: M. Shafroth, R. Chalmers, E. N. Strait, and R. E. Segal, Nuclear Forces and the Few-Nucleon Problem, Vol II, p. 365.

3. D. O. Caldwell and J. R. Richardson, Phys. Rev. 98, 28 (1955).

4. For example, L. Costillejo and L. S. Singh, Nuovo Cimento 11, 131 (1959).

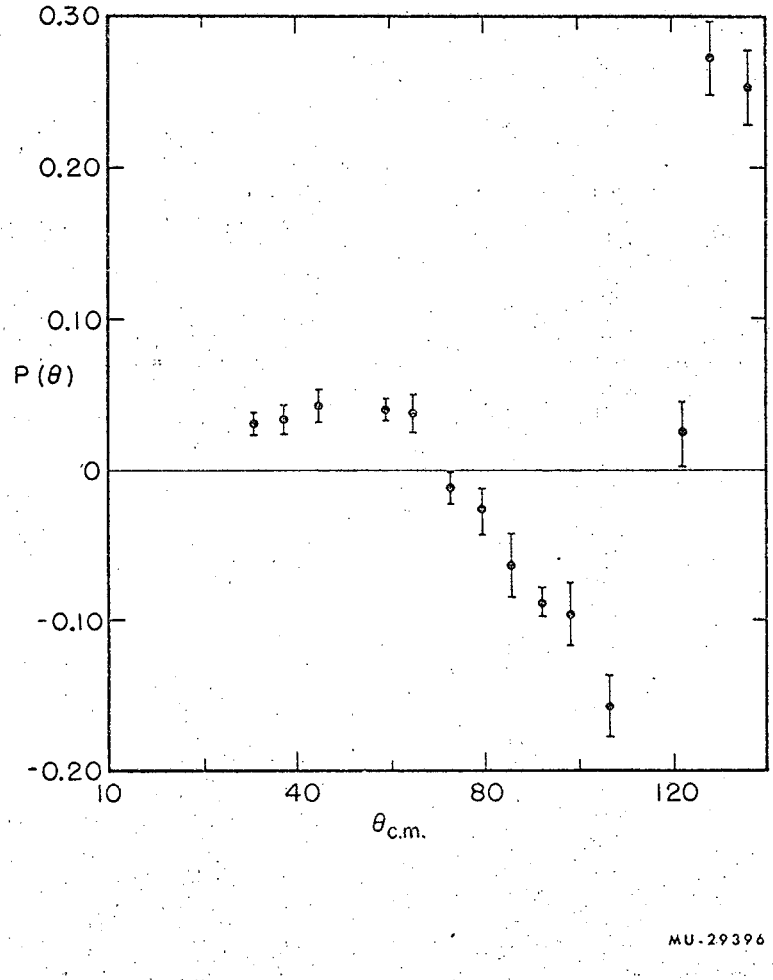


Fig. C. 4-1. Proton polarization in p-d elastic scattering at 22 MeV.

# 5. TOTAL REACTION CROSS SECTIONS FOR 22.4-MeV DEUTERONS(*)

B. Wilkins and G. Igo

The reaction cross section for deuterons is of considerable interest. The deuteron is known to be a relatively large, loosely bound system subject to electric breakup processes[1] in collisions at interaction distances larger than the nuclear radius in heavy elements.[2] In addition, nuclear breakup processes[3] at the nuclear surface in light elements have large cross sections.[2] If interactions occur at a larger radius[4] than for α particles or protons, the total reaction cross section might be expected to be enhanced. Indeed, Hamburger, Cohen, and Price[2] have found that at about 15 MeV the deuteron breakup cross section is larger, by a factor of the order of 2, than the predicted values for electric breakup or nuclear breakup.[1,3] For all elements investigated in our work, however, reaction cross sections for 22.4-MeV deuterons are found to be almost identical with those for 40-MeV α particles. These measurements suggest that reaction cross sections are not enhanced by the large cross sections for deuteron breakup. The comparison is valid, since the Coulomb barrier effects are almost identical in these two cases.

The experimental apparatus used in the reaction cross section measurements has been described in detail elsewhere,[5] and results are presented in the paper from which this report is condensed.

The importance of reaction cross-section measurements for determining optical-model potential parameters (at least under some conditions) has recently been shown by Olkowsky[6] in the optical-model analysis of data for 10-MeV proton elastic scattering on Cu. The same apparently holds for the deuteron optical potential. Halbert et al.[7] have obtained striking fits to the comprehensive elastic-scattering data at 11.8 MeV.[8] They obtain 2051 mb and 2217 mb for the predicted reaction cross section for Sn in two analyses[9] of 11.8-MeV deuteron elastic scattering data.[8] The measured value at 22.4 MeV for tin is 1563 ± 117 mb. The theoretical values for Ni at 11.8 MeV -- 1360 mb and 1396 mb -- and the measured value for Ni -- 1491 ± 63 mb -- at 22.4 MeV are in better agreement. Elastic scattering data taken alone, even when very comprehensive and with small experimental error, are apparently not sufficient to predict the correct value of the reaction cross section. Conversely, the experimental values of the reaction cross section are apparently necessary data for optical-model analyses.

---

*Abstract of contribution to Phys. Letters (to be published).

1. C. J. Mullin and E. Guth, Phys. Rev. 82, 141 (1951).
2. E. W. Hamburger, B. L. Cohen and R. E. Price, Phys. Rev. 121, 1143 (1961).
3. R. Glauber, Phys. Rev. 99, 1515 (1955).
4. C. E. Porter, Phys. Rev. 99, 1400 (1955).
5. B. D. Wilkins and G. Igo, submitted to The Physical Review.
6. J. Olkowsky (Centre d' Etudes Nucléaires Saclay, France), private communication.
7. E. C. Halbert, R. H. Bassel and G. R. Satchler, Bull. Am. Phys. Soc. Series II, Volume 7, No. 4 (1962).
8. G. Igo, W. Lorenz, and U. Schmidt-Rohr, Phys. Rev. 124, 832 (1961).
9. E. C. Halbert (ORNL, Oak Ridge, Tenn.), private communication.

# 6. ALPHA-PARTICLE REACTION CROSS SECTIONS AT 40 MeV AND THE MEAN FREE PATH IN NUCLEAR MATTER IN THE ENERGY RANGE $10^1$ to $10^6$ MeV(*)

George Igo and Bruce D. Wilkins

We have measured the reaction cross section $\sigma_R$ for 40-MeV alpha particles, and we compare it with the predictions $\sigma_I$ of the Igo potential.[1,2] The ratio $\sigma_R/\sigma_I$ plotted against $A^{2/3}$ (A, the atomic number) deviates from unity in a systematic fashion. A straight line with a slope of $5.5\times10^{-3}$ fits the data in Fig. C.6-1. Superimposed on this trend $\sigma_R/\sigma_I$ dips by 18% near A = 28 protons, as was also noted in the 10-MeV proton measurements.[3]

The experimental apparatus used in the measurements of reaction cross section (see Fig. C.6-2) has been described in detail elsewhere[4] and will not be discussed here except where parameters of the experiment have been altered because of the change in the projectile. The raw cross section $\sigma$, obtained from the target-in and target-out measurements, is listed in Table I. Three principal corrections must be made to $\sigma$. A "dummy" foil is placed ahead of the counters when the target is out so that the energy incident on the stopping counter will be the same in the target-in and target-out measurements. The α-particle energy in counter 3 is therefore different for the two configurations. Fortunately the counter 3 scattering-out correction $\eta_3$ can be measured quite accurately.[3] A second correction, $\sigma_{el}$, is due to those elastic events in which scattering occurs outside the solid angle subtended by counter 5, the stopping counter. The corresponding plane angle $\theta_5$ (lab) was set at 28.7° for light and intermediate elements. For elements heavier than tin, $\theta_5$ was set at 43.0°. The third correction, $\sigma_{inel}$, is comprised from part of the inelastic and reaction events scattered into the solid angle subtended by the stopping counter. In order to facilitate the separation of elastic events from the inelastic and reaction events, a degrader foil is placed between the target and counter 5. The thickness of the degrader foil was adjusted so that 25-MeV α particles are stopped by it.

The correction $\sigma_{in}$ is due to several sources. The first is the correction due to (α, α') direct-interaction events[5-9] (evaporation-spectrum α particles stop in the absorber). The correction due to (α, p) events has been obtained by using the Nuclear Monte Carlo Evaporation Model (NMCEM).[10]

---

*Submitted to Nucl. Phys.


1. G. Igo, Phys. Rev. Letters 1, 72 (1958); Phys. Rev. 115, 1665 (1959).
2. J. R. Huizenga and G. Igo, Nucl. Phys. 29, 462 (1962).
3. G. Igo and B. D. Wilkins, Phys. Letters 2, 342 (1962).
4. B. D. Wilkins and G. Igo, 10-MeV Proton Reaction Cross Sections for Several Elements, Phys. Rev. (to be published).
5. R. Beurtey, R. Catillon, R. Chauminades, M. Crut, H. Faraggi, A. Papineau, J. Saudinos, and J. Thirion, Compt. Rend. 252, 1756 (1961).
6. J. Van Heerden and D. J. Prowse, Nucl. Phys. 15, 356 (1960).
7. R. G. Summers-Gill, Phys. Rev. 109, 1591 (1958).
8. J. L. Yntema, B. Zeidman, and B. J. Ray, Phys. Rev. 117, 801 (1960).
9. D. K. McDaniels, J. S. Blair, S. W. Chen, and G. W. Farwell, Nucl. Phys. 17, 614 (1960).
10. I. Dostrovsky, Z. Fraenkel, and G. Friedlander, Phys. Rev. 116, 683 (1959).

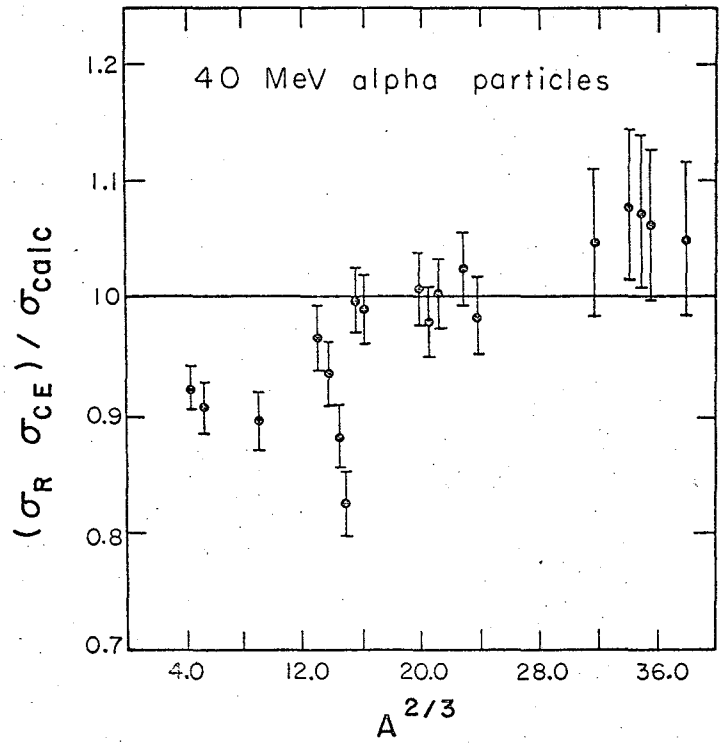


Fig. C.6-1. The ratio of the nonelastic cross section for 40-MeV α particles, $\sigma_R - \sigma_{CE}$, to the corresponding theoretical value $\sigma_I$ versus the two-thirds power of A.

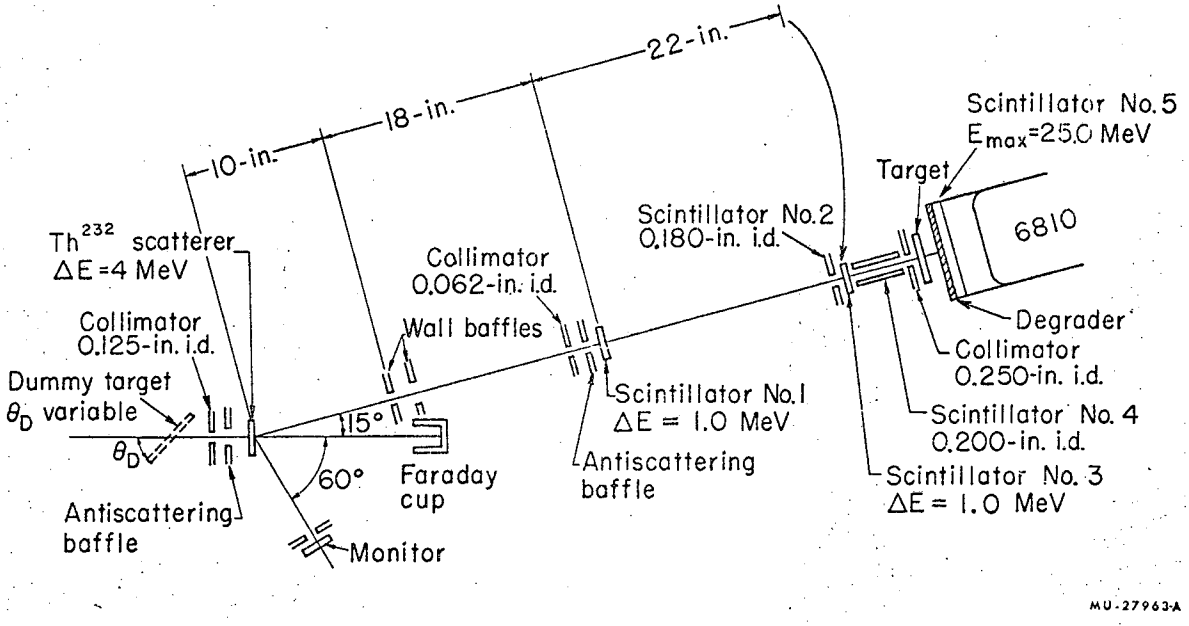


Fig. C.6-2. Schematic diagram of the experimental apparatus.

Table I. The raw cross section $\sigma$, the counter 3 scattering-out correction $\eta_3$, the inelastic and reaction scattering correction $\sigma_{inel}$ (references 5-17), the eastic scattering correction $\sigma_{el}$ (references 7, 8, 18-20), and the nonelastic cross section $\sigma_R - \sigma_{CE}$.

| Element | $\sigma$ (mb) | $\eta_3$ (mb) | $\sigma_{inel}$ (mb) | $\sigma_{el}$ (mb) | $\sigma_R - \sigma_{CE}$ (mb) |
|---|---|---|---|---|---|
| Be | 789± 7 | 9± 4 | 36± 7 | 51± 3 | 783± 11 |
| C | 894±12 | 12± 6 | 60± 9 | 65± 3 | 901± 16 |
| Al | 1105±17 | 23±10 | 54± 8 | 41± 2 | 1141± 21 |
| Ti | 1422±30 | 32±18 | 77±12 | 31± 5 | 1500± 37 |
| V | 1397±32 | 34±18 | 80±12 | 31± 5 | 1480± 39 |
| Fe | 1363±34 | 36±20 | 68±12 | 31± 5 | 1436± 42 |
| Ni | 1271±28 | 40±18 | 79±15 | 36± 2 | 1354± 37 |
| Cu | 1526±36 | 42±19 | 128±26 | 50± 3 | 1646± 48 |
| Zn | 1511±37 | 42±19 | 129±26 | 48± 3 | 1639± 49 |
| Zr | 1753±48 | 45±32 | 97±23 | 124± 7 | 1771± 63 |
| Nb | 1704±52 | 53±27 | 105±24 | 134± 7 | 1728± 64 |
| Mo | 1792±65 | 47±34 | 103±24 | 160±10 | 1782± 78 |
| Ag | 1881±52 | 61±27 | 99±25 | 195±10 | 1846± 64 |
| Sn | 1858±65 | 59±34 | 97±25 | 246±13 | 1768± 78 |
| Ta | 1846±83 | 79±44 | 97±25 | 136± 7 | 1886± 97 |
| Au | 1931±63 | 88±39 | 100±25 | 200±10 | 1919± 79 |
| Pb | 1953±62 | 89±42 | 100±30 | 250±13 | 1892± 82 |
| Bi | 1923±87 | 100±46 | 100±30 | 270±20 | 1853±105 |
| Th | 1973±84 | 92±51 | 100±30 | 404±20 | 1761±105 |

Experimental data,[11-15] fitted with this model, were used to fix the parameters of the model. The predictions of the model for (α, p) cross sections then were calculated. Instead of a parameter for shell corrections fitted to each element (as was used in reference 10), Cameron's empirical shell correction[16] was used. This gave consistently good fits to the experimental data throughout the periodic table. The (α, d) and (α, t) corrections were also calculated and found to be small (about 5 mb). The (α, $He^3$) reaction did not contribute because of the large Q value associated with this reaction. The NMCEM

11. N. T. Porile, Phys. Rev. 115, 939 (1959).

12. R. Vandenbosch, T. D. Thomas, S. E. Vandenbosch, R. A. Glass, and G. T. Seaborg, Phys. Rev. 111, 1358 (1958).

13. Bruce M. Foreman, Spallation and Fission in Thorium-232, and The Masses of the Heaviest Elements (Thesis), UCRL-8223, April 1958.

14. N. O. Lassen and V. A. Sidorov, Nucl. Phys. 19, 579 (1960).

15. N. T. Porile and D. L. Morrison, Phys. Rev. 116, 1193 (1959).

16. A. G. W. Cameron, A Revised Semi-Empirical Atomic Mass Formula, CRP-690, March 1957.

17. R. M. Eisberg, G. Igo, and H. E. Wegner, Phys. Rev. 100, 1309 (1955).

does not treat the direct-interaction (α, p) events properly. To compensate for this the NMCEM calculations were adjusted to fit the average of the forward-peaked, direct-interaction distributions[17] determined experimentally. It is therefore possible that we have underestimated the contribution of the direct-interaction (α, p) events, especially in the light elements with $\sigma_R/\sigma_I < 1$ (see Fig. C.6-1). Unfortunately, there are no measurements at the extreme forward angles corresponding to the solid angle intercepted by counter 5 with which to check this. The values predicted by NMCEM when normalized to the measured $\sigma_R$ fitted the excitation function peaks within 1 MeV, and the absolute magnitude of the excitation function data was usually fitted within 20%.

The elastic scattering correction $\sigma_{el}$ has been estimated from the literature.[7, 8, 18-20] The elastic scattering data consist of the sum of shape elastic scattering $\sigma_{SE}$ and compound elastic scattering $\sigma_{CE}$. The latter is not included in the measured quantity in these experiments. The final result $\sigma_R - \sigma_{CE}$, where $\sigma_R$ is the total reaction cross section, is listed in the last column of Table I. The results for $(\sigma_R - \sigma_{CE})/\sigma_I$ are also shown in Fig. C.6-1, where the deviation from unity can be seen. The most prominent features are the agreement with unity for $A^{2/3} \geq 16$, the dip near 28 proton nuclei, and a 10% deviation for light elements. It has been emphasized above that some of this deviation could be due to an underestimate of the (α, p) direct-interaction cross sections. The data can be fitted by a straight line with slope of $5.5 \times 10^{-3}$ on this plot versus $A^{2/3}$ if the dip near 28-proton nuclei is neglected. It also should be noticed that we plot $(\sigma_R - \sigma_{CE})/\sigma_I$ versus $A^{2/3}$. However, at 40 MeV, $\sigma_{CE}$ is expected to be small, and we do not believe that the dip is due to a resonance in $\sigma_{CE}$. Instead, it probably reflects the decrease in the cross-sectional area of nuclei in this region. The same effect was seen in $\sigma_R - \sigma_{CE}$ for the 10-MeV protons,[3, 4] but not seen in the 22.4-MeV deuteron reaction cross section data.[21] With the completion of these α-particle $\sigma_R$ measurements it is possible to obtain the mean free path of α particles in nuclear matter, $\lambda_{NE}$. The attenuation of 18-MeV flux of α particles[22] in Ar (arrows in Fig. C.6-3) for the region where the Igo potential[1] is well defined has been used. The amount of nuclear material traversed for a 1/e attenuation can be obtained by numerical integration (see Fig. C.6-3). In Fig. C.6-3 are plotted contours for a Woods-Saxon type of nuclear distribution[23] consistent with charge

18. A. I. Yavin and G. W. Farwell, Nucl. Phys. 12, 1 (1959).

19. G. Igo, H. E. Wegner, and R. M. Eisberg, Phys. Rev. 101, 1508 (1956).

20. H. E. Wegner, R. M. Eisberg, and G. Igo, Phys. Rev. 99, 825 (1955).

21. B. D. Wilkins and G. Igo, Phys. Letters, 3, No. 1, 48, (Nov. 15, 1962).

22. I. McCarthy, in Proceedings of the International Conference on the Nuclear Optical Model (Florida State University, Tallahassee, Florida, 1959), p. 24.

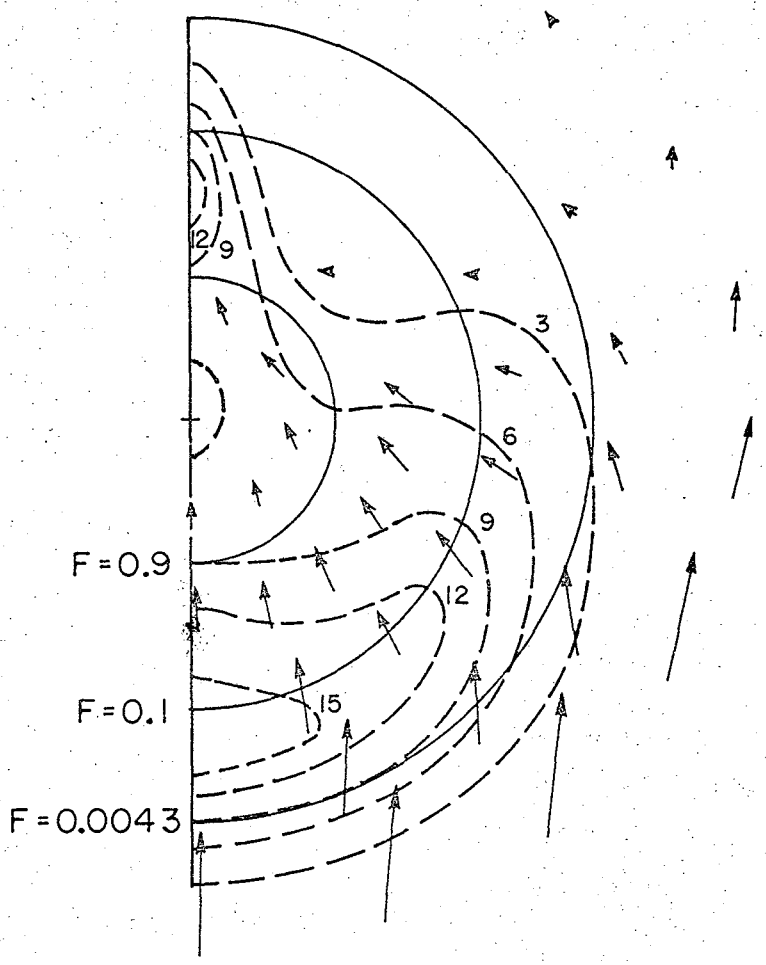


Fig. C.6-3. The flux of 18-MeV α particles in Ar (arrows) (references 1, 2, 22), the flux absorption (dashed lines), and the nuclear matter contours (solid lines) (reference 16).

density measurements.[24] The half-value radius is $1.2\,A^{1/3}\times10^{-3}$ cm; the diffuseness parameter, $0.6\times10^{-13}$ cm; and A, the atomic weight. However, it should be noted that these measurements are sensitive to $\langle r^2\rangle$ rather than the shape of the charge-distribution tail. The justification for putting credence in this shape for the tail of the distribution is that the potential tail[1, 2] has this shape, and Hartree-Fock self-consistent calculations show that the nuclear distribution must therefore have a similar shape. The mean free path obtained in this way from the data up to 50 MeV may be expressed in terms of the mean free path in nuclear matter of uniform density $\rho_0/20$, where $\rho_0$ is the central density. It was decided to express it in terms of a surface density $\rho_0/20$ rather than in terms of a central density $\rho_0$, because the Pauli principle may have a profound effect on the mean free path at low energies in the central part of the nucleus.

The values of $\sigma_R$ at 40 MeV obtained in this experiment can be compared with values obtained at higher energies.[25-27] There is a slow change with energy amounting to about 50% in the energy range $4\times10^1$ MeV to $10^6$ MeV. It is therefore reasonable to assume $\lambda_{NE}$ is inversely proportional to $\sigma_R$. Figure C.6-4 shows a plot of $\lambda_{NE}$ versus energy thus obtained. A straight line is drawn through the experimental points. The slow overall variation with energy and the small average value (12 F) are apparent. These quantitative values for $\lambda_{NE}$ are of considerable importance in interpreting attenuation effects in nuclear reactions involving α particles.[28]

---

23. R. D. Woods and D. S. Saxon, Phys. Rev. 95, 577 (1954).

24. D. G. Ravenhall, Rev. Mod. Phys. 30, 430 (1958).

25. G. P. Milburn, W. Birnbaum, W. E. Crandall, and L. Schechter, Phys. Rev. 95, 1268 (1954).

26. E. Lohrmann and M. W. Teucher, Phys. Rev. 115, 636 (1959).

27. M. W. Teucher, E. Lohrmann, and M. Schein, preprint.

28. G. Igo, L. F. Hansen, and T. J. Gooding, The (α, 2α) Reaction on Heavy Elements at 915 MeV, submitted to Phys. Rev.

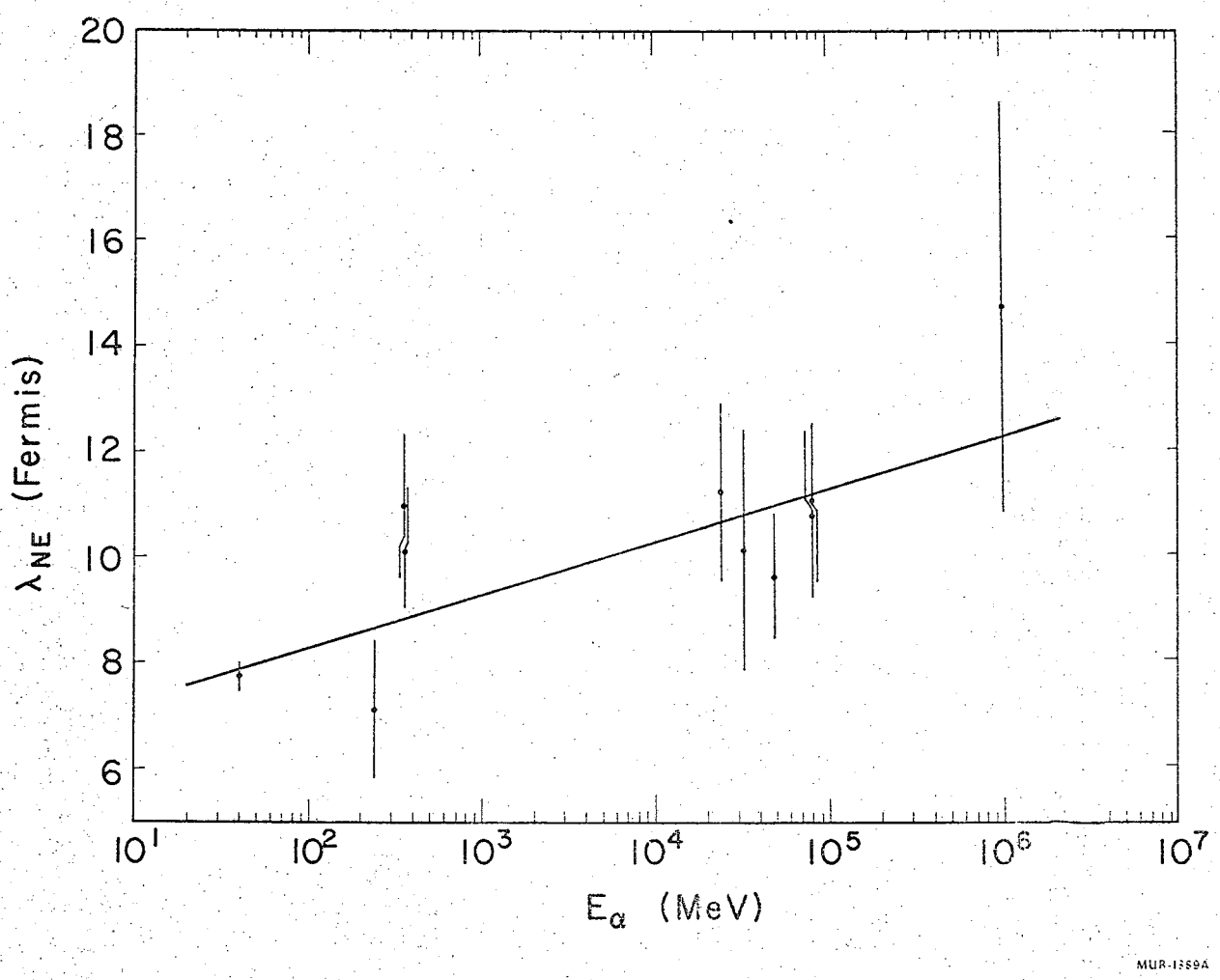


Fig. C.6-4. The nonelastic mean free path $\lambda_{NE}$ versus energy in nuclear matter of density $\rho_0/20$, where $\rho_0$ is the central nuclear density.

# 7. INELASTIC HELIUM-ION SCATTERING AT THE 88-INCH CYCLOTRON

Bernard G. Harvey, John R. Meriwether, William B. Jones
Pierre Darriulat, and Ernest J. M. Rivet

The first experiment to be completed at the 88-inch cyclotron was a study of elastic and inelastic scattering of 65-MeV helium ions from $C^{12}$, $N^{14}$, and $O^{16}$. The cyclotron beam was momentum-analyzed by means of a uniform-field circular-pole magnet and an adjustable slit. An image of the slit was thrown on the target by means of a quadrupole lens doublet.

By use of a slit opening of 0.060 in., a beam of divergence 0.2° (full angle) and size 0.080×0.500 in. was obtained at the target. The intensity was normally about 0.2 μA, but reached 0.4 μA at times in spite of limitation of the internal beam to about 20 μA. (This is about 1/50 of what the cyclotron is expected to produce eventually). With lithium-drifted silicon detectors, an energy resolution of 140 keV (full width at half maximum) was measured for 65-MeV particles scattered from gold foils.

Spectra of helium ions scattered from $N^{14}$ and $C^{12}$ are shown in Figs. C.7-1 and C.7-2. The $(d_{5/2})^2$ J = 5 level at 9 MeV in $N^{14}$ (see preceding section) is not observably excited by inelastic helium ion scattering. To produce it from the $N^{14}$ ground state would require promotion of two nucleons from the $p_{1/2}$ to the $d_{5/2}$ shell, and such double excitations are known to be weak.

The $N^{14}$ levels at 6.23 and 6.44 MeV were not detected. Both of them require double promotion ($p_{1/2}^2 \rightarrow 2sld_{5/2}$) according to True's theoretical wave functions.

The angular distributions of scattered particles corresponding to formation of the $N^{14}$ levels at 3.95 and 7.03 MeV were found to be virtually identical. In both cases, the excitation takes place by the promotion of a $p_{3/2}$ nucleon to the $p_{1/2}$ shell.

The 2- level at 8.88 MeV in $O^{16}$ was quite strongly excited even though it is of "unnatural" parity . . . ; [i.e., $\pi \neq (-1)^J$]. Such a level can be excited only by second-order processes or by a spin-orbit contribution to the interaction.[1]

---

1. W. W. Eidson and J. G. Cramer, Phys. Rev. Letters 9, 497 (1962).

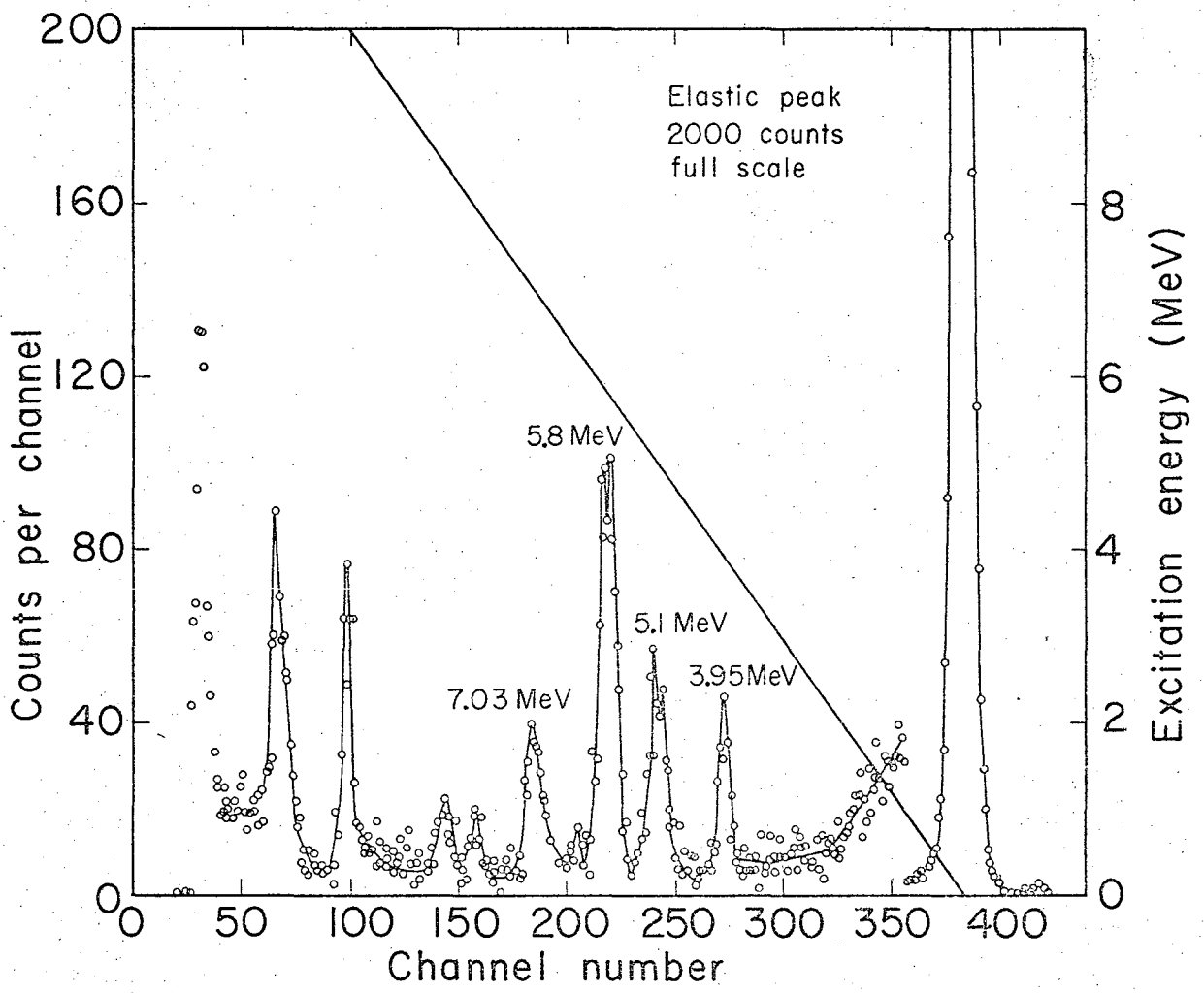


Fig. C.7-1. Elastic and inelastic spectrum of helium ions (initially 65 MeV) scattered from $N^{14}$. $N^{14}(\alpha, \alpha')N^{14*}$, 17 deg(lab).

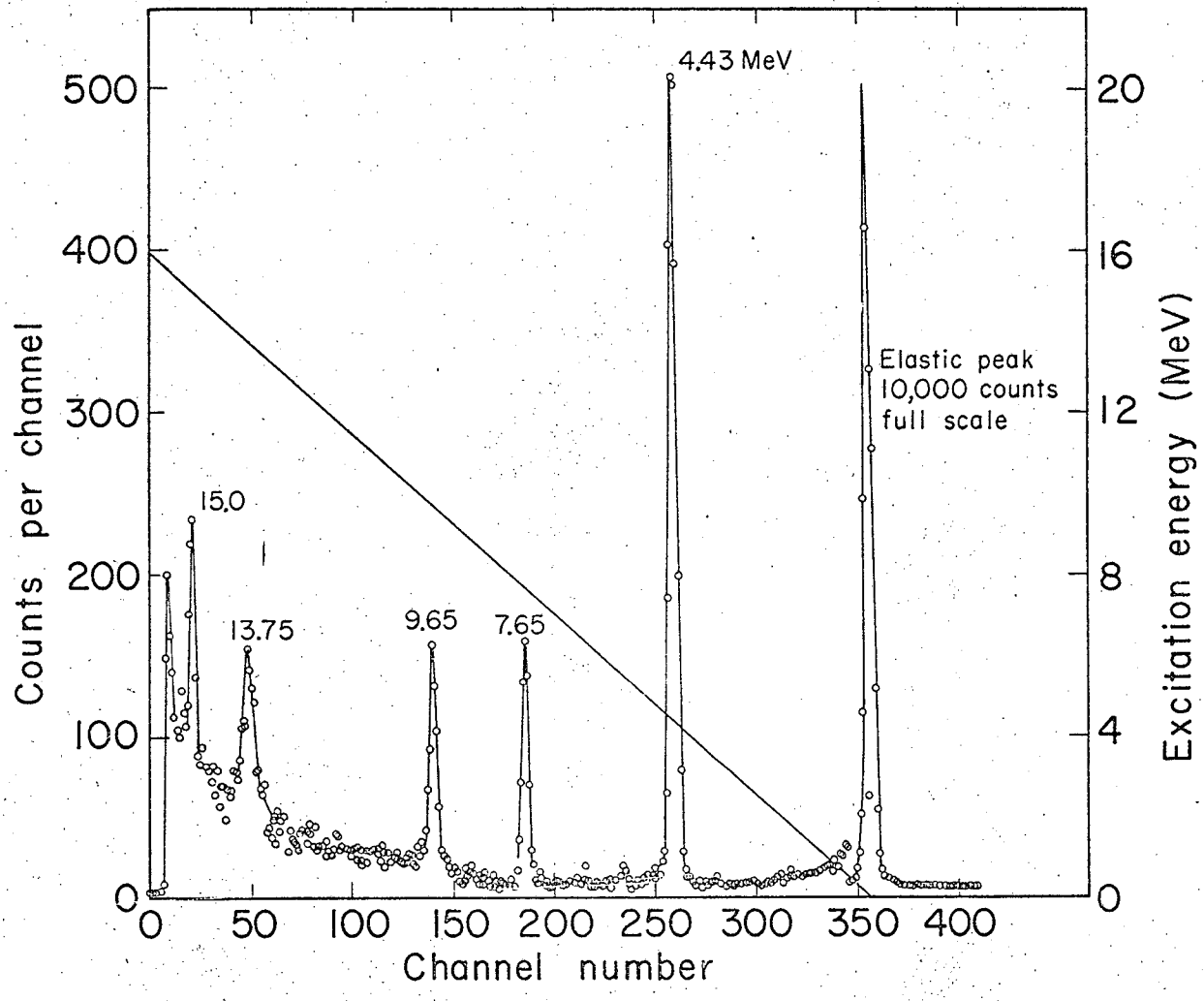


Fig. C.7-2. Elastic and inelastic spectrum of helium ions (initially 65 MeV) scattered from $C^{12}$. $C^{12}(a, a')C^{12*}$, 18 deg(lab).

## 8. "ALPHA-PARTICLE" SATELLITES IN THE "NUCLEAR STRATOSPHERE"(*)

George Igo

We have investigated the "alpha-particle" cluster density in the region $\rho < 1/20\ \rho_0$, utilizing the (α, 2α) reaction at 0.915 BeV. The results are consistent with complete clustering of all nucleons in the density region $\rho < 1/20\ \rho_0$. In the "stratospheric" layers of heavy nuclei, $\rho < 1/20\ \rho_0$, nucleons are less affected by the Pauli principle. When nucleons emerge from the inner region they give the nucleus extra stability by clustering to form "α-particle" satellites. These structures may have a short lifetime and be constantly forming and redissolving. The α-particle nonelastic mean free path in infinite nuclear matter of central nuclear density $\rho_0$ is very short (0.6 F) and almost independent of energy, as determined from elastic scattering and total reaction cross section measurements for α particles. As a consequence the reaction volume in heavy nuclei is known to be that part of the pole caps where $\rho < 1/20\ \rho_0$, and the (α, 2α) reaction is very specifically probing the "stratospheric" layer. Coincident events were observed from a series of heavy target elements in which two emergent α particles were identified and in which the sum of their energies was 0.915 BeV. The energies of the individual α particles and the angular correlation between them were found to correspond to the kinematics of a free, two-body collision for equal-mass particles. The numbers of such events were consistent with complete clustering of all nucleons in the density region $\rho < 1/2\ \rho_0$.

---

*Abstract for presentation at Conference on Advances in Meson and Nuclear Research, Gatlinburg, November 12 and 13, 1962.

## 9. TWO-NUCLEON STRIPPING REACTIONS

Bernard G. Harvey, Joseph Cerny, Richard H. Pehl, and Ernest J. M. Rivet

In each of the nuclear reactions $C^{12}(\alpha, d)N^{14}$, $N^{14}(\alpha, d)O^{16}$, $N^{15}(\alpha, d)O^{17}$, and $O^{16}(\alpha, d)F^{18}$, the energy spectrum of the emitted deuterons shows one or more very large peaks corresponding to particularly strong excitation of one or more energy levels of the product nucleus. For the residual nuclei $N^{14}$ and $F^{18}$, only one such level is excited. In $O^{17}$, there are two such levels and in $O^{16}$ there are two and possibly three. Figure C. 9-1 shows the deuteron spectrum obtained from $O^{16}(\alpha, d)F^{18}$, using 47-MeV helium ions from the Crocker Laboratory 60-inch cyclotron.

The strongly excited levels are believed to be of $(d_{5/2})^2\ J = 5$ character—that is, the target nucleus is unchanged in the reaction while the captured proton and neutron each enter the $d_{5/2}$ shell, which is initially completely empty. The angular momentum of two units per nucleon is consistent with the known linear momentum transfer if the reaction is assumed to occur at the surface of the nucleus.

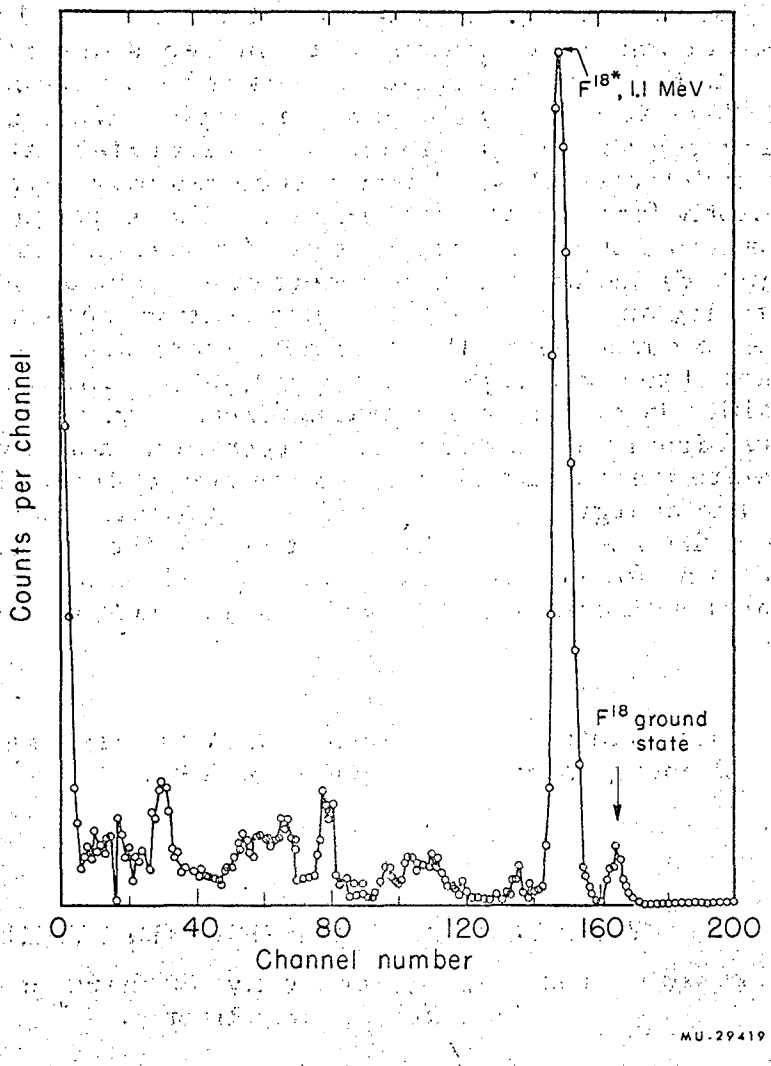


Fig. C.9-1. Spectrum of deuterons from the $O^{16}(a,d)F^{18}$ reaction induced by 47-MeV helium ions.

If most of the linear momentum of the captured particles is due to their center-or-mass motion, then the vector sum of their angular momenta will most probably be 4, since the linear momentum vectors, and therefore the angular momentum vectors, will be parallel. Since the outgoing particle is a triplet-state deuteron, conservation of angular momentum requires that the captured pair should also be in a relative triplet state. The states most strongly populated should therefore be those with a large $^3G$ amplitude. For the $(d_{5/2})^2$ J = 5 state, this amplitude is 1.00. For the $(d_{5/2})^2$ J = 3 state, the amplitude is -4/175, so this state would presumably have to be formed mainly through the $^3D$ amplitude, which is 108/175. This amplitude, however, would require $\ell_n + \ell_p$ equal to 2. The angular momentum vectors $\ell_n$ and $\ell_p$ (the orbital angular momenta of the captured neutron and proton) would thus be far from parallel. Such a situation could arise as a result of the relative internal motion of the captured particles in the incident helium ion, but it becomes less and less probable as the orbital angular momentum of the captured nucleons increases.

A 5+ level is already known in $F^{18}$ at just the energy at which the strongly populated level was found. No such level is known in $N^{14}$, but calculations by W. W. True[1] place it at about 9 MeV, in excellent agreement with the strong level populated in $C^{12}(\alpha, d)N^{14}$.

The doublet in $O^{17}$ (at 7.6 and 9.0 MeV) is believed to be due to the coupling of the J = 5 nucleon pair with the J = 1/2 $N^{15}$ target, to give two levels of spins 9/2 and 11/2. A calculation by Norman K. Glendenning finds the separation between two levels of this type to be about 2 MeV, which is in reasonable agreement with the experimental value. The three levels in $O^{16}$ are believed to be due to coupling of the J = 5 particles with the J = 1 $N^{14}$ target nucleus, giving levels of spin 4, 5, and 6.

As an extension of these observations, a successful attempt was made to find an analogous effect in the $f_{7/2}$ shell. In the reaction $Ca^{40}(\alpha, d)Sc^{42}$, a level in $Sc^{42}$ of $(f_{7/2})^2$ J = 7 character was populated much more strongly than any others. The deuteron energy spectrum is shown in Fig. C. 9-2. A strong level was found at 1.2 MeV in $K^{42}$ by means of the reaction $A^{40}(\alpha, d)K^{42}$.

These experiments were the last to be made at the 60-inch cyclotron before it closed down after 23 years of highly successful operation.

---

1. William W. True, Nitrogen-14 and the Shell Model, to be submitted for publication.

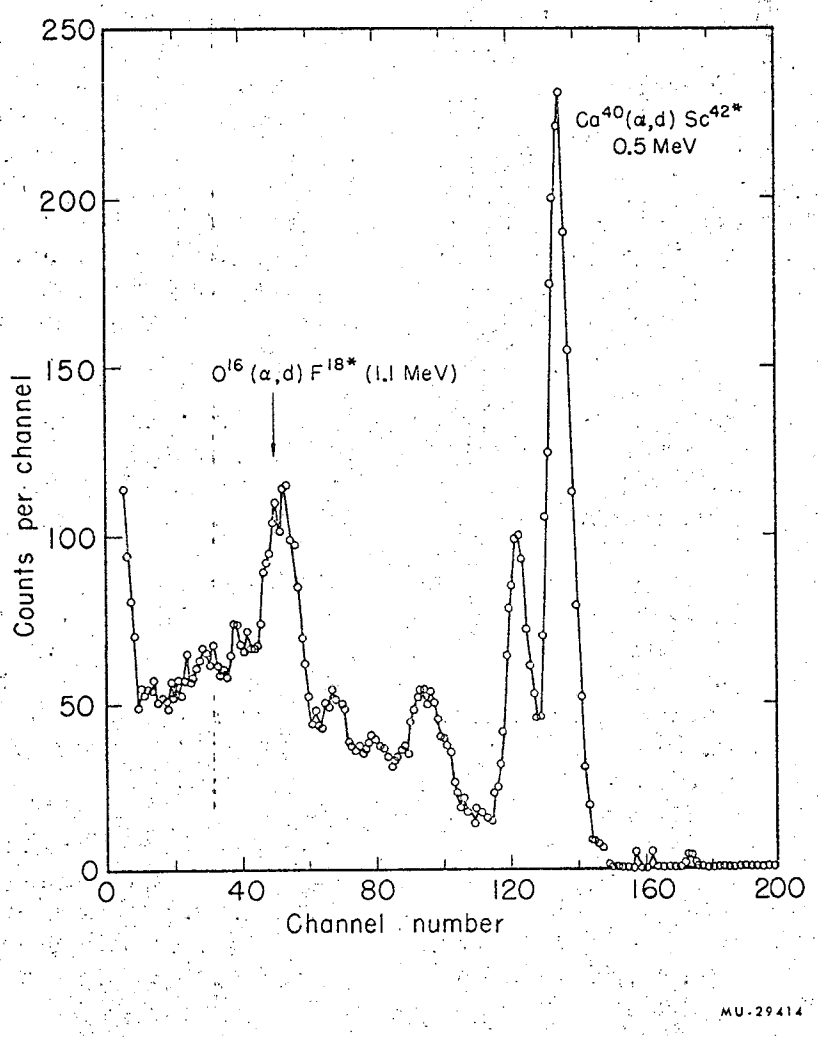


Fig. C. 9-2. Spectrum of deuterons from the $Ca^{40}(\alpha, d)Sc^{42}$ reaction induced by 47-MeV helium ions.

# 10. EQUILIBRIUM CHARGE DISTRIBUTIONS OF PRODUCTS OF HEAVY-ION-INDUCED SPALLATION

Naftali H. Steiger

Heavy particles passing through matter can lose or capture electrons in collisions with the stationary atoms of the medium traversed. This process results in the establishment of an equilibrium distribution of charges from which the characteristic mean charge can be obtained. In general the equilibrium charge $\bar{z}$ of an energetic particle in this case is given by

$$\bar{z} = f\,(Z_1,\ A_1,\ v,\ Z_2,\ A_2,\ \text{state of condensation of medium}), \qquad (1)$$

where $Z_1$, $A_1$, and v are nuclear charge, mass, and velocity of the moving particle and $Z_2$ and $A_2$ are the nuclear charge and the mass of the atoms of the medium.

No rigorous theory about the charge distribution of heavy particles ($Z > 1$) as a function of the various factors shown in Eq. (1) appears to exist at present. The methods used are highly approximate in character, mainly based on statistical considerations, and are not in very satisfactory agreement with experiments.[1-5]

The existing experimental data are mostly for particles of Z up to 20 (Ar), because of the heretofore limited possibilities of accelerating very heavy ions. Measurements on fission fragments that have a continuous spread in Z can be related only very roughly to Sr and Xe as the most representative ones.[6,7] Experimental studies for particles of higher Z would therefore be of interest.

Spallation products resulting from heavy-ion-induced nuclear reactions can be produced in an energy interval from a few MeV up to about 30 MeV. This offers therefore an almost unique possibility for the study of charge equilibria of heavy particles possessing even higher Z than the fission fragments.

This report gives the results of an experimental study of equilibrium charge distributions of heavy particles of nuclear charge $Z = 66 \pm 1$ (Tb, Dy,

---

1. N. Bohr, Phys. Rev. 58, 654 (1940).

2. W. E. Lamb, Phys. Rev. 58, 696 (1940).

3. J. Knipp and E. Teller, Phys. Rev. 59, 659 (1941); J. H. M. Brunings, J. Knipp, and E. Teller, Phys. Rev. 60, 657 (1941).

4. N. Bohr and J. Lindhard, Kgl. Danske Videnskab. Selskab Mat.-Fys. Medd. 28, No. 7 (1954).

5. I. S. Dmitriev, Soviet Phys. JETP 5, 473 (1957).

6. N. O. Lassen, Kgl. Danske Videnskab. Selskab Mat.-Fys. Medd 30, No. 8 (1955).

7. C. B. Fulmer and B. C. Cohen, Phys. Rev. 109, 96 (1958).

and Ho) in the velocity region $2.5\times10^8$ to $5.5\times10^8$ cm/sec. A number of nuclear reactions induced by accelerated heavy ions was chosen, most of them leading to $_{66}Dy^{149}$ as the primary spallation product, and in some cases to $_{65}Tb^{149g}$ or $_{67}Ho^{149}$, which finally decay into $Tb^{149g}$.

The study had to be limited to reactions for which evidence for the compound-nucleus mechanism has been presented.[8] For these reactions the mean velocity of the spallation products can be calculated.

In the experimental setup used, targets of about 100 $\mu g/cm^2$ thickness were bombarded by a well-collimated Hilac beam, which passed through a narrow slit before hitting the target. The resulting spallation products emerging from the target and passing through a second narrow slit were magnetically analyzed and then collected on a thin aluminum catcher foil. The experiments were performed at a pressure of about $10^{-4}$ mm Hg. It could be shown that with the target thickness used, about 95% of the products leave the targets after achieving charge equilibrium in it. The horizontal distribution of the collected products, which is proportional to the effective charge state, was recorded by taking an autoradiograph of the catcher foil. The distribution was then determined by counting microscopically the $\alpha$-particle tracks from the decayed $Tb^{149g}$ (see Fig. C. 10-1).

In all the reactions used, a certain number of neutrons was evaporated. When angular distribution of the evaporated nucleons is assumed either isotropic or symmetric about $\pi/2$ in the c. m. system, the mean velocity of the final product, $\langle v \rangle$, equals the velocity of the compound nucleus, and may be obtained from

$$\langle v \rangle^2 = \frac{2 A_b E_b}{(A_b + A_T)^2} , \qquad (2)$$

where $E_b$ is the bombarding energy in the laboratory system and $A_b$ and $A_T$ are the masses of the bombarding particle and the target respectively. However, the neutron evaporation causes an appreciable velocity spread of the investigated particles for which the curve shown in Fig. C. 10-1 must be corrected.

It can be shown that this spread may be estimated from

$$\frac{\langle V^2 \rangle}{\langle v \rangle^2} = \frac{\left(\frac{E_b A_T}{A_b + A_T} + Q - E_\gamma\right)\left(A_b + A_T\right)^2}{E_b A_b (A_b + A_T - \frac{x+1}{2})^2} , \qquad (3)$$

where $\langle V^2 \rangle$ is the mean square velocity of the products in the c. m. system caused by neutron evaporation, Q is the mass difference (in MeV) between

8. John M. Alexander and David H. Sisson, Recoil Range Evidence for the Compound-Nucleus Mechanism in Reactions Between Complex Nuclei, UCRL-10098, April 1962.

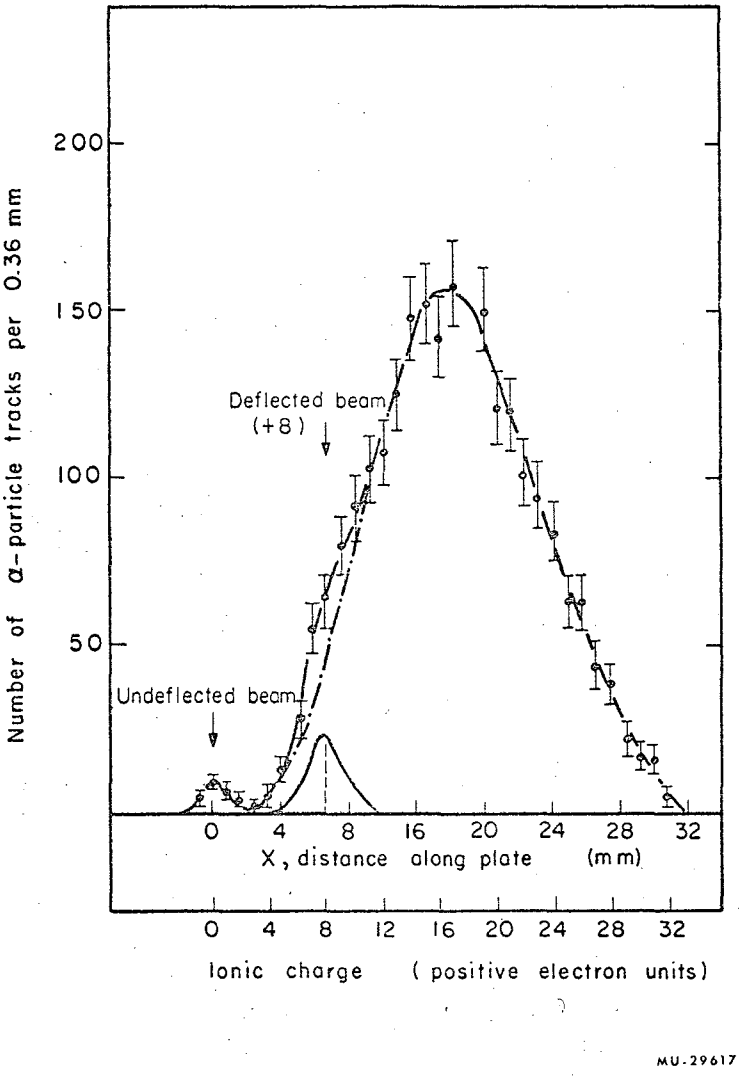


Fig. C.10-1. Experimental charge distribution. Horizontal displacement of particles on catcher foil as a function of α track density. Nuclear reaction: $Pr^{141}(O^{16}, 8n)Ho^{149}$ $E_b$(lab) = 162.0 MeV; Target thickness = 100 μg/cm$^2$ mean velocity of $Ho^{149}$ particles: $\langle v \rangle = 4.50 \times 10^8$ cm/sec. Magnetic field strength = 3150 gauss.

reactants and products, and x is the number of evaporated neutrons. $E_\gamma$ is the average total energy emitted as photons, and is based on angular distribution measurements, assuming isotropic neutron emission.[9] After correction for velocity spread according to Eq. (3), for velocity spread caused by target thickness and geometrical spread, the resultant curve can be converted into a histogram representing the actual charge distribution (Fig. C. 10-2).

In Table I are summarized the reactions used and the resultant mean effective charges as a function of the mean velocity of the particles, $\langle v \rangle$. Figure C. 10-3 is a graphic representation of $\bar{z}$ versus $\langle v \rangle$. Figure C. 10-4 shows the equilibrium charge distribution $\phi_z$ -- that is, the fraction of ions with a charge z -- as a function of particle mean velocity $\langle v \rangle$. The results for z = 5, 10, 15, 20, and 25 are plotted as representative quantities.

Both statistical models, the Bohr model[1] and the model given by Brunings, Knipp, and Teller,[3] relate to an ion in the ground state. In order to be able to apply the Bohr-Lamb theory[1, 2] to a condensed medium, one must have knowledge of the distribution of electronic orbital velocities in an ion that is continually perturbed by collisions at high frequency. As this distribution is unknown, Bohr and Lindhard[4] introduced a semi-empirical factor, which they determined as 1.5 for heavy fission fragments (Z = 54, $v = 8.6 \times 10^8$ cm/sec). In this investigation (Z = 66, $v = 2.5 \times 10^8$ to $5.5 \times 10^8$ cm/sec), the factor found was about 2 for the whole velocity range studied. When applying our $\bar{z}/v$ function to the statistical model given by Brunnings, Knipp, and Teller we obtained the following $\gamma$ values:

(a) For the assumption that the characteristic velocity is that of the energetically most easily removable electron, we get $\gamma = 4.3$ for $v = 2.5 \times 10^8$ cm/sec, and $\gamma = 3.6$ for $v = 5.5 \times 10^8$ cm/sec. Extrapolating from these values to Z = 54, $v = 8.8 \times 10^8$ cm/sec gives a $\gamma$ value close to that obtained for heavy fission fragments in condensed media ($\gamma = 2.1$).

(b) For the assumption that the characteristic velocity is that of the outermost electron, we get, for the whole velocity range measured, the almost constant value of $\gamma = 0.8$.

The results obtained for the measured equilibrium charge distributions will be discussed in greater detail in a forthcoming report. Furthermore, an attempt will be made to use the experimental results for improved calculations of range-energy relations of heavy ions in this velocity and Z region.

---

9. Gabriel N. Simonoff and John M. Alexander, Angular-Momentum Effects on Neutron Emission by $Dy^{156}$, $Tb^{153}$, and $Tb^{157}$ Compound Nuclei, UCRL-10099 Rev., Sept. 1962.

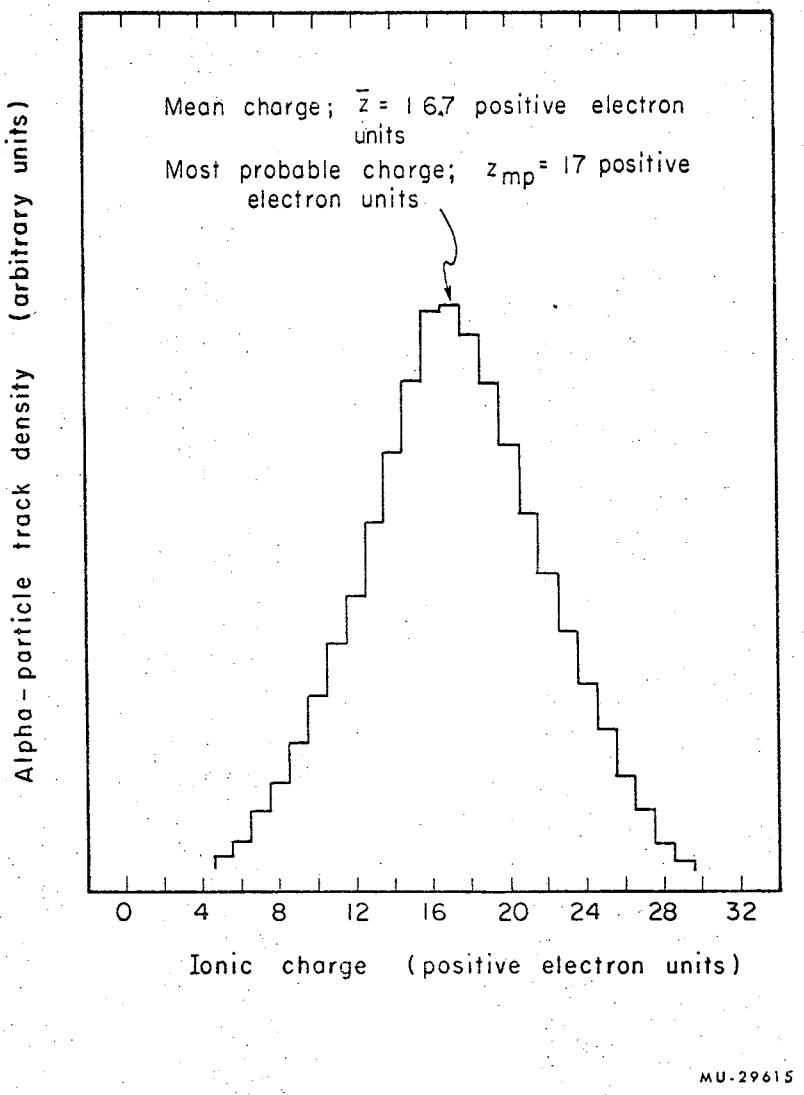


Fig. C. 10-2. Corrected charge distribution. Effective charge state (in positive electron units) as a function of α-particle track density. Nuclear reaction: $Pr^{141}(O^{16}, 8n)Ho^{149}$. Mean velocity of $Ho^{149}$ particles $\langle v \rangle = 4.50 \times 10^8$ cm/sec.

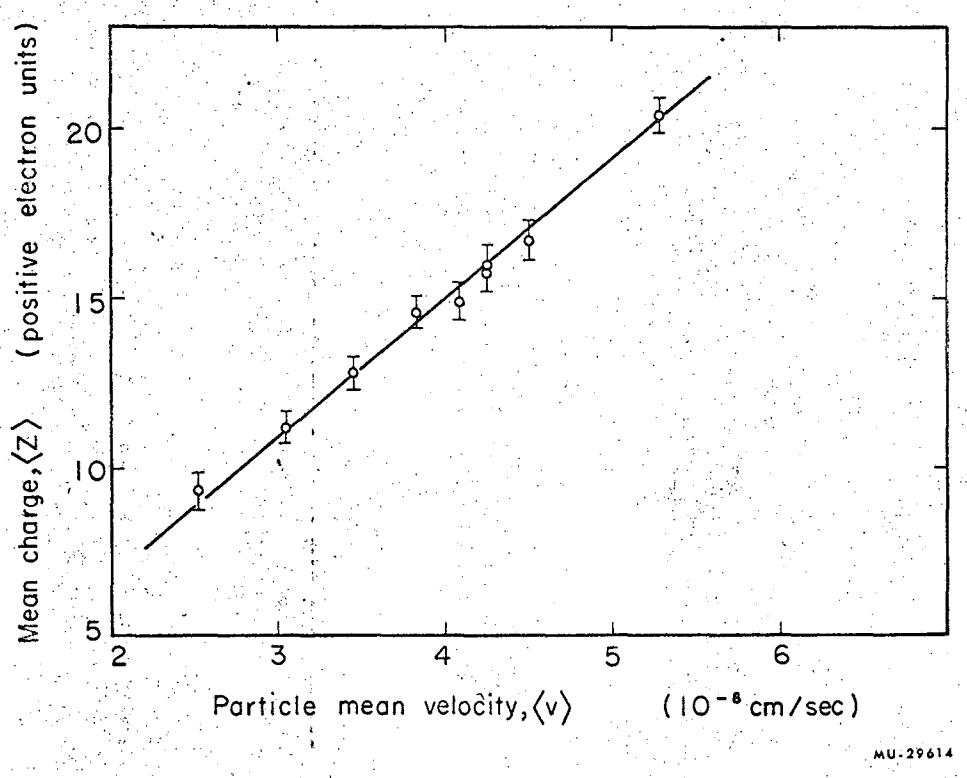


Fig. C. 10-3. Effective mean charge $\bar{z}$ (in positive electron units) as a function of particle mean velocity $\langle v \rangle$; nuclear charges of moving particles $Z_1$ = 65, 66, 67 (see Table I).

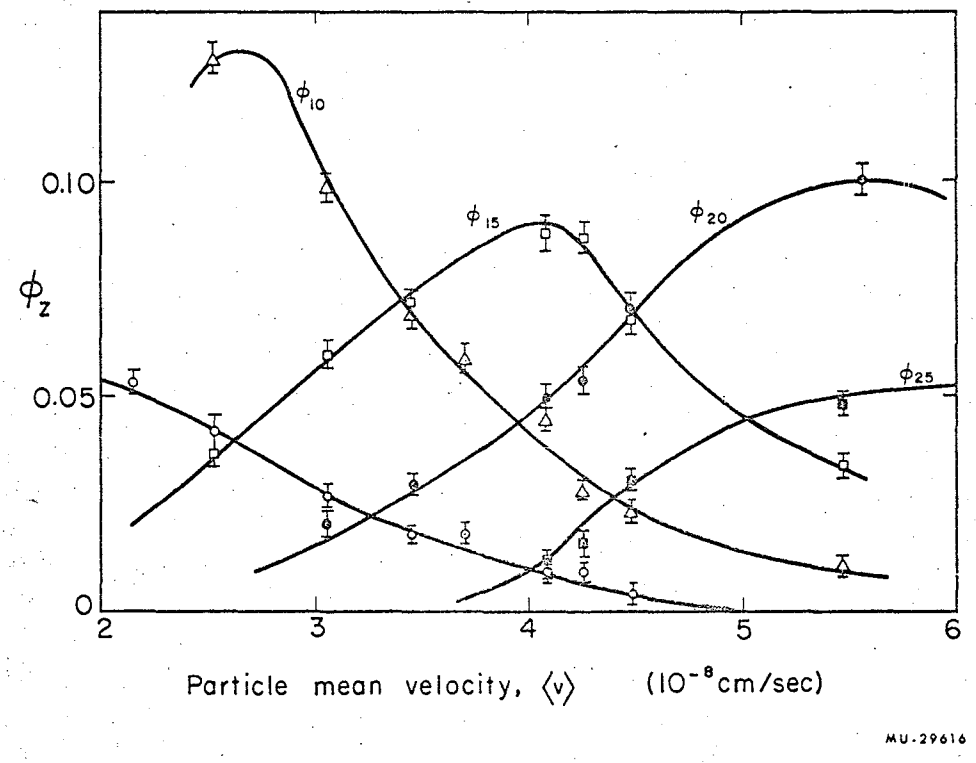


Fig. C. 10-4. Equilibrium charge distribution $\phi_z$ (fraction of ions with charge z) as a function of particle mean velocity $\langle v \rangle$; z = 5, 10, 15, 20, or 25.
$Z_1$ = 65, 66, and 67
$Z_2$ = 56 through 60
see Table I

Table I. Summary of the reactions used and of mean effective charge $\bar{z}$. (Symbols as used in text.)

| Nuclear reaction | $E_b$(lab) [MeV] | $Z_1$ | $Z_2$ | $\langle v \rangle$ ($10^{-8}$ cm/sec) | Velocity spread, $\sigma_{1/2}$, caused by: neutron evaporation (%) | Velocity spread, $\sigma_{1/2}$, caused by: target thickness (%) | $\bar{z}$ (positive electron units) |
|---|---|---|---|---|---|---|---|
| $Pr^{141}(C^{12}, 4n)Tb^{149}$ | 64.0 | 65 | 59 | 2.52 | 9.3 | 3.2 | 9.3 |
| $Nd^{142}(C^{12}, 5n)Dy^{149}$ | 95.2 | 66 | 60 | 3.05 | 11.1 | 2.9 | 11.2 |
| $Pr^{141}(N^{14}, 6n)Dy^{149}$ | 105.7 | 66 | 59 | 3.45 | 10.9 | 2.6 | 12.8 |
| $Pr^{141}(N^{14}, 6n)Dy^{149}$ | 130.0 | 66 | 59 | 3.82 | 11.8 | 2.1 | 14.6 |
| $Ce^{138}(O^{16}, 7n)Dy^{149}$ | 133.1 | 66 | 58 | 4.08 | 10.0 | 1.5 | 14.9 |
| $Ce^{138}(O^{16}, 7n)Dy^{149}$ | 141.0 | 66 | 58 | 4.24 | 10.8 | 1.4 | 15.7 |
| $Pr^{141}(O^{16}, 8n)Ho^{149}$ | 144.5 | 67 | 59 | 4.24 | 10.3 | 1.8 | 15.9 |
| $Pr^{141}(O^{16}, 8n)Ho^{149}$ | 162.0 | 67 | 59 | 4.50 | 10.6 | 1.7 | 16.7 |
| $Ba^{138}(Ne^{20}, 9n)Dy^{149}$ | 181.6 | 66 | 56 | 5.27 | 10.0 | 1.9 | 20.4 |
| $Ba^{138}(Ne^{22}, 11n)Dy^{149}$(a) | 205.0 | 66 | 56 | 5.83 | | | (a) |

a. This type of experiment is to be performed in the very near future.

# 11. DETERMINATIONS OF NUCLEAR "RADII" FROM HEAVY-ION ELASTIC SCATTERING

Homer E. Conzett

Phase-shift analyses[1] of heavy-ion elastic scattering data have yielded "interaction" radii,

$$R = r_a(A_1^{1/3} + A_2^{1/3}),$$

where $A_1$ and $A_2$ are the mass numbers of the projectile and target nuclei, respectively. Hereafter, a radius so determined will be called an absorption[2] radius, since this terminology explicitly defines the method by which the determination was made. The radius parameter has typically been consistent with $r_a = 1.45$ F when obtained, for example, from $C^{12}$, $N^{14}$, $O^{16}$, and $Ne^{20}$ scattering data.[3-5] By contrast, the radius parameter determined by optical-model analyses of elastic proton and α-particle scattering data has been $r_0 \leq 1.30$ F.[6] The purpose of this note is to point out the reason for this apparent discrepancy.

In the optical model, $r_0$ is the radius parameter corresponding to the half-value point of the real nuclear potential,

$$Vf(r) \text{ with } f(r) = \left[1 + \exp\frac{r - R}{a}\right]^{-1};$$

and, also, of the imaginary potential when the same radial form, f(r), is assumed. (This radius is expected to be larger than the nuclear density radius by the range of the nuclear force.) By contrast, a phase-shift analysis determines the actual absorption[2] of particles as a function of the orbital angular momentum, $\ell\hbar$, of the projectile-nucleus system. This can be transformed into a determination of the absorption as a function of impact parameter of the corresponding classical trajectory.[7] Thus, $r_a$ is

---

1. We include here all analyses in which the partial-wave (complex) phase shifts are explicit parameters in the calculation and are not adjusted through an intermediary optical potential; e.g., J. S. Blair, Phys. Rev. 95, 1218 (1954), "sharp-cutoff" model; J. A. McIntyre, K. H. Wang, and L. C. Becker, Phys. Rev. 117, 1337 (1960), modified sharp-cutoff model.

2. As used here, any transition out of the entrance channel is defined as absorption.

3. J. A. McIntyre, S. D. Baker, and T. L. Watts, Phys. Rev. 116, 1212 (1960).

4. Jonas Alster and Homer E. Conzett, Heavy-Ion Elastic Scattering, to be submitted to Phys. Rev. (revision of thesis by Alster, UCRL-9650, April 1961).

5. D. D. Kerlee, H. L. Reynolds, and E. Goldberg, Phys. Rev. 127, 1224 (1962).

6. For example, Proceedings of the International Conference on the Nuclear Optical Model, Florida State University, Tallahassee, 1959.

7. In the simple case of an uncharged projectile, for example, the impact parameter is $r = [\ell(\ell+1)]^{1/2}/k$, where $\hbar k$ is the center-of-mass momentum.

the radius parameter corresponding to the radius at which the amplitude, $A_\ell(r)$,[8] of the outgoing $\ell$th partial wave has been reduced to 1/2. (For complete absorption $A_\ell = 0$, for no absorption $A_\ell = 1$.)

Since $r_0(A_1^{1/3} + A_2^{1/3})$ is the radius at which the optical potential is V/2, whereas $r_a(A_1^{1/3} + A_2^{1/3})$ is the radius at which the absorption of incident particles is 75% [that is, $A_\ell^2 = \frac{1}{4}$ = intensity of outgoing wave; $(1 - A_\ell^2) = \frac{3}{4}$ = fractional absorption], an $r_0 = r_a$ would be purely fortuitous. Figure C. 11-1 demonstrates this point graphically. There, the curve f(r) with $r_0 = 1.30$ F represents the optical potential f(r) appropriate to the scattering of protons from Ta. The curve $A_\ell(r)$, with $r_a = 1.45$ F as determined from analysis of 124-MeV $C^{12}$-Ta scattering data,[4] demonstrates that the strong absorption of the incident particles in the outer region of the potential (and nuclear density) explains the larger value of $r_a$. Thus, it is apparent that $r_a$ should not be a constant, but can be expected to vary with type and energy of the incident particle.

---

8. The argument r in $A_\ell(r)$ is written here to indicate the "equivalence" between $\ell$ and r.

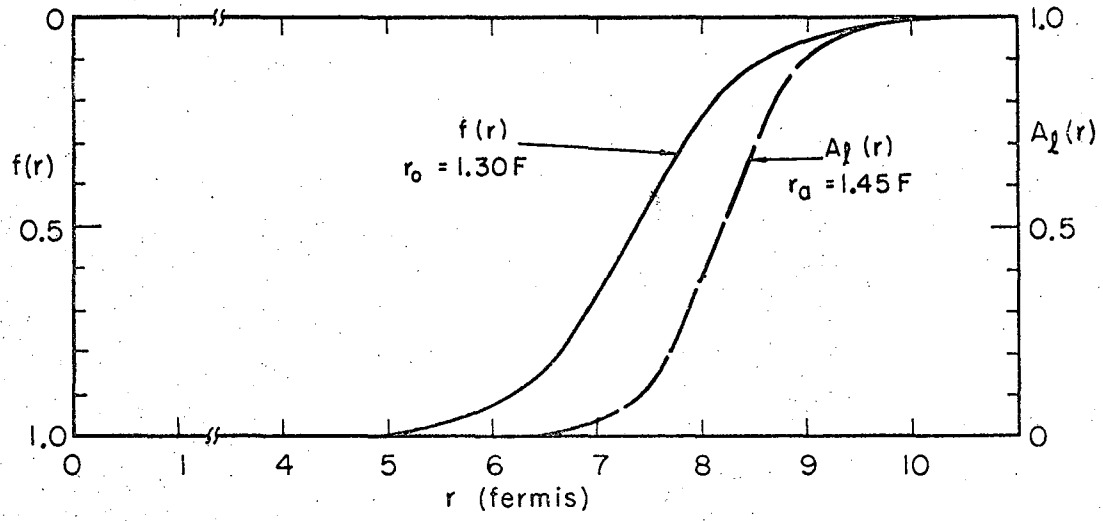


Fig. C. 11-1. Comparison of radius parameters, $r_0$ and $r_a$ (see text).

# D. PHYSICAL CHEMISTRY

## 1. MASS SPECTROSCOPY. SURFACE IONIZATION STUDIES

F. L. Reynolds

This work has to do with the possible improvement of surface ion sources for use in mass spectroscopy and in the evaluation of surface ionization as a method of ascertaining ionization potentials. The latter depends on the assumption that the Saha-Langmuir equation describes the correct relationship between the surface work function $\Phi$ of a metal and the ionization potential I of an atom having thermodynamic equilibrium residence on the metal surface.

The ratio of the number of ions to atoms leaving a hot metal surface is $\alpha = N_+/N_0$, and is known as the degree of ionization. In a simplified case, with $N_0 >> N_+$, $\alpha$ is determined by the relationship expressed in the Saha-Langmuir equation,

$$\alpha = \frac{N_+}{N_0} = \frac{g_+}{g_0} \exp\left[\frac{e(\Phi - I)}{KT}\right] .$$

The ratio $g_+/g_0$ gives the statistical weights of the ionic and atomic states, I the ionization potential of the impinging element, and K and T have their usual meaning. The determination of $\alpha$ experimentally depends not only on the measurement of the metal temperature, on $\Phi$, and on the ionization energy, but is also dependent upon the physical and chemical condition of the metal surface, the degree of surface coverage by foreign atoms and the desired impinging atom. It is influenced by the electric field extracting the ions from the metal surface and is also sensitive to the potential drop along the emitting filament, since in most experimental cases this filament is not an equipotential surface.

To minimize a number of these experimental effects, a homogeneous single-crystal surface was used, ultrahigh vacuum conditions were maintained, low-intensity beams employed, and particular attention given to field extraction conditions.

The work was done on single-crystal tungsten ribbon filaments and studies were made using the (110) and (111) crystal surfaces. These oriented filaments were heated in a mass spectrometer and a beam of either Ba, Sr, or Ca atoms impinged on the hot filament surface. The atomic beam was held constant by effusion from a small Knudsen-type oven. The oven could be heated by radiation alone, or by electron bombardment when higher temperatures were required.

It has been known for some time that the electron emission from the (110) plane of tungsten is considerably lower than from other planes. This has been determined by various methods, but agreement in the work function of this plane is not too impressive. The spread of values reported ranges

from 4.58 to 6.0 eV. For the formation of positive ions, where $I > \Phi$, a high-work-function surface increases the emission. A high-work-function surface is desired for greater sample efficiency in mass spectroscopy, and in addition a factor of stability and reproducibility is required in first-ionization potential determinations.

Only a few values for the first-ionization potential of elements determined by surface ionization methods appear in the literature. Agreement with other values, when available, is again not impressive. For example, the greatest difference involves the element uranium. Bakulina and Ionov[1] gave 6.08 eV, Werning[2] 6.25 eV by surface ionization methods. Spectroscopic (emission) methods quote 4.0 eV.[3] In most other cases the surface ionization method has given a slightly lower value for the elements Nd, Pr, Ce, Er, and Tb than other methods. See Table I.

Table I. Comparison of first-ionization methods determined by different methods.

| Element | Surface-ionization method (eV) | Other methods (eV) | References |
|---|---|---|---|
| Nd | 5.51 | 6.3 | 4, 5 |
| | 6.31 | 5.7 | 6, 7 |
| | 5.10 | | 2 |
| Pr | 5.48 | 5.8 | 5, 6 |
| Ce | 5.60 | 6.54 | 5, 7 |
| | | 6.91 | 5 |
| Tb | 5.98 | 6.7 | 5, 7 |
| U | 6.08 | | 1 |
| | 6.25 | 4.0 | 2, 3 |
| | 4.5 to 5.0 | | 8 |
| Pu | 5.1 | --- | 9 |
| Am | --- | 6.0 | 10 |

1. I. N. Bakulina and N. I. Ionov, Soviet Phys. JETP 9, 709 (1959).

2. Joseph R. Werning, Thermal Ionization at Hot Metal Surfaces (Thesis), UCRL-8455, Sept. 1958.

3. Smithsonian Physical Tables (prepared by William E. Forsythe), 9th Revised Ed. (Smithsonian Institution, Washington, D. C., 1954).

4. R. G. Johnson, D. E. Hudson, and F. H. Spedding, Mass-Spectrometric Determination of Latent Heats of Metals, ISC-293, Dec. 1952.

5. W. Finkelnburg and W. Humback, Naturwiss 42, 35 (1955).

6. N. I. Ionov and M. A. Mitsev, Zhur. Eksptl. i Teoret. Fiz. 38, 1350 (1960); see also Soviet Phys. JETP 13, 518 (1961) and 11, 972 (1960).

7. J. C. Boyce, Rev. Mod. Phys. 13, 1 (1941).

8. E. G. Rauh and R. J. Thorn, J. Chem. Phys. 31, 1481 (1959).

9. Ralph H. V. M. Dawton and Kenneth L. Wilkinson, Plutonium: Evaporation Tests, Ionization Potential, and Electron Emission, AERE-GP/R 1906, Apr. 1955.

10. M. Fred and F. S. Tomkins, J. Opt. Soc. Am. 47, 1076 (1957).

## Filament Preparation

Single-crystal filaments were prepared by slicing bulk-single crystal tungsten into 0.020-in. -thick wafers. The wafers were ground to about 0.005 in. thickness and then slit into 0.035-in. -wide strips by cutting with a miniature sandblast cutter. The strips were then ground to 0.002 in. thickness, and electropolished. Each filament was checked for final orientation and single-crystal properties by back-reflected Lane x-ray technique before being placed in the mass spectrometer.

## Results

Work on polycrystalline tungsten filaments was reported previously.[11] At this time it was ascertained that so-called polycrystalline filaments, upon heating, soon developed single-crystal surfaces of preferred orientation, but a given surface orientation was not often reproducible. The surface could consist of a few large crystals all oriented within 2 or 3° of each other, and from a number of such filaments it was found that the surface plane could be (211), (311), (511), (310), (411) or other closely associated higher-index planes. In spite of the multitude of planes, their work functions must be reasonably close. Impinging Ba on W, Werning obtained 4.58±.01 eV for the work function of a heated polycrystalline tungsten filament; a value of 4.59±.03 eV had been obtained in the previously reported work[11] for the (310) plane using Sr on W. A paper by Allen reported a value of 4.58 eV from the (311) plane of tungsten.[12] This was determined by electron emission. It is indeed remarkable that such close values are obtained for tungsten surfaces whose metallographic history and experimental conditions were not likely to be identical.

A (110) surface-oriented filament, prepared as outlined above, was substituted for the polycrystalline filament. The oven was charged with both Ca and Sr. By accident, the beam intensities of $Ca^{40}$ and $Sr^{88}$ were of the same magnitude. An average of 10 Sr runs gave 5.44±.05 eV for the surface work function, and a similar number of runs with Ca gave 5.45±.05 eV. Values of 5.69 eV for Sr and 6.111 eV for Ca were taken as the first-ionization potentials.[13]

A second (110) surface-oriented filament was substituted for the previous emitter. Four determinations with Ca gave 5.39±.04 eV and 9 runs with Sr gave 5.38±.03 eV for this surface. A comparison of the surface planes of these two filaments by x-ray techniques checked within a degree or two of being (110).

Similar techniques were then used on a filament whose surface normal was the (111) plane. For this surface, the published literature values agree

---

11. F. L. Reynolds, in Chemistry Division Annual Report, UCRL-10023, Jan. 1962, p. 216.

12. F. G. Allen, Phys. Chem. Solids 8, 119 (1959).

13. C. E. Moore, Atomic Energy Levels, Vol II., Natl. Bur. Std. U. S. Circ. 467, 1962.

within ± 0.2 eV and center about an average value of 4.4 eV. Initial runs on this surface were yielding much higher values as shown in Table II.

Table II. Surface work functions (initial runs) on filament with surface normal (111) plane.

| Date | Experiment | $\Phi_{(111)}$ (eV) |
|---|---|---|
| 8-6 | Ba on W | 4.79 |
| 8-7 | Ba on W | 4.79 |
| 8-8 | Ba on W | 4.80 |
| 8-12 | Ba on W | 4.80 |
| 8-13 | Ca on W | 4.81 |
| 8-13 | Ba on W | 4.92 |
| 8-17 | Sr on W | 4.95 |
| 10-17 | Ca on W | 5.01 |
| 10-23 | Ca on W | 4.98 |

There also appeared to be a trend upwards in the work function of the surface with time. It was postulated that the (111) surface was not stable and that other planes were being presented. To check this, the filament was removed and an x-ray orientation picture taken. The Laue pattern indicated a (111) surface plane, the crystal structure giving a perfect single-crystal pattern. The filament Kovar leads had become slightly conducting from filament evaporated metal, which is believed to have biased the results in Table II. The same filament was replaced in the mass spectrometer and the leads protected from recoating. A second series of runs was taken on this surface; the results appear in Table III.

Table III. Surface work functions (second run); surface normal (111) plane.

| Date | Experiment | $\Phi_{(111)}$ (eV) |
|---|---|---|
| 11-27 | Sr on W | 4.50 |
| 11-27 | Sr on W | 4.55 |
| 11-28 | Sr on W | 4.56 |
| 11-28 | Sr on W | 4.52 |
| 11-28 | Sr on W | 4.47 |
| 11-29 | Sr on W | 4.47 |
| 11-29 | Sr on W | 4.41 |
| 11-30 | Sr on W | 4.43 |

Summary

A value for the work function of the (110) plane of tungsten has been determined. It is also demonstrated that this surface is stable and constant at high temperatures over long periods of time. An average value for the (110) plane is 5.41±.04 eV.

A value for the (111) plane of tungsten agrees quite well with previous literature values. This value is 4.49±.04 eV.

These results were determined by using three different elements, whose first-ionization potentials have values of 5.21 eV for Ba, 5.69 eV for Sr, and 6.111 eV for Ca.[13] Essentially, there was good agreement in the experimental work-function value of the surfaces studied by using either of these elements.

The Saha-Langmuir equation can be used to give correct values for unknown ionization potentials provided detailed attention is given the parameters of physical and chemical adsorption, clean surface conditions, low residual gas pressure, and electrical and electric field conditions. The ionization potential should, of course, be greater than Φ for this method. A more detailed account of these experiments will be given in F. L. Reynolds, "Surface Ionization of Tungsten Single-Crystal Filaments," to be submitted to J. Chem. Phys. (UCRL-10618, Feb. 1963).

## 2. CHEMICAL EFFECTS FOLLOWING THE $S^{34}(n, \gamma)S^{35}$ REACTION IN GASEOUS SULFUR COMPOUNDS(*)

M. Lee Hyder† and Samuel S. Markowitz

The chemical behavior of $S^{35}$ formed by the $S^{34}(n, \gamma)$ reaction has been studied in gaseous $H_2S$, $SO_2$, $SF_6$, $CH_3SH$, and thiophene. The gases were sealed in quartz ampules and irradiated with thermal neutrons in the thermal column of the Livermore pool-type reactor. Among the effects studied were those of pressure, surface area of the container, and additive gases including Ar, NO, $O_2$, and $H_2$. The $S^{35}$ was recovered in gaseous compounds and in deposits on the walls of the ampules; the chemical composition of both portions of activity was determined by aqueous chemistry using carriers. The results are consistent with a model in which the original molecule is broken up in the recoil process and the resulting fragments containing $S^{35}$ react with the surroundings only after they have slowed to thermal energies; in general, the final chemical form of the $S^{35}$ is determined by the chemical environment in which it is produced rather than by its original oxidation state or chemical

---

* Condensation of paper (UCRL-10360-Rev., Aug. 1962, based on Ph. D. thesis by M. Lee Hyder) to be published in J. Inorg. Nucl. Chem., 1963.

† Present address: Chemistry Department, Savannah River Laboratory, E. I. duPont deNemours and Co., Aiken, South Carolina.

form. However, irradiations of mixtures of several gases with NO gave results possibly indicating that the chemical form of the $S^{35}$ immediately after molecular disruption may depend upon the nature of the original molecule.

The study of the chemistry of radioactive products of nuclear reactions offers a unique tool for an examination of the chemical behavior of molecular fragments with high kinetic energy. The nuclear reaction imparts a high recoil momentum to the atom involved. This momentum may suffice to break the atom's chemical bonds and give it high kinetic energy as well, so that it recoils through its surroundings as a "hot" atom or ion. Following its subsequent chemical reaction, it can be identified by its radioactivity. A hot atom recoiling through a liquid or solid is restricted to a relatively small region by recoil from surrounding atoms, and when it is finally slowed to thermal energies it may react chemically with the excited chemical species produced in the slowing process. In the gas phase, however, the interval between collisions is so large that chemical reactions with the undisturbed surroundings are possible. Experimental systems of this type have been investigated by a number of authors who studied particularly the reactions of tritium with organic materials,[1] reactions of various halogens,[2,3] and others.[4,5] Estrup and Wolfgang have been able to characterize the reaction of tritium with methane to give $CH_3T$ as being due to tritium atoms with kinetic energy above thermal energy.[6] Gordus and Hsiung have further extended the theory and have given a theoretical treatment of the bond-breaking process.[7]

In our work the reactions of $S^{35}$ produced by $S^{34}(n,\gamma)$ were studied in a variety of gaseous systems. The reactions of $S^{35}$ were first investigated by Levey, Milham, Rice, and Willard,[8] and have recently been studied by Herber, who reviews earlier work.[9] In most of these experiments the $S^{35}$ was produced in condensed systems by the $Cl^{35}(n,p)S^{35}$ reaction. It was felt that study of gas-phase reactions of $S^{35}$ would help answer questions regarding oxidation or reduction resulting from the nuclear process, and might additionally indicate to what extent multiple bonds are broken.

---

1. This work is reviewed by (a) Alfred P. Wolf, Ann. Rev. Nucl. Sci. 10, 259-290 (1960), and in (b) Proceedings of a Symposium on Chemical Effects of Nuclear Transformations, Prague, 1960 (International Atomic Energy Agency, Vienna, 1961) Vol. 2, pp. 67-148.

2. J. B. Evans, J. E. Quinlan, M. C. Sauer, Jr., and J. E. Willard, J. Phys. Chem. 62, 1351 (1958).

3. Edward P. Rack and Adon A. Gordus, J. Phys. Chem. 65, 944 (1961).

4. C. MacKay, M. Pandow, P. Polak, and R. Wolfgang, Reference 1(b), op. cit., 2, p. 38.

5. W. S. Koski, H. Schmied, and W. C. Perkins, Reference 1(b), op. cit., 2, p. 217.

6. Peder J. Estrup and Richard Wolfgang, J. Am. Chem. Soc. 82, 2665 (1960).

7. Adon A. Gordus and Ch-hua Hsiung, J. Chem. Phys. 36, 947 (1962).

8. Gerrit Levey, Robert Milham, William Rice, and John E. Willard, in Conference on Hot-Atom Chemistry Brookhaven National Laboratory Report AECU-50, Aug. 1948, p. 6.

9. R. H. Herber, Reference 1(b), op. cit., 2, pp. 201-208.

The radioisotope $S^{35}$ is formed from $S^{34}$, which is 4.2% abundant in natural sulfur,[10] with a cross section that is 0.26 b for thermal neutrons.[11] The half-life of $S^{35}$ is 87 days, and it decays by emission of $\beta^-$ particles with a maximum energy of 0.168 MeV. No gamma radiation accompanies decay.[10]

Breakup of the original molecule has been shown to be general following the $S^{34}(n, \gamma)S^{35}$ reaction, but there remains a possibility that not all bonds will be broken, depending on the nature of the original species.

Except possibly for the results obtained with added NO, oxidation or reduction of the sulfur activity appears to depend upon the surroundings -- walls, reactive gases, etc. -- rather than upon the oxidation state or nature of the original molecule.

The $H_2S^{35}$ has been found to be a major product in irradiations of $H_2S$, $CH_3SH$, and thiophene. (The $H_2S^{35}$ fraction may also include $H_2SS^{35}$.) The results of $SO_2$ irradiations are complex; an important contribution to the reactions appears to involve the walls. Oxidation on the walls seems to take place readily when gas-phase reactions do not compete; this is not unexpected in view of the ease with which oxidation occurs in $C^{11}$ recoils[4] and in $S^{35}$ formed in crystals.[9]

Implicative results were obtained from irradiations of various gases mixed with NO. Although $S^{35}$ was recovered in gaseous compounds that were not definitely identified, the study of the hydrolysis products of these compounds implies that the chemical form of the $S^{35}$ immediately following breakup may vary with the chemical form of the original compound.

No epithermal reactions have been identified as such for $S^{35}$ recoils; they have probably been ruled out in the $SO_2$ and $H_2S$ systems. The results from the irradiation of $CH_3SH$ or thiophene suggest that hot reactions may take place in these systems.

---

10. D. Strominger, J. M. Hollander, and G. T. Seaborg, Rev. Mod. Phys. 30, 615 (1958).

11. D. J. Hughes and R. B. Schwartz, Neutron Cross-Sections (2nd Ed.), Brookhaven National Laboratory Report BNL-325, 1958.

## 3. THE RADIATION CHEMISTRY OF ISOPROPYL COMPOUNDS(*)

Michael P. Sweeney and Amos S. Newton

A study has been made of the effect of radiation quality on the radiolysis of a variety of liquid organic compounds. One major aspect of this study was to investigate the extent of molecular rearrangements of the type

$$i\text{-}C_3H_7X \longrightarrow C_3H_6 + HX.$$

Because many such rearrangements have been postulated to occur from H atoms on carbons β to the group X, the aliphatic group in each compound was the isopropyl group and X was any one of the functional groups Cl, OH, $C_6H_5$, CN, COOH, $CH_2COOH$, $COCH_3$, and $OCOCH_3$. In each case purified degassed liquid samples of each of the compounds were irradiated at a number of dosage levels with $Co^{60}$ γ rays or 40-MeV helium ions. The volatile products of each irradiation were isolated and determined, and the zero bombardment yield of each product was found by extrapolation to zero time of irradiation. The yields of products are shown in Table I.

Certain products in Table I can be formed only by radical-radical reactions. In these cases it was found that the yields of these products by the two types of radiation were in the ratio $G_{He^{++}}/G_{\gamma} = 1.8 \pm 0.2$. Propylene can be formed in the irradiation of these compounds by

(1) a disproportionation reaction of isopropyl radical and another radical, and

(2) a molecular dissociation of the excited molecule to propylene and HX.

The radical part of the propylene yield should bear the relation of a factor of 1.8 between the two radiations, while the unimolecular part should be independent of radiation quality if it is assumed that no deactivation of the excited state leading to the dissociation occurs that is a function of radiation quality. Thus one can set up two equations in two unknowns and solve for the extent of rearrangement to form $C_3H_6$.

(1) $He^{++}$: $G_{rearrangement} + 1.8\, G_{disp.} = G_{He^{++}}$,

(2) $Co^{60}$ γ rays: $G_{rearrangement} + G_{disp.} = G_{\gamma}$ .

The results are shown in Table II.

The results show the rearrangement to propylene to be a major mechanism in the radiolysis of isopropyl chloride, isobutyronitrile, methyl isopropyl ketone, and isopropyl acetate, and a minor contributor to the radiolysis products of the other compounds irradiated.

---

*Brief presentation from thesis by Michael P. Sweeney (UCRL-9983, March 1962).

Table I. Initial product yields (G values) from $He^{++}$ and $Co^{60}$ γ-ray irradiation of various liquid isopropyl compounds

| Product | Isopropyl chloride | | Isopropyl alcohol | | Isopropyl benzene | | Isobutyro-nitrile | | Isobutyric acid | | Isovaleric acid | | Methyl iso-butyl ketone | | Isopropyl acetate | |
|---|---|---|---|---|---|---|---|---|---|---|---|---|---|---|---|---|
| | $He^{++}$ | $Co^{60}$ | $He^{++}$ | $Co^{60}$ | $He^{++}$ | $Co^{60}$ | $He^{++}$ | $Co^{60}$ | $He^{++}$ | $Co^{60}$ | $He^{++}$ | $Co^{60}$ | $He^{++}$ | $Co^{60}$ | $He^{++}$ | $Co^{60}$ |
| $H_2$ | 1.31 | 1.31 | 3.48 | 3.08 | 0.27 | 0.21 | 1.06 | 0.84 | 0.84 | 0.73 | 0.77 | 0.67 | 0.90 | 0.70 | 0.88 | 0.76 |
| $CH_4$ | 0.24 | 0.25 | 1.35 | 1.68 | 0.075 | 0.108 | 0.39 | 0.44 | 0.091 | 0.102 | 0.12 | 0.15 | 0.43 | 0.58 | 0.98 | 1.85 |
| $C_2H_6$ | 0.010 | 0.003 | 0.16 | 0.079 | 0.0038 | 0.0016 | 0.026 | 0.014 | 0.01 | ≤0.005 | ≈0.008 | ≈0.005 | 0.065 | 0.034 | 0.59 | 0.34 |
| $C_3H_8$ | 1.14 | 3.38 | 0.10 | 0.11 | 0.0069 | 0.012 | 0.26 | 0.51 | 1.40 | 3.47 | ≈0.04 | ≈0.1 | 0.032 | 0.083 | 0.15 | 0.43 |
| $C_3H_6$ | 2.68 | ≈2.16 | 0.37 | 0.25 | 0.028 | 0.017 | 0.79 | 0.63 | 1.71 | 1.04 | ≈0.29 | ≈0.26 | 0.52 | 0.82 | 0.82 | 0.78 |
| $iC_4H_{10}$ | 0.040 | 0.02 | 0.050 | 0.028 | 0.001 | 0.0005 | 0.045 | 0.020 | 0.055 | 0.035 | ≈1.04 | ≈2.8 | 0.27 | 0.56 | 0.26 | 0.15 |
| $iC_4H_8$ | 0.002 | 0.002 | 0.007 | 0.002 | 0.0002 | 0.0001 | 0.010 | 0.005 | 0.008 | 0.005 | <0.48 | <0.26 | 0.23 | 0.15 | 0.024 | 0.011 |
| $iC_5H_{12}$ | | | | | | | | | | | >0.07 | >0.03 | 0.13 | 0.08 | | |
| CO | | | 0.04 | 0.03 | | | | | 0.33 | 0.42 | 0.15 | 0.22 | 0.47 | ≈0.38 | 1.19 | 1.02 |
| $CO_2$ | | | | | | | | | 4.46 | 4.78 | 3.5 | 4.2 | | | 0.79 | 0.76 |
| HCl | 5.13 | 5.55 | | | | | | | | | | | | | | |

Table II. Propylene yield by rearrangement.

| Compound | Total $G_{(C_3H_6)}$ | | $G_{(C_3H_6)}$ |
|---|---|---|---|
| | $He^{++}$ | γ-ray | (rearrangement) |
| $i\text{-}C_3H_7Cl$ | 2.68 | 2.16 | 1.5 |
| $i\text{-}C_3H_7OH$ | 0.37 | 0.25 | 0.1 |
| $i\text{-}C_3H_7C_6H_5$ | 0.028 | 0.017 | 0.003 |
| $i\text{-}C_3H_7CN$ | 0.79 | 0.63 | 0.4 |
| $i\text{-}C_3H_7COOH$ | 1.17 | 1.04 | 0.2 |
| $i\text{-}C_3H_7CH_2COOH$ | 0.29 | 0.26 | 0.2 |
| $i\text{-}C_3H_7COCH_3$ | 0.52 | 0.82 | 0.5, 0.8[a] |
| $i\text{-}C_3H_7OCOCH_3$ | 0.82 | 0.78 | 0.7 |

a. All propylene must be formed by rearrangement, as almost no propyl radicals are present. Hence the assumption of no deactivation obviously fails in this case.

## 4. ION-EXCHANGE STUDIES IN CONCENTRATED SOLUTIONS. I. THE ALKALI CATIONS WITH A SULFONIC ACID RESIN(*)

David C. Whitney and Richard M. Diamond

The elution of tracer alkali metal cations from sulfonic acid cation-exchange resin (Dowex-50) columns by several uni-univalent salts and acids has been investigated. The tracers used in this study were Na, Rb, and Cs, and the eluting agents were $HClO_4$, $HNO_3$, HCl, HBr, HI, the corresponding Li salts, and CsCl. The elution order in dilute solution is explained as resulting from the water-water, ion-water, and ion–resin sulfonate interactions. Reversals in this order, and deviations of the elution behavior from the simple mass action law as the salt or acid concentration is increased, are interpreted as being due to three main effects. The first is that the availability of water to solvate the ions decreases, as shown by the decreasing water activities. The decrease in water acitivity diminishes the hydration of the ions and makes them more susceptible to anion-cation interactions, particularly the sulfonate-cation interaction in the resin phase. The result is to increase the elution volume for the smaller ions and decrease the elution volume for the larger ions, causing a reversal in the elution order. The second effect is that cation-anion interactions are becoming more important in the aqueous phase also, and the extent depends on the nature of

*Brief form of forthcoming report, UCRL-10595, 1963.

both cation and anion, being stronger for the smaller of the alkalis. The more strongly the anion reacts with the cation, the better it is able to replace the diminishing hydration of the cation with anion solvation, thus extending the dilute solution order to higher external phase concentrations. Thirdly, the effect of nonexchange electrolyte increasingly entering the resin phase and providing more "exchange" sites tends to increase the elution volumes of all cations. These three effects are sufficient to account for the variation in behavior of the tracer alkalis when eluted from sulfonate resin column by concentrated solutions as diverse as $LiClO_4$, LiAc, $HNO_3$, and CsCl.

## 5. ION-EXCHANGE STUDIES IN CONCENTRATED SOLUTIONS. II. THE ALKALI CATIONS WITH A CARBOXYLIC ACID RESIN

David C. Whitney and Richard M. Diamond

The previous summary described the elution of alkali tracers from Dowex-50, a sulfonic-acid type ion-exchange resin, by concentrated salts and acids. In order to investigate more throughly the role of resin ion-cation interactions, the elution of Na and Cs tracers from Bio-Rex-70, a carboxylic-acid type resin, by solutions of $LiClO_4$, LiCl, $LiNO_3$, and LiAc was studied. It would be expected that the much stronger attraction of the carboxylate group than of the sulfonate groups for cations would cause resin ion-cation effects to play a much greater role in selectivity. Since the smallest alkali ion is most strongly complexed by the carboxylate group, the effect would be a reversal of the elution order of Na and Cs at lower concentrations than in the sulfonate case. This is seen for the first three Li salts, where the reversal occurs at concentrations only 1/4 or 1/5 as great in Bio-Rex-70 as in Dowex-50. Since the complexing groups in both resin and aqueous phases are the same when the elution is carried out with LiAc, no reversal would be expected; none occurs. Thus it is seen that the selectivity of a resin for (alkali) cations from concentrated electrolyte solutions is related to its complexing ability compared with that of the electrolyte in the external solution. As described in these papers, this cation-anion complexing may be of a more subtle nature than the usually considered complex-ion formation, resembling the "localized hydrolysis" hypothesis of Robinson and Harned.[1]

---

1. R. A. Robinson and H. S. Harned, Chem. Rev. 28, 419 (1941).

# 6. THE EXTRACTION OF ACIDS BY BASIC ORGANIC SOLVENTS. II. TRIBUTYL PHOSPHATE-HBr

David C. Whitney and Richard M. Diamond

In order to determine the generality of the extraction model previously proposed for $HClO_4$ into dilute $CCl_4$ solutions of tributyl phosphate (TBP),[1,2] studies were extended to the extraction of HBr. The results obtained were very similar to those for $HClO_4$. That is, the extracting species has the formula $H_3O^+ \cdot 3TBP \cdot mH_2O \cdots Br^-$, $0 \leq m \leq 1$ for the range from 1 to 10% by volume TBP in $CCl_4$, and the proposed structure for the species is ($R = C_4H_9O$):

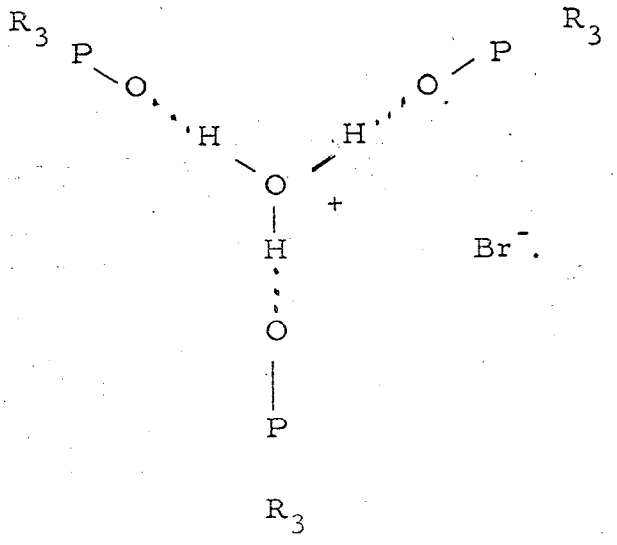


It is suggested that as the TBP concentration rises, the excess $H_2O$ is included in the species as a bridge between the TBP and $H_3O^+$; this is discussed in the $HClO_4$ paper.[2]

Owing to the lower extraction coefficient and ready oxidation of HBr, the experimental difficulties are much greater than in the $HClO_4$ case and presumably account for minor differences between the two acids. It is hoped that these problems can be surmounted by use of a stronger base, trioctyl phosphine oxide, to extract HCl from aqueous solutions; this work is currently in progress.

---

1. Preceding annual report (UCRL-10023, Jan. 1962), p. 160.

2. David C. Whitney and Richard M. Diamond, The Extraction of Acids by Basic Organic Solvents. I. Tributyl Phosphate-$HClO_4$ and Tributyl Phosphate-$HReO_4$, J. Phys. Chem. (in press).

# 7. THEORY OF FOCUSING ELECTROPHORESIS

Ernst J. Schumacher*

A former theoretical study on electrophoresis of cations with a superimposed concentration gradient of a complex-forming ligand parallel to the electric field[1] was based on a number of idealizing assumptions. The work mentioned in the next report stimulated some further thoughts and experiments, especially concerning a system in which the ligand concentration gradient is coupled with a pH gradient (pH-pL gradient). The aim was to predict the composition of anode and cathode solutions to optimize the pH-pL gradient for a given separation problem in regard to separation time and component purity.

Ordinary zone electrophoresis -- e.g., on a paper strip -- implies a mobility difference $\Delta U(IK)$ for the separability of two components I and K. It is usually possible to choose some ligand L, complexing both I and K, which makes $\Delta U(IK)$ much larger than that of the uncomplexed components. At a certain concentration $C_L(IK)$, $\Delta U(IK)$ shows a maximum. If the mixture contains the set $AB\cdots IK\cdots N$ of components, ordered along decreasing complex stability with L, the concentration $C_L(IK)$ gives only optimum separation conditions for the pair IK but not for any other pair of the set. It is therefore necessary to provide a range of $C_L$ values along the separation system that covers all $C_L(IK)$ values characteristic of the components. Two questions arise:

(a) Since $C_L(IK)$ is the optimum L concentration for the separation of IK, any other concentration (also a concentration distribution) is less desirable. How do we choose a $C_L$ distribution that is optimal for the whole set $A\cdots N$?

(b) If the range of $C_L$ covers all $C_L(IK)$ values, how do we provide conditions such that each pair IK of the set migrates to that part of the apparatus where its separability is optimal?

The answer to (a) is a $C_L$ distribution of the form

$$
\begin{array}{lll}
C_L \ll C_L(AB) & & X \ll X_A \\
= C_L(AB) & & X_A < X < X_B \\
= C_L(BC) & & X_B < X < X_C \\
\vdots & & \vdots \\
= C_L(IK) & & X_I < X < X_K \\
\vdots & & \vdots \\
= C_L(N\text{-}1;N) & & X_{N-1} < X < X_N \\
\gg C_L(N\text{-}1;N) & & X_N \ll X
\end{array}
$$

---

*On leave from Anorganisch-Chemisches Institut der Universität, Zurich, Switzerland.

1. E. Schumacher, Helv. Chim. Acta 40, 2322 (1957); UCRL Transl. -627 (L).

where $X_A$, $X_B \cdots X_I$, $X_K \cdots X_N$ are points along the direction of the electric field where the first moment of the concentration distribution of the components A, B$\cdots$I, K$\cdots$ will be, i.e., a stepwise increase of $C_L$ from the anode to the cathode, the $C_L(IK)$ values being the plateau concentrations between steps, and with as many steps as there are components.

Condition (b) can be satisfied only if L is an anion and the complexes are anions too. The plateau values $C_L(IK)$ are then concentrations for which $U_I < 0$; $U_K > 0$ and $|\Delta U(IK)| = \max$.

Such a system separates all the components and enriches each one at that particular $C_L$ step where it passes its isoelectric point (focus). Gradient electrophoresis is, therefore, the best electrophoretic separation for a multicomponent mixture provided that the $C_L$ distribution is optimal.

The separation pattern is not dependent on the initial zone width of the applied sample as long as the component concentrations are small compared with the buffer capacity of the ligand-concentration gradient. Since the mobility of each component is finite everywhere except at its focus position, the component spectrum develops in a finite time. The latter is directly proportional to the current density.

The well-known theory of moving boundaries in electrophoresis shows that a system of concentration steps can be maintained in an electric field by an appropriate choice of anode and cathode electrolytes and of their concentrations. In our case, we have to choose weak acid-base systems in which the steps develop between a strong acid anode solution and a subsequent series of acids, with increasing pK values terminating with a cathode solution containing the conjugate bases in various defined concentrations. An expansion of the weak-electrolyte moving-boundary theory is necessary to cover this problem, which has by now been solved for up to eight components of which six are chemically interacting. This leads to six "natural" pH steps (maintained by a constant current at a stationary height and five moving with a constant velocity) in which six pL steps can be established. This is sufficient for the separation of six very similar components like actinides and rare earths.

The mathematical details of the theory have been worked out for metal ions, but may also be interesting for the separation of other electrolytes whose mobility is pH-dependent or pL-dependent (or both), like polypeptides.[2] The applicability of the theory to a practical problem of separation of metal ions implies the knowledge of the complex stability constants for each component or, more exactly, of the "isoelectric function" in a pH-pL diagram (which has to be measured). As a corollary, a separation pattern with known (measured) $C_L$ steps yields interesting information on the isoelectric function and, therefore, on the nature and charges of complexes present.

Several series of experiments confirm the features of the calculated pH step function and its voltage-time behavior (with constant current) or current-time behavior (with constant voltage).

---

2. Harry Svensson, Acta Chem. Scand. 15, 325 (1961); 16, 456 (1962).

I thank Dr. Harry Svensson for a very stimulating correspondence on the problem of "natural" pH gradients in electrophoresis. I would like to express my deepest gratitude to Dr. I. Perlman and Dr. S. G. Thompson for their hospitality at the Lawrence Radiation Laboratory.

## 8. SEPARATION OF ACTINIDES AND RARE EARTHS BY FOCUSING ELECTROPHORESIS

Ernst J. Schumacher*

Focusing electrophoresis has recently been used to separate all the rare earths from one another within a few minutes.[1] The study presented here has been undertaken to work out a similar separation scheme for mixtures of actinides and of actinides and rare earths.

The mobility differences between aqueous three-valent actinides or rare earth ions are not large enough for zone electrophoresis to produce a clean separation in a reasonable time, even in very high electrical fields. As with ion exchange techniques, one increases the differences, therefore, by partly complexing some or all of the components. Suitable ligands in this connection are chelate ligands like EDTA, NTA, or similar polyaminoacetates. They convert, in certain pH-pL areas [pL = -log (ligand conc.)], the $A^{3+}$ or $R^{3+}$ cations (A:actinide; R:rare earth) into $AL^-$, $RL^-$ or $AL_2^{3-}$, $RL_2^{3-}$ anions (where L refers to EDTA and NTA). For each component $A_i$, $R_i$ there exists a specific function $I_{A_i}$, $I_{R_i}$ of the variables pH and pL, called isoelectric function. It defines the locus on the pH-pL area where the transport of that component in an electrical field applied to the solution vanishes exactly. This function is related to the transport properties of $A_i^{3+}$, $R_i^{3+}$, $A_iL^-$, $R_iL^-$, etc., to the stability constants of the complexes, and to the protolysis constants of the complexes and ligands. Among these parameters the transport coefficients are the least accurately known. The isoelectric function must therefore be measured directly. For this work, only ratios of these functions are necessary, for which the assumption of equal transport coefficients among the respective $A_i^{3+}$ and $A_iL^-$ ions is sufficiently accurate. A knowledge or an estimate of the complex-stability constants is then the only requirement for the choice of experimental conditions.

If a pH-pL gradient is maintained in the water solution along a filter paper strip, a sample of actinides will be collected or focused under the influence of an electric field at a number of specific isoelectric points $(pH, pL)_i$ characteristic for each component i. The time necessary for the formation of the isoelectric separation pattern depends on the initial spread of the sample and on the current density. For the latter there is a limit, set by the efficiency of heat transfer from the paper strip to a cooling bath. Under favorable conditions 30 sec is the lower limit, a few minutes being the average for a five- to ten-component solution.

---

*On leave from Anorganisch-chemisches Institut der Universität, Zurich, Switzerland.

1. W. Friedli and E. Schumacher, Helv. Chim. Acta 44, 1829 (1961), UCRL-Transl. No. 851.

Experimental procedure

A sample of 5 to 20 λ of a solution containing not more than 500 μg total of actinides and rare earths (and no excess of mineral acids and as little as possible of inert salts) is applied in the middle of a filter paper strip about 14 cm long and 1 cm wide (Whatman #1, Schleicher & Schuell #2043). The strip is held by a plastic holder with a free gap of about 10 cm.[1] On one side of the sample the anode solution is applied, on the other side the cathode solution, and both ends are connected with the respective electrode compartments, usually by means of a filter paper bridge. The whole strip is cooled in a bath of carbon tetrachloride (< 35°C). Current is applied from a constant current supply, furnishing 1 to 15 mA (as preselected, usually 5 mA for EDTA or 10 mA for NTA, and capable of delivering up to 2000 V filtered dc. After 1 to 10 min, depending on the problem, the strip is dried over a hair drier (requiring approx 30 seconds) and is ready for inspection. All these operations are carried out conveniently in a standard Berkeley Box.

A typical choice of anode and cathode solutions is given in Table I.

Table I. Solutions used for obtaining autoradiographs shown in Fig. D. 8-1.

| Number on Fig. D. 8-1 | Anode solution | Cathode solution |
|---|---|---|
| 1, 2, 3, 5, 7 | 0.2 M HCl | 0.05 M $(NH_4)_2$HNTA<br>0.10 M $NH_4$ClAc |
| 4 | 0.6 M HCl | 0.08 M $(NH_4)_2H_2$EDTA<br>0.13 M $NH_4$Ac<br>0.10 M $NH_4$ClAc<br>0.20 M $HCl_2$Ac<br>0.30 M $NH_4Cl_3$Ac,<br>pH = 3.5 adjusted<br>with $NH_3$ |
| 6 | 0.2 M HCl | 0.15 M $(NH_4)_2$ HNTA<br>0.20 M $NH_4$Ac<br>0.16 M $NH_4$ClAc<br>pH ≈ 5 |

(Ac = acetate; ClA = chloroacetate)

The experiments were done before the theory described in the previous report had been sufficiently developed. Improvements in the composition of the solutions and therefore in the separation, especially between Es and Cf, are easily possible.

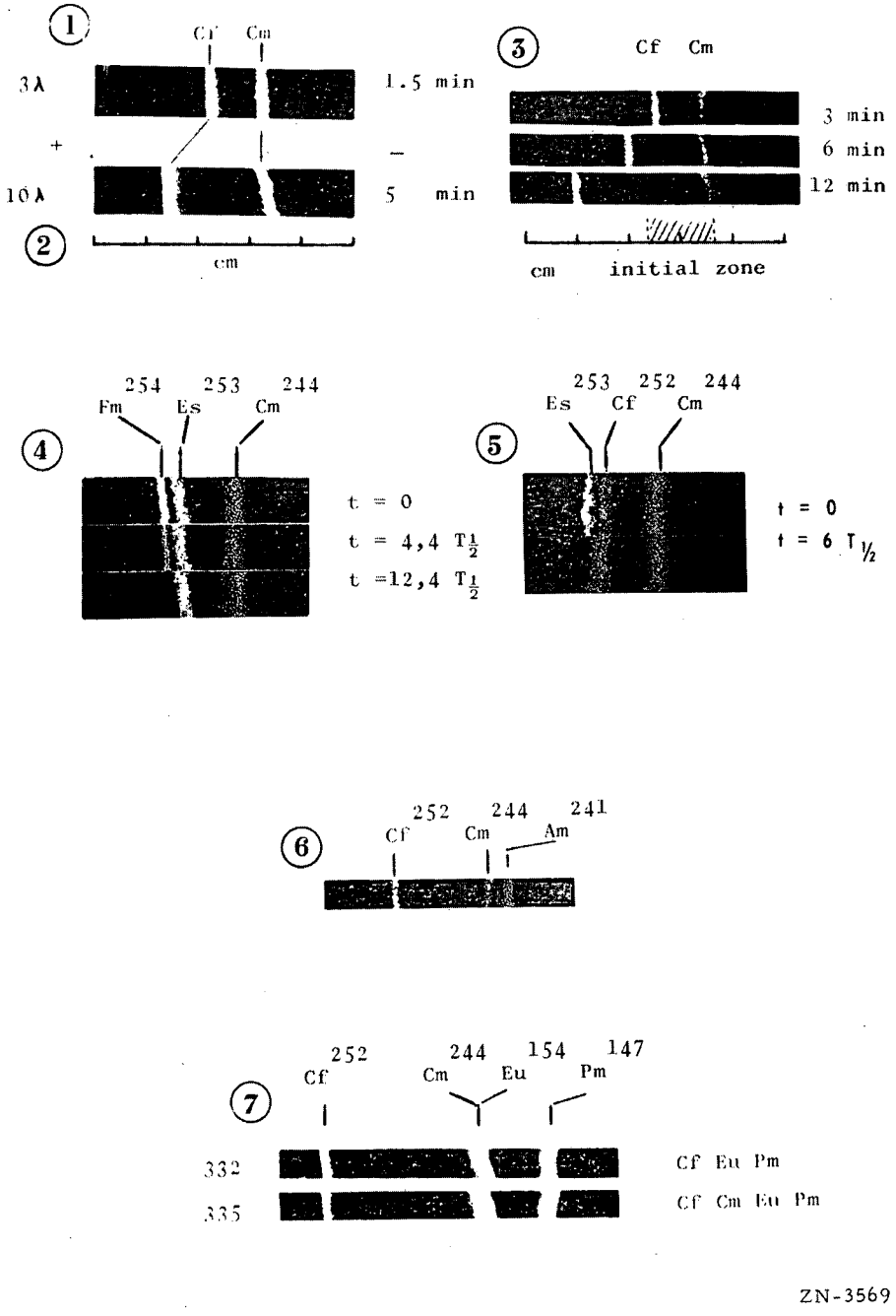


Fig. D.8-1. Autoradiographs of actinide separations.

## Results

A separation scheme was worked out for the actinides from Am to and including Fm (except for Bk, which was available only as a very weak tracer and not detectable accurately enough on the paper strip); see Fig. D. 8-1 for typical separation patterns. The autoradiographs were obtained by the method of Latimer, Larsh, and Corum,[2] which has been very helpful for this work. The paper strips are held between two very thin Mylar foils on the block of the camera. Five strips can be exposed simultaneously. An exposure of 2 to 5 min is necessary for a sample of 1000 α counts/min. Numbers 1 and 2 on Fig. D. 8-1 are overexposed considerably (2 hours for 2000 α counts/min for $Cf^{252}$ and $Cm^{244}$) to show the background between the focused lines. Numbers 3 through 7 are exposed between 5 and 10 min, to 5000 to 10,000 α counts/min and $5 \times 10^4$ β counts/min. The radiochemical purity can be estimated to be better than $1:10^4$ from these autoradiographs (e.g., see also #4, showing the background after disappearance of $Fm^{254}$) and from quantitative studies during rare earth separation.[1,3] For better separation one can wait longer (see #3) or repeat the procedure after cutting out the desired line: elute with 1 drop 3 M HCl onto a Pt disc, evaporate and take up in 10 λ 0.1 M HAc. Decontamination factors -- e.g., for Fm from Cf -- of the order of $1:10^7$ can easily be obtained in about 16 min (6 min first separation, drying; 3 min autoradiography for location of Fm; 2 min cutting out, elution and application to prepared strip; 5 min for second separation) or in about 11 min by the use of a cross-form paper.[3] See Table II.

Table II. Separation times for cases demonstrated in Fig. D. 8-1

| Number on Fig. D. 8-1 | Time (min) |
|---|---|
| 1 | 1, 5 |
| 2 | 5 |
| 3 | 3, 6, 12 |
| 4, 5 | 5 |
| 6 | 8 |
| 7 | 10 |

The Fm, Es, Cf, Bk, and Cm are separated from all the rare earths below Eu, which make the largest contribution of fission rare earths; see #7, in which Cm coincides with Eu. Other ligands may give an even larger shift between actinides and rare earths (EDTA?).

The identifications of all the lines have been confirmed by various means: half-life (Fm, Es), isotope dilution, cross separations, alpha spectrum, or relative position in the separation pattern.

---

2. Chemistry Division Annual Report, 1961, UCRL-10023, Jan. 1962, p. 230. I thank A. E. Larsh for the introduction to this beautiful technique and for the loan of equipment.

3. E. Schumacher and W. Friedli, Helv. chim. acta 43, 1706 (1960).

The reproducibility of a separation depends somewhat on the skill of the experimenter. After a training of a couple of days a technician is able to perform the operations reliably. They are as simple as with ion-exchange columns.

There are no detectable losses of alpha activity during the usual handling of the paper strips, especially during separation (into the $CCl_4$), drying (into the hot air), and autoradiography (onto the Mylar foils).

The technique seems applicable to remote handling as well. The short duration should make it attractive in strong radiation fields where damage to ion-exchange resins and eluting ligands is so excessive as to prevent the applicability of the much slower ion-exchange chromatography. The filter paper can be replaced by glass fiberpaper (fine version) or, for alpha spectroscopy, by a very thin sulphonated polystyrene film.[4]

An extensive report is in preparation.

I would like to thank Dr. Stanley G. Thompson for his interest and hospitality and Ray Gatti for providing me with suitable tracers.

4. Sven Bjørnholm and C. Michael Lederer, Nucl. Instr. Methods 15, 233 (1962).

## 9. CHEMICAL SEPARATION OF TRANSURANIUM ELEMENTS FROM Si ROCK

Raymond C. Gatti, Stanley G. Thompson, Sherman Fried, and Reinhardt Brandt

One of the programs under the Plowshare Program of the AEC is the production of large quantities of transuranium elements by nuclear explosions. As in the "Mike" experiment the presence of $U^{238}$ in a very high neutron flux produces very neutron-rich uranium isotopes which decay by $\beta^-$ emission to $\beta^-$-stable end products. Some of the possible reactions are shown in the chart on the following page.

Since the nuclear explosion is set off underground, a chemical procedure was devised so that the transuranium elements could be chemically separated from one another in a 4- to 5-hour period. The flow sheet is shown on pages 216, 217, and 218.

In general a chemical yield of about 70% was achieved for the fast chemistry (4 to 5 h). In the $BiPO_4$ precipitate step, the more dilute the solution is made, and the lower the $HNO_3$ concentration, the better the $BiPO_4$ carries the 3+ actinides. Therefore a much higher chemical yield (approx 90%) can be expected if more care is taken at each chemical step.

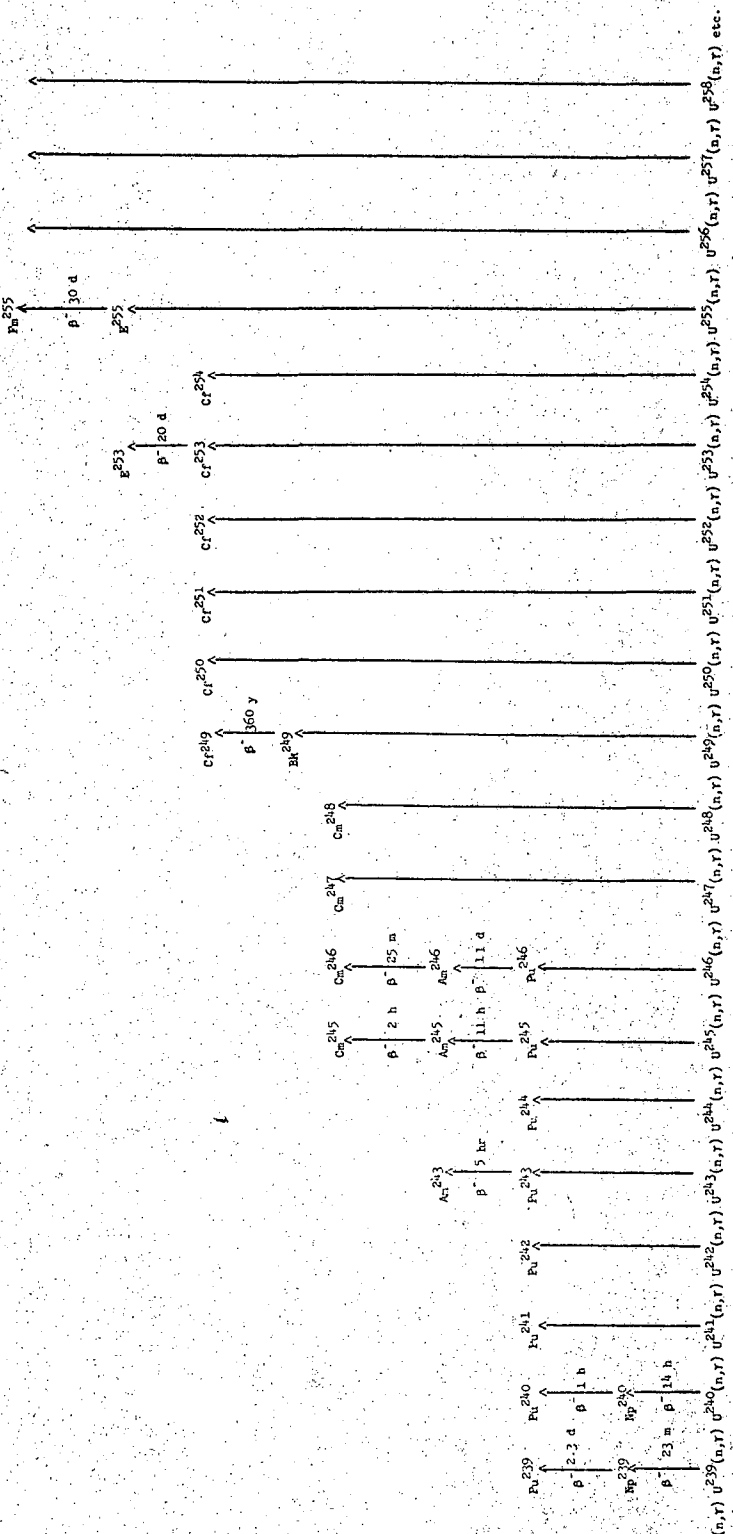
Fm255
β- 30 d
Es255
Es253
β- 20 d
Cf254
Cf253
Cf252
Cf251
Cf250
Cf249
β- 360 y
Bk249
Cm248
Cm247
Cm246
β- 25 m
Am246
11 d
Pu246
Cm245
β- 2 h
Am245
11 h β-
Pu245
Pu244
Am243
β- 5 hr
Pu243
Pu242
Pu241
Pu240
β- 1 h
Np240
14 h β-
Pu239
β- 2.3 d
Np239
β- 23 m β-
U238(n,r) U239(n,r) U240(n,r) U241(n,r) U242(n,r) U243(n,r) U244(n,r) U245(n,r) U246(n,r) U247(n,r) U248(n,r) U249(n,r) U250(n,r) U251(n,r) U252(n,r) U253(n,r) U254(n,r) U255(n,r) U256(n,r) U257(n,r) U258(n,r) etc.

FLOW SHEET

Part A.

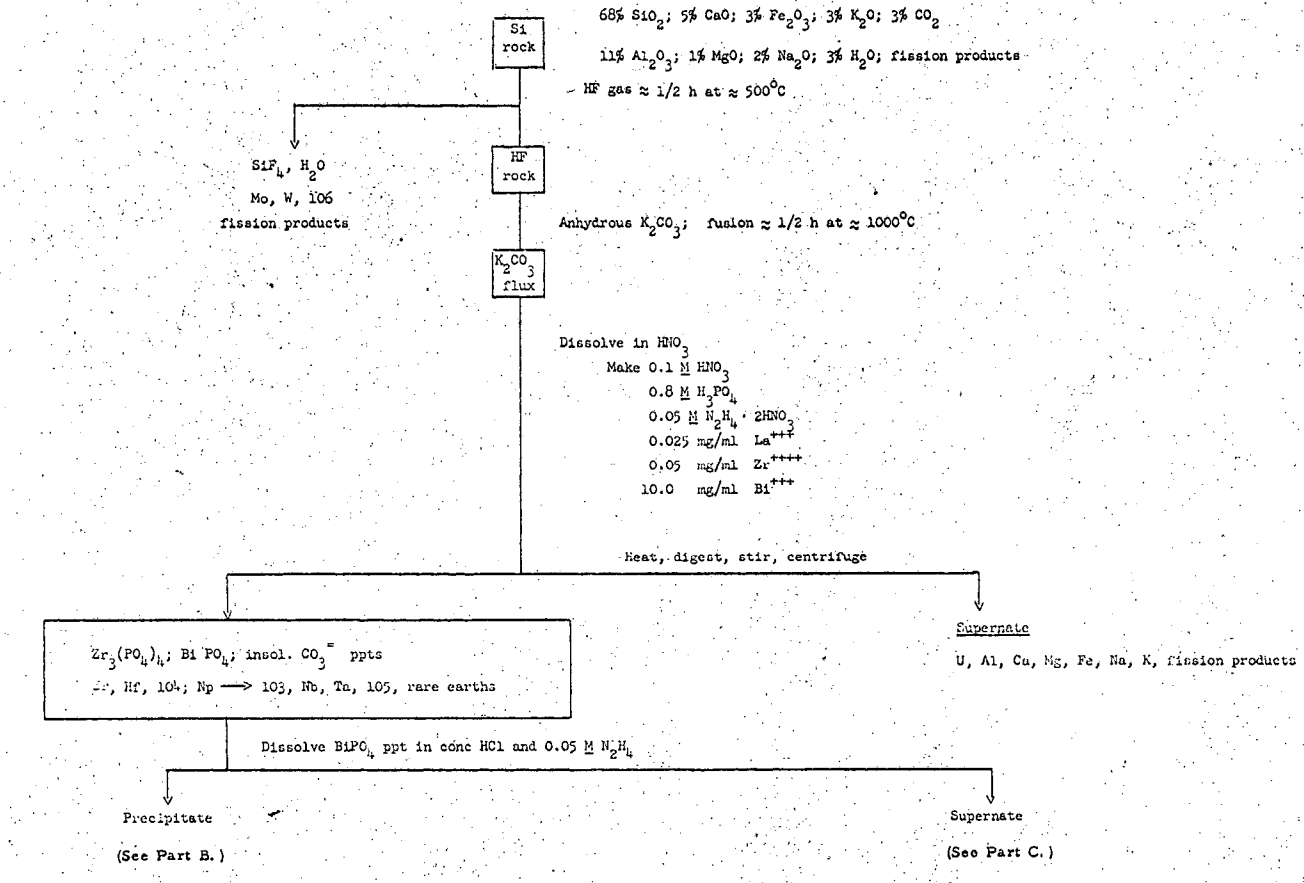

Part B.

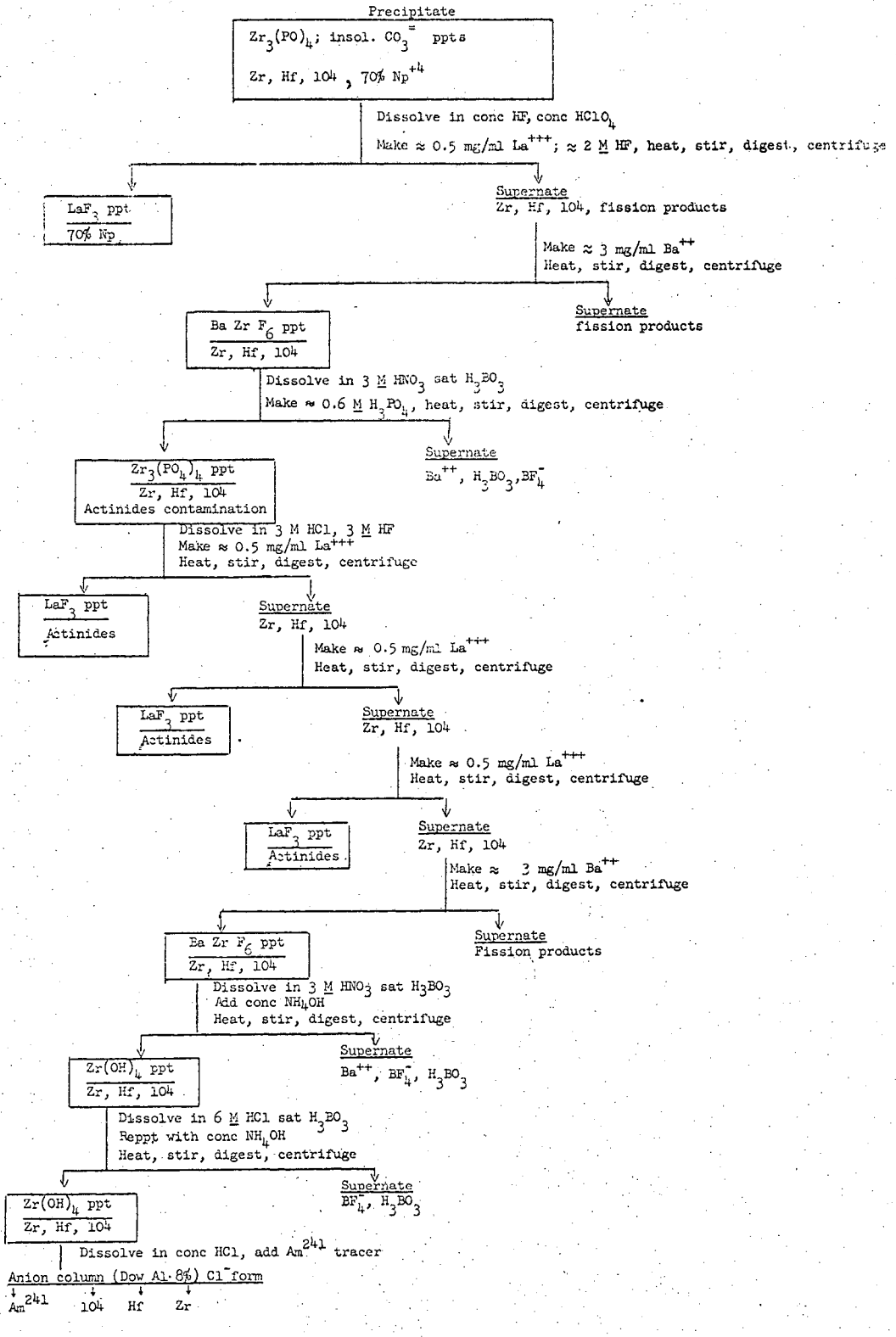
Precipitate
$Zr_3(PO)_4$; insol. $CO_3^=$ ppts
Zr, Hf, 104 , 70% $Np^{+4}$
Dissolve in conc HF, conc $HClO_4$
Make ≈ 0.5 mg/ml $La^{+++}$; ≈ 2 M HF, heat, stir, digest., centrifuge
$LaF_3$ ppt
70% Np
Supernate
Zr, Hf, 104, fission products
Make ≈ 3 mg/ml $Ba^{++}$
Heat, stir, digest, centrifuge
Ba Zr $F_6$ ppt
Zr, Hf, 104
Supernate
fission products
Dissolve in 3 M $HNO_3$ sat $H_3BO_3$
Make ≈ 0.6 M $H_3PO_4$, heat, stir, digest, centrifuge
$Zr_3(PO_4)_4$ ppt
Zr, Hf, 104
Actinides contamination
Supernate
$Ba^{++}$, $H_3BO_3$, $BF_4^-$
Dissolve in 3 M HCl, 3 M HF
Make ≈ 0.5 mg/ml $La^{+++}$
Heat, stir, digest, centrifuge
$LaF_3$ ppt
Actinides
Supernate
Zr, Hf, 104
Make ≈ 0.5 mg/ml $La^{+++}$
Heat, stir, digest, centrifuge
$LaF_3$ ppt
Actinides
Supernate
Zr, Hf, 104
Make ≈ 0.5 mg/ml $La^{+++}$
Heat, stir, digest, centrifuge
$LaF_3$ ppt
Actinides
Supernate
Zr, Hf, 104
Make ≈ 3 mg/ml $Ba^{++}$
Heat, stir, digest, centrifuge
Ba Zr $F_6$ ppt
Zr, Hf, 104
Supernate
Fission products
Dissolve in 3 M $HNO_3$ sat $H_3BO_3$
Add conc $NH_4OH$
Heat, stir, digest, centrifuge
$Zr(OH)_4$ ppt
Zr, Hf, 104
Supernate
$Ba^{++}$, $BF_4^-$, $H_3BO_3$
Dissolve in 6 M HCl sat $H_3BO_3$
Reppt with conc $NH_4OH$
Heat, stir, digest, centrifuge
$Zr(OH)_4$ ppt
Zr, Hf, 104
Supernate
$BF_4^-$, $H_3BO_3$
Dissolve in conc HCl, add $Am^{241}$ tracer
Anion column (Dow A1·8%) $Cl^-$ form
$Am^{241}$
104
Hf
Zr

Part C.

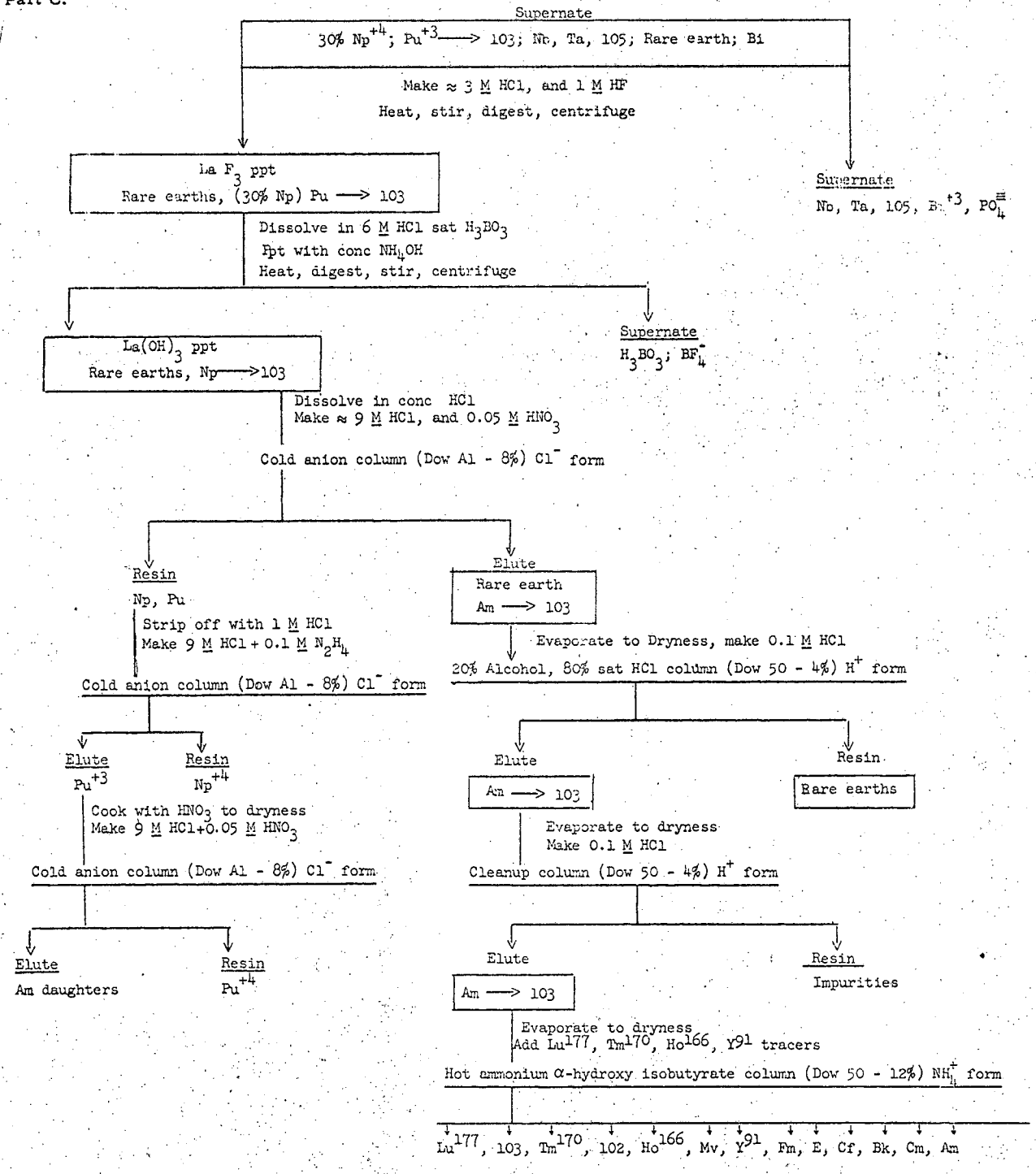
Supernate
30% $Np^{+4}$; $Pu^{+3}$ ⟶ 103; Nb, Ta, 105; Rare earth; Bi
Make ≈ 3 M HCl, and 1 M HF
Heat, stir, digest, centrifuge
$LaF_3$ ppt
Rare earths, (30% Np) Pu ⟶ 103
Supernate
Nb, Ta, 105, $Bi^{+3}$, $PO_4^{\equiv}$
Dissolve in 6 M HCl sat $H_3BO_3$
Ppt with conc $NH_4OH$
Heat, digest, stir, centrifuge
$La(OH)_3$ ppt
Rare earths, Np⟶103
Supernate
$H_3BO_3$; $BF_4^-$
Dissolve in conc HCl
Make ≈ 9 M HCl, and 0.05 M $HNO_3$
Cold anion column (Dow A1 - 8%) $Cl^-$ form
Resin
Np, Pu
Strip off with 1 M HCl
Make 9 M HCl + 0.1 M $N_2H_4$
Elute
Rare earth
Am ⟶ 103
Evaporate to Dryness, make 0.1 M HCl
Cold anion column (Dow A1 - 8%) $Cl^-$ form
20% Alcohol, 80% sat HCl column (Dow 50 - 4%) $H^+$ form
Elute
$Pu^{+3}$
Resin
$Np^{+4}$
Elute
Am ⟶ 103
Resin
Rare earths
Cook with $HNO_3$ to dryness
Make 9 M HCl+0.05 M $HNO_3$
Evaporate to dryness
Make 0.1 M HCl
Cold anion column (Dow A1 - 8%) $Cl^-$ form
Cleanup column (Dow 50 - 4%) $H^+$ form
Elute
Am daughters
Resin
$Pu^{+4}$
Elute
Am ⟶ 103
Resin
Impurities
Evaporate to dryness
Add $Lu^{177}$, $Tm^{170}$, $Ho^{166}$, $Y^{91}$ tracers
Hot ammonium α-hydroxy isobutyrate column (Dow 50 - 12%) $NH_4^+$ form
$Lu^{177}$, 103, $Tm^{170}$, 102, $Ho^{166}$, Mv, $Y^{91}$, Fm, E, Cf, Bk, Cm, Am

Paper presented at
IAEA meeting, Vienna, May 21-25, 1962

UCRL- 0624
(from UCRL-10176)

# 10. THERMODYNAMICS OF THE ACTINIDES

Burris B. Cunningham

Department of Chemistry
and
Lawrence Radiation Laboratory
University of California, Berkeley, California

## INTRODUCTION

Herein, the term "actinides" is applied to the elements of atomic number 89-103. All members of the series have now been discovered[1] but the production of weighable amounts of the elements has not been extended beyond einsteinium (atomic number 99). There is little hope that experiments with macroscopic quantities of the transeinsteinium elements ever will be possible, owing to the very short half lives of even their most stable isotopes. It has been of particular interest, therefore, to attempt to discover whether the properties of the more stable elements of this series vary in a sufficiently systematic way to justify confidence in the prediction of the properties of macroscopic amounts of the heavier elements. In this connection, at the Lawrence Radiation Laboratory in Berkeley, particular effort has been devoted to the investigation of the transplutonium elements.

### Electronic Configurations

Optical and atomic beam resonance methods have been used to determine the electronic configurations[2,3] of the neutral gaseous atoms of the actinides through curium, with the results shown in Table I. On the basis of their electronic configuration the transactinium elements, with the exception of thorium, are members of a 5f transition series. The gaseous ion $Th^{+3}$ (spectroscopic notation, Th IV) has been shown to have a $5f^1$ configuration,[2]

TABLE I

Electronic Configurations of the Actinides
Radon core plus $7s^2$ plus:

| Element | Ac | Th | Pa | U | Np | Pu | Am | Cm |
|---|---|---|---|---|---|---|---|---|
| Configuration | 6d | $6d^2$ | $5f^2 6d$ | $5f^3 6d$ | $5f^4 6d$ | $5f^6$ | $5f^7$ | $5f^7 6d$ |

and $Th^{+3}$ may therefore be included in the series. The lighter actinides are more readily oxidized beyond the +3 state than are the 4f (lanthanide) elements, doubtless because the lighter 5f elements have smaller values for their fourth, fifth and sixth ionization potentials.[3]

Properties of Metals

A. Americium

Americium metal was first prepared by Westrum and Eyring[4] who noted that it was less dense (bulk density 11.7 ± 0.3 gm $cm^{-3}$) and more malleable and ductile than plutonium. Westrum and Eyring,[4] as well as Lohr and Cunningham,[5] measured the heat of solution of the metal in 1.5 M HCl, and found a value of 162 ± 3 Kcal $mol^{-1}$.

The first investigation of the crystal structure of americium metal revealed the existence of an alpha lanthanum-like double hexagonal close packed phase (space group $P6_3/mmc$) with lattice parameters:

$a_o = 3.642 \pm 0.005A, \quad c_o = 11.76 \pm 0.01A$

at room temperature, with a calculated density of 11.87 ± 0.05 gm.[6]

A second double hexagonal close packed phase, having lattice parameters:

$a_o = 3.474 \pm 0.005A$, and $c_o = 11.25A$,

as well as a face centered cubic phase (obtained by condensation of americium metal vapor on tantalum) with $a = 4.895 \pm 0.005A$, have been reported by McWhan, Wallmann, Cunningham, Asprey, Ellinger and Zachariasen.[7] Both of these phases have calculated densities of 13.7, and a metallic radius (C. N. 12) = 1.73A.

The thermodynamics relationship among these phases is not clear at the present time. In an attempt to establish the temperature order of stability McWhan, Cunningham and Wallmann[8] investigated the crystal structure of the more dense double hexagonal phase of the metal from -120 to +605°C. No change in the structure or discontinuity in the expansion behavior was observed in this temperature interval. Because of rapid volatilization of americium and reaction with the quartz x-ray capillaries, the extension of the investigation to higher temperatures was not feasible at the exposure times required for the standard x-ray equipment. Exposure times were shortened, however, by wrapping the protected film directly around the high temperature oven (~3 cm diameter). By this means diffraction patterns were obtained at 700 and 850°C. Although extensive volatilization of the metal and oxidation to AmO still occurred during the exposure, a few lines were obtained which could be indexed as fcc with $a = 4.91A$. This cell constant is consistent with the room temperature value for the fcc phase and its experimentally determined thermal coefficient of expansion. (See below.)

Coefficients of thermal expansion were calculated for both the fcc and double hexagonal close packed phases, the former from diffraction patterns taken on a single sample at about 50° intervals from 22 to

360°C, and the latter on two samples of metal, the first from 20 to 605°C, and the second from -121 to 588°C.

The data were then fitted to a polynomial of second order by the method of least squares, with the results:

Sample No. 1.

$$a_T = 3.4671 + 2.62 \times 10^{-5} T + 0.56 \times 10^{-8} T^2$$

$$c_T = 11.238 + 6.59 \times 10^{-5} T + 6.3 \times 10^{-8} T^2$$

Sample No. 2.

$$a_T = 3.4673 + 2.57 \times 10^{-5} T + 0.52 \times 10^{-8} T^2$$

$$c_T = 11.236 + 7.31 \times 10^{-5} T + 7.3 \times 10^{-8} T^2$$

As mentioned previously, in contrast to the behavior of plutonium, no anomalies were noted in the expansion behavior of americium.

Melting Point of Americium.

A number of early attempts to determine the melting point of americium failed to yield satisfactory values, owing, no doubt to the formation of a hard oxide skin on the surface of the small samples of metal. McWhan, Cunningham and Wallmann[8] overcame this difficulty by "soldering" fine tantalum wires together with freshly produced americium metal, and subjecting the join to a mild strain at gradually increasing temperatures until parting occurred.

The method was first investigated with similar quantities of pure rare earth metals of known melting point and found to be reliable to about ± 5°C. The best value for the melting point of americium, as determined by this method, is 995 ± 7°C.

Magnetic Susceptibility of Americium.

McWhan and Cunningham[9] have investigated the susceptibility of several samples of americium metal in the temperature range from -196 to 550°C. Accurate measurements are difficult because of the low susceptibility of the metal, but from these measurements the temperature variation of the susceptibility may be set at less than 7% in the interval studied. The value for the susceptibility at room temperature is:

$$\chi_{20^\circ C} = (881 \pm 46) \times 10^{-6} \text{ erg gauss}^{-2}\text{mol}^{-1}$$

There have been several measurements of the susceptibility of $Am^{+3}$, both in aqueous solution and in compounds. The data are in poor agreement, especially as regards the magnitude of the temperature dependence. Howland and Calvin[10] found $\chi_M$ for $Am^{+3}$ ion in dilute acid solution to be $720 \times 10^{-6}$ ergs $\text{gauss}^{-2}\text{mol}^{-1}$ at room temperature. Crane, Wallmann and Cunningham[11] found a much higher value (namely, 1040) for $AmF_3$ at 295°K and a marked temperature dependence (1740 at 77°K). Recent measurements [9] on $Am^{+3}$ adsorbed on a single bead of cation exchange resin ("Dowex 50") give a value of 670 ± 100 at 20°C and 744 ± 120 at 77°K. The room temperature value agrees with that of Howland and Calvin within experimental error. The higher susceptibility and more pronounced temperature dependence observed by Crane, et al, for americium trifluoride may have been due to the presence of a small amount of curium impurity in their sample ($\chi_{M_{20^\circ}}$ $Cm^{+3}$ = 24,000 cgs units).

The susceptibility of americium metal appears to be slightly higher than that of the +3 ion and the temperature dependence to be

slightly less. These differences, however, are barely outside the present rather large experimental errors.

An analysis by Gruber[12] of the low lying electronic levels of $Am^{+3}$ in a lanthanum trichloride matrix gives a separation of 2215 $cm^{-1}$ between the ground state, $^7F_o$, and the next higher J = 1 level. The separation is such that the higher level is only slightly populated, even at temperatures as high as 850°K (~ 600 $cm^{-1}$).

The susceptibility of $Am^{+3}$ arises, then, almost entirely from temperature independent second order terms of the ground level, in agreement with those measurements which show but little temperature dependence.

Although both $Am^{+3}$ and $Eu^{+3}$ have an $f^6$ configuration for the ground state, the calculation of a theoretical value for the susceptibility of $Am^{+3}$ is more difficult than for $Eu^{+3}$, since the departure from pure LS coupling is quite significant for americium.

Gruber[12] has made a preliminary calculation of the mixing of the $^5D_o$ and $^3P_o$ levels with the ground state of $Am^{+3}$. From his results McWhan and Cunningham[9] calculate a value of 682 x $10^{-6}$ ergs $gauss^{-2}$ for the molar susceptibility of the ion. The agreement with the experimental values is considered reasonably satisfactory.

The susceptibility data strongly suggest that there are close to three electrons per atom in the conduction bond in the metal, in disagreement with the valence assignment proposed by Zachariasen.[13]

B. Curium

Wallmann, Cunningham and Fuger[14] have obtained data on the crystal structure, melting point and heat of solution of curium metal

in 1 M HCl. Marei and Cunningham[15] have measured the magnetic susceptibility from 77 to 350° K.

A mixture of face centered cubic and hexagonal phases is obtained by reduction of the trifluoride with barium vapor at ~ 1300° C.

Preliminary values for the lattice parameters of the hexagonal phase are:

$a_o$ = 3.50 A

$c_o$ = 11.3 A

The unit cell volume is about three percent more than that of the more dense hexagonal phase of americium

The melting point is 1340 ± 40° C.

The susceptibility data are given in Table II.

TABLE II

Magnetic Susceptibility of

Curium Metal

| T (°K) | $\chi_m$ (c g s units) × $10^6$ |
|---|---|
| 329 | 16,700 ± 400 |
| 306 | 17,600 ± 400 |
| 297 | 17,700 ± 400 |
| 273 | 18,400 ± 400 |
| 230 | 20,100 ± 400 |
| 77 | 32,200 ± 400 |

Within the accuracy of measurements, the metal obeys the Curie-Weiss relationship down to liquid nitrogen temperatures. The molar susceptibility of the metal is similar to that of the trifluoride as measured by Crane, Wallmann and Cunningham.[11]

The heat of solution of curium metal in 1 M HCl is -138 ± 7 Kcal $mol^{-1}$, similar to that of plutonium, but some 20 kilocalories more positive than that of americium. The more electropositive nature of americium may be associated with its low heat of vaporization.[15]

SUMMARY OF PROPERTIES OF THE METALS

In the metallic state, the next two elements beyond plutonium are rare-earth-like in character in conformity with their general rare earth-like chemical behavior. As shown by tracer experiments on the actinide elements through mendelevium the +3 state persists with high stability throughout the rest of the series. It appears probable that the metals beyond curium will, in general, resemble the rare earth elements in structure and properties.

Zachariasen[13] has calculated values for the numbers of valence and 5f electrons in the actinide metals, on the basis of observed inter-atomic distances in the solid phases. He assigns 5.5 f electrons and 3.5 valence electrons to the face centered cubic and more dense double hexagonal close packed phases of americium. Our lattice parameters for metallic curium, a predominantly trivalent element, suggests that the number of valence electrons in both curium and the more dense form of americium is close to three.

II. Properties of Actinide Crystals

CRYSTAL FIELD SPLITTING IN THE ACTINIDE TRICHLORIDES

Crystal field stabilization plays an important part in determining the thermodynamic stability of "d" transition element compounds and it has been of interest, therefore, to determine crystal field splittings for some compounds of the actinide elements. Lammermann and Stapleton[17] have examined the optical and paramagnetic resonance spectrum of tripositive plutonium in both a lanthanum trichloride and a lanthanum ethyl sulfate matrix and find that the crystal field splitting of the levels is small and of about the same magnitude as observed in the analagous lanthanide ion, $Sm^{+3}$. Gruber[12] has observed crystal field splittings for $Am^{+3}$ in a $LaCl_3$ matrix to be similar to those found for $Eu^{+3}$. For the trivalent actinides, crystal field effects appear to have little more importance in determining the stability of various compounds than in the case of the lanthanides.

CRYSTAL STRUCTURES OF THE TRICHLORIDES OF CURIUM AND CALIFORNIUM

The trichlorides of the lanthanide elements exhibit the hexagonal $UCl_3$ structure type from lanthanum through gadolinium, a triclinic structure from holmium to lutecium, while $TbCl_3$ and $DyCl_3$ have a structure which has not yet been identified. It seems reasonable to suppose that the transition from one structure type to another is determined primarily by the ratio of the radius of the metal cation to that of the chloride ion. For a given number of electrons in the f subshell the trivalent actinide ions are 0.02 to 0.03A larger than the corresponding trivalent rare earths. Hence, if radius ratio is the critical factor, the $UCl_3$ structure might be expected to persist

in the actinide trichlorides to about element 99 (einsteinium). Wallmann and Cunningham[18] have obtained the diffraction patterns of $CmCl_3$ and $CfCl_3$ and find that both have the hexagonal structure, as expected.

III. Magnetic Properties of the Actinide Compounds

As have been mentioned previously, analyses of the optical absorption spectra of the trivalent actinides in a $LaCl_3$ matrix by Gruber,[12] and by Lammermann and Stapleton[17] have shown that the departure from pure LS coupling in the ground state is considerably greater for the heavier f transition elements than for the lanthanides. The analysis of the spectrum of $Pu^{+3}$ in $LaCl_3$ by Lammermann and Stapleton is sufficiently extensive to allow a good comparison to be made between calculated magnetic susceptibilities for $PuCl_3$ and the experimental values reported by Dawson, Mandleberg and Davies.[19]

The comparison[9] is shown in Table III.

The susceptibility minimum indicated by the experimental point at 548° K is not predicted by the theoretical calculations, and perhaps should be reinvestigated. The magnetic susceptibilities of $Bk^{+3}$ and $Cf^{+3}$ (adsorbed on the cation exchange resin Dowex 50) have been measured from 77° K to somewhat above room temperature, but analyses of the spectra of the ions are not sufficiently detailed as yet to permit an accurate comparison of experimental and theoretical values.

Cunningham, Wallmann, Phillips and Gatti[20] have attempted to measure the magnetic susceptibility of the tripositive ion of einsteinium, using approximately 0.003 μg of the oxide.

TABLE III

Magnetic Susceptibility of $PuCl_3$

| Temp | Experimental $\chi_m$ ($\times 10^6$) | Theoretical |
|---|---|---|
| 90°K | 1607 | 1567 |
| 200 | 887 | 829 |
| 300 | 658 | 628 |
| 334 | 606 | 587 |
| 373 | 571 | 549 |
| 397 | 548 | 529 |
| 428 | 525 | 507 |
| 457 | 515 | 490 |
| 491 | 484 | 472 |
| 520 | 464 | 458 |
| 548 | 462 | 447 |
| 583 | 472 | 434 |
| 300 | 659 | |

Complications arise in measuring the susceptibilites of highly radioactive samples because of paramagnetism induced in the supporting matrix by the radioactive disintegration of the sample. The principal isotope used for the susceptibility measurements on einsteinium was the 20 day $\alpha$-emitting $E^{253}$.

In order to correct for the induced paramagnetism, the susceptibility of the sample was measured as a function of time, and extrapolated to zero time. The data thus corrected gives $\mu_{eff}$ for $E^{+3}$ = 8.1 ± 1.5 Bohr magnitons.

CONCLUSIONS

On the basis of present knowledge of the properties of the actinide elements, it would appear probable that the thermodynamic properties of the transcurium elements probably will be rather similar to those of curium with a more or less regular variation as a function of atomic number, as observed in the lanthanide elements.

The remaining elements in the series will be predominantly tripositive, and their crystallography will resemble that of the corresponding rare earth element of similar ionic radius.

Magnetic and optical properties will resemble those of the analogous lanthanide elements, after making allowance for the greater multiplet splitting and more significant departure from LS coupling for the heavier elements.

BIBLIOGRAPHY

[1] A. Ghiorso, T. Sikkeland, A. E. Larsh and R. M. Latimer, Phys. Rev. V. 6, No. 9, p. 473 (1961)

[2] P. F. A. Klinkenberg, Physica 16, 618, 185 (1950)

[3] (a) J. C. Hubbs, R. Marrus and J. Winocur, Phys. Rev. 114, 586 (1959)

(b) J. C. Hubbs, R. Marrus, W. A. Nierenberg and J. L. Worcester, Phys. Rev. 109, 390 (1958)

(c) R. G. Albridge, J. C. Hubbs and R. Marrus, Phys. Rev. 111, 1137, (1958)

(d) A. Cabezas, E. Lipworth, R. Marrus and J. Winocur, Phys. Rev. 118, 233 (1960)

(e) R. Marrus, Biorganic Chemistry Quarterly Report, June-July-August, Nov. 23, 1958 (UCRL-8457)

(f) A. Cabezas, I. Lindgren, E. Lipworth, R. Marrus and M. Rubenstein, Nucl. Phys. 20, 509-512 (1960)

(g) R. Marrus, W. A. Nierenberg, and J. Winocur, Hyperfine Structure of Americium-241, May, 1960. (UCRL-9207)

(h) A. Cabezas and I. P. K. Lindgren, Atomic Beam Study of the Hyperfine Structure of the Thulium-170, May 9, 1960. (UCRL-9163)

(i) J. Winocur, Some Nuclear and Electronic Ground-State Properties of $Pa^{233}$, $Am^{241}$ and 16-Hour $Am^{242}$, April 13, 1960 (UCRL-9174)

[4] E. F. Westrum and L. Eyring, J. Am. Chem. Soc. 73, 3396 (1951)

[5] H. R. Lohr and B. B. Cunningham, J. Am. Chem. Soc 73, 2025 (1951)

[6] P. Graf, B. B. Cunningham, C. H. Dauben, J. C. Wallmann, D. H. Templeton and H. Ruben. J. Am. Chem. Soc., 78, 2340 (1956)

[7] D. B. McWhan, J. C. Wallmann, B. B. Cunningham, L. B. Asprey, F. H. Ellinger and W. H. Zachariasen, J. Inorg. Nucl. Chem., 15, 185 (1960)

[8] D. B. McWhan, B. B. Cunningham and J. C. Wallmann, J. Inorg. Nucl. Chem. (in press)

[9] D. B. McWhan and B. B. Cunningham, unpublished data.

[10] J. J. Howland, Jr. and M. Calvin, J. Chem. Phys. 18, 239 (1950)

[11] W. W. T. Crane, J. C. Wallmann and B. B. Cunningham, The Magnetic Susceptibilities of Some Compounds of Americium and Curium. Aug., 1950 (UCRL-846)

[12] J. B. Gruber, An Analysis of the Absorption Spectra of Tm (IV) and Am (IV). Thesis. University of California, 1961.

[13] W. H. Zachariasen, Chapter X in THE METAL PLUTONIUM. A. S. Coffinberry and W. N. Miner, Editors. The University of Chicago Press, Chicago, 1961.

[14] J. C. Wallmann, B. B. Cunningham and J. Fuger, unpublished data.

[15] S. Marei and B. B. Cunningham, unpublished data.

[16] S. C. Carniglia and B. B. Cunningham, J. Am. Chem. Soc. 73, 3396 (1951).

[17] H. Lammermann and H. J. Stapleton, J. Chem. Phys. 35, 1514 (1961).

[18] J. C. Wallmann and B. B. Cunningham, unpublished data.

[19] J. K. Dawson, C. J. Mandleberg and D. Davies, J. Chem. Soc., 2047 (1951)

[20] B. B. Cunningham, J. C. Wallmann, L. Phillips and R. Gatti, unpublished data.

# 11. CRYSTAL AND MOLECULAR STRUCTURE OF XENON TETRAFLUORIDE(*)

David H. Templeton, Allan Zalkin, J. D. Forrester, and Stanley M. Williamson

Because of interest in the molecular structure of xenon tetrafluoride[1] we have determined the structure of the crystals by x-ray diffraction at room temperature. The structure consists of a molecular packing of square-planar molecules of $XeF_4$.

A 4-to-1 molar ratio of $F_2$ and Xe was passed through a nickel tube at 300°C. With a residence time in the hot zone of 1 minute, essentially all the xenon reacted, and crystals condensed in the cooler part of the flow system. The solid was then sublimed under vacuum into other Pyrex containers and finally into thin-walled vitreous silica capillaries for x-ray examination.

Preliminary crystal data were obtained from oscillation and Weissenberg photographs of several crystals. The accurate cell dimensions and the intensities of the reflections were measured with a goniostat and scintillation counter with Mo Kα radiation, $\lambda(K\alpha_1) = 0.70926$ Å. The well-formed dodecahedral crystal had diameters ranging from 0.13 to 0.24 mm, corresponding to μR about unity. No correction was made for absorption. Because the crystal grew about 30% during the intensity observations, the data were normalized by repeated measurements of a few reflections.

The monoclinic unit cell has dimensions $a = 5.050$, $b = 5.922$, $c = 5.771$ Å (each ± 0.003 Å), and $\beta = 99.6° \pm 0.1°$, in reasonable agreement with values found elsewhere.[2, 3, 4] With two molecules per cell the density is 4.04 g/ml. Systematically absent reflections correspond to space group $P2_1/n$. Reflections are strong when $h+k+\ell$ is even and weak when it is odd, showing that the Xe atoms are at 0, 0, 0 and 1/2, 1/2, 1/2. Fluorine atoms are in two sets of general positions 4(e): $\pm(x, y, z; \frac{1}{2} - x, \frac{1}{2} + y, \frac{1}{2} - z)$.

Intensities were measured for the 329 independent reflections of the primitive cell with $\theta$ less than 25°. Of these, 36 are absent because of the space group symmetry. Of the other 133 reflections with $h+k+\ell$ odd, whose intensities depend only on the fluorine scattering, 96 were recorded as non-zero. An extensive search for other weak reflections which would demand a larger unit cell was made by sweeping along many lattice rows and by counting at approximately 100 positions corresponding to reflections of cells with some or all of the axes doubled. No such reflections were found, with the sensitivity about $10^{-4}$ of the strongest reflection.

---

*Letter to be published, J. Am. Chem. Soc. (Jan. 20, 1963).

1. H. H. Claassen, H. Selig, and J. G. Malm, J. Am. Chem. Soc. 84, 3593 (1962).

2. Stanley Siegel (Argonne National Laboratory), private communication.

3. Henri A. Levy (Oak Ridge National Laboratory), private communication.

4. James A. Ibers and Walter C. Hamilton (Brookhaven National Laboratory), private communication.

A trial structure was derived by simple calculations involving a few reflections. It was refined by least squares in several series of calculations. With independent isotropic temperature factors and equal weights for 286 reflections (omitting the seven at the lowest angles) the conventional $R = \Sigma||F_o| - |F_c||/\Sigma|F_o|$ was reduced to 0.086 with the parameters:

| | x | y | x | B |
|---|---|---|---|---|
| Xe | (0) | (0) | (0) | 1.6 $Å^2$ |
| $F_1$ | 0.261 | 0.147 | 0.847 | 3.6 |
| $F_2$ | 0.228 | 0.033 | 0.295 | 3.7 |

Standard deviations are 0.003 for each coordinate. Calculations with anisotropic temperature factors gave the same coordinates within 0.002 or less. Isotropic refinement with the 96 nonzero reflections with $h+k+\ell$ odd gave the same coordinates within 0.005 or less.

The above coordinates correspond to Xe-F bond distances of 1.92 and 1.90 Å, with standard deviations of 0.02 Å. The F-Xe-F bond angles are 89.7° (and 90.3°) with $\sigma = 0.9°$. The molecule is planar by the symmetry, and we find it to be square within the experimental uncertainty.

The thermal motion of the fluorine atoms exceeds that of the xenon atoms. As a result, the average Xe-F distance is greater than that given above. With the assumption that F "rides" on Xe, we estimate (from the anisotropic temperature parameters) that the average corrected distance is 1.93 Å.

The F-F distances within the molecule are 2.69 and 2.71 Å ($\sigma$ = 0.03 Å). The shortest F-F contact between molecules is 3.03 Å.

Ibers and Hamilton have deduced two structures by refinement of data with $h+k+\ell$ even. These data do not permit determination of the relative signs of the two y coordinates. One of these two structures is in approximate agreement with our result.

The structure and molecular dimensions are shown in Figs. D. 11-1 and D. 11-2.

We thank Dr. Henri A. Levy for helpful information concerning the space group.

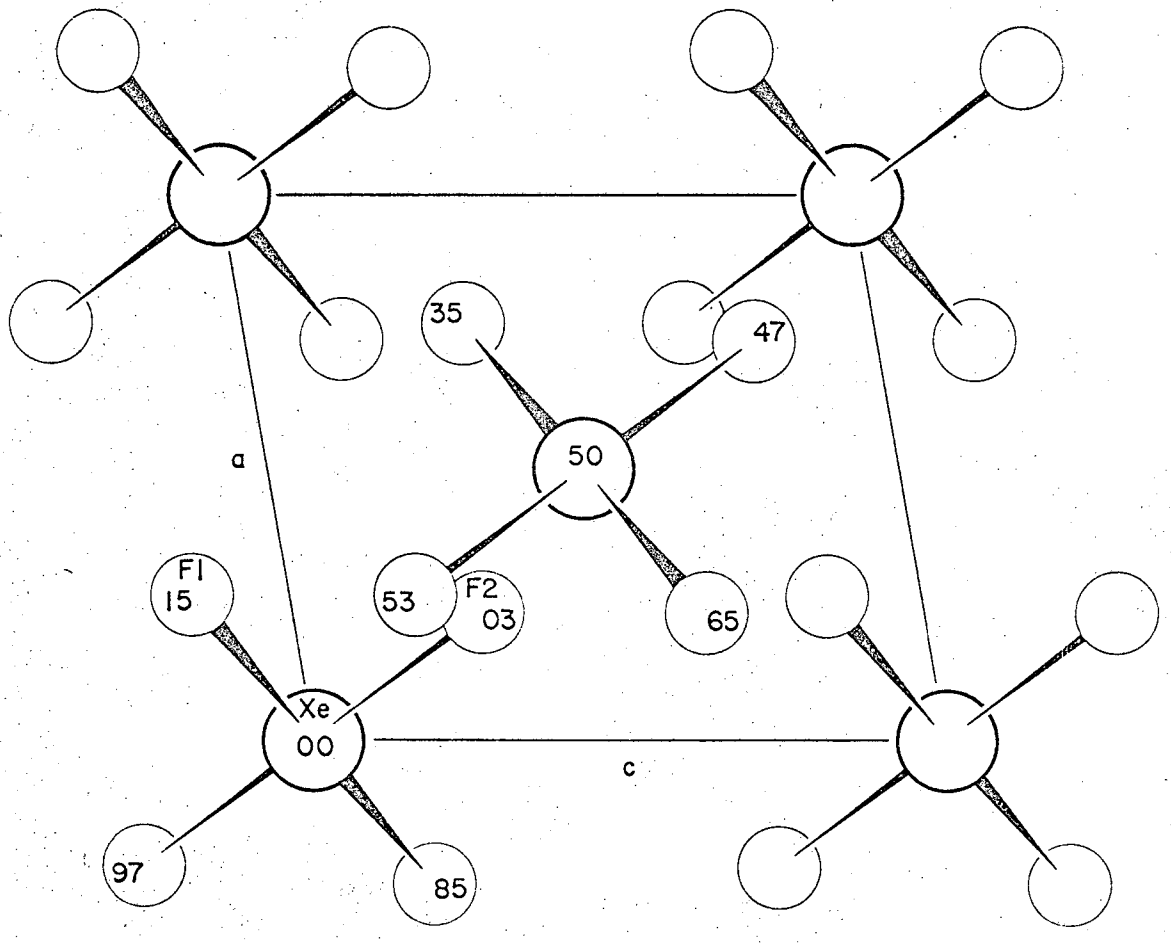


Fig. D. 11-1. Structure of $XeF_4$.

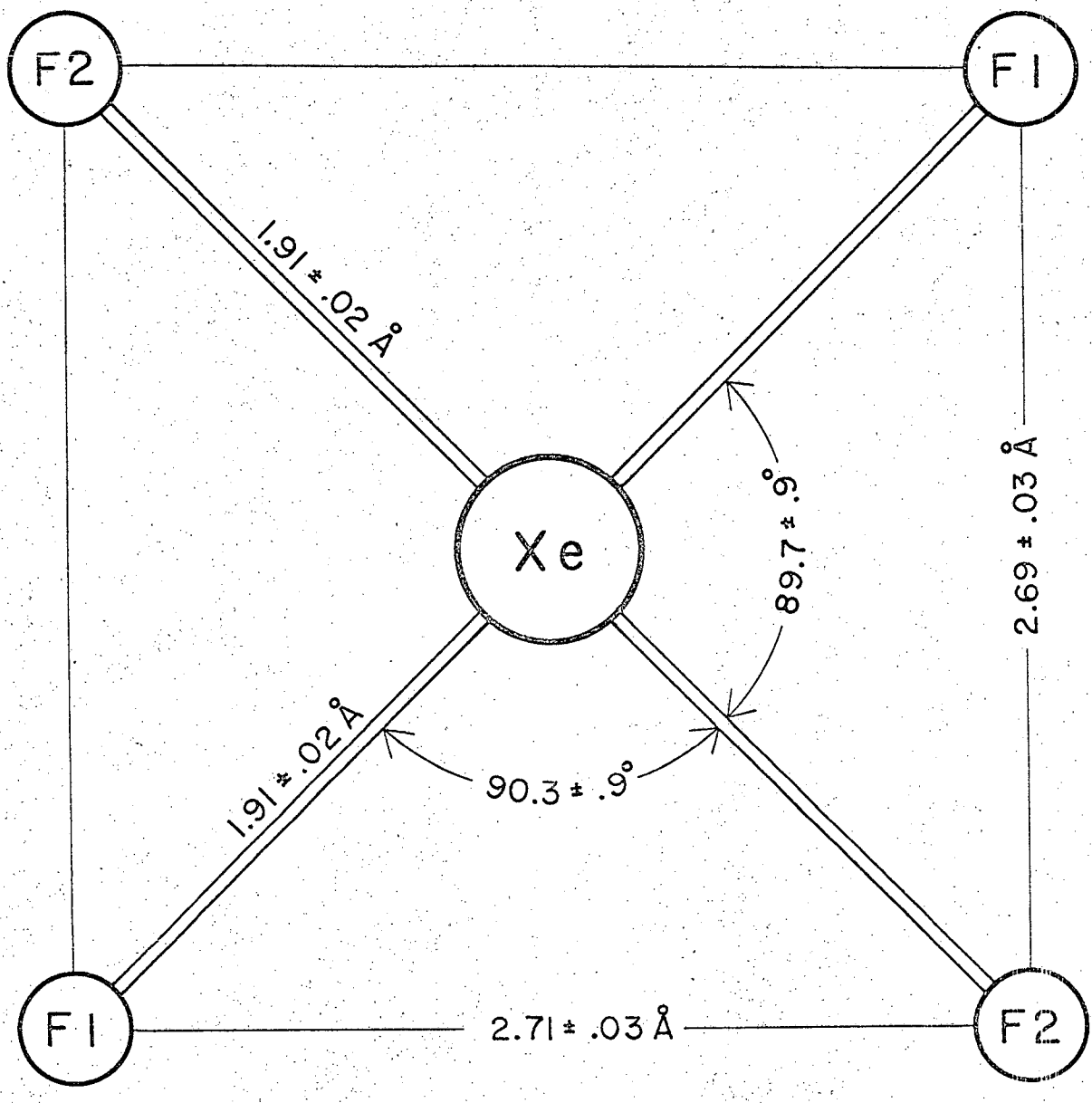


Fig. D. 11-2. Molecular dimensions of $XeF_4$.

# 12. CRYSTAL AND MOLECULAR STRUCTURE OF $In_2I_6$

John D. Forrester, Allan Zalkin, and David H. Templeton

## Experimental Procedure

$InI_3$ was synthesised by heating indium metal at 250°C in an atmosphere of iodine vapor. The $InI_3$ was distilled to a clean portion of the glass tube which was then sealed off from the rest of the apparatus and opened in a dry box, as the trihalide is extremely hygroscopic. Small quantities of the $InI_3$ were loaded into quartz capillary tubes (0.6 mm diameter and 0.015 mm wall) and recrystallized by heating in an oven to 250°C (mp of $InI_3$ is 210°C -- Handbook of Physics and Chemistry) and allowed to cool slowly.

## Unit Cell and Space Group

The dimensions of the monoclinic unit cell of $InI_3$ are

$$a = 9.837 \pm 0.004 \text{ Å},$$

$$b = 6.102 \pm 0.004 \text{ Å},$$

$$c = 12.195 \pm 0.009 \text{ Å},$$

$$\beta = 107.69 \pm 0.05^\circ.$$

Reflections of the type $h0\ell$ are absent for $\ell$ odd, and of the type $0k0$ are absent for k odd. This indicates $P2_1/c$ ($C_{2h}^5$) as the space group, and the success of our structure determination supports this.

With four formula units ($InI_3$) per unit cell, the density is calculated as 4.72 $g/cm^3$, as compared with the reported measured densities of 4.69 $g/cm^3$,[1] and 4.66 $g/cm^3$.[2]

## Structure Determination

This monoclinic unit cell, of space group $P2_1/c$, has four $InI_3$ formula units per unit cell, with the iodine atoms arranged ideally in a close-packed cubic array. Placing the origin of the unit cell at a center of symmetry midway between two iodine atoms allows the symmetry elements to be inserted satisfactorily and the close-packed iodine array preserved. This puts the iodine atoms in three different fourfold general positions of the type

$$4(e): x, y, z;\ \bar{x}, \bar{y}, \bar{z};\ \bar{x},\ 1/2 + y,\ 1/2 - z;\ x,\ 1/2 - y,\ 1/2 + z,$$

with the ideal coordinates of

---

1. W. Z. Klemm, Anorg. u. Allgem. Chem. 163, 235 (1927).
2. W. Klemm and F. Dierks, ibid 219, 42 (1934).

$I_1$ 0, 1/4, 1/8,

$I_2$ 1/3, 3/4, 5/24,

$I_3$ 2/3, 3/4, 1/24,

and In at 1/6, 0, 1/24.

## Discussion of the Structure

The overall packing of the dimers in the structure is shown in Fig. D. 12-1. The closeness of the arrangement of the iodine atoms to a close-packed cubic arrangement can be seen in this figure, where the background grid of side a/2 for the ideal face-centered cubic cell is drawn to accentuate the relation. Table I, in which are listed the ideal and the final positional parameters, also demonstrates the nearness to the ideal structure. The shortest I-I distance in this structure is 4.110 Å, and the mean I-I distance for nearest neighbors is 4.353 Å, in comparison with the shortest I-I distance of 4.44 Å in InI.

The indium atoms are in tetrahedral holes in the close-packed iodine arrangement but are slightly further from the ideal positions than the iodine atoms, probably owing to repulsion between the two metal atoms.

The dimeric molecule $In_2I_6$ is formed by two tetrahedra of iodine atoms around the indium atoms sharing an edge, and is analogous to the dimer in solid $Al_2Br_6$ and in $Al_2Cl_6$ vapor. The entire structure, in fact, is very similar to that of $Al_2Br_6$, which has both a dimeric molecule and close packing of the halogen atoms. The shape and dimension of the dimer are depicted in Fig. D. 12-2. The crystal symmetry gives the dimer a center of symmetry, but, in addition to this, the dimer has a mirror plane through the bridge iodines to an accuracy better than the standard deviation. This is not demanded by the crystal symmetry.

The dimensions of the dimer are in reasonable agreement with those reported by Wood and Ritter[3] for x-ray-diffraction measurements on fused $InI_3$, provided the assignment of the bond distances to the bridge and terminal iodine atoms have been reversed. The In-In distance is, however, not in such good agreement, being only 3.15 Å, as opposed to 3.883 Å as found in this work. This distance compares with the shortest In-In distance of 3.58 Å found by Jones and Templeton in InI.[4]

The repulsion and increased separation of the metal atoms leaves four of the angles at the indium atom from the iodine atoms in the tetrahedron very close to the tetrahedral angle (107.4, 107.7, 109.3, and 109.3°) but distorts the other two, making the angle to the terminal iodine atoms larger (125.1°) and that to the bridge iodine atoms smaller (93.7°).

---

3. R. E. Wood and H. L. Ritter, J. Am. Chem. Soc. 74, 1760 (1952).

4. R. E. Jones and D. H. Templeton, Acta Cryst. 8, 847 (1955).

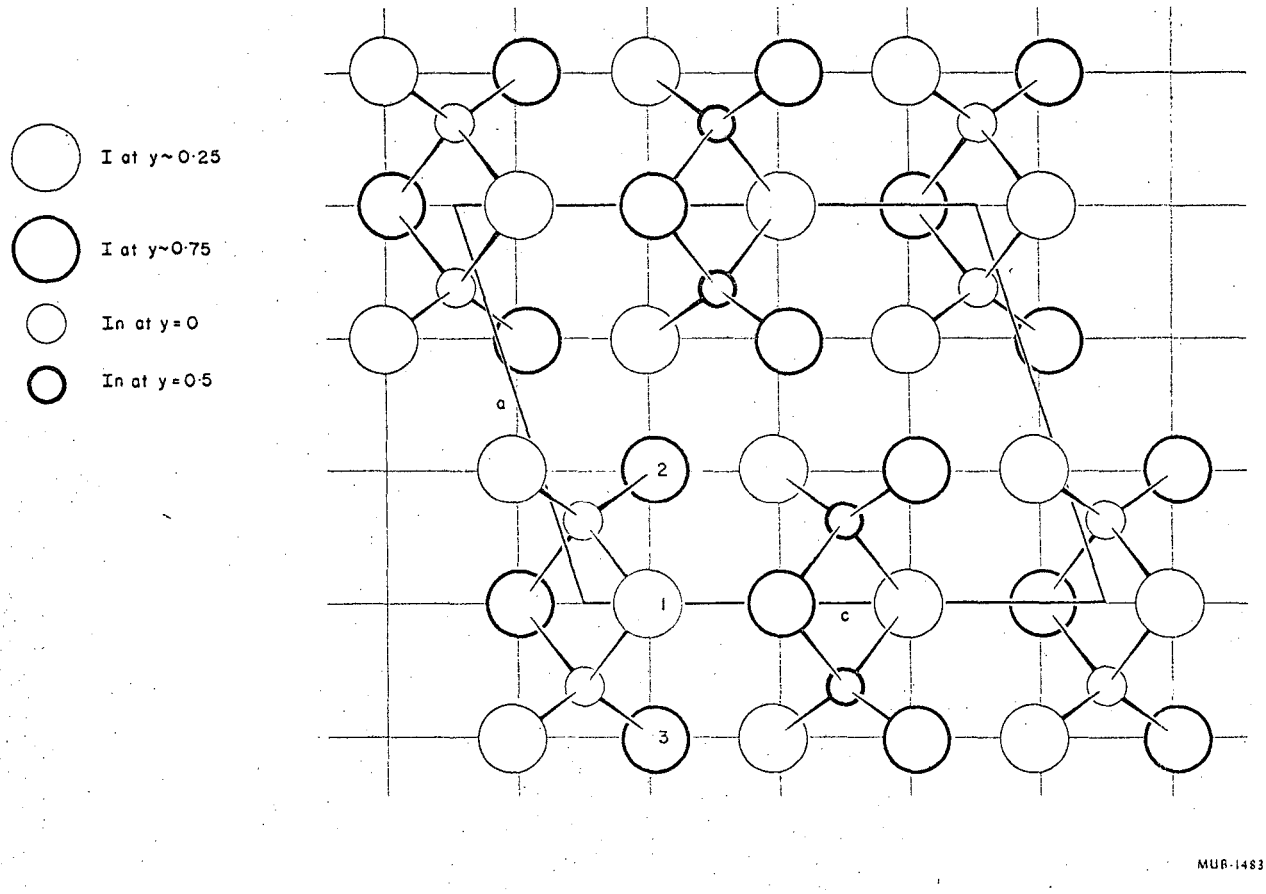


Fig. D. 12-1. The packing of the dimers of $In_2I_6$, together with the approximately face-centered cubic arrangement of the iodine atoms. The square grid is drawn with side = 3.05 Å = a/2 for the face-centered cubic lattice. The actual values of y for the iodine atoms are: $I_1$, y = 0.236; $I_2$, y = 0.229; $I_3$, y = 0.231.

Table I. Final and ideal positional parameters.

| Atom | x | | y | | z | |
|---|---|---|---|---|---|---|
| | Final | Ideal | Final | Ideal | Final | Ideal |
| In | 0.2072 | 0.1667 | -0.0005 | 0.00 | 0.0510 | 0.0417 |
| I(1) | 0.0001 | 0.0000 | 0.2360 | 0.25 | 0.1220 | 0.1250 |
| I(2) | 0.3361 | 0.3333 | 0.7293 | 0.75 | 0.2198 | 0.2083 |
| I(3) | 0.6617 | 0.6667 | 0.7306 | 0.75 | 0.0531 | 0.0417 |

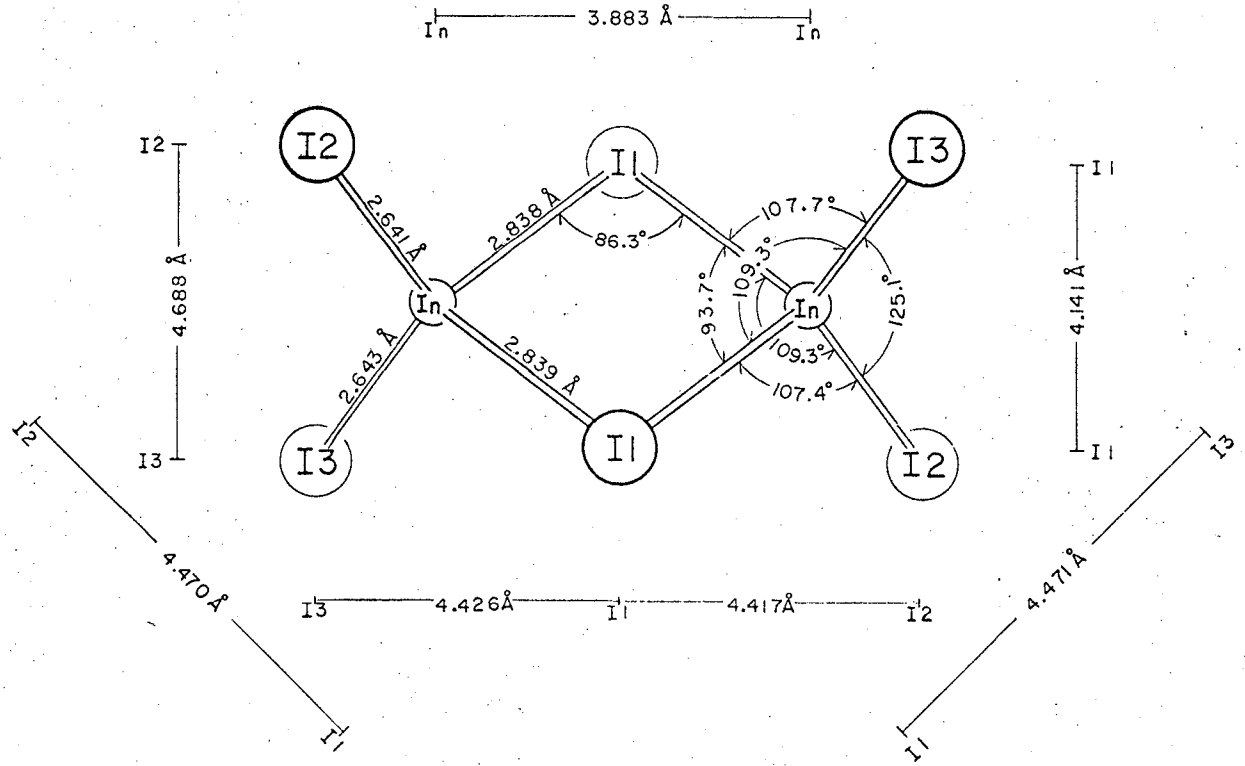


$In_2I_6$

MUB-1484

Fig. D. 12-2. The $In_2I_6$ dimer. This is formed by the sharing of an edge by two tetrahedra and is very similar to the $Al_2Br_6$ dimer. The estimated standard deviation of the shorter distances is ± 0.005 Å and for the longer distances, ± 0.007 Å.

## 13. CRYSTAL STRUCTURE OF THE HYDRATED DOUBLE NITRATE OF MAGNESIUM AND CERIUM(*)

David H. Templeton, Allan Zalkin, and J. D. Forrester

According to single-crystal x-ray diffraction data, crystals of $Mg_3Ce_2(NO_3)_{12}(H_2O)_{24}$ are rhombohedral, space group $R\bar{3}$. The hexagonal cell with $a = 11.00$ and $c = 34.59$ Å contains three formula units. By least-squares refinement the conventional unreliability factor R was reduced to 0.04 for about 1600 reflections. The Ce atoms, on the threefold axis at $z = \pm 0.2497$, are each surrounded by 12 oxygen atoms at an average distance of 2.64 Å. These oxygen atoms, belonging to six nitrate ions, are at the corners of a somewhat irregular icosahedron. The Mg atoms are at the origin and on the threefold axis at $z = \pm 0.4279$. Each Mg atom is surrounded by six water molecules with the oxygen atoms at the corners of an octahedron with an average Mg-O distance of 2.07 Å. One-fourth of the water molecules are not coordinated to cations. Evidence for the hydrogen atom positions from the diffraction data indicates that six of the eight independent hydrogen atoms are involved in normal hydrogen bonds. The structure is shown in Fig. D. 13-1.

---

*Abstract for American Physical Society Meeting at Stanford University, December 27-29, 1962, Bull. Am. Phys. Soc. 7, 608 (1962).

## 14. CRYSTAL STRUCTURE OF $KH_2F_3$ AND GEOMETRY OF THE $H_2F_3^-$ ION(*)

J. D. Forrester, Michael E. Senko,† Allan Zalkin, and David H. Templeton

Alkali fluorides crystallize from HF solutions in the form of many solvates. For example, in the KF-HF system Cady observed the phases KF·HF, KF·2HF, 2KF·5HF, KF·3HF, and KF·4HF.[1] It is well known that in KF·HF the fluorine atoms are connected in pairs by strong hydrogen bonds, and it is convenient to consider this substance as a salt of $K^+$ and $HF_2^-$ ions. We speculated that in the higher solvates other polymeric ions occur: $FHFHF^-$, $FHFHFHF^-$, etc. By a determination of the crystal structure by x-ray diffraction, we have confirmed that in KF·2HF the fluorine atoms are grouped into $FHFHF^-$ ions, and consequently we write the formula as $KH_2F_3$.

Crystals were prepared and photographed (by M. E. S.) in 1954, and the unit cell and space group were determined. The prospect of locating eight atoms in the asymmetric unit of a noncentric crystal with data of doubtful accuracy and with rather inadequate computing facilities was not as interesting as several other problems, and the work was suspended. In

---

*Brief version of published paper, Acta. Cryst. 16, 58 (1963).

†Now at International Business Machines Corp., Yorktown Heights, N. Y.

1. G. H. Cady, J. Am. Chem. Soc. 56, 1431 (1934).

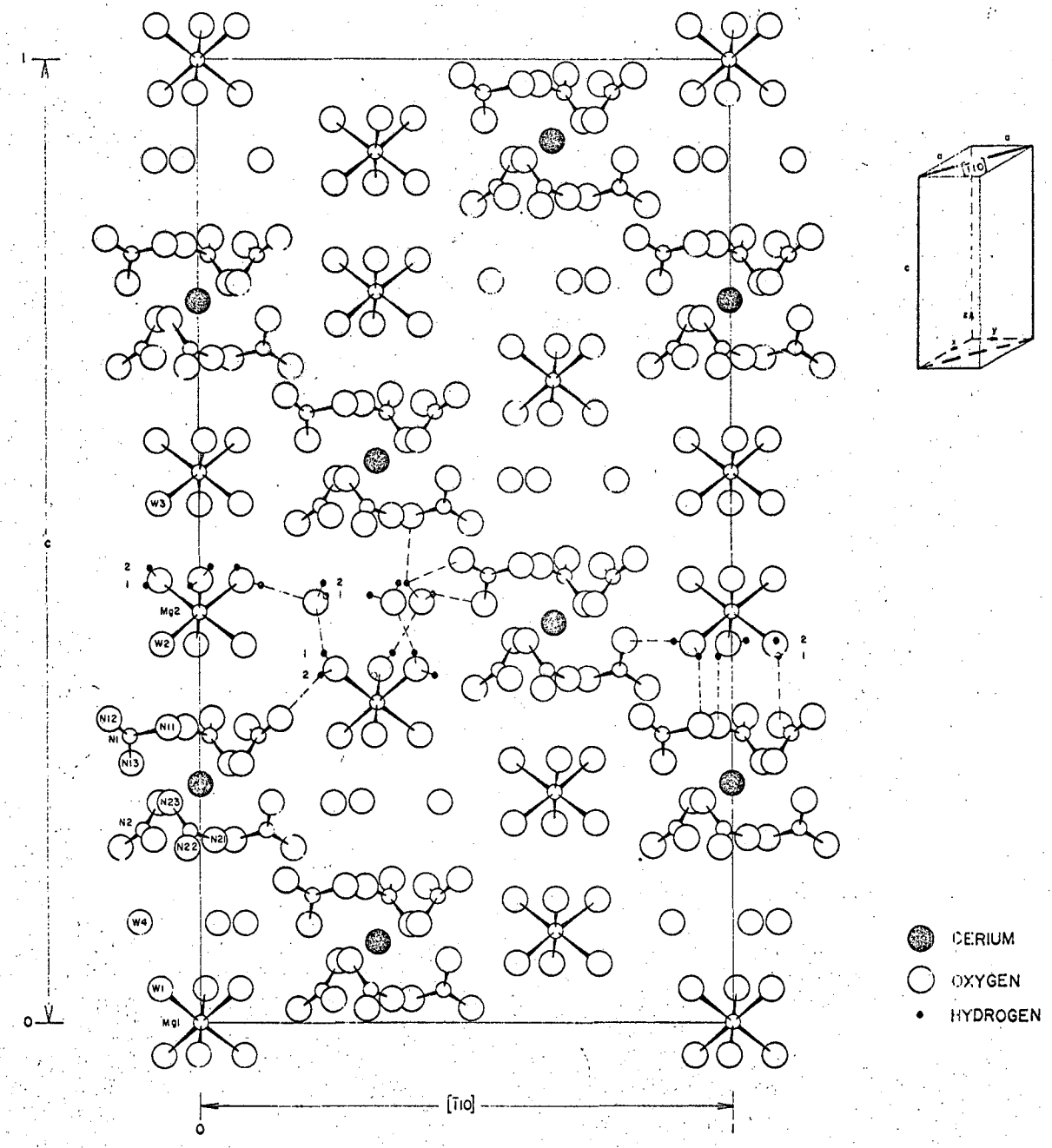


Fig. D. 13-1. A section through a unit cell of the structure along a [1̄10] plane. Only the cerium and magnesium atoms in this plane, together with the atoms closely coordinating them, are shown. One example of each type of hydrogen position and each type of hydrogen bond are shown.

1961 and 1962 the old photographs were examined again and were used to determine the structure reported here.

## Unit Cell and Space Group

The diffraction patterns show orthorhombic symmetry with unit cell dimensions

$$a = 8.52 \pm 0.02 \text{ Å},$$

$$b = 11.09 \pm 0.03 \text{ Å},$$

$$c = 6.69 \pm 0.02 \text{ Å}.$$

Reflections are absent for h00 with h odd, for 0k0 with k odd, and for 00$\ell$ with $\ell$ odd. These absences correspond to space group $P2_12_12_1$, which is confirmed by the success of the structure determination. The number of formula units per unit cell must be divisible by 4. Ionic volumes in other crystals suggest that $8(KH_2F_3)$ is the only reasonable content of the unit cell. On this basis the calculated density is 2.06 g/cm$^3$.

## Determination of the Structure

The asymmetric unit contains two potassium atoms and six fluorine atoms. The coordinates of the potassium atoms were determined uniquely from a three-dimensional Patterson function.

The three-dimensional electron density function was calculated by using phases calculated from the potassium atoms. This function was perplexing, but we identified four fluorine atoms by rejecting peaks that corresponded to unreasonably short interatomic distances and those for which we could not find $K_1$-F and $K_2$-F peaks in the Patterson function.

A second electron density function was calculated with phases determined by the two potassium atoms and the four fluorine atoms. With the same criteria, we were able to identify the remaining two fluorine atoms.

The structure was then refined by least squares with an IBM-7090 computer and a full-matrix program written by P. K. Gantzel, R. A. Sparks, K. N. Trueblood, with minor changes.

Refinement with all the data made it evident that absorption errors were present. Refinement was continued with 551 reflections (of which 56 are zero) where $\sin\theta/\lambda$ exceeded 0.2. For these data the conventional reliability factor $R = \Sigma ||F_o| - |F_c|| / \Sigma |F_o|$ was reduced to 0.202 after six cycles.

The computer program used had no provision for refining the separate scale factors of the different layers, so these factors were adjusted by hand, and R fell to 0.186. Because the low-angle data still seemed to be affected by absorption, further refinement was done with reflections for which $\sin\theta/\lambda$ exceeded 0.3 (487 terms of which 54 are zero). After further

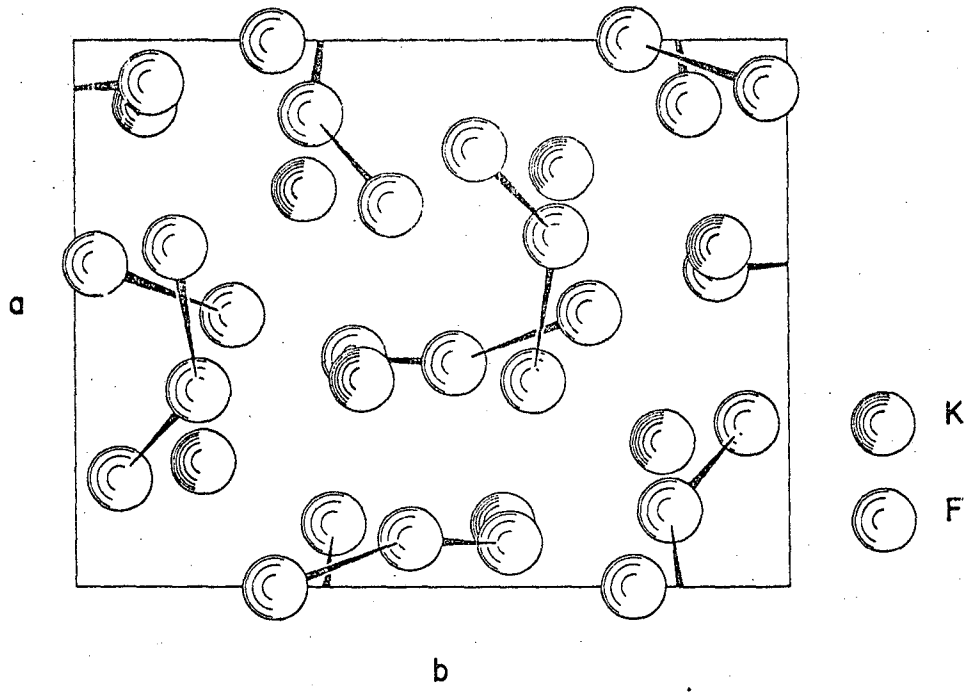


Fig. D. 14-1. Crystal structure of $KH_2F_3$, projected along c.

rescaling, R was reduced to 0.142. At this stage, shifts of coordinates were negligible. A total of 37 parameters (including scale factors) was used to achieve this fit.

Fluorine atoms occur in the structure in groups of three, as was expected for hydrogen-bonded $H_2F_3^-$ ions (Fig. D. 14-1). The two non-equivalent groups permit independent measurement of four hydrogen-bond distances and two bond angles, which are listed in Table I. These bond distances average 2.33 Å, and the deviations from this average are of doubtful significance. The difference in the two bond angles is significant, and we infer that the molecule is not very rigid and that it bends to improve the crystal packing. This idea is consistent with the F-F-F angles reported for hydrogen fluoride. In the solid, HF occurs in zig-zag chains with angles of 120.1°.[2] In the gaseous polymer, the angle is observed as 144° by electron diffraction.[3]

The distances that we observe for the hydrogen bonds in $KH_2F_3$ imply that these bonds approach in stability those in bifluoride ions. This fact suggests that the potential curve for the proton in one of these bonds may also be of the single-minimum type. The accuracy of our x-ray-diffraction data does not permit us to test this conjecture, nor do we know of any other evidence that bears on the question. If such a minimum does occur, symmetry does not require it to be at the center of the bond.

The structure as a whole is saltlike, with the potassium ions well dispersed among the $H_2F_3^-$ ions. The shortest K-K distance is 4.34 Å. Each potassium atom has eight fluorine neighbors, each a member of a different $H_2F_3^-$ ion, at distances averaging 2.83 Å for $K_1$ and 2.82 Å for $K_2$.

---

2. M. Atoji and W. N. Lipscomb, Acta Cryst. 7, 173 (1954).

3. S. H. Bauer, J. Y. Beach, and J. H. Simons, J. Am. Chem. Soc. 61, 19 (1939).

Table I. Interatomic distances and angles in $KH_2F_3$.
(The standard deviation of each distance is 0.02 Å.)

| | Distances (Å) | | Angles (deg) |
|---|---|---|---|
| $F_1$-$F_2$ | 2.35 | $F_2$-$F_1$-$F_3$ | 130 ± 2 |
| $F_1$-$F_3$ | 2.34 | | |
| $F_4$-$F_5$ | 2.29 | $F_5$-$F_4$-$F_6$ | 139 ± 2 |
| $F_4$-$F_6$ | 2.34 | | |
| | | | Distances (Å) |
| $K_1$-$F_1$ | 2.69 | $K_2$-$F_4$ | 2.67 |
| $K_1$-$F_3$ | 2.69 | $K_2$-$F_1$ | 2.69 |
| $K_1$-$F_5$ | 2.78 | $K_2$-$F_6$ | 2.72 |
| $K_1$-$F_6$ | 2.80 | $K_2$-$F_2$ | 2.78 |
| $K_1$-$F_2$ | 2.81 | $K_2$-$F_4$ | 2.80 |
| $K_1$-$F_5$ | 2.85 | $K_2$-$F_5$ | 2.94 |
| $K_1$-$F_6$ | 2.94 | $K_2$-$F_3$ | 2.96 |
| $K_1$-$F_2$ | 3.05 | $K_2$-$F_3$ | 2.99 |

# 15. ELECTRON TRANSFER IN DILUTE GOLD ALLOYS(*)

P. H. Barrett, R. W. Grant, Morton Kaplan, D. A. Keller, and D. A. Shirley

The chemical properties of systems involving two metals, rather than one metal and one nonmetal, fall in one of the least understood areas of modern physical chemistry. In contrast to the situation for "conventional" chemical compounds, there is no satisfactory theoretical model available for the metallic bond, let alone the bonding in intermetallic compounds. Similarly, unlike the case of ions in dilute solutions, even the charge states are unknown for metal atoms in dilute solid solutions with other metals. To attack the charge-state problem one must study some parameter other than just the spatial disposition of atoms in solid solutions. The disposition of the outer electron is required; this can be studied in part by nuclear resonance. We have used the Mössbauer resonance technique in a survey experiment to study the charge states of gold atoms in very dilute solid solutions in eighteen metallic elements.

In these experiments the isomeric chemical shift of the gold resonance line was measured in each case. The results are given in Table I. The shifts are all taken relative to metallic gold, which was used as an absorber.

We believe this to be the first experimental investigation into this type of chemical bonding. There are so few guides available that a precise quantitative interpretation seems out of the question. However, several qualitative features may be extracted from the shift data. First we note that the theoretical expression for the chemical shift in a Mössbauer resonance experiment may be written as the product of an electronic factor and a nuclear factor:

$$\Delta E = \frac{2\pi Z e^2}{5} R^2 \left[ \Delta \langle X^{2\rho} \rangle \right] \left[ \Delta \langle \psi | \psi \rangle_0 \right] \qquad (1)$$

The nuclear factor, given in the first square brackets, is the difference between the average $2\rho$th reduced radial charge moments of the nuclear states: it is usually unknown. The second set of square brackets contains the electronic factor: the difference, between source and absorber, of the electron densities at the nucleus. Thus the chemical shift is directly proportional to this difference.

The concept of electronegativity is frequently useful for discussing electron transfer in more conventional chemical systems. We have tested its applicability here by plotting the chemical shift against the electronegativity of the host (Fig. D. 15-1). There is a strong correlation between the two quantities. This is established directly from the experimental data, and rests on no further assumptions.

---

*Brief version of paper to be submitted to J. Chem. Phys. (UCRL-10608, March 1963).

Table I. Isomeric chemical shifts of $Au^{197}$ in several metals (probable error in the last place given in parenthesis).

| Host | Chemical shift (cm/sec) |
|---|---|
| Be | 0.59 (5) |
| Cu | 0.42 (4) |
| Ca | 0.87 (5) |
| Ag | 0.14 (2) |
| Ge | 0.45 (4) |
| Y | 0.76 (3) |
| Li | 0.74 (5) |
| Sn | 0.43 (4) |
| Al | 0.76 (4) |
| Pd | 0.24 (3) |
| Te | 0.19 (3) |
| Si | 0.33 (3) |
| Mg | 0.63 (3) |
| Fe | 0.53 (2) |
| Co | 0.52 (2) |
| Ni | 0.47 (2) |
| Zn | 0.34 (5) |
| Pt | 0.13 (2) |

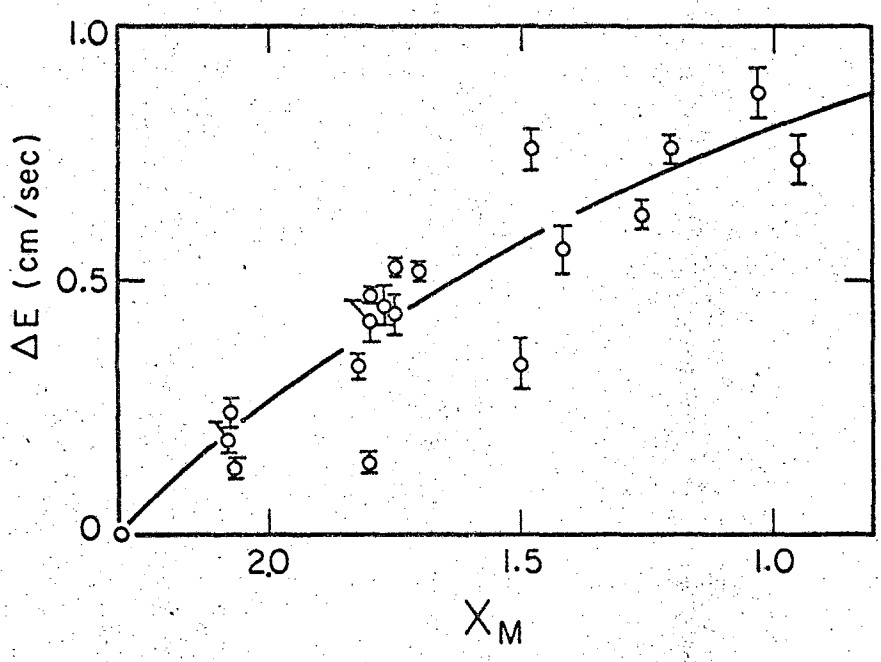


Fig. D. 15-1. Isomeric chemical shift vs host electronegativity for solid solutions of $Au^{197}$ in the metals listed in Table I, plus gold. The curve, representing an empirical best fit, shows some evidence of saturation.

By further rather qualitative reasoning we have reached the following tentative conclusions:[1]

1. Electrons are transferred toward the gold atom, which is more electronegative than the hosts, in every case.
2. In each alloy gold gains electron density equivalent to a fraction (up to 0.4 to 0.8 in calcium) of a 6s electron.

These tentative conclusions should be tested by further work. If they are correct, the data for charge transfer in these systems fit quite naturally into a simple chemical model: the more electronegative host metals contribute electrons to the gold solute atom, roughly in proportion to the electronegativity difference, until the 6s shell is nearly full. Then the Pauli principle prevents further transfer, and the shift-vs-electronegativity curve begins to saturate. There is some evidence in Fig. D. 15-1 for the onset of saturation.

1. The arguments are too complicated to reproduce here. They may be found in the paper from which this report is condensed.

## 16. INTERNAL FIELDS IN EUROPIUM

P. H. Barrett and D. A. Shirley

The internal magnetic fields at the nuclei of rare earth metals and divalent europium compounds are of interest in studying the "canted spiral" type of antiferromagnetism. These fields can be measured by Mössbauer resonance techniques in elements that have suitable isotopes. Europium-151 is such an isotope;[1] it exhibits a sizable Mössbauer effect, and single-line sources can be made. We have used this isotope to characterize the hyperfine structure in europium metal at low temperatures, thereby deriving the internal magnetic field and the spin and magnetic moment of the 21.7-keV state of $Eu^{151}$.

The hyperfine spectrum of $Eu^{151}$ in metallic europium is shown for several temperatures in Fig. D. 16-1. The Néel point[2] of 87°K is confirmed by the transition between the 90°K and 86°K spectra from a single line characteristic of paramagnetic relaxation to a wider pattern characteristic of materials below the collective magnetic transition point, where spin-lattice relaxation is slow compared with lifetimes of the isomeric level ($\tau \approx 10^{-8}$ sec).

At 4.2°K, where europium is presumably ferromagnetic, a well-resolved pattern is observed (Fig. D. 16-2). This spectrum may be reproduced theoretically by referring to a "g-factor diagram" (Fig. D. 16-3), on which the ratio of g factors of the isomeric states is plotted against the

1. D. A. Shirley, M. Kaplan, R. W. Grant, and D. A. Keller, Phys. Rev. 127, 2097 (1962).

2. C. Olsen, N. Nereson, and G. Arnold, J. Appl. Phys., Vol. 33 Supplement, April 1962.

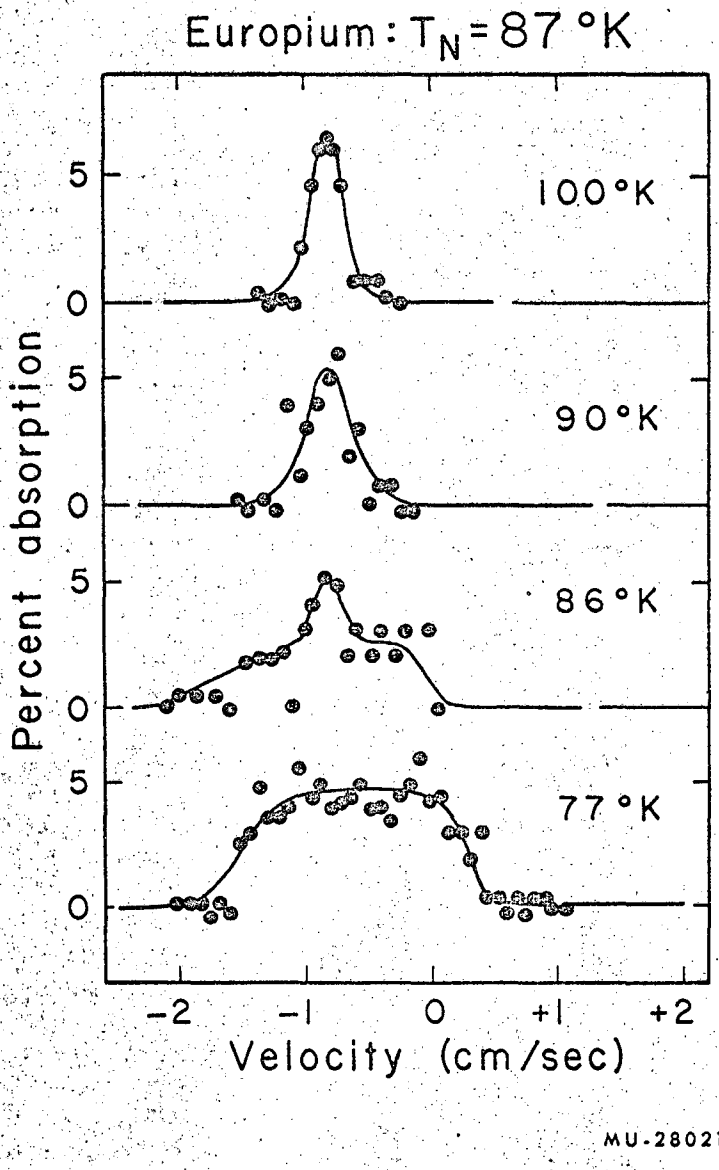


Fig. D. 16-1. The resonant absorption spectra of $Eu^{151}$ in europium metal at several temperatures near the Néel point of 87°K.

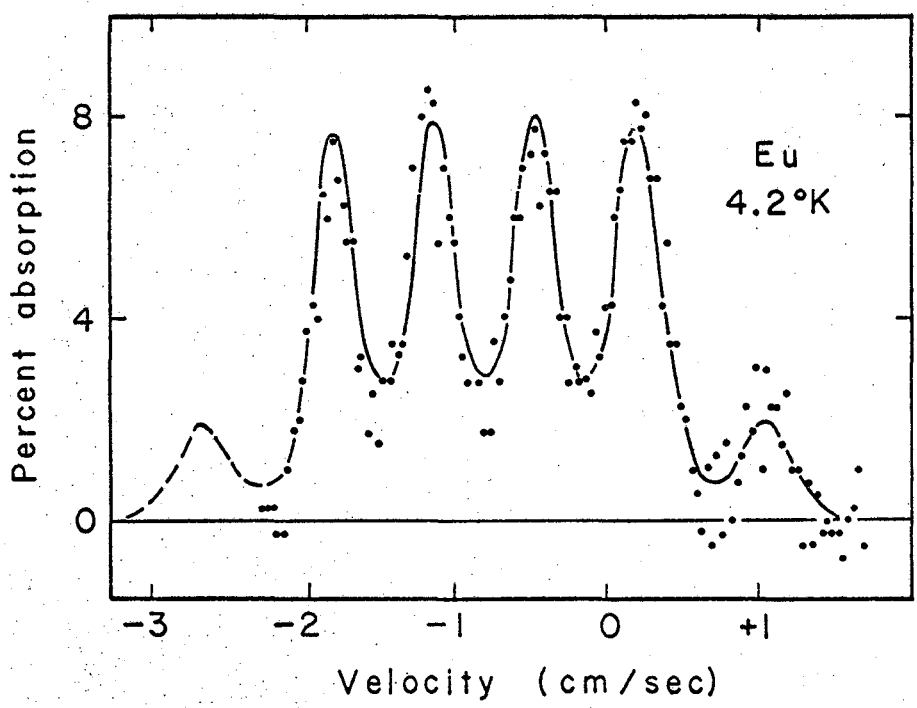


Fig. D. 16-2. The resonant absorption spectrum of $Eu^{151}$ in europium metal at 4.2°K. The sweep did not go to high enough velocities to detect the weak line at -2.6 cm/sec in this run. In other runs this line was observed. The theoretical curve is for a g-factor ratio of + 0.528.

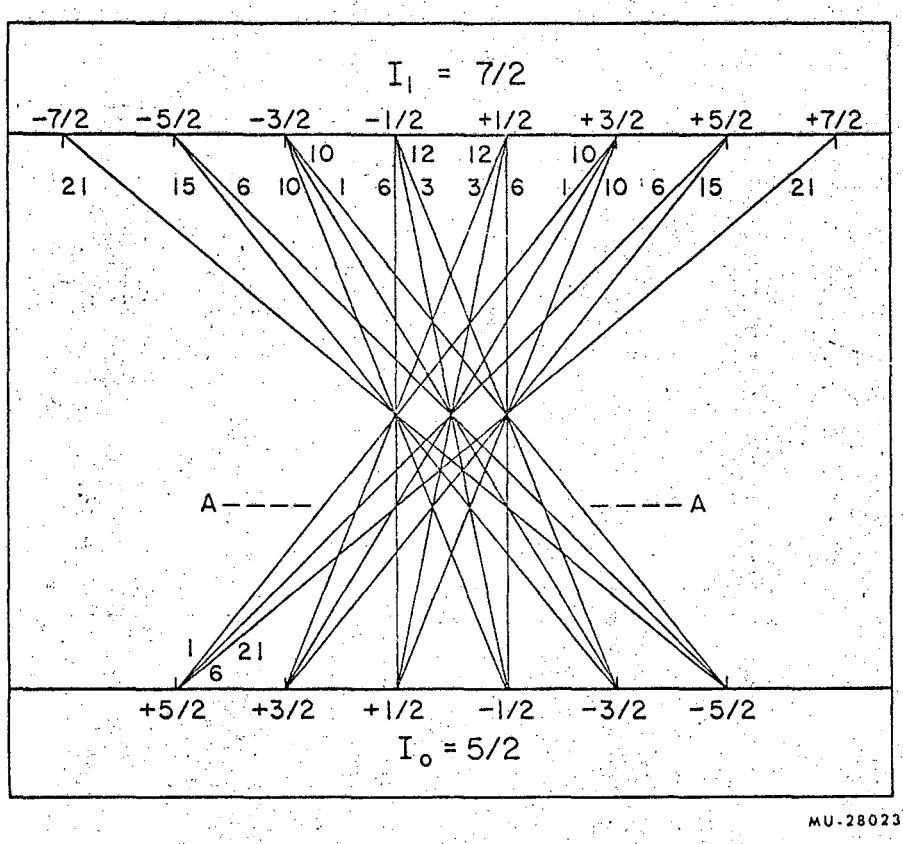


Fig. D. 16-3. The g-factor diagram for a dipole transition between two states of spins 5/2 and 7/2, having magnetic moments of the same sign. The line A-A fits the $Eu^{151}$ spectrum. Numbers near lines denote relative intensities.

energy of splitting. Zeeman components of the isomeric M1 transition are drawn in with appropriate intensities. Only for the g-factor ratio given by the line A-A does the theoretical spectrum fit the experimental data. The curve in Fig. D. 16-2 is derived for this ratio. There are eighteen Zeeman components: accidental degeneracies leave only six strong, and two very weak, lines. Similar g-factor diagrams were drawn for the other possible spins of the 21.7-keV state allowed by conservation of angular momentum in dipole transition to a spin 5/2 state, as well as for negative g-factor ratios. Only the diagram in Fig. D. 16-3 gave a satisfactory fit. Thus the spin of the 21.7-keV state is 7/2 from the g-factor ratio $+0.528 \pm 0.005$ and the known ground-state moment of +3.419 nm;[3] we find, for the excited state, $\mu = +2.53 \pm 0.03$ nm.

The internal field, derived by comparison of the nuclear moment with the numerical value of the splitting, is $264 \pm 8$ kgauss. This is comparable to the 311 to 343 kgauss which may be derived from paramagnetic resonance data on divalent europium ions,[4, 5] and tends to confirm the idea that the $4f^7 6S^2$ europium configuration forms ion cores characterized as $4f^7$, $^8S_{7/2}$, which produce the internal field via configuration mixing, plus two 6s conduction electrons, which remain unpolarized in the conduction band.

---

3. F. M. Pichanick, P. G. H. Sandars, and G. K. Woodgate, Proc. Roy. Soc. (London) A257, 277 (1960).

4. B. Bleaney and W. Low, Proc. Phys. Soc. (London) A68, 55 (1955).

5. W. Low, Phys. Rev. 106, 1827 (1956).

## 17. THE INTERNAL MAGNETIC FIELDS AT NUCLEI OF GOLD DISSOLVED IN IRON, COBALT, AND NICKEL

R. W. Grant, Morton Kaplan, D. A. Keller, and D. A. Shirley

Since the discovery of large magnetic fields at nuclei of diamagnetic atoms dissolved in ferromagnets,[1] these fields have been of particular interest in connection with conduction-electron polarization, from which they are believed to arise. The sign of the internal field is especially important in elucidating the mechanism of this polarization. The magnitude can be useful in deciding whether conduction-electron polarization is indeed the origin of the fields.

For solutions of gold in iron, cobalt, and nickel the measurements have been particularly uncertain. Two general experimental techniques have been applied; Mössbauer resonance[2] and nuclear polarization.[3] The

---

1. B. N. Samoilov, V. V. Sklyarevskii, and E. P. Stepenov, Zh. Eksperim. i. Teor. Fiz. 36, 644 (1959).

2. D. A. Shirley, M. Kaplan, and P. Axel, Phys. Rev. 123, 816 (1961); L. D. Roberts and J. O. Thomson, Bull. Am. Phys. Soc. 6, 75 (1961); 6, 230 (1961); 7, 350 (1962); 7, 351 (1962).

3. N. G. Stone and B. G. Turrell, Phys. Letters 1, 39 (1962).

Mössbauer experiments have suffered from the fact that the magnetic moment of the 77-keV state of $Au^{197}$ is unique in being nearly in the wrong "Schmidt group." This has impeded the measurement of the internal fields for some time. Now the moment is known to be small, however. This moment helps to establish a new kind of nuclear excitation, "core excitation."[4] The polarization experiments require several assumptions for their interpretation and are probably less reliable. Recently several groups have studied these fields intensively, all by different methods.[3, 5, 6, 7] Our experiments have involved direct comparison of the internal fields with external fields up to 94,000 gauss, using the Low-Temperature Laboratory 7-megawatt magnet. The hyperfine structure of the Mössbauer resonances in $Au^{197}$ was measured.

The maximum effective external field (i.e., the difference between the field at the source and that at the absorber) was only 65,000 gauss. In iron this is only 5% of the internal field; it causes each resonance line to move only 0.03 cm/sec, or 1/20 of one line width. To measure such a small effect accurately it was necessary to take all the data at points of maximum slope on the intensity-vs-Doppler velocity curve (Fig. D. 17-1).

In Fig. D. 17-2 are shown the observed hyperfine splittings for $Au^{197}$ in iron, cubic and hexagonal cobalt, and nickel. This splitting arises from an effective field $\vec{H}_{eff}$ given by the vector sum of the internal and external fields plus a "magnetostrictive field," which varies with the magnetization $\vec{M}$ of the specimen, i.e.,

$$\vec{H}_{eff} = \vec{H}_{int} + \vec{H}_{ext} + \vec{H}_{mag}(\vec{M}). \qquad (1)$$

Here the "magnetostrictive field" includes effects actually due to magnetostriction as well as those due to strains and domain orientation. For large external fields ($H_{ext}$ larger than about 10,000 gauss) the magnetization, and hence the "magnetostrictive field," saturates. Thus at these high fields it is possible to compare the internal and external fields (which are now collinear) directly by measuring the magnitude of their sum. The straight lines in Fig. D. 17-2 were fitted to the data and used to derive the internal fields given in Table I. The signs of these fields were obtained from the signs of the slopes of the lines in Fig. D. 17-2.

---

4. A. Braunstein and A. de-Shalit, Phys. Letters 1, 264 (1962).

5. Louis D. Roberts and J. O. Thomson, Phys. Rev. Letters 9, A8 (1962).

6. B. N. Samoilov, V. V. Sklarevski, and V. D. Gorobchenko, Soviet Physics JETP 14, 1267 (1962).

7. R. W. Grant, M. Kaplan, D. A. Keller, and D. A. Shirley, Bull. Am. Phys. Soc. 7, 601 (1962).

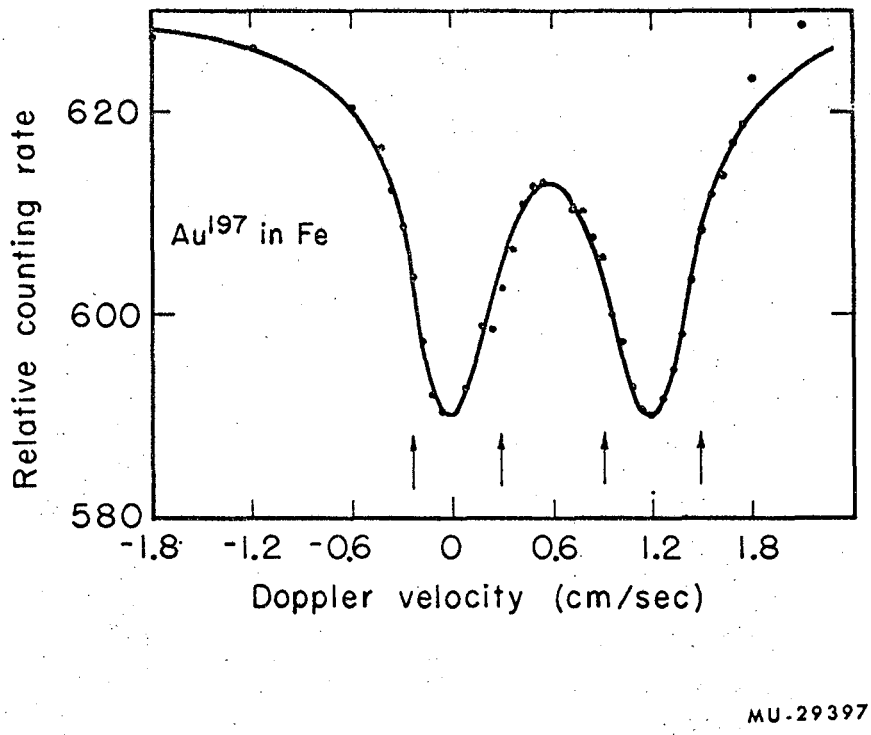


Fig. D. 17-1. Transmission curve for resonant 77-keV γ rays from a source of $Au^{197}$ in iron, using a single-line absorber of metallic gold. Data at various external fields were taken at points indicated with arrows which are near the points of maximum slope. Between 2.5 and 3.0 million counts were taken at each point for every value of the external magnetic field.

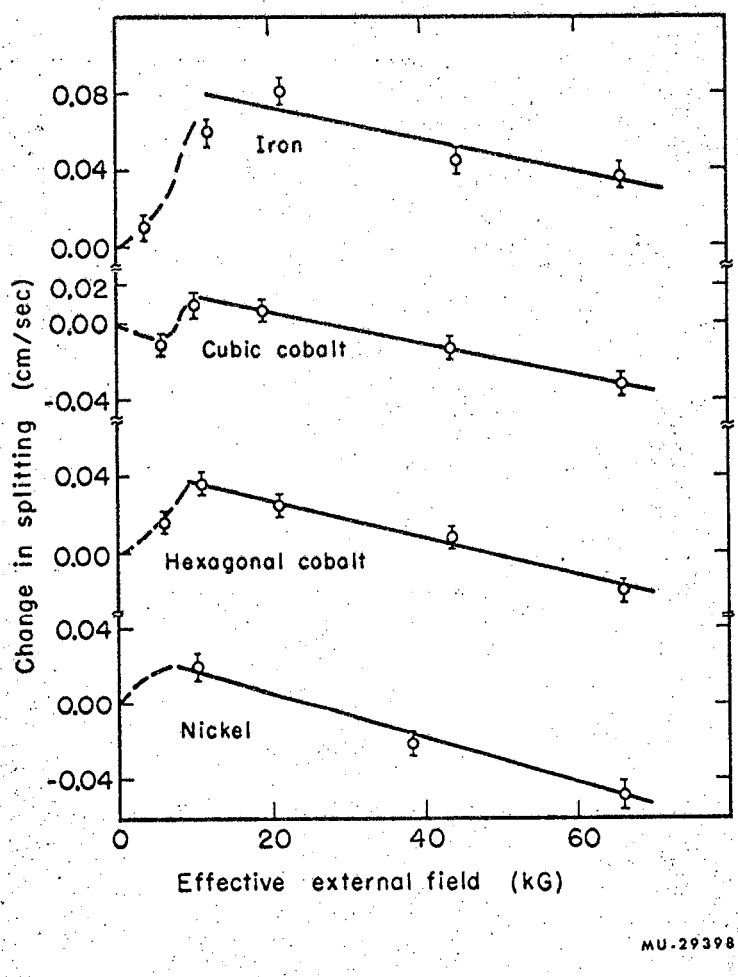


Fig. D. 17-2. Total splitting of the Mössbauer resonance pattern for $Au^{197}$ in Fe, Co, and Ni. The straight lines were used to determine internal fields.

Table I. Internal fields for $Au^{197}$ in ferromagnets, derived from slopes.

| Host | Internal field (kG) | $\mu_{77}$ (nm) |
|---|---|---|
| Fe | - 1350 ± 300 | 0.34 ± .09 |
| Co (cubic) | - 910 ± 150 | 0.36 ± .06 |
| Co (hex) | - 830 ± 150 | 0.39 ± .06 |
| Ni | ≈ - 200 | ----- |

The internal fields are all negative, supporting the conduction-electron polarization hypothesis. Moreover, the magnitudes of the fields are larger than for the lighter elements, suggesting again that it is the 6s conduction electron of gold, with its very large hfs field, which is being polarized. In Fig. D. 17-3 the magnitude of the internal field is plotted against the atomic magnetic moment of the host. The internal field follows the atomic magnetic moment closely.

By comparing the internal fields with the total splitting in each case, we find a value of

$$\mu_{77} = 0.37 \pm 0.04 \text{ nm}$$

for the magnetic moment of the 77-keV isomeric state of $Au^{197}$.

## 18. THE INFLUENCE OF HIGH PRESSURES ON THE MÖSSBAUER EFFECT IN DYSPROSIUM-161

John A. Stone

An experimental study[1] has been performed to determine the influence of pressure up to 100 kbar on the resonant absorption of γ rays emitted without recoil.[2] The system under study was the 25.6-keV gamma ray of $Dy^{161}$ from the decay of $Tb^{161}$ situated in gadolinium metal, using thin dysprosium absorbers.

---

1. The experimental portion of this work was performed with the assistance of Malcolm Nicol and Dr. George Jura of the Inorganic Materials Group.

2. R. L. Mössbauer, Z. Physik 151, 125 (1958); Naturwiss. 45, 538 (1958); Z. Naturforsch. 14a, 211 (1959).

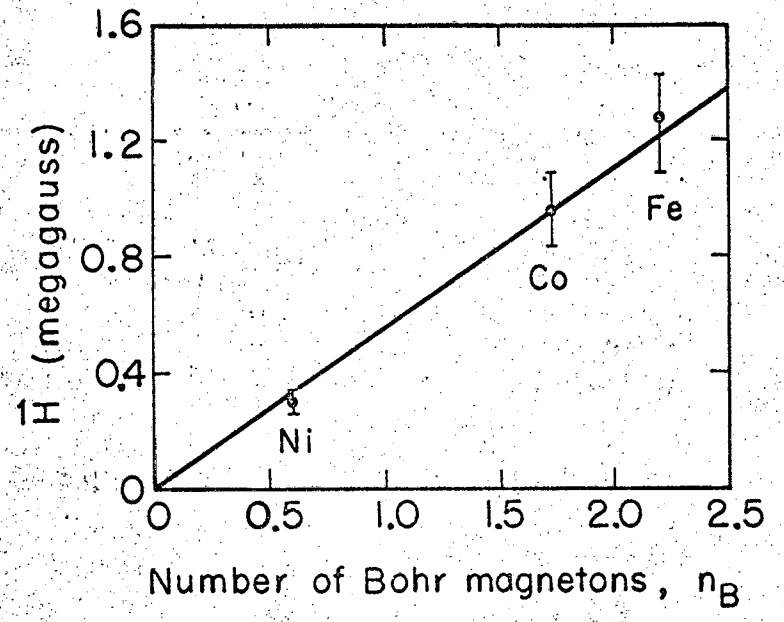


MU-29399

Fig. D. 17-3. Magnitude of the internal field at the nucleus of a gold atom dissolved in a ferromagnetic host, vs atomic magnetic moment of the host.

The results of this work are summarized in Figs. D. 18-1 through D. 18-3 and in Table I. Figures D. 18-1 and D. 18-2 show the spectra of transmitted $\gamma$-ray intensity versus relative absorber velocity at pressures of approximately 30 kbar and 50 kbar, respectively. Considerable hyperfine structure is evident in these spectra. Figure D. 18-3 is a comparison of spectrum envelopes, where the hyperfine structure has been smoothed out and ignored, at 30 kbar, 50 kbar, and 100 kbar.

Table I. Quantities measured in high-pressure Mössbauer absorption experiments. (See text for explanation of symbols.)

| P (kbar) | x | $\frac{f_P}{f_{30}}$ | $\Delta E_P - \Delta E_{30}$ (cm/sec) | $\frac{\Delta E_P}{\Delta E_{30}}$ | $\bar{v}$ (mm/sec) |
|---|---|---|---|---|---|
| 0 (1 atm) | $\approx 0$ | $\leq 0.3$ | --- | --- | --- |
| 30 | 1.00 | 1 | 0 | 1 | $4.0 \pm 0.2$ |
| 50 | 1.71 | $1.81 \pm 0.05$ | $2.67 \pm 0.05$ | $\geq 1.9$ | $2.0 \pm 0.4$ |
| 100 | 3.14 | $3 \pm 1$ | $5.5 \pm 0.2$ | $\geq 2.8$ | --- |

Table I gives several quantitative results derived from the experimental data. Because the absorption effect at atmospheric pressure was too small to be measured in these experiments, all quantities are quoted relative to the 30-kbar spectrum, where the most precise data were obtained. The nomenclature used in Table I is defined as follows:

P = approximate pressure at which an experiment was performed;

x = ratio of the experimentally measured loading pressures on the oil in the hydraulic press, at pressure P and at 30 kbar; this is equal to the ratio of the pressures;

$\frac{f_P}{f_{30}}$ = ratio of the fraction of $\gamma$ rays emitted without recoil, at pressure P and at 30 kbar; this is equal to the ratio of the areas above the transmission curves at these pressures;

$\Delta E_P$ = energy difference between the highest- and lowest-energy components of the recoil-free $\gamma$-ray emission spectrum, at pressure P; the observed width of a velocity spectrum is the sum of this quantity and a corresponding quantity for the absorber, so that the difference between the observed widths at pressures P and 30 kbar is independent of the absorber and is equal to $\Delta E_P - \Delta E_{30}$; lower limits on $\Delta E_P / \Delta E_{30}$ may also be obtained;

$\bar{v}$ = velocity coordinate of the centroid of a velocity spectrum; this is related to the chemical shift between the source and the absorber.

Two qualitative conclusions may be drawn immediately from these comparisons. With increasing pressure,

(a) recoil-free fractions increase;
(b) hyperfine splittings increase.

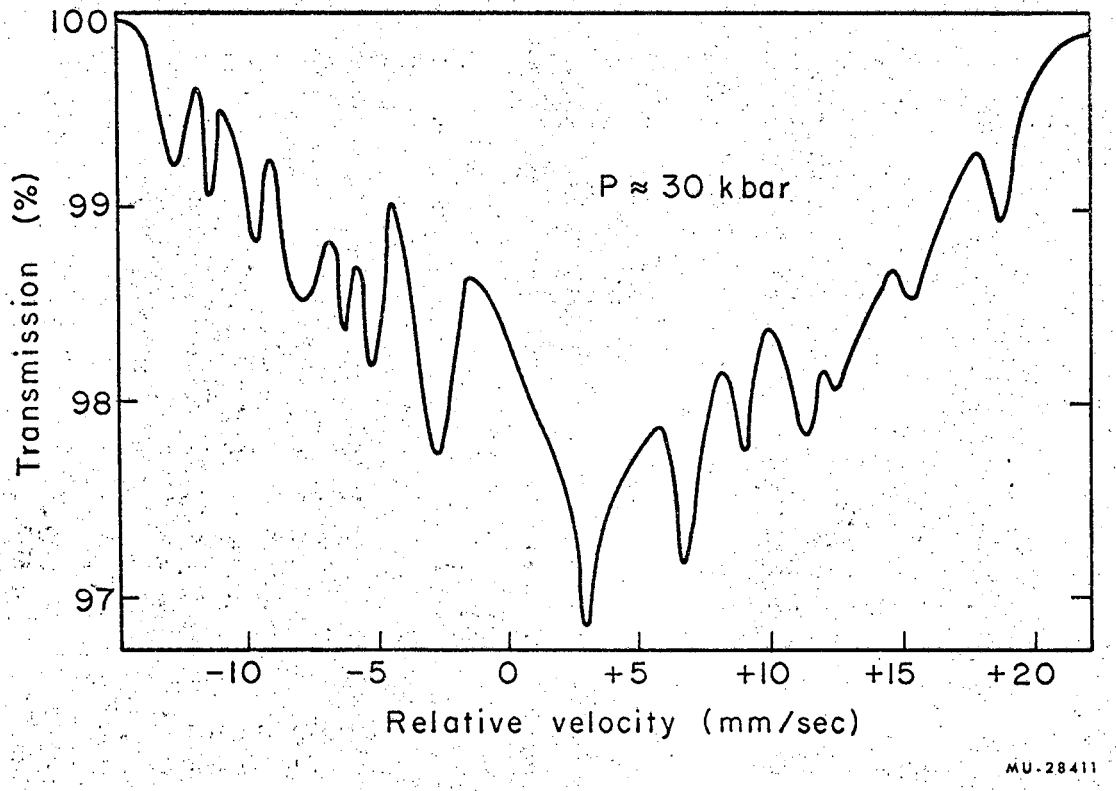


Fig. D. 18-1. Velocity spectrum of the 25.6-keV γ ray of $Dy^{161}$ situated in Gd metal at approximately 30 kbar.

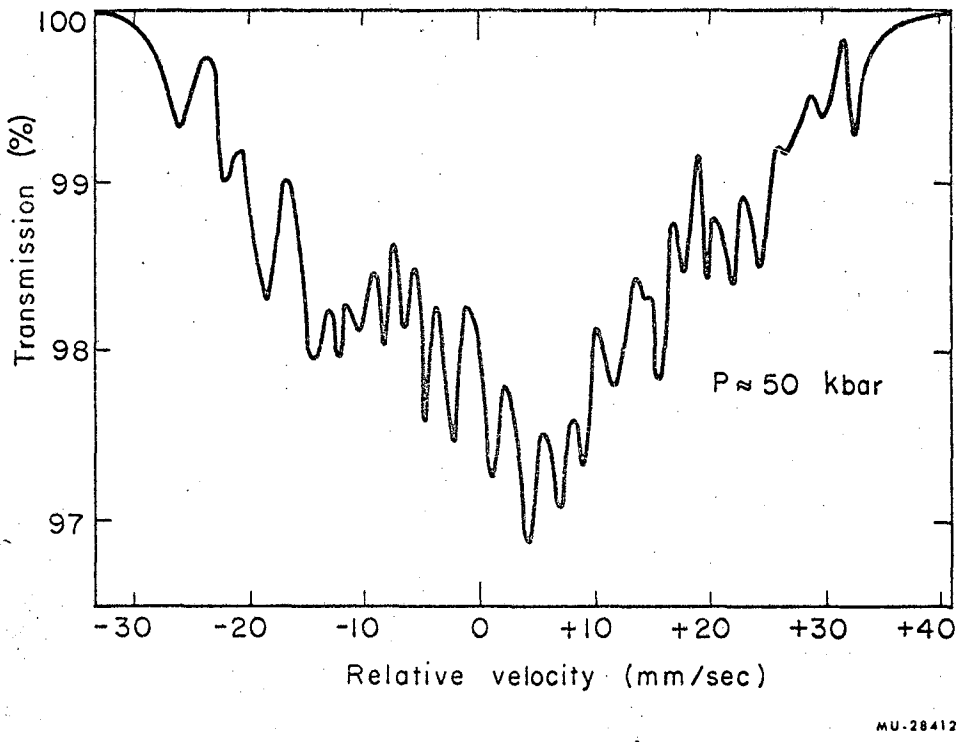


Fig. D. 18-2. Velocity spectrum of the 25.6-keV γ ray of $Dy^{161}$ situated in Gd metal at approximately 50 kbar.

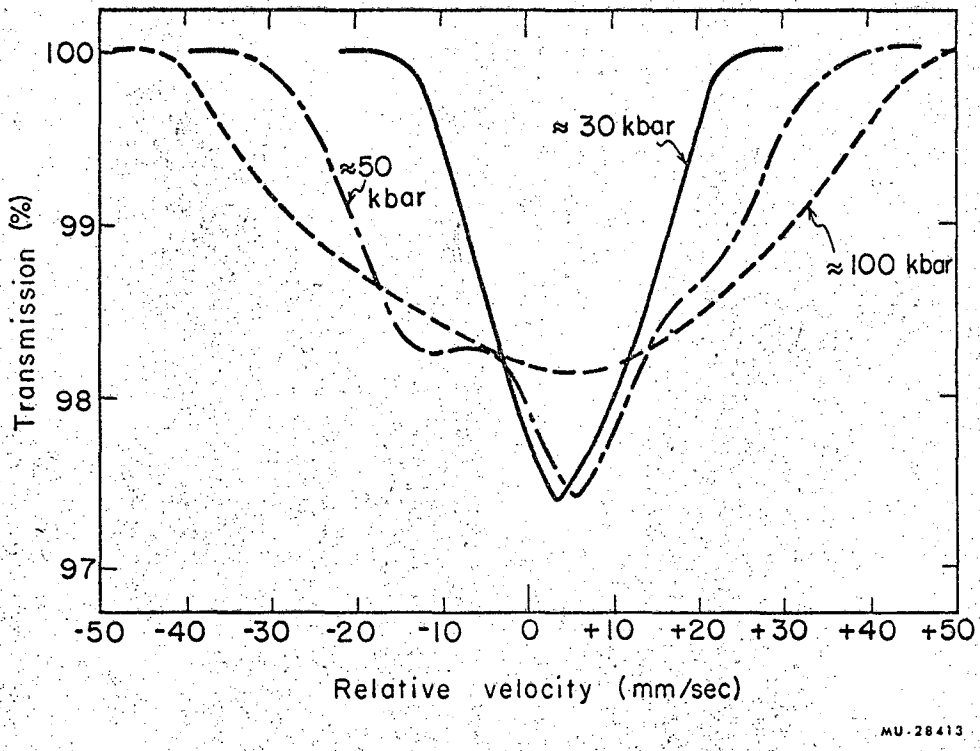


Fig. D. 18-3. Comparison of the envelopes of velocity spectra at several pressures, for the 25.6-keV γ ray of $Dy^{161}$ situated in Gd metal.

These two effects summarize the influence of high pressures on the Mössbauer effect in $Dy^{161}$ as determined from this experimental work.

An interpretation of the increase in recoil-free fractions with pressure may be made by using a treatment similar to that of Hanks.[3] To do this it is necessary to derive equations for the case in which the ambient temperature T is higher than the Debye temperature $\theta$. Starting with the expression for the recoil-free fraction f from the Debye model of lattice vibrations,

$$\ln f = -\frac{3}{2}\frac{R}{k\theta}\left[1 + 4\left(\frac{T}{\theta}\right)^2 \int_0^{\theta/T} \frac{t\,dt}{e^t - 1}\right],$$

where R is the normal recoil energy of an atom due to emission of the $\gamma$ ray, and k is Boltzmann's constant, one may introduce the pressure dependence by the following series of approximations and assumptions.

(a) The volume dependence of $\theta$ is given by the Grüneisen relation,

$$\frac{d \ln \theta}{d \ln V} = -\gamma,$$

where $\gamma$ is the Grüneisen constant for the material.

(b) Volume changes in the system are small.

(c) $T/\theta > 1.6$; this allows the use of the high-temperature approximation,

$$4\left(\frac{T}{\theta}\right)^2 \int_0^{\theta/T} \frac{t\,dt}{e^t - 1} \approx 4\left(\frac{T}{\theta}\right) - 1.$$

(d) Volume changes can be expressed by

$$\frac{\Delta V}{V_0} \approx aP - bP^2,$$

where a and b are empirically determined coefficients.

(e) Pressure is proportional to loading.[4]

Using these assumptions, one finally obtains

$$\ln \frac{f_2}{f_1} = \frac{12\,RT\gamma}{k\theta_0^2}\left(\frac{\Delta V_1}{V_0} - bP_1^2 x\right)(x - 1),$$

---

3. R. V. Hanks, Phys. Rev. 124, 1319 (1961).

4. Peter W. Montgomery, Harold Stromberg, George H. Lura, and George Jura, Calibration of Bridgman Anvils, A Pressure Scale to 125 kbars, UCRL-9807, Aug. 1961.

where the subscript 1 refers to the reference state near 30 kbar, and the subscript 0 refers to the atmospheric pressure reference state. With $\theta_0^2/\gamma$ as an adjustable parameter, Fig. D. 18-4 shows the fit of the calculated curve to the experimental points for $\theta_0^2/\gamma = 6000$. The experimental results appear to be consistent with values of $\theta_0$ from 75 to 100 for a dysprosium impurity in gadolinium metal. This is somewhat lower than the values for the pure metals, which are near 150.

Work is being continued on the interpretation of the hyperfine splittings.

## 19. ANION EFFECTS ON THE $Pr^{3+}$ SPECTRUM*

Ralph D. McLaughlin and John G. Conway

Shifts in spectral lines of $Pr^{3+}$ that result from changing the cation-anion distance have been studied. This was done by recording the spectra of a few per cent of $Pr^{3+}$ which had been incorporated into the anhydrous trichlorides of Ce, Nd, Sm, Gd, and the anhydrous tribromides of La and Ce. In addition, data for $Pr^{3+}$ in $Gd(EtSO_4)_3 \cdot 9H_2O$ were compared with existing data on $Pr^{3+}$ in $Ce(EtSO_4)_3 \cdot 9H_2O$. In all these systems $Pr^{3+}$ has the same point symmetry. The results are displayed in Fig. D. 19-1.

Two types of shifts occur. The main shift results from the change in position of the center of gravity of the crystal-field states. A minor shift of crystal-field states with respect to each other is also observed.

---

*Brief version of note to be published in J. Chem. Phys. (UCRL-10458, Sept. 1962).

## 20. THE ABSORPTION SPECTRUM OF $Pu^{3+}$ IN LANTHANUM TRICHLORIDE AND LANTHANUM ETHYLSULFATE*

Hildelore Lämmermann and John G. Conway

Studies of the polarized absorption spectrum and some special effects were conducted on crystals of lanthanum trichloride and lanthanum ethylsulfate containing 0.1 and 5 mol % of $Pu^{3+}$ at various low temperatures. The ground-state levels as well as several excited states are well characterized. Attempts at fitting the positions of levels to 5f hydrogenic free-ion states give good agreement for $F_2 = 245\ cm^{-1}$ and $\zeta = 2290\ cm^{-1}$. Figure D. 20-1 is an energy level scheme showing the data and the calculations.

---

*Abstract of paper to appear in J. Chem. Phys. 38 (Jan. 1963).

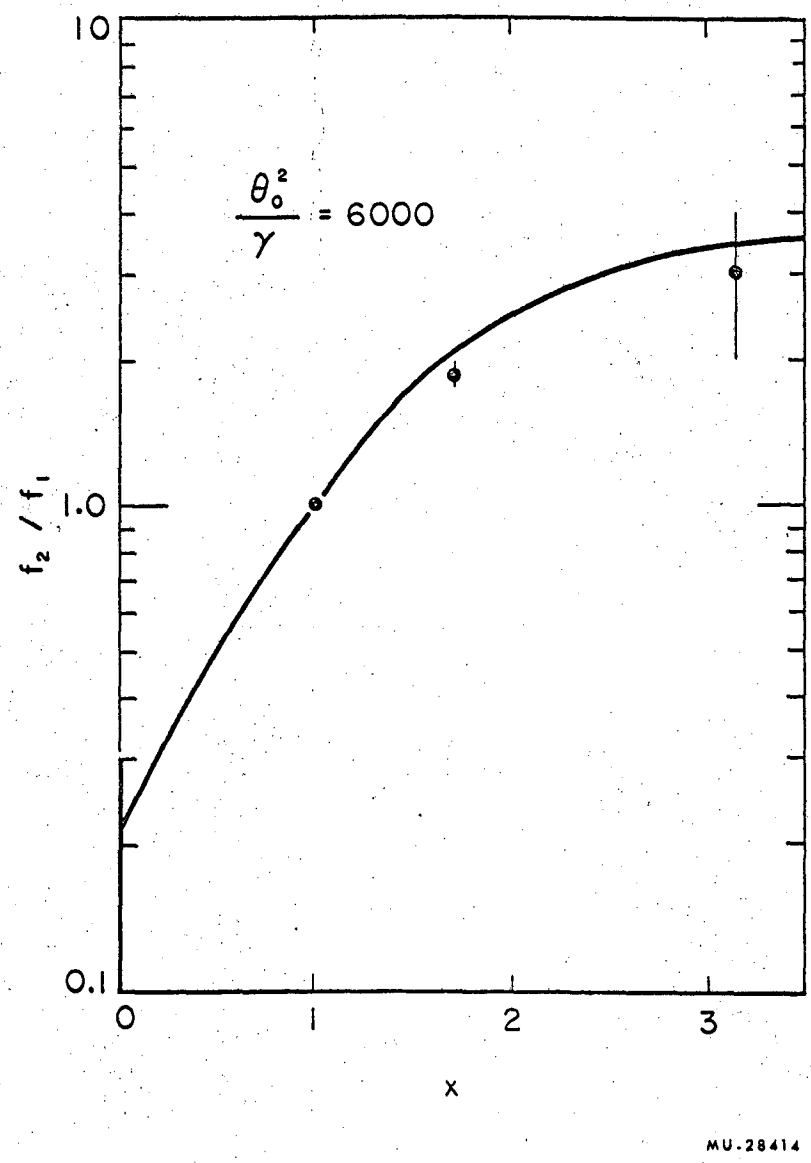


Fig. D. 18-4. Comparison of calculated and experimental pressure dependence of recoil-free fraction ratios. The solid line is the curve calculated for $\theta_0^2/\gamma = 6000$. The variable x is proportional to pressure.

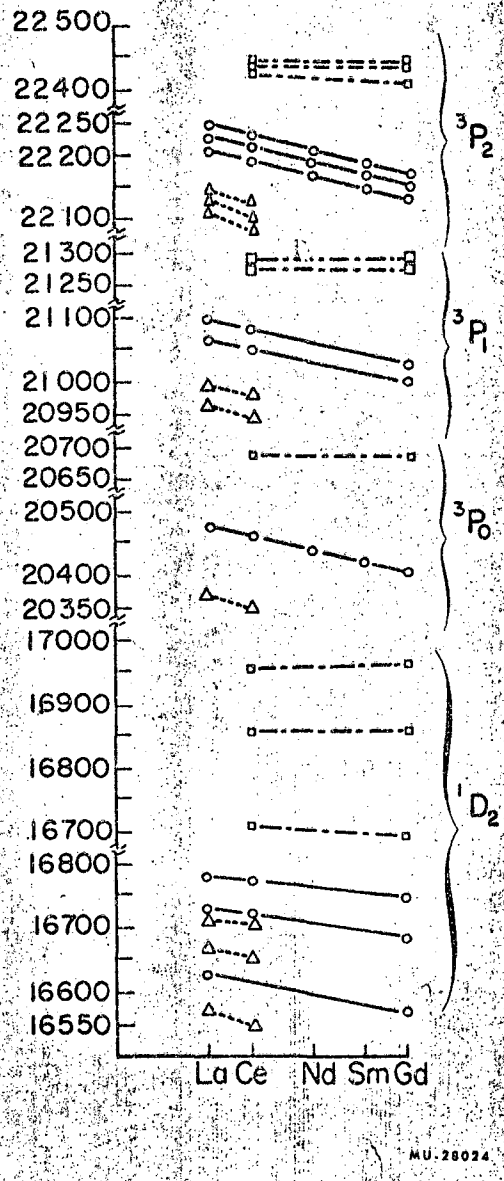


Fig. D. 19-1. Positions of states as a function of ionic radii of rare-earth ions of the host crystals. The squares are points for the ethyl-sulfates, the circles are points for the trichlorides, and the triangles are points for the tribromides.

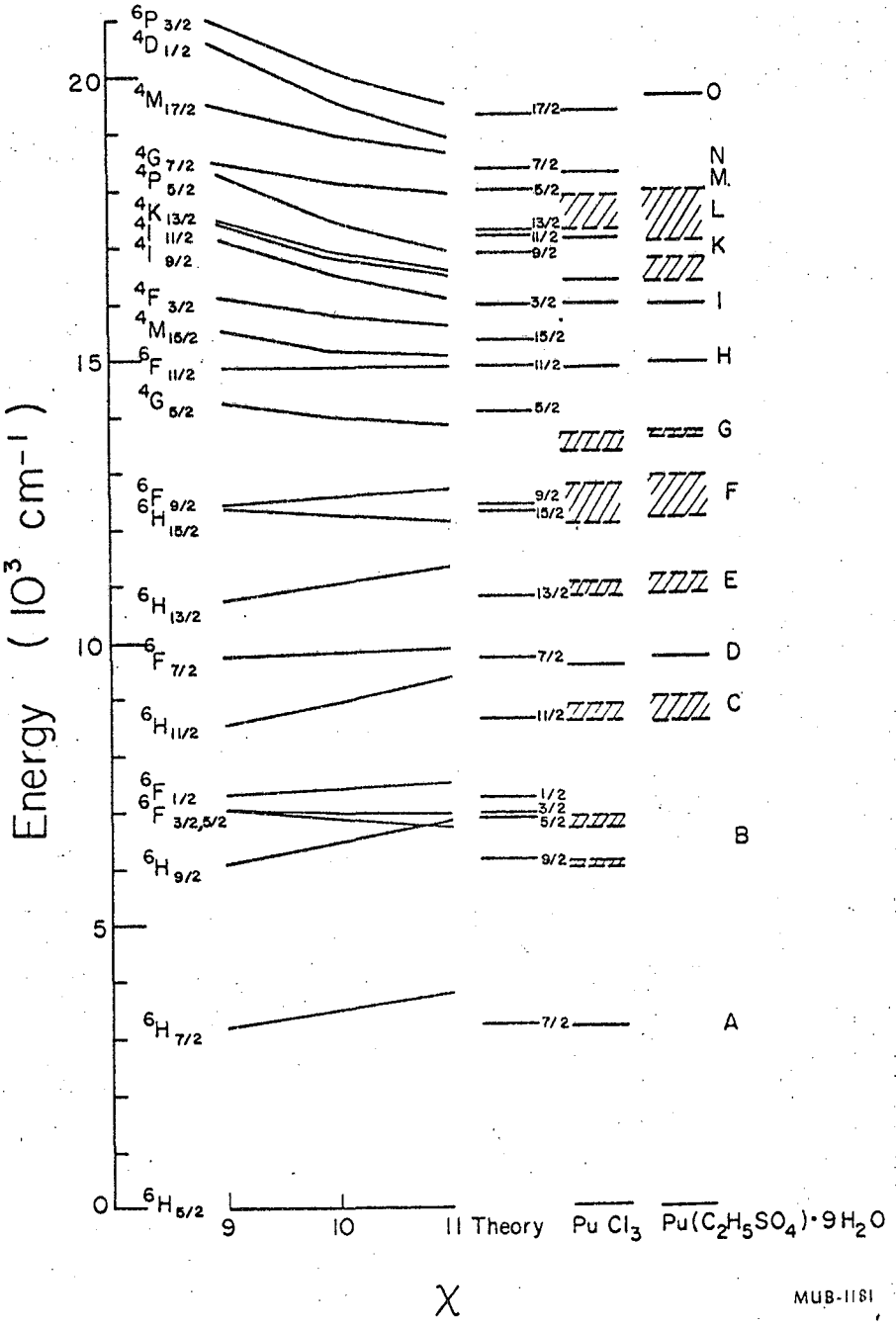


Fig. D. 20-1. Energy-level scheme of trivalent plutonium between 0 and 20 000 $cm^{-1}$. Right side: the levels observed in the crystal of $PuCl_3$ and $Pu(C_2H_5SO_4)_3 \cdot 9\,H_2O$ (A, B, ··· O are arbitrary designations of the levels). To the left: the free-ion levels calculated as functions of $\chi$ for $\chi$ = 9 to 11, with $^6H_{5/2}$ adjusted to 0 $cm^{-1}$ and $^6F_{11/2}$ to 14 860 $cm^{-1}$. The states are labeled in the LSJ coupling scheme. The values for $\chi$ = 9.35 ($\zeta$ = 2290 $cm^{-1}$, $F_2$ = 245 $cm^{-1}$) are considered the best fit.

Abstract from J. Opt. Soc. Am. 52, 1311 (1962).

21.

WB12. Ground Term of the First Spectrum of Curium. EARL F. WORDEN, RALPH G. GUTMACHER, AND E. KENNETH HULET, *Lawrence Radiation Laboratory, University of California, Livermore, California,* AND JOHN G. CONWAY, *Lawrence Radiation Laboratory, University of California, Berkeley, California,* AND MARK FRED, *Argonne National Laboratory, Argonne, Illinois.*—The emission spectrum of curium has been observed in the region 2400–9000 Å. Electrodeless discharge lamps containing 100 μg $CmI_3$ were used as sources. In operation of the lamps at high temperature, a number of arc lines were observed in reversal. Wavenumber differences of these lines were calculated with an IBM 650 computer. Analysis of the differences yielded the ground-term levels. Approximately 200 lines can be assigned to combinations with the ground term. Zeeman patterns were used to confirm $J$ values and calculate Lande $g$ factors. The $g$ factors are in agreement with those found by the atomic-beam method.[1] The data show that the ground term of CmI is $^9D^0$, arising from the electronic configuration $5f^7\,6d^1\,7s^2$. The observed levels of the $^9D^0$ term and $g$ factors are $J=2$ (0.00 $cm^{-1}$) $g=2.56$; $J=3$ (302.15 $cm^{-1}$), 2.00; $J=4$ (815.65 $cm^{-1}$), 1.78; $J=5$ (1764.26 $cm^{-1}$), 1.67; $J=6$ (3809.34 $cm^{-1}$), 1.62. (15 min.)

[1] J. C. Hubbs, R. Marrus, and J. O. Winocur, Phys. Rev. 114, 586 (1959).

## 22. LOW-LYING ENERGY LEVELS OF LANTHANIDE ATOMS AND INTERMEDIATE COUPLING(*)

John G. Conway and B. G. Wybourne

The effects of intermediate coupling on the properties of the low-lying levels of lanthanide atoms have been examined in detail. Particular attention has been given to the effects of a breakdown of Russell-Saunders coupling on the energies and magnetic properties of the levels of the ground multiplets. The energy levels were calculated by diagonalization of the combined electrostatic and spin-orbit matrices of the $f^n$ configurations. It is found possible to fit the energy levels of the ground multiplets of NdI and SmI to within 2 $cm^{-1}$ of their observed energies using 4f-hydrogenic ratios for the Slater $F_k$ integrals. The g values are found to agree within the experimental errors of the atomic-beam measurements. An explanation for the apparent success of the 4f-hydrogenic eigenfunctions is offered, and it is demonstrated that the success of these eigenfunctions does not imply that the actual eigenfunctions are hydrogen-like. The effects of intermediate coupling on the relativistic and diamagnetic corrections to the g values are examined and shown to fall within the range of atomic-beam measurements. The importance of intermediate coupling in the actinides is noted.

---

*Abstract of paper to be submitted to Phys. Rev. (UCRL-10566, Nov. 1962).

## 23. OPTICAL ABSORPTION INTENSITIES OF RARE EARTH IONS(*)

B. R. Judd†

Electric dipole transitions within the 4f shell of a rare-earth ion are permitted if the surroundings of the ion are such that its nucleus is not situated at a center of inversion. An expression is found for the oscillator strength of a transition between two states of the ground configuration $4f^N$, on the assumption that the levels of each excited configuration of the type $4f^N n'd$ or $4f^N n'g$ extend over an energy range small as compared to the energy of the configuration above the ground configuration. On summing over all transitions between the components of the ground level $\psi_J$ and those of an excited level $\psi'_{J'}$, both of $4f^N$, the oscillator strength P corresponding to the transition $\psi_J \rightarrow \psi'_{J'}$ is found to be given by

$$P = \Sigma T_\lambda \nu (\psi_J \| U^{(\lambda)} \| \psi'_{J'})^2,$$

where $U^{(\lambda)}$ is a tensor operator of rank $\lambda$, and the sum runs over the three values 2, 4, and 6 of $\lambda$. Transitions that also involve changes in the vibrational modes of the complex comprising a rare-earth ion and its surroundings, provide a contribution to P of precisely similar form. It is shown that sets of parameters $T_\lambda$ can be chosen to give a good fit with the experimental data on aqueous solutions of $NdCl_3$ and $ErCl_3$. A calculation on the basis of a model, in which the first hydration layer of the rare-earth ion does not possess a center of symmetry, leads to parameters $T_\lambda$ that are smaller than those observed for $Nd^{3+}$ and $Er^{3+}$ by factors of 2 and 8 respectively. Reasons for the discrepancies are discussed.

---

*Abstract of published paper, Phys. Rev. 27, 750 (1962).

†Present address: Laboratoires de Bellevue, Bellevue (Seine et Oise), France.

## 24. ENERGY MATRICES OF THE $f^5$ ELECTRON CONFIGURATION(*)

B. G. Wybourne†

In a recent paper the calculation of the complete spin-orbit matrices for the $f^5$ electron configuration was reported. In an earlier paper the complete electrostatic matrices were presented. Using the results of these calculations it has been possible to construct the energy matrices of the $f^5$ configuration. These energy matrices have been applied to the analysis of the crystal spectra of trivalent samarium, dysprosium, and plutonium ions. To permit a wider usage of these energy matrices they have been tabulated by a direct print-out of the matrix elements which were checked and stored on punched cards.

---

*Abstract of UCRL-10448, Sept. 1962.

†Now at: Division of Chemistry, Argonne National Laboratory, Lemont, Illinois.

## 25. ELECTROSTATIC INTERACTIONS IN COMPLEX ELECTRON CONFIGURATIONS(*)

B. G. Wybourne†

Simplified expressions for the matrix elements of electrostatic interactions both within and between several types of complex electron configurations have been obtained by the application of angular-momenta recoupling techniques. The use of these recoupling techniques avoids the usual extensive calculation of the sums of products of the matrix elements of tensors of the types $V^{\kappa k}$ and $U^{k}$. The derived expressions involve the sums of products of coefficients of fractional parentage and n-j symbols, and as such are amenable to machine computation.

---

*Abstract of paper to be published in J. Math. Phys., March 1963 (UCRL-10443, Aug. 1962).

†Now at: Division of Chemistry, Argonne National Laboratory, Lemont, Illinois.

## 26. PARAMAGNETIC RESONANCE OF THE TRIPOSITIVE CURIUM ION IN ETHYLSULFATE AND TRICHLORIDE CRYSTALS(*)

Marvin Abraham,† B. R. Judd,‡ and H. H. Wickman

The paramagnetic resonance of the ion $Cm^{3+}$ has been studied by incorporating various amounts of curium in crystals of lanthanum ethylsulfate and anhydrous lanthanum trichloride. For the ethylsulfate crystals, a single line was observed at helium temperatures, characterized by $g_{\parallel} = 1.925 \pm 0.002$ and $g_{\perp} = 7.73 \pm 0.02$. A similar line, for which $g_{\parallel} = 1.925 \pm 0.002$ and $g_{\perp} = 7.67 \pm 0.02$, occurs for the trichloride crystals. These lines are interpreted as corresponding to transitions within the lowest doublet of the ground level $5f^7\ {}^8S_{7/2}$, which, owing to the high degree of intermediate coupling, does not possess the extremely small splitting typical of S states. The Landé g value of the ground level is found to be 1.925. Previous experimental results on the paramagnetic resonance of $Cm^{3+}$, which were difficult to account for theoretically, are shown to be spurious; evidently the reported spectra should have been ascribed to $Gd^{3+}$.

---

*Abstract of paper submitted to Phys. Rev. (UCRL-10567, Nov. 1962).

†Temporary address: Institute of Physics, San Carlos de Bariloche, Rio Negro, Argentina.

‡Present address: Laboratoires de Bellevue, Bellevue (Seine et Oise), France.

## E. INSTRUMENTATION

### 1. PERFORMANCE OF THE IRON-FREE BETA SPECTROMETER

Jack M. Hollander and Robert L. Graham

The new iron-free 50-cm double-focusing beta spectrometer was brought into initial operation in the sping of 1962.[1] Much of the past year has been devoted to solving the many technical problems that usually attend the initial operating period of an entirely new instrument. As a result of these efforts, the instrument was operating at the close of the year on a fairly routine basis.

During the initial operation of the cooling system, a serious overheat occurred which was caused by the failure of a safety interlock. Decomposition of the Freon-11 coolant and chemical attack of ferrous materials in parts of the cooling system resulted, which necessitated that the whole system be disassembled for thorough cleaning. All ferrous materials were subsequently replaced by copper or aluminum or chemically protected by "Bisonite" coating. The cooling system was restored to operation in September 1962.

During October, a detailed study of the focusing properties of the instrument was undertaken. This is of fundamental importance because the practical utility of the instrument as a precision research tool will ultimately be determined by the available transmission and resolution.

It had originally been hoped that the spectrometer would achieve resolutions as sharp as $\leq 0.02\%$ (in momentum) and also that it could be "opened up" for transmissions in excess of 1% (at appropriately reduced resolution).[1] Indeed, in the initial "post-factory" tests in Uppsala, Sweden, a resolution of 0.018% was achieved with the ThB I line. In the early stages of operation in Berkeley, it was realized that the transmission of the instrument was less than expected, however, at given resolution settings. It therefore appeared desirable to carry out a set of detailed experimental tests of the focusing properties, with the aim of gaining a fuller knowledge of the present capabilities of the coil system and of gaining the information needed to design a system of baffles that would give the maximum transmission for particular resolution settings.

The essential details of the test arrangement are shown in Fig. E. 1-1. A small aperture in the test baffle permitted only a "pencil beam" of electrons to pass. The position of the aperture could be varied vertically by ± 20 cm and radially by ± 8 cm.

At each of 90 different aperture "positions" $(h^*, t^*)$, the K661.6 conversion electron line of Cs-137 was scanned to establish its intensity, shape and "position" (mean current setting). The results for $h^* = 0$, shown in Fig. E. 1-2, reveal that there is an up-down asymmetry, i. e., the radial

1. K. Siegbahn, C. L. Nordling, and J. M. Hollander, in Chemistry Division Annual Report, 1961, UCRL-10023, Jan. 1962.

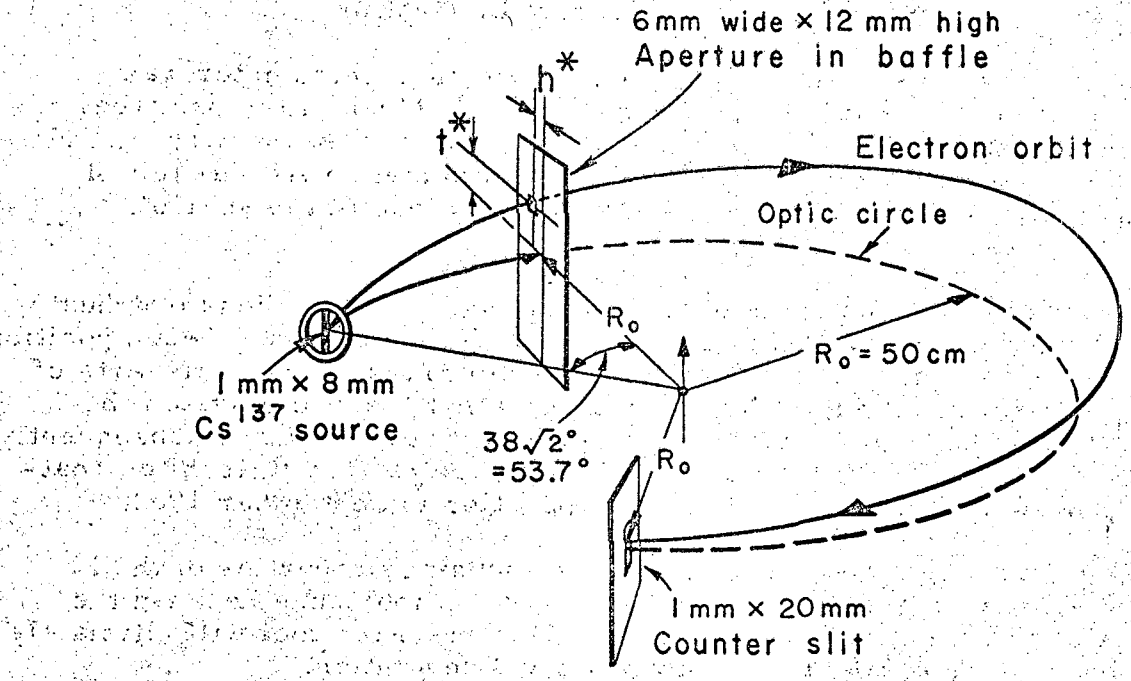


Fig. E. 1-1. Schematic diagram of the "exploration" baffle used to study the focusing properties.

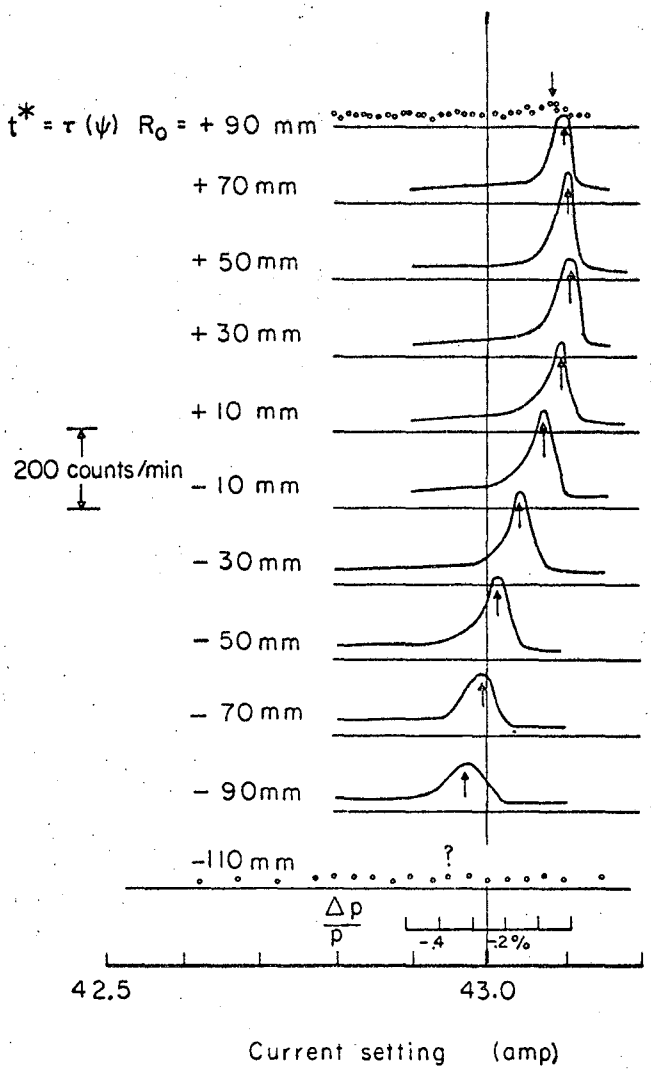


Fig. E. 1-2. Variation of the K661.6 peak position as a function of the height, $t^*$, of the exploration baffle aperture. All curves are for a radial position of $h^* = 0$. The disappearance of counting rate at $t^* = +9$ and -11 cm is due to vertical displacement of the focused image (axial aberrations).

position of the image is not independent of the axial departure angle from the source, as one would expect for a "high aperture" double-focusing spectrometer.

By graphical interpolation of the peak positions one can deduce contour lines in the baffle plane representing the family of electron orbits which all come to focus at the same current setting $I_0(1+\Delta)$, i.e., at the same radial position in the counter plane, $r_0[1+\eta(\pi)]$, where $\eta(\pi)$ is called the radial aberration. Figure E. 1-3 shows a map of these "isoaberration" lines in the baffle plane. The contours labeled 0 correspond to K661.6 conversion electron orbits that come to focus at 43.11 amperes (see Fig. E. 1-2) and, for example, the contours labeled -0.2% correspond to orbits that come to focus at a current setting of 0.2% lower than 43.11 amperes.

The information in Fig. E. 1-3 has been used directly to design a set of baffles for different resolutions, two of which are shown in Fig. E. 1-4. We have retained the original mouting plate with its fiducial markings and have made a set of interchangeable plates with apertures shaped to match the contour lines in Fig. E. 1-3.

The substantial improvement in the performance of the spectrometer so obtained is illustrated in Fig. E. 1-5. All three curves were obtained by using the same calibrated 1×6 mm source of $Cs^{137}$ (strength - 200 μCi) as was used in the tests. Curve A shows the results obtained with what were the "best" settings for a rectangular baffle and 0.5×10-mm counter slit, taken prior to the focusing study. Curve B shows the results with the same "best" rectangular baffle aperture after the counter slit aperture had been enlarged to 1×20 mm. Curve C shows the improvement on going to the 0.05% shaped baffle aperture. The line width of 0.07% is due in part to source thickness. With thinner sources under identical conditions the line width is ≤ 0.065% in momentum.

From the areas between the contour lines in Fig. E. 1-3 and the known geometry (Fig. E. 1-1) we can compute the transmission as a function of resolution for the ideal case of a perfect "point" source. This relationship is displayed graphically in Fig. E. 1-6, where it is compared with some other precision spectrometers.[2,3,4] The rapid drop in transmission for the Berkeley spectrometer at better resolutions is a consequence of the distorted contour lines shown in Fig. E. 1-3. Some improvement might be expected if the inaccuracies or distortions in the present coil system were corrected. However, as yet we have no detailed theoretical basis to use as a guide in such a modification.

A more profitable line of attack would seem to be a completely new theoretical approach aimed toward a great increase in the transmission of a high-resolution double-focusing iron-free system.

At the close of 1962, detailed experimental studies were being carried on of the conversion-electron spectra associated with the decays of $Ce^{143}$, $Np^{238}$, and $Ba^{131}$.

2. R. L. Graham, G. T. Ewan, and J. S. Geiger, Nucl. Instr. Meth. 9, 245 (1960).

3. J. A. Jungerman, M. E. Gardner, C. G. Patten, and N. F. Peek, Nucl. Instr. Methods 15, 1 (1962).

4. A. A. Bartlett, R. A. Ristenin, and R. P. Bird, Nucl. Instr. Methods 17, 188 (1962).

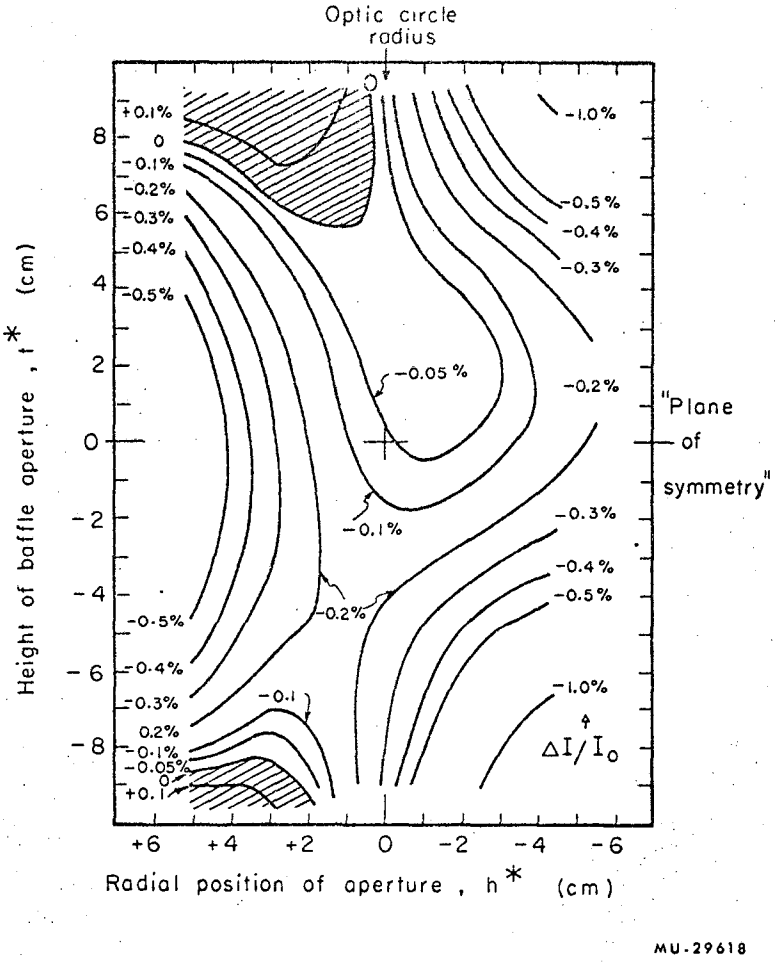


Fig. E. 1-3. Radial "isoaberration" contours in the baffle plane. Electron orbits intersecting any point on a given line all come to focus at the same current setting.

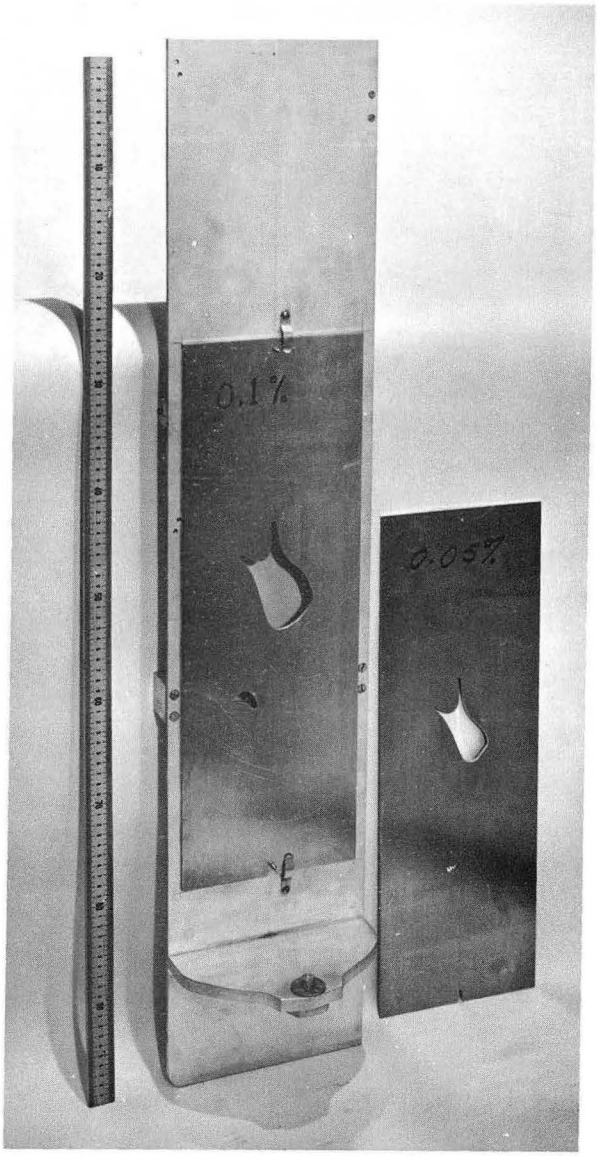


ZN-3591

Fig. E.1-4. Photograph of two of the contoured baffle plates prepared with the aid of Fig. E.1-3.

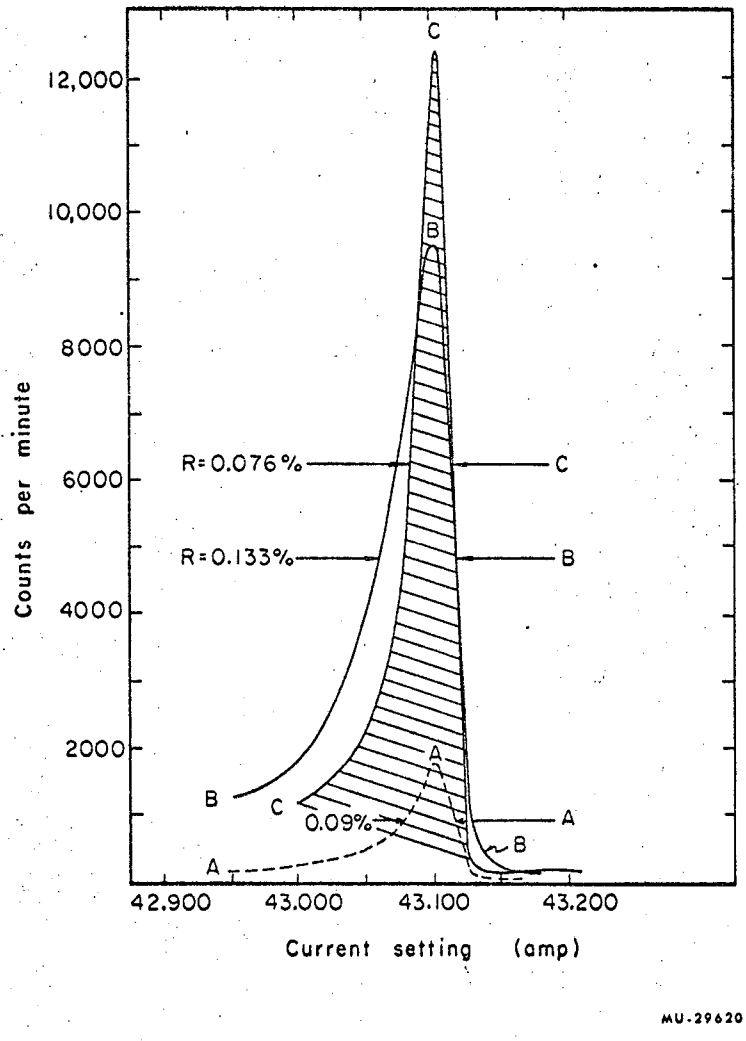


Fig. E. 1-5. The K661.6 inversion line from a 200-μCi source (1×8 mm) as observed with three different settings. This illustrates how the resolution obtained with the 0.05% contoured baffle, Curve C, is improved over the best resolution obtainable with the rectangular baffle system originally supplied, Curves B ("best" rectangular baffle, slit 1×20 mm) and A ("best" rectangular baffle, counter slit 0.5×10 mm).

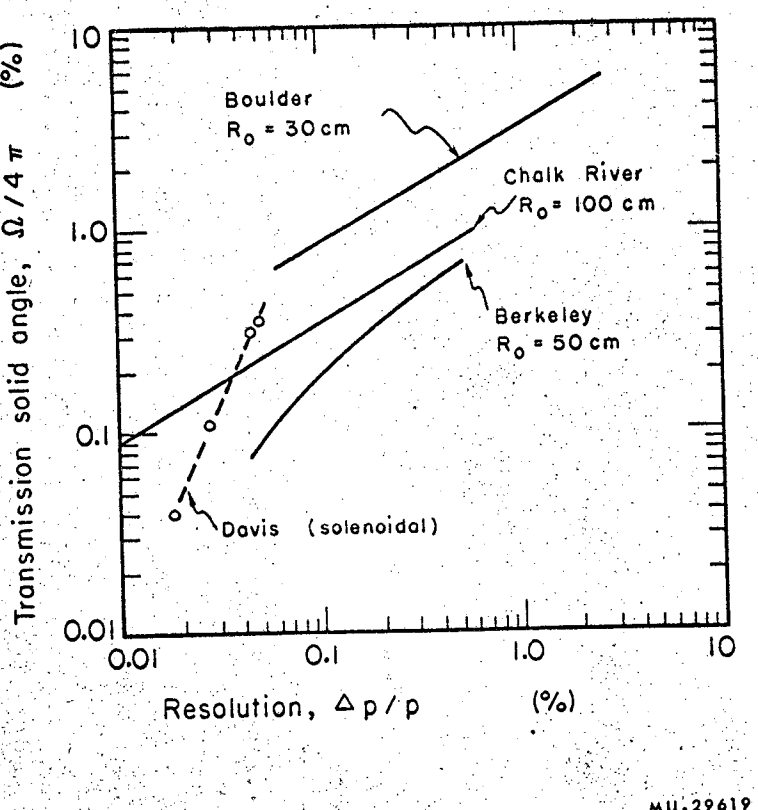


Fig. E. 1-6. Theoretical transmissions for several β spectrometers as a function of momentum resolution.

## 2. LITHIUM-DRIFTED SURFACE-BARRIER DETECTORS

Robert M. Latimer and Walter E. Stockton

Semiconductor detectors that combine the advantages of both the surface barrier and lithium-drift processes have been developed. When lithium-drift silicon is used instead of the normal N-type silicon in producing large-area surface-barrier counters, the resolution improves markedly. This improvement results not only from the reduced capacity associated with the deep depletion layer but also from the improved quality of silicon obtainable through the lithium-drift process.

At room temperature, a lithium-drifted surface-barrier detector with an active area of 3.5 $cm^2$ resolved $Am^{241}$ $\alpha$ particles to 30 keV (FWHM) and had a 20-keV window ($\approx 0.1$ $\mu$). The depletion depth was about 1 mm, which permitted it to count Hilac-produced 10.4-MeV protons and 41.6-MeV $\alpha$ particles. The resolution on protons and $\alpha$ particles was limited by the beam energy spread to 1%. Small (0.5 $cm^2$) lithium-drifted surface-barrier detectors have resolved $Am^{241}$ $\alpha$ particles to 19 keV with windows as thin as 8 keV.

## 3. A MULTICHANNEL SAMPLE COUNTER

Alfred A. Wydler

Oftentimes in Nuclear Chemistry many similar samples of a material are prepared for both qualitative and quantitative analysis. This analysis and recording is generally time-consuming, as these samples are typically handled in succession. An example is the collecting and counting of the elutant from an ion-exchange resin column. A machine has been built to reduce the overall time required for these operations. It is named "Elution Monitoring System," which may be shortened to "EMS."

In its present form this system accepts sample plates, either 5/8 in. or 1 in. in diameter, in amounts of twenty or less. For 1% coincidence loss, these samples should have fewer than 200 dis/min of alpha and spontaneous fission in any total combination. An eight-channel pulse-height analyzer is incorporated for rough analysis of alpha energy (about 1 MeV/channel) and determination of spontaneous fission events. Also an electronic timer with a capacity of 800 minutes is included. Neon lamps and mechanical registers provide instantaneous data readout.

To facilitate data processing and to provide for permanent storage, all data are contained in a paper tape record, produced by a "Tally" perforator.

This counting system is completely transistorized and self-contained in a 48-in. standard electronic cabinet.

Each sample position is a plug-in module, consisting of reversible sample carrier, silicon particle detector, switches for control and identification, preamplifier, and other necessary electronics.

The resolution of these detectors is within less than 80 keV for 6-MeV α particles at a geometry of 40%.

A He atmosphere surrounds the detector and sample, instead of the more conventional vacuum. This is considered an inexpensive replacement for the messy vacuum pumps normally required. Each counting chamber consumes about 10 $cm^3$ of helium per minute, 3 to 5 times the minimum necessary to restrict the back-diffusion of air.

Each sample has an arbitrarily assigned number. By means of decaded switches, this number is included with the time and pulse-height data and punched into paper tape for later processing or storage. Data are recorded at the rate of twenty words per second, hence this is ultimately the limiting counting rate.

A device to read back the punched tape is currently being constructed. This reader will reduce the data from any selected sample into their constituent parts, such as energy, activity at each of eight energy levels, and time of event. It will also give half-life information. Because this reader is not yet available, data are presently being taken from the scalers and mechanical registers of each module.

## 4. DEVELOPMENT OF A MULTIPARAMETER PULSE-HEIGHT RECORDING SYSTEM

Michiyuki Nakamura and George S. Simonof

During the past year a flexible multiparameter pulse-height recording system was successfully checked and utilized. The system has been used principally for experiments on nuclear fission.

The general operation of the system is as follows: $\underline{N}$ coincident parameters (where $\underline{N}$ is any number from 2 to 16) arrive at the system in the form of pulses from the experimenter's electronics. These $\underline{N}$ pulses are temporarily stored in $\underline{N}$ pulse stretchers, and then serially read into an analog-to-digital conversion unit (pulse-height–to–time converter). The resultant digitized pulse heights are stored in specific locations of a buffer magnetic-core storage system. The buffer storage is capable of storing 512 pulse heights, e.g., 256 two-parameter events. When the buffer storage is filled, the binary information is dumped onto magnetic tape in IBM-compatible format. This basic cycle is repeated until the experimenter has gathered sufficient information.

The fundamental system speed is limited primarily by the time taken to empty the information from core storage onto magnetic tape (80 msec). With this speed and the abundant storage on magnetic tape (over one million two-parameter events, for example) the experimenter is given much freedom to vary parameters. Consequently, a given tape may contain many experiments.

A subsystem permitting the experimenter to read back the information for a single parameter of any given experiment into a multichannel pulse-height analyzer was also successfully developed and checked this past year.

The experimenter is thus able to evaluate his information within minutes after he has written an experiment on tape.

The worthwhile experimental information on magnetic tape can then at any time be sorted, analyzed, and reduced via an IBM 7090 or 709 computer. A report is presently being written which describes the system in detail.

## 5. USE OF A VARIABLE-GAIN AMPLIFIER FOR SYSTEM GAIN STABILIZATION

Michiyuki Nakamura and James E. Ream

In a long-range α experiment, $Cf^{252}$ was used as a source.[1] In order to obtain a reasonably high triple-coincidence rate, close spacings between a strong source of $Cf^{252}$ ($\approx 10^7$ fissions/min) and large-area semiconductor detectors were used. After a week's run damage to the detectors was noted. The signal pulse amplitudes had decreased to 20% of their initial value. The total number of fission fragments causing this much damage depends on the characteristics of the detector, but most detectors are unusable after $10^9$ total fission fragments.

We sought a means for gain stabilization for semiconductor detector systems. The technique of altering the high voltage to photomultipliers or proportional counters is often used for system gain stabilization. The semiconductor counters used for fission-fragment and α-particle detection must be operated at a bias voltage where the charge-collection efficiency is constant, but not in a region where the leakage current increases abruptly.[2] We felt the answer to semiconductor-detector system stabilization lay in an electrically controlled variable-gain amplifier.

We developed a transistorized amplifier whose gain can be changed by an electrical signal. The gain of the amplifier is varied by altering the current in a lamp bulb (G. E. No. 344) placed in the amplifier circuit. The lamp bulb resistance changes as a result of the temperature change caused by the current. The G. E. No. 344 lamp bulb was used because its hot and cold resistance values (2000 and 300 ohms, respectively) were compatible with impedances of transistorized circuits.

Our stabilized system consisted of a stable discriminator, a count-rate circuit, and this variable-gain amplifier in addition to the usual system components. The variable-gain amplifier was placed between the pre-amplifier and the main linear amplifier. The discriminator was placed after the linear amplifier and set on the peak of the heavier fission fragment. The discriminator output fed into the count-rate circuit, which in turn controlled

---

1. Zeev Fraenkel, Long-Range α Particles Emitted in the Spontaneous Fission of $Cf^{252}$ (in preparation).

2. W. M. Gibson and G. L. Miller, Charge Collection in Semiconductor Radiation Detectors, in Proceedings of the Conference on Nuclear Electronics, Belgrade, Yugoslavia, 15-20 May 1961 (International Atomic Energy Agency, Vienna, 1962), Vol. I.

the gain of the variable-gain amplifier. By this method of stabilization we were able to keep the fission peaks to approximately one or two channels of the original peaks although the system gain had degraded to 70% of its original magnitude.

Under development are two methods of gain stabilization using the variable-gain amplifier. One is the use of a single-channel analyzer whose base line is modulated over a peak to determine gain changes. The other is a digital stabilization approach whereby the pulse train from a pulse-height analyzer is digitized, and a digital single-channel analyzer is used to determine gain shifts.[3] The last two methods should be superior to our simple discriminator approach because these methods can be used in experiments with varying count rates.

---

3. J. A. Ladd and J. M. Kennedy, A Digital Spectrum Stabilizer for Pulse Analyzing Systems, AECL-1417, Dec. 1961, Chalk River, Ontario, Canada.

## 6. MASS SPECTROMETER DATA ACCUMULATOR

Michiyuki Nakamura, Frederick E. Vogelsberg, and Maynard C. Michel

Ion counting for data readout in solid-sample mass spectrometers has been in use here and elsewhere[1] for several years, and has contributed significantly to the recent increase in sensitivity and precision of isotope abundance measurements.

After using a manually summed counting system for several years, we have developed a semiautomatic system which is now in constant use, with quite satisfactory results, on a 12-inch-radius (60-degree sector) isotope-abundance mass spectrometer. This is planned as one step in the development of a very fast, completely automatic scan system similar to that described by Barton.[2]

The present system consists of a simple step-voltage scan of the spectrum at the rate of approximately 1 mass number per second, magnetic core storage of accumulated data, summation of successive scans, and readout (by printed tape) of the total events for each mass number. Data are stored in the core array of a RIDL 34-12 pulse-height analyzer operated in a modified "time mode." Each mass number is represented by an address in the memory. Circuit logic steps the ion-accelerating potential so that it presents successive mass numbers to the entrance slit of the detector, and provides for readout

---

1. F. A. White and T. L. Collins, Appl. Spectry. 8, 17 (1954).

2. George W. Barton, Jr., Leonard E. Gibson, and Laurin F. Tolman, An Ion Counting and Accumulation System for Mass Spectroscopy, UCRL-5464, Aug. 1959.

of previously stored data at the corresponding address. These stored data are transferred by parallel entry from the analyzer add-subtract scaler to a fast 10-Mc scaler. Then, during a precise fixed gate time, new counts are added to the existing count and the new total is written back into the memory. The fast and slow scalers are reset as the accumulator addresses the next mass number, where the operation is repeated. This sequence is controlled by a digital clock, which cycles until the operator determines that sufficient data have been stored to give the desired accuracy.

Source-sample considerations require the system to handle count rates as high as $10^5$ per sec for the most abundant masses. To keep counting errors due to coincidence or dead time less than 0.5%, the input amplifier and scaler recovery must be not greater than $10^{-7}$ sec. For this reason the count is handled by a 10-Mc scaler and then transferred to the slower add-subtract scaler of the analyzer. Modification of the analyzer for this parallel access does not preclude its operation in the normal "pulse height" mode.

It will in the future be desirable to extend this system to store perhaps 20 addresses per mass number with a maximum capacity of $10^8$ counts per channel. Rapid step scan of 200 to 400 channels at a rate of about 200 channels per second, continuous scope presentation, and variable scan programs will render the system even more flexible. The improvement in operation of the mass spectrometer, compared with either a stepped single-channel counting system or the older current-integration system is appreciable. Isotopic abundance ratios with a standard deviation of approx 0.5% are now easily attained, and the time required for data collection is much less than formerly. Previously, manual computations could exceed half the total run time when high precision was required. In contrast, the present system often allows the computations to be completed during the run, and evaluated concurrently.

# F. CHEMICAL ENGINEERING

## 1. A METHOD FOR ESTIMATING THE HEAT OF FORMATION AND FREE ENERGY OF FORMATION OF SIMPLE INORGANIC COMPOUNDS(*)

Darrell E. Wilcox and LeRoy A. Bromley

A general method of independently estimating the standard heat of formation $\Delta H_f^\circ$ and free energy of formation $\Delta F_f^\circ$ of inorganic compounds at 25°C has been developed. The result is a simple equation involving three parameters characteristic of each ion. Each valence state of an element or group may be assigned a value for each of the parameters. These parameters may be evaluated for any ion if at least three experimental heats of formation or free energies of formation are known.

The equation has been applied to the correlation of known $\Delta H_f^\circ$ data for 34 monovalent and divalent cations and 32 anions, including the metallic halides, oxides, sulfides, and compounds such as the sulfates, carbonates, and tungstates. The average deviation obtained for 427 compounds was 1.98 kcal/M, and the maximum deviation was 8.73 kcal/M. Similar results were obtained in a correlation of $\Delta H_f^\circ$ for a set of trivalent and tetravalent cations, and in the correlation of $\Delta F_f^\circ$ of many of the same compounds.

An error of less than 15 kcal/M may generally be expected in estimating an unknown if one uses parameters evaluated from three or more experimental data.

---

*Abstract of paper based on Wilcox's M. S. Thesis (UCRL-10397, Aug. 1962).

## 2. DOWNFLOW FORCED-CONVECTION BOILING OF n-BUTANOL IN AN ELECTRICALLY HEATED TUBE(*)

Graham Sommerville and LeRoy A. Bromley

Local heat-transfer coefficients and two-phase total pressure drops have been measured for the downflow forced-convection boiling of n-butanol in electrically heated tubes having an inside diameter of 0.4670 in. and heated lengths of 5.69 and 4.10 ft respectively. Heat fluxes ranged from $2.8 \times 10^4$ to $6.6 \times 10^4$ Btu/h ft$^2$, and mass fluxes from 136 to 440 lb mass/sec ft$^2$. Exit qualities up to 31% were measured at pressures between 16.9 and 50.0 psia.

---

*Brief summary from Graham F. Sommerville, Downflow Boiling of n-Butanol in a Uniformly Heated Tube (M. S. Thesis), UCRL-10527, Oct. 1962.

The boiling heat-transfer data have been compared with previous correlations that had been based on the water-steam system. New boiling-heat-transfer correlations have been derived and found to be successful in correlating data for both water and n-butanol to within ±30%. The best correlation is

$$St = 0.90\ Re_l^{-0.268}\ X_{tt}^{-0.292}\ Bo^{0.191}\ Pr_l^{-0.233},$$

where

$St$ = Stanton number = $h_b/CpG$,

$Re_l$ = Reynolds number for the liquid = $DG_l/\mu_l$,

$X_{tt}$ = Lockhart-Martinelli parameter[1] =

$$\left[\frac{\rho_g}{\rho_l}\right]^{0.5}\left[\frac{\mu_l}{\mu_g}\right]^{0.1}\left[\frac{1-x}{x}\right]^{0.9},$$

$Bo$ = Boiling number = $q/G\lambda$

$Pr_l$ = Prandtl number for the liquid = $(\mu Cp/k)_l$

The individual symbols have the following meaning:

$h_b$ = boiling-heat-transfer coefficient, in Btu/h ft$^2$ °F
$Cp$ = heat capacity of liquid, in Btu/lb mass °F
$G$ = total mass velocity of flow, in lb mass/h ft$^2$
$G_l$ = mass velocity of liquid only
$D$ = diameter of tube
$\mu_l$ = viscosity of liquid
$\mu_g$ = viscosity of vapor
$\rho_g$ = density of vapor
$\rho_l$ = density of liquid
$x$ = vapor quality = mass fraction of vapor
$q$ = heat flux, in Btu/h ft$^2$
$\lambda$ = latent heat of vaporization, in Btu/lb mass
$k$ = conductivity of liquid, in Btu/h ft °F

Local two-phase total-pressure gradients have been successfully correlated by the method of Schrock and Grossman. Local two-phase frictional-pressure gradients have been obtained and compared with previous results for the water-steam system.

Complete details of this study are contained in Sommerville's thesis.

1. R. W. Lockhart and R. C. Martinelli, Chem. Eng. Progr. 45, 39 (1949).

## 3. CONCENTRATION AND VELOCITY PROFILES IN A STEFAN DIFFUSION TUBE(*)

Fred J. Heinzelmann, Darshanlal T. Wasan, and Charles R. Wilke

The Stefan diffusion tube has been widely used as a means of determining vapor-phase diffusion coefficients.[1, 2, 3] By this method the diffusion coefficients have been calculated from the measured mass flux, assuming flat concentration and velocity profiles in the diffusion tube. These assumptions have not previously been verified. The study presented here involves a theoretical analysis of the flow system and an experiment designed to determine whether or not the flat-profile assumptions are valid.

In the theoretical analysis the axial component of the steady-state momentum equation for a fluid with constant properties, with zero axial pressure gradient, and with zero azimuthal velocities is coupled with the corresponding steady-state diffusion equation. Theoretical velocity and concentration profiles are obtained by assuming perturbations in flat profiles and by satisfying the boundary values of the diffusion system: namely, that the concentration of the diffusing species A at the liquid-gas interphase is constant, the concentration of A at the top of the tube is zero, and the concentration profile is axially symmetric. There is no transfer from the walls of the tube into the gas, there is no slip in velocity at the wall, the velocity profile is axially symmetric, and at the evaporating surface the diffusion velocity is given by the mass flux of the nondiffusing species. For the benzene-air system described below, calculated values of the ratio of the axial velocity $u$ to the uniform velocity $u_0$ versus the percent cross-sectional area for a 13-cm-long diffusion tube are shown in Fig. F. 3-1. The theoretical study shows that the velocity profile starts out flat at the evaporating surface and develops into what is essentially a parabolic profile. By use of the calculated parabolic velocity profile the concentration profile was obtained. The values of the profile of the ratio of the concentration perturbation $C_1$ to the surface concentration $C_s$ calculated at several values of the radial and axial distances are shown in Table I.

Table I. Profile of concentration perturbation, $C_1$, given as $C_1/C_s$, where x = axial distance (in cm), r = radial distance (in cm), and $r_0$ = radius of the tube (in cm).

| | $r/r_0$ | | | |
|---|---|---|---|---|
| x | 0 | 0.24 | 0.71 | 0.87 |
| 6 | $-2.7\times10^{-5}$ | $-2.2\times10^{-5}$ | $0.4\times10^{-5}$ | $1.0\times10^{-5}$ |
| 13 | 0 | 0 | 0 | 0 |

*Summary of paper based on Heinzelman's M. S. thesis, UCRL-10421, Aug. 1962.

1. J. Stefan, Sitzber. Akad. Wiss. Wien, Math.-naturw. Kl 63, Abt II (1871).

2. Ibid. 65, Abt II, 323 (1872).

3. C. Y. Lee and C. R. Wilke, Ind. Eng. Chem. 46, 2381 (1954).

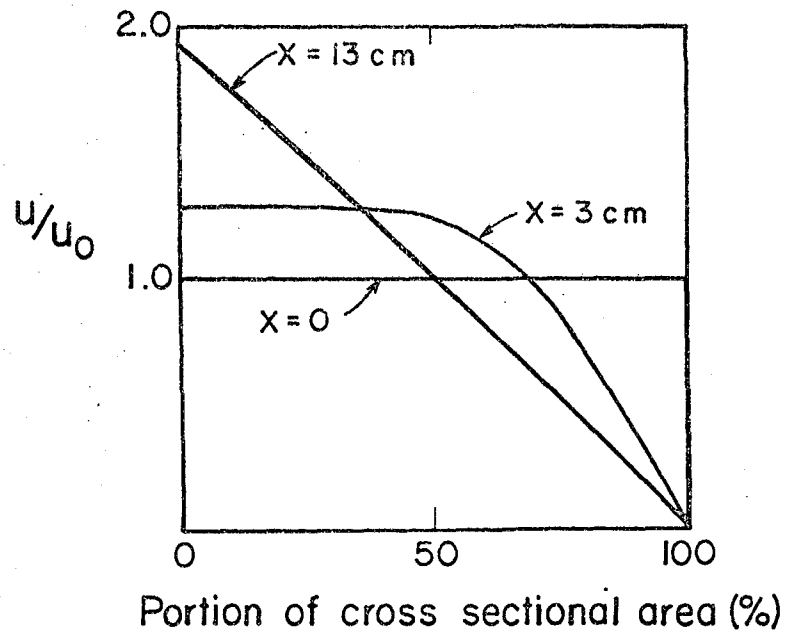


Fig. F.3-1. Velocity profiles in a Stefan diffusion tube.

The system used for the experiment was benzene diffusing through stagnant air at 35°C and 748 mm Hg pressure. The apparatus was substantially the same as that used by Getzinger for measuring diffusion coefficients.[4] However, semicircular probes made of tungsten wire were used for measuring the radial and axial concentration gradients. Measurements of change in resistance of the probes by means of a Wheatstone bridge permitted calculation of the concentration profiles. The experimental data corrected for end effects[3] are shown in Fig. F. 3-2. The solid curve is the calculated concentration gradient based on the assumption of flat concentration profile throughout the tube.

The theoretical study and the experimental results both indicate that the concentration profile is sufficiently flat across the diffusion tube to justify the plug flow assumption.

---

4. Richard W. Getzinger, Steady-State Diffusion in Ternary Gas Mixtures (M. S. Thesis), UCRL-9987, Jan. 1962.

## 4. KINETICS OF CONSECUTIVE-REACTION SYSTEMS

H. R. Siewert, P. N. Tenney, and T. Vermeulen

Both the interpretation of experimental results and the prediction of conversion in new situation, in multiple-reaction systems, are quite difficult because of the mathematical complexity of such systems. In many instances, the differential rate equations cannot be integrated analytically. Even when an analytic result is available, it may prove to be implicit rather than explicit in the desired unknown, and its numerical evaluation may be quite involved.

The investigation summarized here and reported fully in Siewert's thesis,[1] was undertaken to examine ways of handling the data in a particular group of multiple reactions, and to assemble the numerical solutions for these systems so as to facilitate further development of data-handling techniques. The reaction models selected were consecutive-competitive (second-order); and consecutive-reversible (with each step either first- or second-order). Among the latter, solutions were developed for all the two-reaction sequences in which either the first reaction or the second (but not both) is reversible.

These solutions for consecutive-reversible cases are of two types, one applicable to batch and tubular-flow reactors under constant-density isothermal conditions, and the other applicable to stirred-tank-flow reactors involving perfect mixing. A dimensionless time $\tau$, obtained as the product of the first reaction coefficient $k_1$ and true elapsed time, is used as the

---

1. Howard R. Siewert, Kinetic Analysis of Consecutive-Reaction Model Systems (M. S. Thesis), UCRL-10575, November 1962.

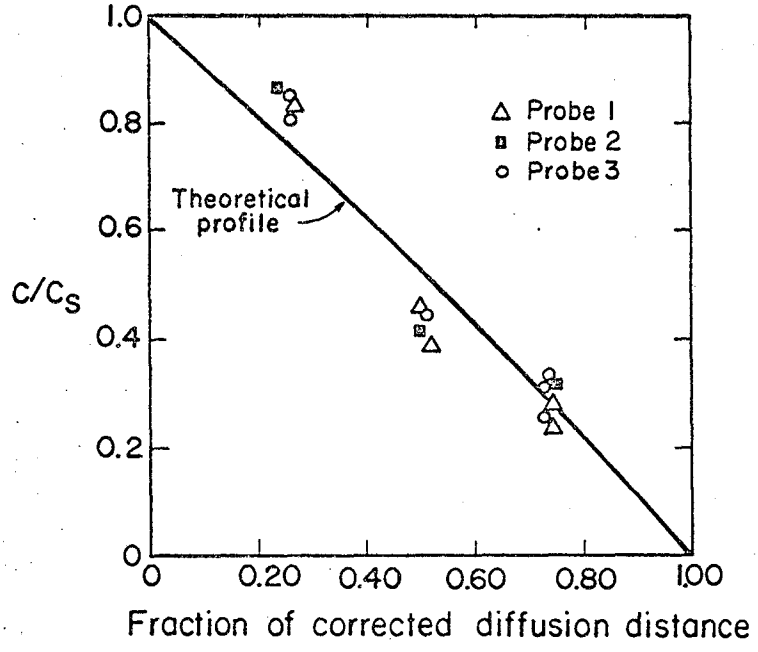


Fig. F. 3-2. Experimental concentration profile corrected for end effects.

independent variable; the concentration ratios--moles of first reactant remaining to moles of first reactant initially fed, $\alpha$, and moles of second product formed to moles of first reactant initially fed, $\gamma$ --are plotted as dependent variables, with two ratios of rate coefficients required as contour parameters.

As an example of possible data-handling methods, a time-ratio method of analysis is illustrated for the reaction case $A \rightleftharpoons 2B$, $B \rightarrow C$. Because there are three rate coefficients (and hence two ratios of rate coefficients), two independent time ratios are required. Figure F. 4-1 shows the ratio of times at $\alpha = 0.35$ and $\alpha = 0.7$, and Fig. F. 4-2 the ratio at $\gamma = 0.5$ and $\gamma = 0.05$. For experimental values of the two time ratios, different values of $\kappa_2$ must be tried in these two plots until the value is found that also makes $\kappa_1$ equal. The resulting values of $\kappa_1$ and $\kappa_2$, with an $\alpha$ or $\gamma$ value at an actual time, can be used in one of the parent plots to evaluate $k_1$ (and, from this, the other rate coefficients).

## 5: LONGITUDINAL DISPERSION IN PACKED GAS-ABSORPTION COLUMNS(*)

W. E. Dunn, T. Vermeulen, C. R. Wilke, and T. T. Word

To complete work started in the preceding year, longitudinal-mixing experiments were conducted in a packed cylindrical column 2 ft in inside diameter and 6 ft high. Air and water were used as carrier streams, with helium and sodium nitrate as the respective tracers. As packing materials, 1-in. Berl saddles and 1- and 2-in. Raschig rings were used.

The mixing results were expressed in terms of Peclet-number (P) values, determined as the product of effective particle diameter and superficial velocity divided by dispersion coefficient. The method of obtaining P from experimental data has been described by Jacques and co-workers.[1] Experimental data are shown in Fig. F. 5-1 for the gas phase, and in Fig. F. 5-2 for the liquid phase. The higher P values for the gas correspond to lower extents of mixing. The gas-phase P values are seen to decrease with increasing liquid or gas flow rates. Liquid-phase P values increase with increasing liquid flow rate, and are relatively insensitive to gas rate. The results are believed to be independent of the particular fluids used for measurement. Application of these results to typical experimental data[2] has shown that longitudinal mixing contributes significantly to absorption-column performance for relatively short columns.

---

*Summary of work reported by William E. Dunn, Longitudinal Mixing in Packed Gas-Absorption Columns (thesis), UCRL-10394, July 1962.

1. G. L. Jacques, J. E. Cotter, and T. Vermeulen, Longitudinal Dispersion in Packed Extraction Columns, UCRL-8658, April 1959.

2. L. Fellinger, Absorption of Ammonia by Water and Acid in Various Standard Packings (Sc. D. thesis), Massachusetts Institute of Technology, 1941.

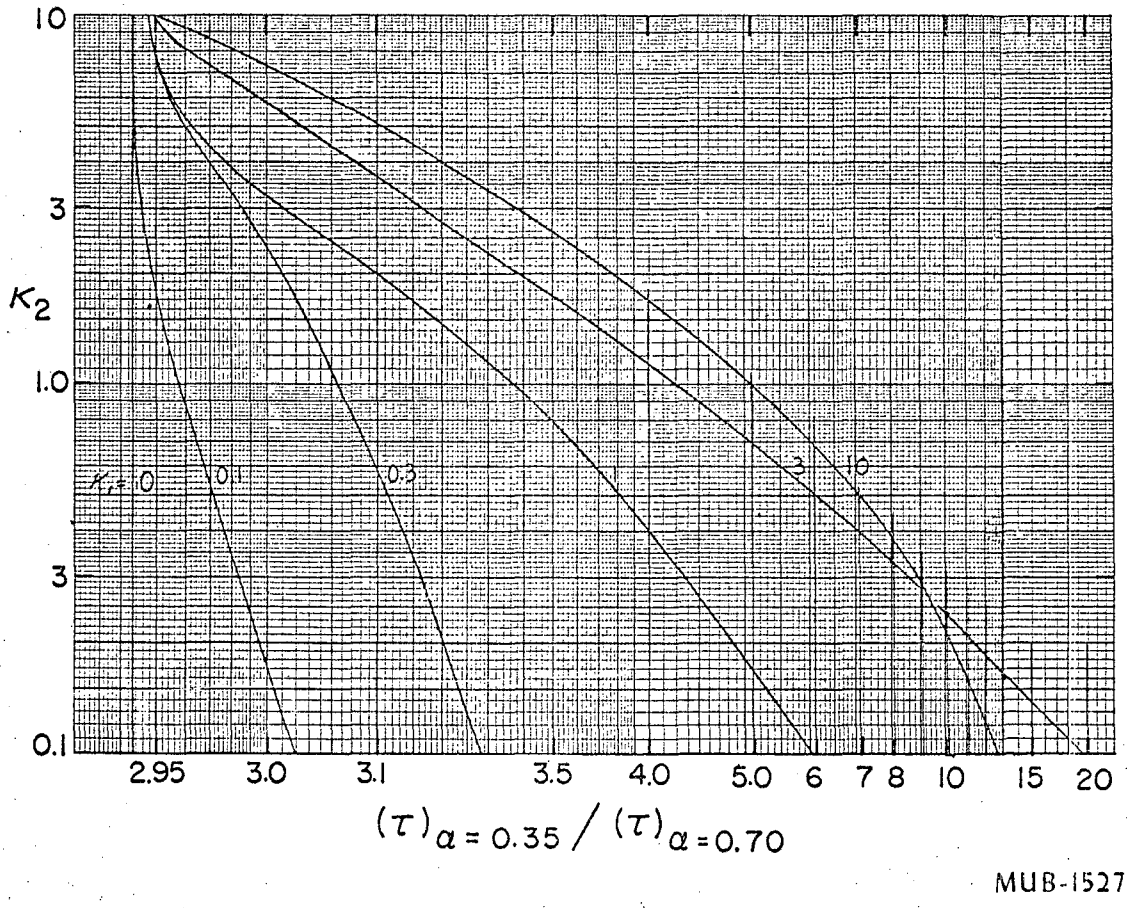


Fig. F. 4-1. Time-ratio plot for given α values, in consecutive-reaction system with two first-order-forward steps and reverse of first step second-order. $\kappa_1$ is a dimensionless ratio based on reverse and forward rate coefficients for first step; $\kappa_2$ is the ratio of forward rate coefficients for second step and first step.

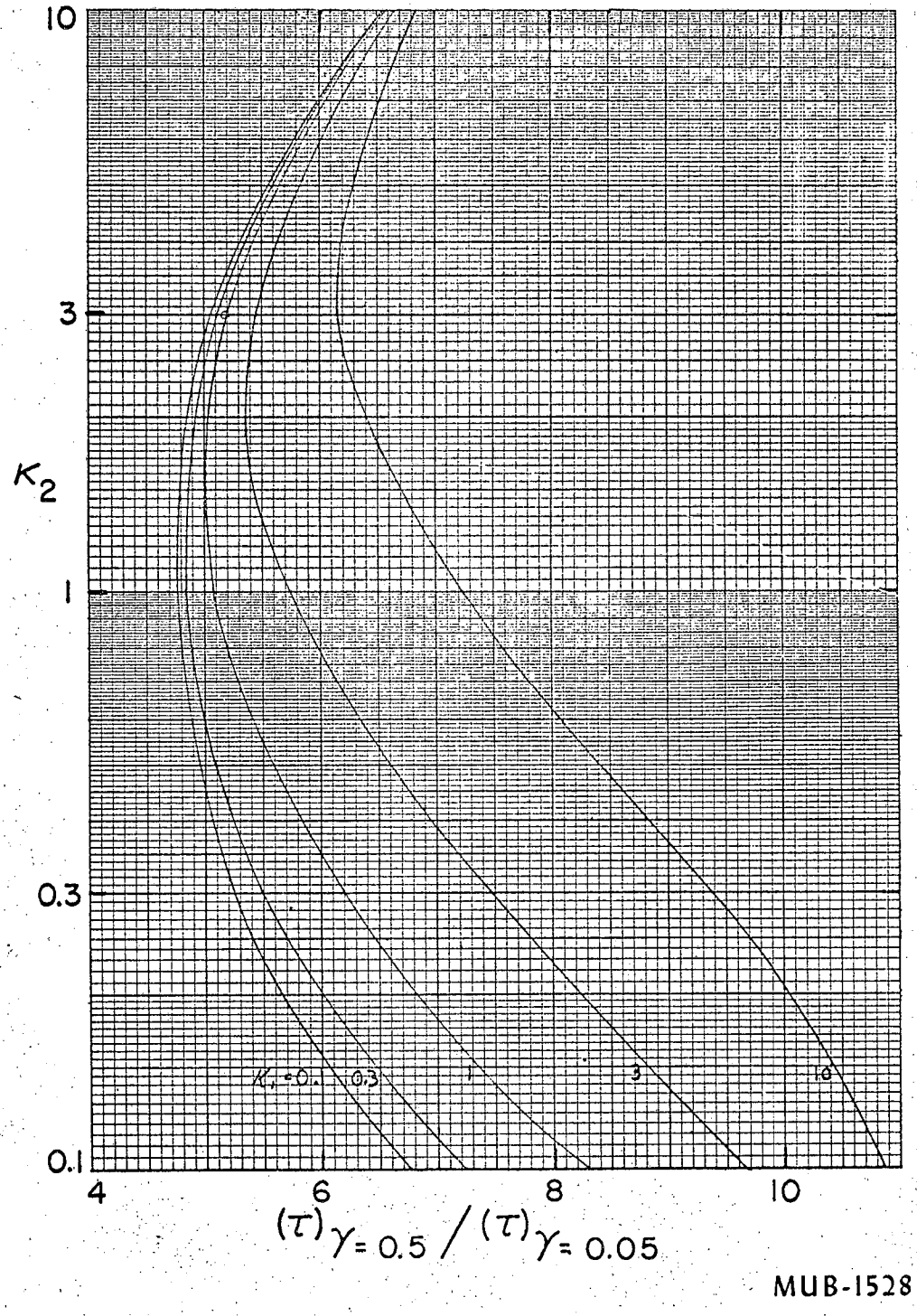


Fig. F.4-2. Time-ratio plot for given γ values, in consecutive-reaction system with two first-order forward steps and reverse of first step second-order.

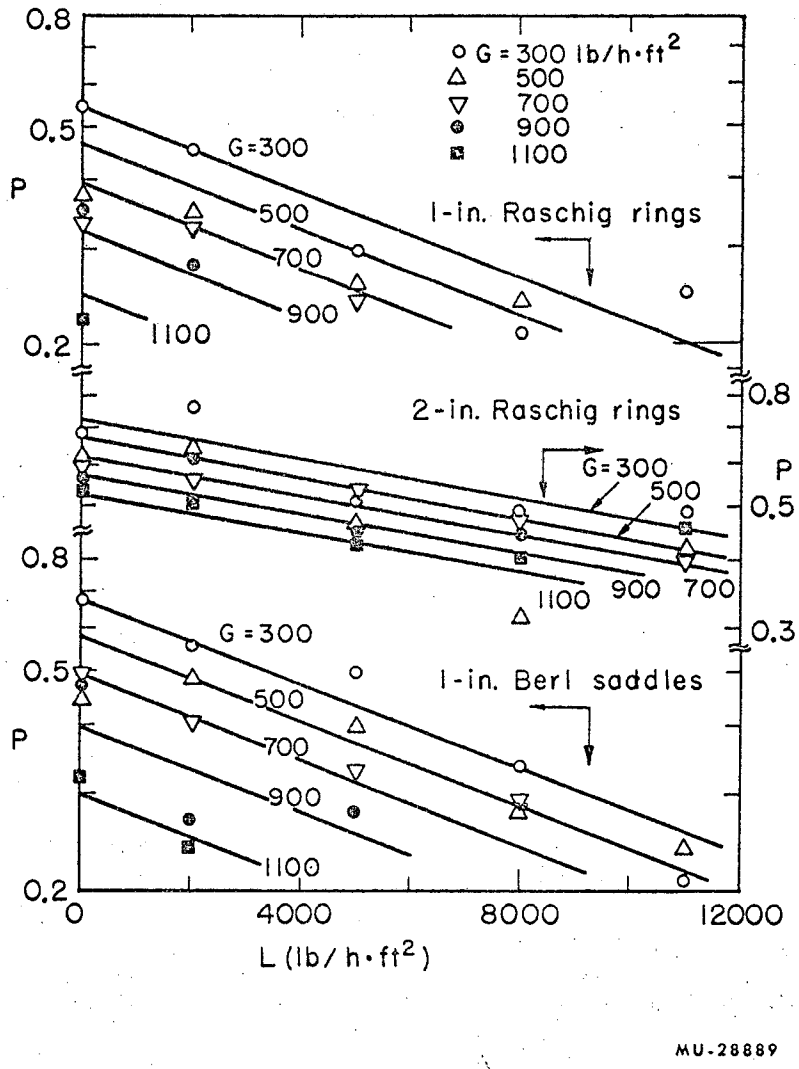


Fig. F. 5-1. Gas-phase Peclet-number values for countercurrent flow of air and water.

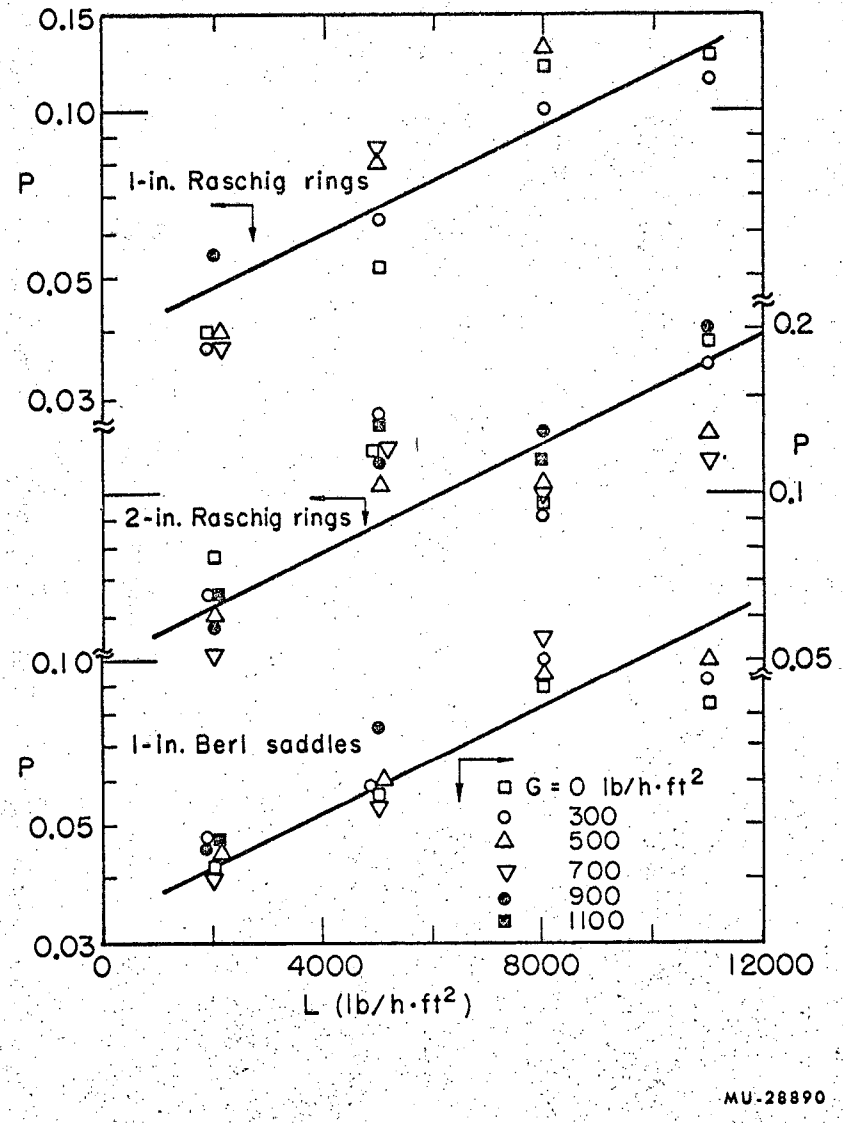


Fig. F. 5-2. Liquid-phase Peclet-number values for counter-current flow of air and water.

## G. THESIS ABSTRACTS

On the following pages the abstracts of theses issued in 1962 are reproduced from the original documents.

Papers elsewhere in this report cover work described in theses by

| | |
|---|---|
| William E. Dunn (M. S.) | (Paper F. 5) |
| Eldon Lee Haines (Ph. D.) | (Paper B. 11) |
| Fred J. Heinzelmann (M. S.) | (Paper F. 3) |
| Monte Lee Hyder (Ph. D.) | (Paper D. 2) |
| Paul L. Reeder (Ph. D.) | (Paper C. 1) |
| Michael A. Sweeney (Ph. D.) | (Paper D. 3) |
| David C. Whitney (Ph. D.) | (Papers D. 4, D. 5, D. 6) |
| Darrell E. Wilcox (M. S.) | (Paper F. 1) |

# I. THEORY OF COLLECTIVE VIBRATIONS OF EVEN-EVEN SPHEROIDAL NUCLEI

Eugene R. Marshalek

Lawrence Radiation Laboratory
University of California
Berkeley, California

March 1962

## ABSTRACT

A version of the Inglis "cranking model" is presented which describes nuclear shape oscillations without the adiabatic approximation. The collective frequencies of a system of particles moving in a time-dependent shell model potential are obtained as solutions of a dispersion equation usually associated with the random phase approximation (RPA). The method used is equivalent to an extension of the cranking model first devised by Araujo. It is shown that the form of the dispersion equation follows from a suitable definition of "vibrational spectrum" in a system with coupled collective and intrinsic degrees of freedom. It is also shown that the generalized cranking model is equivalent to the time-dependent self-consistent field method applied to an appropriate long-range two-body force.

Extensive numerical applications are made to quadrupole vibrations of even-even deformed nuclei, using Nilsson's single particle eigenvalues and asymptotic wave functions, and taking residual pairing interactions into account by means of the Bogolyubov canonical transformation method. Vibrational frequencies, mass

parameters, force constants, reduced electric quadrupole transition probabilities, and vibration-rotation interaction coefficients of the "$\beta$" and "$\gamma$" quadrupole modes are theoretically estimated for rare earth and actinide isotopes, and compared with experimental values.

# 2. A HYDRODYNAMIC MECHANISM FOR THE COALESCENCE OF LIQUID DROPS

Sidney B. Lang

Lawrence Radiation Laboratory
University of California
Berkeley, California

May, 1962

## ABSTRACT

The coalescence of liquid drops at planar interfaces was studied theoretically and experimentally. The mechanism of coalescence was found to occur in two parts. In the first part, the drop (phase 1) approaches the interface through the continuous medium (phase 2) and deforms the interface by creating a spherical depression in it. The thin spherical shell of phase 2 material between the drop and the interface is slowly squeezed out under the combined action of surface and gravity forces. The phase 2 film becomes thinner at a rate inversely proportional to the cube of its thickness. When the film becomes sufficiently thin, the second part of the mechanism occurs. Because a denser liquid always overlies a less dense liquid at one of the interfaces of the film, the interface is inherently unstable with respect to long-wavelength disturbances (Taylor instability). If such a disturbance is introduced into the proper interface, the disturbance will grow exponentially in time until the film disintegrates, causing coalescence of the drop. A sufficiently intense disturbance of any wavelength can also rupture the metastable film, causing coalescence. The ease of rupture of the phase 2 film increases with decreasing thickness of the film. The disturbances can originate from any source yielding a fluctuating pressure at the interface, i.e., mechanical vibration, thermal convection currents, Marangoni instability, or other. Because these disturbances arrive randomly in time, coalescence times are also random. Drop rest-times were predicted to decrease with decreasing drop radius, decreasing phase 2 viscosity and decreasing frequency of disturbance.

UCRL-10624
(from UCRL-10097,
Ph. D. Thesis)

The effect of density difference and interfacial tension depends upon whether film thinning or film rupture is the rate-determining step in coalescence.

Coalescence measurements were made in an all-glass thermostatted cell. The two-component systems water-benzene, water-anisole, ethylene glycol-benzene, tributyl phosphate-water, and water-Aroclor 1248 were studied. Both artificial sonic and artificial subsonic disturbances were found to decrease the drop rest-times, as predicted by the theory. Measurement of the natural sonic pattern present in the coalescence cell by means of a special microphone showed the presence of intense but short-time disturbances. Studies with surfactants showed that concentrations of less than 0.02 mM of surface-active agent in the water-benzene system could increase coalescence times by a factor of 2. Experimental changes in drop size and system properties agreed with the theory, qualitatively. Because of the microscopic nature of the theory and the macroscopic nature of the experimental results, exact experimental verification of the theory is not possible.

# 3. PREFERENTIAL POLAR ALPHA-PARTICLE EMISSION IN ORIENTED CALIFORNIUM AND EINSTEINIUM

Quirino Oli Navarro

Lawrence Radiation Laboratory
University of California
Berkeley, California

July 12, 1962

ABSTRACT

Nuclear alignment experiments were performed on $E^{253}$ and $Cf^{249}$, incorporated as the tripositive ions, in single crystals $Nd(C_2H_5SO_4)_3 \cdot 9H_2O$. The actinides and lanthanides were shown to be isomorphous in this salt. The low temperatures needed were attained by adiabatic demagnetization of the samples. Alpha particles emitted from the samples and detected with germanium surface-barrier detectors were found to be highly anisotropic; in the case of einsteinium the nuclear orientation was saturated at a relatively high temperature. The alpha particles from these nuclei were shown to be preferentially emitted from the "tips," thus providing two independent confirmations of the prediction of Hill and Wheeler. The S- and D-waves in the "favored" transitions in these isotopes were found to be in phase. The L = 2, 4 waves in einsteinium were interpreted as being out of phase; the L = 3,5 components in californium could not be determined with certainty, although an out-of-phase relationship was indicated.

By use of the theory of Elliott and Stevens, the electronic ground state resulting from the crystal-field splitting of the ground level of tripositive einsteinium in $Nd(C_2H_5SO_4)_3 \cdot 9H_2O$ was calculated. It was found that the theory, developed for the lanthanides, can be applied to the actinides as well. Values of $\langle r^{-3} \rangle$ for the 5f electrons were estimated; these values and the above theory were used in deriving values of the nuclear moments. From assumed nuclear spins I = 7/2 and I = 9/2 for $E^{253}$ and $Cf^{249}$, respectively, nuclear moments of $|\mu_{253}|$ = 4.9 n.m. and $|\mu_{249}|$ = 1.3 n.m. were derived. Errors of about 20%,

of which one-half comes from uncertainties in the theory, should be attached to these values.

The gamma rays of $Cm^{245}$, following the alpha decay of $Cf^{249}$, were found to be anisotropic. Appreciable attenuation of the gamma-rays was found, indicating some reorientation of the nuclear spin of the daughter nucleus.

Nuclear-alignment experiments were also performed on $Dy^{155}$ and $Dy^{157}$. The angular distributions of the gamma rays following the decays of both isotopes were found to be anisotropic. Spin 5/2-was assigned to the states at 227 keV in $Tb^{155}$ and at 327 keV in $Tb^{157}$. The nuclear moments $|\mu_{155}| = 0.21 \pm 0.05$ n.m. and $|\mu_{157}| = 0.32 \pm 0.02$ n.m. were derived, based on $I = 3/2$ for both isotopes as well as pure $L = 1$ beta decay to the 5/2 - states.

The practicality of germanium surface-barrier detectors was again demonstrated. It was found that these are suitable for use at low temperatures for detecting alpha and beta particles. Experiments indicated that under the conditions demanded in this line of investigation, these detectors are superior to other means of detection of charged particles.

# 4. A CRYSTALLOGRAPHIC STUDY OF MAGNESIUM AMMONIUM SULFATE HEXAHYDRATE

by

Thomas N. Margulis

Department of Chemistry and Lawrence Radiation Laboratory

University of California, Berkeley, California

July 1962

## ABSTRACT

The structure of $Mg(NH_4)_2(SO_4)_2 \cdot 6H_2O$ has been redetermined in order to assign the hydrogen bonds. The crystals are monoclinic, space group $P2_1/a$, with a = 9.324, b = 12.597, c = 6.211 Å, and $\beta = 107.14^\circ$. The structure previously reported by Hofmann has nearly correct coordinates for the Mg, S, and N atoms, but incorrect coordinates for the oxygen atoms. Three-dimensional x-ray diffraction data were taken with the General Electric goniostat. The structure, including hydrogen atoms, was determined by Fourier and least-squares methods. The magnesium atom is surrounded by an octahedron of water molecules, each forming two hydrogen bonds to oxygen atoms of the sulfate ions. Three hydrogen atoms of each ammonium ion are bonded to sulfate oxygen atoms, but the fourth is equidistant from two sulfate oxygen atoms with the geometry which previous authors have called a "bifurcated hydrogen bond". Average interatomic distances (uncorrected for thermal motion) are: Mg-O = 2.07, S-O = 1.47, O-O (hydrogen bonded) = 2.77, N-O (hydrogen bonded) = 2.90, and N-O (bifurcated bond) = 3.08 Å. The average S-O bond length after correction for thermal motion is 1.49 Å.

An attempted calculation of the distribution of electrons in the sulfate ion was unsuccessful. Possible reasons for this are discussed.

# 5. HIGH-ENERGY NUCLEAR REACTIONS OF NIOBIUM WITH INCIDENT PROTONS AND HELIUM IONS

Ralph Garret Korteling

Lawrence Radiation Laboratory
University of California
Berkeley, California

September 10, 1962

## ABSTRACT

High-energy nuclear reactions initiated by protons and helium ions on niobium have been investigated. Specific reaction products were selected to represent the low and high deposition-energy processes as well as the production of low-mass products. Excitation functions for these products were determined between the energies 240 to 720 MeV for incident protons, and 320 to 880 MeV for incident helium ions. The results from the proton bombardments were compared with values obtained from a Monte Carlo calculation of the cascade-evaporation model. The results from the proton bombardments were also compared with those from helium-ion bombardments.

In general, the comparison of experimental proton results with the results from the calculation gives satisfactory agreement for the low and high deposition-energy processes with the exception of specific cases such as the (p, pxn) reactions. This agreement might be improved with suitable refinements of the calculation. However, the calculation is not able to predict the production of low-mass products, and therefore another mechanism must be invoked to explain their production.

The comparison between the experimentally determined proton and helium-ion results shows a remarkable similarity. This similarity was unexpected from a consideration of high-energy processes such as meson production and interaction. The inconsistencies which arise from this observation are presented.

In addition, experimental information for the identification and decay properties of the previously unreported niobium-88 isotope is given.

# 6. SPONTANEOUS FISSION OF SOME HEAVY ISOTOPES

Reinhard Brandt

Lawrence Radiation Laboratory
University of California
Berkeley, California

September 26, 1962

## ABSTRACT

A back-to-back semiconductor counter system was used to study the energy and mass distributions of the fragments in the spontaneous fission of $Fm^{254}$, $E^{253}$, $Cf^{254}$, $Cf^{250}$, and $Cm^{248}$. The results are compared with the spontaneous-fission properties of $Cf^{252}$, which is used as a standard.

All distributions (including those of the odd-mass isotope $E^{253}$) are rather similar, but not identical with the standard. The total kinetic energy of the fragments increases with Z. The asymmetry of the mass distribution shows only small differences between the isotopes. The variances (widths) of all distributions increase with Z and seem to increase with A.

A new fermium isotope with a spontaneous-fission half life of $(11^{+10}_{-6})$ days has been observed. The mass is most likely 258 or 257. The spontaneous-fission half life of $(1.0^{+0.6}_{-0.3}) \cdot 10^4$ y has been observed for $Fm^{255}$. The $Cf^{254}$ spontaneous-fission half life has been redetermined and is 60.5 ± 0.2 days. The alpha/fission ratio in the decay of $Cf^{250}$ has been redetermined and is (1330±45). The redetermined alpha-decay half life of $Fm^{255}$ is (19.9±0.3) h.

G.

UCRL-10624
(from UCRL-10482,
Ph. D. Thesis)

# 7. A MOLECULAR-BEAM ELECTRIC RESONANCE SPECTROMETER AND THE RADIO-FREQUENCY SPECTRA OF LITHIUM FLUORIDE

Alvin Joseph Hebert

Lawrence Radiation Laboratory and Department of Chemistry
University of California, Berkeley, California

September 26, 1962

ABSTRACT

The construction and operation of a radio-frequency electric resonance molecular beam apparatus are described. The resolution of the apparatus is consistent with theoretical expectations. A simple mass spectrograph and an automated counting-recording scheme allow the procurement of spectra from signals that correspond to as few as one hundred detected transitions per second.

The experimental results obtained for lithium fluoride are presented and discussed. Spectra were observed for the first three vibrational states of $Li^6F^{19}$ and $Li^7F^{19}$. A value for the lithium quadrupole coupling constant, the spin-rotation constant, the Stark-effect constant, and the dipole moment is reported for each vibrational state. Results for the V = 2 vibrational state of $Li^7F^{19}$ are reported for the first time.

An analysis of the $Li^7F^{19}$ spectra has resolved an uncertainty in the rotational and vibrational constants previously reported. This in turn has allowed a much more accurate determination of the dipole moments of LiF.

# 8. STEADY-STATE DIFFUSION IN TERNARY GAS MIXTURES

Richard W. Getzinger

Lawrence Radiation Laboratory and Department of Chemical Engineering
University of California, Berkeley, California

January 17, 1962

## ABSTRACT

The Stefan diffusion-tube approach was utilized to experimentally determine the rate of mass transfer in three ternary systems in which two gases were simultaneously diffusing into a third stagnant gas. Constant evaporating binary liquid mixtures were used. The experimentally determined values were compared with the quantities predicted by the Gilliland, or exact, solution of the Stefan-Maxwell equations. Similar comparisons were made with several approximate sets of equations from the literature for typical experimental runs.

Results of these comparisons indicate that: (a) unless the interacting influence of the two diffusing gases upon each other is considered, any predictive method will be seriously in error; (b) the validity of the Stefan-Maxwell equations has been established under experimental conditions more stringent than any that have been employed previously. These results, together with earlier data for stagnant gas mixtures, provide some proof of the applicability of the Stefan-Maxwell equations to diffusion in complex, multicomponent, gas systems.

# 9. SEPARATION OF IMMISCIBLE LIQUIDS BY GRAVITY SETTLING AND INDUCED COALESCENCE

## PART ONE: HORIZONTAL GRAVITY SETTLERS

## PART TWO: GRAVITY SETTLING WITH INDUCED COALESCENCE

Robert J. Graham

Lawrence Radiation Laboratory
University of California
Berkeley, California

February 5, 1962

ABSTRACT

The separation of water from Aroclor 1248 by use of gravity settlers was investigated. The water concentration in the effluent Aroclor was found to depend on several factors, including the inlet and baffle positions, the initial water concentration, and the degree of turbulent mixing upstream from the settler, as well as on the Aroclor flow rate and depth, and the settler length. At high flow rates, an emulsion of water and Aroclor droplets formed at the Aroclor-water interface. This emulsion influenced the water concentration in the effluent Aroclor. Although the general influence of these factors on the separation of water from Aroclor 1248 was established, it was not possible to correlate them in designing full-scale gravity settlers from laboratory-scale settlers.

Fiberglas coalescers mounted in the settlers were effective in coalescing the emulsion and removing Aroclor droplets from the water layer. The coalescers with the most surface area were the most efficient in removing water from the Aroclor. Pressure drops through the coalescers were negligible.

# 10. DIRECT CONTACT CONDENSATION WITH TWO IMMISCIBLE FLUIDS

Daryl Lee Lackey

Department of Chemical Engineering and
Lawrence Radiation Laboratory
University of California
Berkeley, California

June 29, 1962

## ABSTRACT

The theory, design techniques, and relative economics are presented for three basically different direct-contact condensation processes involving fluids whose condensed phases are immiscible. The specific system developed for this study used Aroclor 1248 (Monsanto Chemical Corporation) and steam. The processes investigated were (a) the injection and (b) induction of steam into a high-velocity stream of Aroclor in the throat section of a Venturi, and (c) bubbling of steam into a low-velocity stream of Aroclor, using a packed tower to artificially increase the surface of contact.

The induction, injection, pressure drop, and heat-transfer characteristics of a Venturi in direct-contact condensation service were experimentally investigated, and empirical correlations for the performance of the unit are included.

The performance of a direct-injection device was also experimentally determined, and correlations obtained.

Finally, the theoretical development of relationships predicting the performance of a packed tower in direct-contact condensation service is discussed.

# H. AUTHOR INDEX

## 1. PAPERS PUBLISHED AND UCRL REPORTS ISSUED, 1962 (including some from late 1961)

Alster, J. (see H. E. Conzett, UCRL-10137-Abstract)

Asaro, F., M. C. Michel, S. G. Thompson, and I. Perlman
The Alpha Decay Scheme of 152-Year $Am^{242m}$
UCRL-9758, June 1961 — For Proceedings of the Rutherford Jubilee International Conference, Manchester, 1961 (Heywood and Co., Ltd., London, 1961)

Asaro, F. (see Bjørnholm, UCRL-9938)

Asaro, F. (see I. Perlman, UCRL-10094)

Asaro, F. (see E. Flamm, UCRL-10199)

Asaro, F. (see K. Siegbahn, UCRL-10419)

Baltzinger, C. (see J. M. Alexander, UCRL-10268)

Barloutaud, M., R. Chaminade, H. Farraggi, D. Garetta, and B. G. Harvey
Excitation of Rotational Levels in $Mg^{24}$ by Inelastic Scattering of 43-MeV Alpha Particles
(No UCRL number) Sept. 1962 — Abstract for Padua, Italy, Meeting on Direct Nuclear Interactions, Sept. 1962

Barloutaud, M., R. Chaminade, H. Faraggi, D. Garetta, and B. G. Harvey
Excitation of Vibrational Levels in $Fe^{54}$ by Inelastic Scattering of 43-MeV Alpha Particles
(No UCRL number) Sept. 1962 — Abstract for Padua, Italy Meeting on Direct Nuclear Interactions, Sept. 1962

Barrett, P. H., R. W. Grant, M. Kaplan, D. A. Keller, and D. A. Shirley
Conduction-Electron Transfer and Electronegativity
UCRL-10514-Abs., Oct. 1962 — Abstract for APS Meeting, Stanford, Dec. 1962

Barrett, P. H. (see R. B. Frankel, UCRL-10517-Abstract)

Bennett, W. (see W. M. Garrison, UCRL-9813)

Bjørnholm, S., M. Lederer, F. Asaro, and I. Perlman

Alpha Decay to Vibrational States
UCRL-9938, Sept. 1962 Phys. Rev.

Bjørnholm, S., and C. M. Lederer

Thin Cation-Exchange Foils
UCRL-9957, Dec. 1961 Nuclear Instr. Methods 15, 233 (1962)

Bloom, S. D., and N. K. Glendenning

(p, n) Reactions in Mirror Nuclei and the Nuclear Two-Body Force
(No UCRL number) 1961 For Proceedings of the Rutherford Jubilee International Conference, Manchester, 1961 (Heywood and Co., Ltd., London, 1961)

Bolotin, H. H. (see D. J. Horen, UCRL-10592)

Bolotin, H. H. (see D. J. Horen, UCRL-10594-Abs.)

Bowman, H. R., S. G. Thompson, J. C. D. Milton, and W. J. Swiatecki

Velocity and Angular Distributions of Prompt Neutrons from Spontaneous Fission of $Cf^{252}$
UCRL-9713-Rev., Oct. 1961 Phys. Rev. 126, 2120 (1962)

Bowman, H. R., J. C. D. Milton, Stanley G. Thompson, and W. Swiatecki

Further Studies of the Prompt Neutrons from the Spontaneous Fission of $Cf^{252}$
UCRL-10139-Rev., May 1962 Phys. Rev.

Brandt, R. (see R. C. Gatti, UCRL-10456)

Brandt, R. (see L. Phillips, UCRL-10464)

Brandt, R.

Spontaneous Fission of Some Heavy Isotopes
UCRL-10481, Sept. 1962 Ph. D. Thesis

Breivogel, F. W., and M. D. Holtz

Tables of Kinetic Energy vs Magnetic Rigidity for Electrons
UCRL-10494, Nov. 1962

Brown, M. (see G. Igo, UCRL-10148-Abs.)

Budick, B. (see S. S. Alpert, UCRL-10005-Abs.)

Cerny, J., B. G. Harvey, and R. H. Pehl

(α, d) Reactions on Odd-Odd Targets
UCRL-9525, Feb. 1961 Nucl. Phys. 29, 120 (1962)

Cerny, J. (see B. G. Harvey, UCRL-10142 Abs., 10143-Abs., 10144-Abs.)

Cerny, J. (see B. G. Harvey, UCRL-10190)

Chaminade, R. (see M. Barloutaud, No UCRL number)

Chaminade, R. (see M. Barloutaud, No UCRL number)

Choppin, G. R., and T. Sikkeland

Ratio of $Cd^{115}$ Isomers Produced in Heavy-Ion-Induced Fission
UCRL-10226, May 1962 Phys. Rev.

Cole, S. (see W. M. Garrison, UCRL-9903)

Conway, J. G. (see E. F. Worden, No UCRL number-Abstract)

Conway, J. G. (see J. B. Gruber, UCRL-9555)

Conway, J. G., J. B. Gruber, E. K. Hulet, R. J. Morrow, and R. C. Gutmacher

Absorption and Self-Luminescence Spectra of $Cf^{+3}(5f^9)$
UCRL-9654, April 1961 J. Chem. Phys. 36, 189 (1962)

Conway, J. G., E. K. Hulet, and R. J. Morrow

Emission Spectrum of Californium
UCRL-9776, July 1961 J. Opt. Soc. Am. 52, 222 (1962)

Conway, J. G. (see H. Lämmermann, UCRL-10257)

Conway, J. G. (see R. D. McLaughlin, UCRL-10458)

Conway, J. G., and B. G. Wybourne

Low-Lying Energy Levels of Lanthanide Atoms and Intermediate Coupling
UCRL-10566, Nov. 1962 Phys. Rev.

Conzett, H. E., and J. Alster

Comparison of Optical-Model and Diffraction-Theory Analyses of Heavy-Ion Elastic Scattering
UCRL-10056-Abs., Feb. 1962 — Abstract for APS Meeting, Washington, D. C., April 1962

Conzett, H. E., G. Igo, and W. K. Knox

Polarization of 21-MeV Protons Elastically Scattered from Deuterium
UCRL-10136-Abs., March 1962 — Abstract for Padua, Italy, Meeting on Direct Nuclear Interactions, Sept. 1962

Conzett, H. E., and J. Alster

Heavy-Ion Elastic Scattering
UCRL-10137-Abs., March 1962 — Abstract for Padua, Italy, Meeting on Direct Nuclear Interactions, Sept. 1962

Conzett, H. E. (see A. Isoya, UCRL-10159-Abs.)

Crespo, V. P., J. M. Alexander, and E. K. Hyde

Ejection of Large Fragments in High-Energy Nuclear Reactions
UCRL-10496, Oct. 1962 — Phys. Rev.

Cunningham, B. B.

The Metal Plutonium
No UCRL number — Review for Science Magazine

Cunningham, B. B. (see D. B. McWhan, No UCRL number)

Cunningham, B. B.

Thermodynamics of the Actinides
UCRL-10176, April 1962 — Report for the Proceedings of International Atomic Energy Agency Symposium on the Thermodynamics of Nuclear Materials, Vienna, May 1962

Demildt, A. C.

Microactivation Analysis for Oxygen in the Actinide Metals
UCRL-10324, July 1962 — Anal. Chem.

Diamond, R. M. (see D. C. Whitney, UCRL-10063)

Diamond, R. M. (see D. C. Whitney, UCRL-10595)

Dunn, W. E.

Longitudinal Mixing in Packed Gas-Absorption Columns
UCRL-10394, July 1962 M. S. Thesis

Elliott, J. H., and R. H. Pehl

A Thin Semiconductor Transmission-Counter System for Nuclear Particle Detection
UCRL-10030, Jan. 1962 Rev. Sci. Instr., 33, 713 (1962)

English, M. K., and W. M. Garrison

Dehydropeptide Production in the Radiolysis of Solid Peptides: A Radiolytic Synthesis of Pyrazine Derivatives from Cyclic Dipeptides
UCRL-10186, Sept. 1962 Nature

Faraggi, H. (see M. Barloutaud, No UCRL number)

Faraggi, H. (see M. Barloutaud, No UCRL number)

Fick, J. L. (see L. H. Weiss, UCRL-9787)

Flamm, E., and F. Asaro

Perturbation of Alpha-Particle–Gamma-Ray Angular Correlations in $Am^{241}$, $Am^{243}$, and $Cm^{243}$
UCRL-10199, May 1962 Phys. Rev.

Forrester, J. D., E. Senko, A. Zalkin, and D. H. Templeton

Crystal Structure of $KH_2F_3$ and Geometry of the $H_2F_3^-$ Ion
UCRL-10150-Abs., March 1962 Abstract for American Crystallographic Association, Villanova University, June 1962

Forrester, J. D., M. E. Senko, A. Zalkin, and D. H. Templeton

Crystal Structure of $KH_2F_3$ and Geometry of the $H_2F_3^-$ Ion
UCRL-10197, April 1962 Acta Cryst. 16, 58 (1963)

Forrester, J. D. (see D. H. Templeton, UCRL-10485-Abs.)

Forrester, J. D. (see D. H. Templeton, UCRL-10597)

Frankel, R. B., P. H. Barrett, and D. A. Shirley

Quadrupole Coupling in Tellurium
UCRL-10517-Abs., Oct. 1962 Abstract for APS Meeting, Stanford, Dec. 1962

Fred, M. (see E. F. Worden, No UCRL number-Abstract)

Garetta, D. (see M. Barloutaud, No UCRL number)

Garetta, D. (see M. Barloutaud, No UCRL number)

Garrison, W. M. and B. M. Weeks

Radiation Chemistry of Compounds Containing the Peptide Bond
No UCRL number, 1962 Radiation Res. 17, 341 (1962)

Garrison, W. M., M. E. Jayko and W. Bennett

Radiation-Induced Oxidation of Protein in Aqueous Solution
UCRL-9813, Aug. 1961 Rad. Res. 16, 483 (1962).

Garrison, W. M., B. M. Weeks, and S. Cole

pH Effects in the Radiolysis of Aquo-organic Systems
UCRL-9903, Oct. 1961 Nature, 193, 1291 (1962)

Garrison, W. M. (see M. K. English, UCRL-10186)

Garrison, W. M.

Recent Development in the Radiation Chemistry of Aqueous Systems
UCRL-10543-Abs., Nov. 1962 Abstract for the Third Annual California Section Meeting-In-Miniature, Dec. 17-18, 1962

Gatti, R. C., R. Brandt, L. Phillips, and S. G. Thompson

The Discovery of a New Fermium Isotope
UCRL-10456, Sept. 1962 J. Inorg. Nucl. Chem.

Gatti, R. C. (see L. Phillips, UCRL-10464)

Gazdik, M. G. (see J. M. Alexander, UCRL-10193)

Gazdik, M. F. (see J. M. Alexander, UCRL-10268)

Getzinger, R. W.

Steady-State Diffusion in Ternary Gas Mixtures
UCRL-9987, Jan. 1962 M. S. Thesis

Ghiorso, A.

The Search for New Elements
No UCRL number Discovery Magazine, Nov. 1961, p. 488-494

Ghiorso, A., T. Sikkeland, A. E. Larsh, and R. M. Latimer

Discovery of Element 103
No UCRL number, 1961 — 1962 Encyclopedia Britannica Year Book, Physics Section, p. 548-549

Ghiorso, A. (see I. Perlman, UCRL-10094)

Gilmore, J., S. G. Thompson, and I. Perlman

An Investigation of the Influence of Angular Momentum on Fission Probability
UCRL-9304-Rev., June 1962 — Phys. Rev. 128, 2276 (1962)

Glendenning, N. K. (see S. D. Bloom, No UCRL number)

Glendenning, N. K.

The Two-Nucleon Stripping Reaction
UCRL-9505, Nov. 1960 — Nucl. Phys. 29, 109 (1962)

Glendenning, N. K. (see S. G. Nilsson, UCRL-9803)

Glendenning, N. K., and G. Kramer

Nucleon-Nucleon Triplet-Even Potentials
UCRL-9904, Nov. 1961 — Phys. Rev. 126, 2159 (1962)

Glendenning, N. K., and G. Kramer

The Scalar Nucleon Form Factor $F_1^n + F_1^p$
UCRL-9905, Oct. 1961 — Phys. Rev. Letters 7, 471 (1961)

Glendenning, N. K. (see S. G. Nilsson, UCRL-9975)

Glendenning, N. K.

Note on an Isomeric State of $Po^{212}$
UCRL-10095, March 1962 — Phys. Rev. 127, 923 (1962)

Gooding, T. J. (see G. Igo, UCRL-10574)

Gordon, G. E. (see T. D. Thomas, UCRL-9950)

Graham, R. J.

Separation of Immiscible Liquids by Gravity Settling and Induced Coalescence
UCRL-10048, Feb. 1962 — M. S. Thesis

Grant, R. W. (see D. A. Shirley, UCRL-10168)

Grant, R. W., M. Kaplan, D. A. Keller, and D. A. Shirley

Nuclear Zeeman Effect in $Au^{197}$
UCRL-10322-Abs., June 1962 Abstract for APS Meeting, Seattle, Aug. 1962

Grant, R. W., and D. A. Shirley

Pseudo-Quadrupole Coupling Constants and Nuclear Moments of Several Promethium Isotopes
UCRL-10472, Sept. 1962 Phys. Rev.

Grant R. W., M. Kaplan, D. A. Keller, and D. A. Shirley

Sign of the Internal Field at Gold Nuclei Dissolved in Iron, Cobalt, and Nickel
UCRL-10513-Abs., Oct. 1962 Abstract for APS Meeting, Stanford, Dec. 1962

Gruber, J. B., and J. G. Conway

Absorption Spectrum and Zeeman Effect of $Am^{3+}$ in $LaCl_3$
UCRL-9555, Feb. 1961 J. Chem. Phys. 36, 191 (1962)

Gruber, J. B. (see J. G. Conway, UCRL-9654)

Gutmacher, R. C. (see E. F. Worden, No UCRL number-Abstract)

Gutmacher, R. C. (see J. G. Conway, UCRL-9654)

Haag, J. N., D. A. Shirley, and David Templeton

Nuclear Alignment of $Ce^{137m}$, $Ce^{137}$, $Ce^{139}$, $Ce^{141}$, and $Ce^{143}$
UCRL-10242, July 1962 Phys. Rev.

Haines, E. L. (see T. Sikkeland, UCRL-9751)

Haines, E. L.

Mass-Energy Relations in the Fission of Highly Excited Heavy Nuclei
UCRL-10342, June 1962 Ph. D. Thesis

Hansen, L. (see G. Igo, UCRL-10148-Abs.)

Hansen, L. F. (see G. Igo, UCRL-10574)

Harvey, B. G. (see J. Cerny, UCRL-9525)

Harvey, B. G. (see J. R. Morton, UCRL-9595-Rev.)

Harvey, B. G., J. Cerny, R. Pehl, and E. Rivet

Investigation of Light-Element Energy Levels by Two-Nucleon Transfer Reactions
UCRL-10142-Abs., May 1962 — Abstract for Padua, Italy, Meeting on Direct Nuclear Interactions, Sept. 1962

Harvey, B. G., J. Cerny, R. Pehl, and E. Rivet

Parities of Some $N^{14}$ Levels
UCRL-10143-Abs., May 1962 — Abstract for Padua, Italy, Meeting on Direct Nuclear Interactions, Sept. 1962

Harvey, B. G., J. Cerny, R. Pehl, and E. Rivet

Configurations of Some $N^{14}$ Levels Formed by Direct Interactions
UCRL-10144-Abs., May 1962 — Abstract for Padua, Italy, Meeting on Direct Nuclear Interactions, Sept. 1962

Harvey, B. G., J. Cerny, R. H. Pehl, and E. Rivet

Levels of $(d_{5/2})^2_5$ Configuration in Light Nuclei
UCRL-10190, April 1962 — Nucl. Phys.

Hebert, A. J.

A molecular Beam Electric Resonance Spectrometer and the Radio-Frequency Spectra of Lithium Fluoride
UCRL-10482, Sept. 1962 — Ph. D. Thesis

Heinzelmann, F. J., D. Wasan, and C. R. Wilke

Concentration and Velocity Profiles in a Stefan Diffusion Tube
UCRL-10421, Aug. 1962 — Heinzelmann's M.S. Thesis

Hennico, A., and T. Vermeulen

Nonequilibrium Thermodynamic Theory for Concentration Profiles in Liquid Extraction
UCRL-9415, Sept. 1960 — A. I. Ch. E. Journal 8, 394 (1962)

Hollander, J. M. (see S. Hultberg, UCRL-9608)

Hollander, J. M. (see J. Valentin, UCRL-9731)

Hollander, J. M. (see J. Valentin, UCRL-9780)

Hollander, J. M. (see Y. E. Kim, UCRL-9812)

Hollander, J. M., C. L. Nordling, and K. Siegbahn
Some Properties of the Levels of $_{100}Fm^{254}$
UCRL-10123, March 1962 Arkiv Fysik, Band 23, Häfte 2

Holtz, M. (see F. W. Breivogel, UCRL-10494)

Horen, D. J. (see S. Hultberg, UCRL-9608-Rev.)

Horen, D. J. (see J. Valentin, UCRL-9730)

Horen, D. J. (see J. Valentin, UCRL-9780)

Horen, D. J. (see Y. E. Kim, UCRL-9812)

Horen, D. J. (see V. Maxia, UCRL-9995)

Horen, D. J., and W. H. Kelly
Isomerism in $Y^{85}$
UCRL-10044-Abs., Feb. 1962 For APS Meeting, Washington, April 1962

Horen, D. J., W. H. Kelly, and L. Yaffe
Characteristics of the Decay of $Ba^{131m}$
UCRL-10413, Aug. 1962 Phys. Rev.

Horen, D. J. (see W. H. Kelly, UCRL-10582)

Horen, D. J., H. H. Bolotin, and W. H. Kelly
Lifetime of the 21.7-keV State in $Eu^{151}$
UCRL-10592, Dec. 1962 Nucl. Phys.

Horen, D. J., H. H. Bolotin, and W. H. Kelly
Lifetime of the 21.7-keV State in $Eu^{151}$
UCRL-10594-Abs., Dec. 1962 Abstract for APS Meeting, Houston, Texas, Feb. 1963

Houston, R. H. (see L. H. Weiss, UCRL-9787)

Hulet, E. K. (see E. F. Worden, No UCRL number; Abstract)

Hulet, E. K. (see J. G. Conway, UCRL-9654)

Hulet, E. K. (see J. G. Conway, UCRL-9776)

Hultberg, S., D. J. Horen, and J. M. Hollander

Measurements of Internal-Conversion Coefficients
UCRL-9608-Rev., April 1961 Nucl. Phys. 28, 471 (1962)

Hyde, E. K.

A Revised Version of a Review of Nuclear Fission, Part One: Fission Phenomena at Low Energy
UCRL-9036-Rev., April 1962

Hyde, E. K. (see V. P. Crespo, UCRL-10496)

Hyder, M. L.

Chemical Effects Following the $S^{34}(n, \gamma)S^{35}$ Reaction in Gaseous Sulfur Compounds
UCRL-10360, July 1962 Ph. D. Thesis

Hyder, M. L., and S. S. Markowitz

Chemical Effects Following the $S^{34}(n, \gamma)S^{35}$ Reaction in Gaseous Sulfur Compounds
UCRL-10360-Rev., Aug. 1962 J. Inorg. Nucl. Chem.

Igo, G., S. S. Markowitz, and J. G. Vidal

Elastic Scattering of 31-MeV $He^3$ Ions from Several Elements
UCRL-9996, Dec. 1961 Phys. Rev.

Igo, G. (see H. E. Conzett, UCRL-10136-Abs.)

Igo, G., and B. Wilkins

Alpha-Particle Reaction Cross Sections near 40 MeV
UCRL-10145-Abs., March 1962 Abstract for Padua, Italy, Meeting on Direct Nuclear Interactions, Sept. 1962

Igo, G., and B. Wilkins

Alpha-Particle Reaction Cross Sections Near 40 MeV
No UCRL number For Padua, Italy, Meeting on Direct Nuclear Interactions, Sept. 1962

Igo, G., and B. Wilkins

Deuteron Reaction Cross Sections at 11.8 MeV and at 20 MeV
UCRL-10146-Abs., March 1962 Abstract for Padua, Italy, Meeting on Direct Nuclear Interactions, Sept. 1962

Igo, G., and B. Wilkins

Proton Reaction Cross Sections at 10 MeV
UCRL-10147-Abs., March 1962 — Abstract for Padua, Italy, Meeting on Direct Nuclear Interactions, Sept. 1962

Igo, G., M. Brown, L. Hansen, and T. Gooding

The (α, 2α) Reaction on Heavy Elements at 915 MeV
UCRL-10148-Abs., March 1962 — Abstract for Padua, Italy, Meeting on Direct Nuclear Interactions, Sept. 1962

Igo, G., and B. Wilkins

10-MeV Proton Reaction Cross Sections for Several Elements
UCRL-10281-Abs., June 1962 — Abstract for APS Meeting, Seattle, Aug. 1962

Igo, G. (see B. Wilkins, UCRL-10281)

Igo, G., and B. Wilkins

10-MeV Proton Reaction Cross Sections
UCRL-10480, Sept. 1962 — Phys. Letters

Igo, G. (see B. Wilkins, UCRL-10500)

Igo, G.

Alpha-Particle Satellites in the Nuclear Stratosphere
UCRL-10528-Abs., Oct. 1962 — Abstract for Conference on Advances in Meson and Nuclear Research, Gatlinburg, Tenn., November 12, 1962

Igo, G., and B. D. Wilkins

Alpha-Particle Reaction Cross Sections at 40 MeV and the Mean Free Path in Nuclear Matter in the Energy Range $10^1$-$10^6$ MeV
UCRL-10568, Nov. 1962 — Nucl. Phys.

Igo, G., L. F. Hansen, and T. J. Gooding

Evidence for Alpha-Particle Clusters in Several Nuclei from the (α, 2α) Reaction at 0.91 BeV
UCRL-10574, Nov. 1962 — Phys. Rev.

Isoya, A., and Conzett, H. E.

Study of the Nuclear Surface by Means of the Elastic Scattering of Heavy Ions
UCRL-10159-Abs., April 1962 — Abstract for APS Meeting, Evanston, June 1962

Jayko, M. E. (see W. M. Garrison, UCRL-9813)

Johansson, S. A. E.

Spontaneous Fission of the Heaviest Elements
UCRL-10474, Sept. 1962

Judd, B. R.

Low-Lying Levels in Certain Actinide Atoms
UCRL-9779, July 1961 Phys. Rev. 125, 613 (1962)

Judd, B. R., and L. C. Marquet

Energy Levels of Er II
UCRL-9830, Aug. 1961 J. Opt. Soc. Am. 52, 504 (1962)

Judd, B. R.

Double-Tensor Operators for Configurations of Equivalent Electrons
UCRL-9868, Sept. 1961 J. Math. Phys. 3, (1962)

Judd, B. R.

Optical Absorption Intensities of Rare Earth Ions
UCRL-10019, Jan. 1962 Phys. Rev. 127, 750 (1962)

Judd, B. R., C. A. Lovejoy, and D. A. Shirley

Anomalous Quadrupole Coupling in Europium Ethylsulfate
UCRL-10202-Rev., June 1962 Phys. Rev. 128, 1733 (1962)

Judd, B. R. (see M. Abraham, UCRL-10567)

Kaplan, M. (see D. A. Shirley, UCRL-10168)

Kaplan, M., and D. A. Shirley

Identification of a Spin 5 State in $Cr^{52}$
UCRL-10207, May 1962 Nucl. Phys. 37, 522 (1962)

Kaplan, M. (see R. W. Grant, UCRL-10322-Abs.)

Kaplan, M. (see R. W. Grant, UCRL-10513-Abs.)

Kaplan, M. (see P. H. Barrett, UCRL-10514-Abs.)

Keller, D. A. (see D. A. Shirley, UCRL-10168)

Keller, D. A. (see R. W. Grant, UCRL-10322-Abs.)

Keller, D. A. (see R. W. Grant, UCRL-10513-A)

Keller, D. A. (see P. H. Barrett, UCRL-10514-A)

Kelly, W. H. (see V. Maxia, UCRL-9995)

Kelly, W. H. (see D. J. Horen, UCRL-10044 Abs.)

Kelly, W. H. (see D. J. Horen, UCRL-10413)

Kelly, W. H., and D. J. Horen

Conversion Electron Measurements in the Decay of 11.5-d $Ba^{131}$
UCRL-10582, Dec. 1962

Kelly, W. H. (see D. J. Horen, UCRL-10592)

Kelly, W. H. (see D. J. Horen, UCRL-10594-Abs.)

Kim, Y. E., D. J. Horne, and J. M. Hollander

Isomeric State in $Y^{86}$
UCRL-9812, Aug. 1961 Nucl. Phys. 31, 447 (1962)

Knox, W. K. (see H. E. Conzett, UCRL-10136-Abs.)

Korteling, R. G.

High-Energy Nuclear Reactions of Niobium with Incident Protons and Helium Ions
UCRL-10461, Sept. 1962 Ph. D. Thesis

Kramer, G., and S. G. Nilsson

On the Penetration Effect in Electric Dipole Internal Conversion
UCRL-9877-Rev., Oct. 1961 Nucl. Phys.

Lackey, D. L.

Direct Condensation with Two Immiscible Fluids
UCRL-10339, June 1962 M. S. Thesis

Lämmermann, H., and J. G. Conway

The Absorption Spectrum of $Pu^{3+}$ in Lanthanum Trichloride and Lanthanum Ethylsulfate
UCRL-10257, May 1962 J. Chem. Phys.

Lang, S. B.

A Hydrodynamic Mechanism for the Coalescence of Liquid Drops
UCRL-10097, May 1962 Ph. D. Thesis

Larsh, A. E. (see I. Perlman, UCRL-10094)

Latimer, R. (see T. D. Thomas, UCRL-9950)

Latimer, R. (see I. Perlman, UCRL-10094)

Lederer, M. (see S. Bjørnholm, UCRL-9938)

Lederer, M. (see S. Bjørnholm, UCRL-9957)

Lee, K. (see A. Zalkin, UCRL-10149-Abs.)

Lee, K. (see A. Zalkin, UCRL-10166)

Levy, R. M., and D. A. Shirley

The g Factor of the 2.083-MeV 4+ State of $Ce^{140}$
UCRL-10454, Oct. 1962 Phys. Letters

Lipworth, E. (see W. W. Alpert, UCRL-10005-Abs.)

Lovejoy, C. A. (see D. A. Shirley, UCRL-10202)

Macfarlane, R. D.

Alpha-Emitting Isomeric State of $Tb^{149}$
UCRL-9870-Rev., Nov. 1961 Phys. Rev. 126, 274 (1962)

Macfarlane, R. D., and I. Almodovar

Study of the $Sm^{149}(n, \alpha)$ $Nd^{146}$ Reaction with Thermal Neutrons
UCRL-10064, April 1962 Phys. Rev. 127, 1665 (1962)

Mahony, J. D. (see S. S. Markowitz, UCRL-9908)

Mahony, J. D., and S. S. Markowitz

The Half Life of Fluorine-18
UCRL-10512, Oct. 1962 Phys. Rev.

Maleh, I. (see R. Schlecht, UCRL-10518 Abs.)

Maleh, I.

Hyperfine Structure of $_{69}Tm^{171}$
UCRL-10520-Abs., Oct. 1962 — Abstract for APS Meeting, Stanford, Dec. 1962

Maleh, I.

Hyperfine Structure of $Er^{171}$
UCRL-10550-Abs., Nov. 1962 — Abstract for APS Meeting, New York, Jan. 1963

Mang, H. J., and J. O. Rasmussen

Shell-Model Calculations of Alpha Decay Rates of Even-Even Spheroidal Nuclei.
No UCRL number — Kgl. Danske Videnskab. Selskab Mat.-fys. Skr. 2, 1 (1962)

Mang, H. J., and J. O. Rasmussen

Theoretical Alpha-Decay Hindrance Factors
No UCRL number — For Proceedings of the Rutherford Jubilee International Conference, Manchester, 1961 (Heywood and Co., Ltd., London, 1961)

Margulis, T. N., and D. H. Templeton

Crystal and Molecular Structure of Triethylscarphane
UCRL-9803, Sept. 1961 — Chem. Phys. 34, No. 9, 2311 (1962)

Margulis, T. N., and D. H. Templeton

Crystal Structure and Hydrogen Bonding of Magnesium Ammonium Sulfate Hexahydrate
UCRL-10151-Abs., March 1962 — Abstract for Amer. Cryst. Assoc., Villanova University, June 18-22, 1962

Margulis, T. N.

A Crystallographic Study of Magnesium Ammonium Sulfate Hexahydrate
UCRL-10386, July 1962 — Ph. D. Thesis

Markowitz, S. S., and J. D. Mahony

Activation Analysis for Oxygen and other Elements by Means of the Helium-3-Induced Nuclear Reactions
UCRL-9908, Nov. 1961 — Anal. Chem. 34, 329 (1962)

Markowitz, S. S. (see G. Igo, UCRL-9996)

Markowitz, S. S. (see P. Reeder, UCRL-10312)

Markowitz, S. S. (see M. L. Hyder, UCRL-10360-Rev.)

Markowitz, S. S. (see J. D. Mahony, UCRL-10512)

Markowitz, S. S. (see P. L. Reeder, UCRL-10548-Abs.)

Marquet, L. C. (see B. R. Judd, UCRL-9830)

Marrus, R. (see S. S. Alpert, UCRL-10005-Abs.)

Marshalek, E. R.

Theory of Surface Vibration of Even-Even Deformed Nuclei
UCRL-10046, March 1962 Ph. D. Thesis

Marshalek, E., L. W. Person, and R. K. Sheline

Systematics of Deformations of Atomic Nuclei
UCRL-10364, July 1962 Rev. Mod. Phys.

Maxia, V., W. H. Kelly, and D. J. Horen

The Neutron-Deficient Yttrium Isotopes
UCRL-9995, Dec. 1961 Inorg. Nucl. Chem.

Michel, M. C. (see F. Asaro, UCRL-9758)

Milton, J. C. D.

Fission Energy Tables and an Application to Nuclear Charge Division
UCRL-9883-Rev., Jan. 1962

Milton, J. C. D. (see H. R. Bowman, UCRL-9713)

Milton, J. C. D. (see H. R. Bowman, UCRL-10139)

Milton, J. C. D., (see H. R. Bowman, UCRL-10139 Rev.)

Morrow, R. J. (see J. G. Conway, UCRL-9654)

Morrow, R. J. (see J. G. Conway, UCRL-9776)

Morton, J. R., III, and B. G. Harvey

Application of Recoil Techniques to Study of the Reactions $Ra^{226}(\alpha, 4n)\ Th^{226}$, $Pb^{208}(\alpha, 2n)\ Po^{210}$, and $Pb^{207}(\alpha, n)\ Po^{210}$
UCRL-9595-Rev., July 1961 Phys. Rev. 126, 1798 (1962)

McColm, D. (see R. Schlecht, UCRL-10518-Abs.)

McLaughlin, R.

Spectrum of $UCl_4$
UCRL-9937, Nov. 1961 J. Chem. Phys. 36, 2699 (1962)

McLaughlin, R. D., and J. G. Conway

Anion Effects on the $Pr^{3+}$ Spectrum
UCRL-10458, Sept. 1962 J. Chem. Phys.

McWhan, D. B., B. B. Cunningham, and J. C. Wallmann

Crystal Structure-Thermal Expansion and Melting Point of Americium Metal
No UCRL number J. Inorg. Nucl. Chem.

Navarro, Q. O., J. O. Rasmussen, and D. A. Shirley

Preferential Polar Emission in the Alpha Decay of Deformed $Cf^{249}$ and $E^{253}$
UCRL-9960-Rev., Sept. 1962 Phys. Letters 2, 353 (1962)

Navarro, Q. O.

Preferential Polar Alpha-Particle Emission in Oriented Californium
UCRL-10362, July 1962 Ph. D. Thesis

Nilsson, S. G., N. K. Glendenning, and J. Sawicki

The Giant E1 Resonance for Deformed Nuclei
UCRL-9803, Sept. 1961 For Proceedings of the Rutherford Jubilee International Conference, Manchester, 1961 (Heywood and Co., Ltd., London, 1961)

Nilsson, S. G., J. Sawicki, and N. K. Glendenning

The Giant E1 Resonance for Deformed Nuclei Treated by the Random-Phase Approximation
UCRL-9975, Dec. 1961 Nucl. Phys. 33, 239 (1962)

Nordling, C. L. (see J. M. Hollander, UCRL-10123)

Pehl, R. H. (see J. Cerny, UCRL-9525)

Pehl, R. H. (see J. H. Elliott, UCRL-10030)

Pehl, R. H. (see B. G. Harvey, UCRL-10142-Abs.)

Pehl, R. H. (see B. G. Harvey, UCRL-10143-Abs.)

Pehl, R. H. (see B. G. Harvey, UCRL-10144-Abs.)

Pehl, R. H. (see B. G. Harvey, UCRL-10190)

Perlman, I. (see J. Gilmore, UCRL-9304-Rev.)

Perlman, I. (see F. Asaro, UCRL-9758)

Perlman, I. (see S. Bjørnholm, UCRL-9938)

Perlman, I., F. Asaro, A. Ghiorso, A. Larsh, and R. Latimer
An Isomeric State of $Po^{212}$
UCRL-10094, Feb. 1962 Phys. Rev. 127, 917 (1962)

Person, L. W., and J. O. Rasmussen
Rotational Energies for the Asymmetric Rotor Model for Odd-Mass Nuclei
UCRL-9876, Jan. 1962 Nucl. Phys. 36, 666 (1962)

Person, L. W. (see E. Marshalek, UCRL-10364)

Phillips, L. (see R. C. Gatti, UCRL-10456)

Phillips, L., R. C. Gatti, R. Brandt, and S. G. Thompson
Spontaneous-Fission Half Lives of $Cf^{254}$, $Fm^{255}$, and $Cf^{250}$
UCRL-10464, Sept. 1962 J. Inorg. Nucl. Chem.

Rasmussen, J. O. (see H. J. Mang, No UCRL number)

Rasmussen, J. O. (see H. J. Mang, No UCRL number)

Rasmussen, J. O. (see J. W. Person, UCRL-9876)

Rasmussen, J. O. (see Q. O. Navarro, UCRL-9960)

Rasmussen, J. O. (see Q. O. Navarro, UCRL-9960-Rev.)

Rasmussen, J. O.
Simplified Shell-Model Alpha Decay Rate Calculations Near $Pb^{208}$
UCRL-10414, Aug. 1962 Nucl. Phys.

Reeder, P., and S. S. Markowitz
Excitation Function for the $C^{12}(\pi^-, \pi^- n)C^{11}$ Reaction
UCRL-10312, June 1962 Phys. Rev. Letters

Reeder, P. L.

Nuclear Reactions Induced by Pions and Protons
UCRL-10531, Nov. 1962 Ph. D. Thesis

Reeder, P. L., and S. Markowitz

Quasi-Elastic Scattering in $C^{12}(\pi^-, \pi^- n)C^{11}$ Excitation Function
UCRL-10548-Abs., Nov. 1962 Abstract for APS Meeting, New York, Jan. 1962

Rivet, E. (see B. G. Harvey, UCRL-10142-Abs.)

Rivet, E. (see B. G. Harvey, UCRL-10143-Abs.)

Rivet, E. (see B. G. Harvey, UCRL-10144-Abs.)

Rivet, E. (see B. G. Harvey, UCRL-10190)

Sawicki, J. (see S. G. Nilsson, UCRL-9803)

Sawicki, J. (see S. G. Nilsson, UCRL-9975)

Schlecht, R., D. McColm, and I. Maleh

Hyperfine Structure of the Lithium Isotopes
UCRL-10518-Abs., Oct. 1962 Abstract for APS Meeting, Stanford, Dec. 1962

Seaborg, G. T. (see T. D. Thomas, UCRL-9950)

Seaborg, G. T. (see V. E. Viola, Jr., UCRL-10248)

Senko, E. (see J. D. Forrester, UCRL-10150-Abs.)

Senko, E. (see J. D. Forrester, UCRL-10197)

Sheline, R. K., T. Sikkeland, and R. N. Chanda

Experimental Observation of a New Region of Nuclear Deformation
UCRL-9888, Oct. 1961 Phys. Rev. Letters 7, 446 (1961)

Sheline, R. K. (see E. Marshalek, UCRL-10364)

Shirley, D. A. (see Q. O. Navarro, UCRL-9960)

Shirley, D. A. (see Q. O. Navarro, UCRL-9960-Rev.)

Shirley, D. A., M. Kaplan, R. W. Grant, and D. A. Keller

The Mössbauer Effect in $Eu^{151}$; Possible Influence of Optical Branches
UCRL-10168, April 1962 Phys. Rev. 127, 2097 (1962)

Shirley, D. A., and C. A. Lovejoy

Anomalous Quadrupole Coupling in Europium Ethylsulfate
UCRL-10202, June 1962 Phys. Rev. 128, 1733 (1962)

Shirley, D. A. (see M. Kaplan, UCRL-10207)

Shirley, D. A. (see J. N. Haag, UCRL-10242)

Shirley, D. A. (see R. W. Grant, UCRL-10322-Abs.)

Shirley, D. A. (see R. M. Levy, UCRL-10454)

Shirley, D. A. (see R. W. Grant, UCRL-10472)

Shirley, D. A. (see R. W. Grant, UCRL-10513-Abs.)

Shirley, D. A. (see P. H. Barrett, UCRL-10514-Abs.)

Shirley, D. A. (see R. B. Frankel, UCRL-10517-Abs.)

Siegbahn, K. (see J. M. Hollander, UCRL-10123)

Siegbahn, K., and F. Asaro

Magnetic Field Dependence of $Am^{243}$ $\alpha$-$\gamma$ Angular Correlations
UCRL-10419, Aug. 1962 Phys. Letters

Sikkeland, T., and V. Viola, Jr.

Direct Interaction in Reactions Between Heavy Ions and $U^{238}$
No UCRL number, June 1962 For Padua, Italy, Meeting on Direct Nuclear Interactions Sept. 1962

Sikkeland, T., E. Haines, and V. Viola, Jr.

Momentum Transfer in Heavy-Ion-Induced Fission
UCRL-9751, July 1961 Phys. Rev. 125, 1350 (1962)

Sikkeland, T. (see V. E. Viola, Jr., UCRL-10088)

Sikkeland, T. (see G. R. Choppin, UCRL-10226)

Sikkeland, T. (see V. E. Viola, Jr., UCRL-10284)

Sikkeland, T., and V. E. Viola, Jr.

Kinetic Energy Release in Fission Induced by Heavy Ions
UCRL-10355-Abs., Aug. 1962 — Abstract for "Discussion on Nuclear Chemistry Fission, and Other Low Energy Nuclear Processes," Oxford, England, Sept. 19, 1962

Simonoff, G. N., and J. M. Alexander

Angular Momentum Effects on Neutron Emission by Dy and Tb Compound Nuclei
UCRL-10099-Rev., Sept. 1962 — Phys. Rev.

Simonoff, G. N. (see J. M. Alexander, UCRL-10525)

Singh, S., and J. M. Alexander

Recoil Study of the Reaction $C^{12}(p, pn)C^{11}$
UCRL-9911, Dec. 1961 — Phys. Rev. 128, 711 (1962)

Sisson, D. H. (see J. M. Alexander, UCRL-10098)

Strieter, F. J., and D. H. Templeton

Crystal Structure of the Carbon Tetrabromide p-Xylene Complex
UCRL-9955, Dec. 1961 — Chem. Phys. 37, 161 (1962)

Sweeney, M. A.

Radiation Chemistry of Isopropyl Compounds
UCRL-9983, March 1962 — Ph. D. Thesis

Swiatecki, W. (see H. R. Bowman, UCRL-10139)

Swiatecki, W. (see H. R. Bowman, UCRL-10139-Rev.)

Templeton, D. H.

Dispersion Corrections for Atomic Scattering Factors
UCRL-9146, March 1960 — International Tables for X-Ray Crystallography, Vol. III (1962), 213-216

Templeton, D. H. (see T. N. Margulis, UCRL-9803)

Templeton, D. H. (see F. J. Strieter, UCRL-9955)

Templeton, D. H. (see A. Zalkin, UCRL-10149-Abs.)

Templeton, D. H. (see J. D. Forrester, UCRL-10150-Abs.)

Templeton, D. H. (see T. N. Margulis, UCRL-10151-Abs.)

Templeton, D. H. (see A. Zalkin, UCRL-10166)

Templeton, D. H. (see J. D. Forrester, UCRL-10197)

Templeton, D. H. (see J. N. Haag, UCRL-10242)

Templeton, D. H., and A. Zalkin

Crystal Structure of Europium Tungstate
UCRL-10344, June 1962 Acta Crystallog.

Templeton, D. H., A. Zalkin, and J. D. Forrester

Crystal Structure of the Hydrated Double Nitrate of Magnesium and Cerium
UCRL-10485-Abs., Oct. 1962 Abstract for APS Meeting, Stanford, Dec. 1962

Templeton, D. H., A. Zalkin, J. D. Forrester, and S. M. Williamson

Crystal and Molecular Structure of Xenon Tetrafluoride
UCRL-10597, Jan. 1963 J. Am. Chem. Soc.

Thomas, T. D., G. E. Gordon, R. M. Latimer, and G. T. Seaborg

Spallation-Fission Competition in Astatine Compound Nuclei Formed by Heavy-Ion Bombardment
UCRL-9950, Nov. 1961 Phys. Rev. 126, 1805 (1962)

Thomas, T. D. (see V. E. Viola, Jr., UCRL-10248)

Thompson, S. G. (see J. Gilmore, UCRL-9304-Rev.)

Thompson, S. G. (see H. R. Bowman, UCRL-9713-Rev.)

Thompson, S. G. (see F. Asaro, UCRL-9758)

Thompson, S. G. (see H. R. Bowman, UCRL-10139)

Thompson, S. G. (see H. R. Bowman, UCRL-10139-Rev.)

Thompson, S. G. (see R. C. Gatti, UCRL-10456)

Thompson, S. G. (see L. Phillips, UCRL-10464)

Tobocman, W.

A Shell-Model Theory of the R Matrix
UCRL-10432, Aug. 1962

Tobocman, W.

Theory of Alpha Decay
UCRL-10434, Aug. 1962

True, W. W.

Nitrogen-14 and the Shell Model
No UCRL number, Oct. 1962

Valentin, J., D. J. Horen, and J. M. Hollander

The Decay of $_{72}Hf^{173}$
UCRL-9731, June 1961 Nucl. Phys. 31, 353 (1962)

Valentin, J., D. J. Horen, and J. M. Hollander

Energy Levels of $_{71}Lu^{172}_{101}$
UCRL-9780, July 1961 Nucl. Phys. 31, 373 (1962)

Vermeulen, T. (see A. Hennico, UCRL-9415)

Vermeulen, T. (see L. H. Weiss, UCRL-9787)

Vermeulen, T. (see W. E. Dunn, UCRL-10394)

Vidal, J. G. (see G. Igo, UCRL-9996)

Viola, V. E., Jr. (see T. Sikkeland, No UCRL number)

Viola, V. E., Jr. (see T. Sikkeland, UCRL-9751)

Viola, V. E., Jr., and T. Sikkeland

Total Cross Sections for Fission of $U^{238}$ Induced by $He^4$ and Heavy Ions
UCRL-10088, Feb. 1962 Phys. Rev.

Viola, V. E., Jr., T. D. Thomas, and Glenn T. Seaborg

Angular Distribution of Fragments from Fission Induced by Heavy Ions in Gold and Bismuth
UCRL-10248, May 1962 Phys. Rev. 128, 767 (1962)

Viola, V. E., Jr., and T. Sikkeland

Kinetic Energy Release in Heavy-Ion-Induced Reactions
UCRL-10284, Oct. 1962 Phys. Rev.

Viola, V. E., Jr. (see T. Sikkeland, UCRL-10355-Abs.)

Wallmann, J. C. (see D. B. McWhan, No UCRL number)

Wasan, D. (see F. J. Heinzelmann, UCRL-10421)

Wasif, S. (see J. M. Alexander, UCRL-10193)

Weeks, B. M. (see W. M. Garrison, No UCRL number)

Weeks, B. M. (see W. M. Garrison, UCRL-9903)

Weiss, L. H., J. L. Fick, R. H. Houston, and T. Vermeulen

Dispersed-Phase Distribution Patterns in Liquid-Liquid Agitation
UCRL-9787, Sept. 1962

Whitney, D. C., and R. M. Diamond

The Extraction of Acids by Basic Organic Solvents.
I. Tributyl Phosphate-$HClO_4$ and Tributyl Phosphate-$HReO_4$
UCRL-10063, April 1962 J. Phys. Chem.

Whitney, D. C.

The Effects of Ion Hydration in Solvent Extration and Ion Exchange
UCRL-10505, Oct. 1962 Ph. D. Thesis

Whitney, D. C., and R. M. Diamond

Ion-Exchange Studies in Concentrated Solutions.
I. The Alkali Cation with a Sulfonic Acid Resin
UCRL-10595, Dec. 1962

Wickman, H. H. (see M. Abraham, UCRL-10567)

Wilcox, D. E.

Method for Estimating the Heat of Formation and Free Energy of Formation of Inorganic Compounds
UCRL-10397, Aug. 1962 Chem. Eng. M. S. Thesis

Wilcox, W. R., and C. R. Wilke

Pure Diffusional Mass Transfer in Zone Melting
UCRL-10433, Aug. 1962 A. I. Ch. E. Journal

Wilke, C. R. (see W. E. Dunn, UCRL-10394)

Wilke, C. R. (see F. J. Heinzelmann, UCRL-10421)

Wilke, C. R. (see W. R. Wilcox, UCRL-10433)

Wilkins, B. D. (see G. Igo, No UCRL number)

Wilkins, B. D. (see G. Igo, UCRL-10145-Abs.)

Wilkins, B. D. (see G. Igo, UCRL-10146-Abs.)

Wilkins, B. D. (see G. Igo, UCRL-10147-Abs.)

Wilkins, B. D. (see G. Igo, UCRL-10281-Abs.)

Wilkins, B. D., and G. Igo

10-MeV Proton Reaction Cross Sections for Several Elements
UCRL-10281, Aug. 1962 Phys. Rev.

Wilkins, B. D. (see G. Igo, UCRL-10480)

Wilkins, B. D., and G. Igo

Total Reaction Cross Sections for 22.4-MeV Deuterons
UCRL-10500, Oct. 1962 Phys. Letters 3, 48 (1962)

Wilkins, B. D. (see G. Igo, UCRL-10568)

Williamson, S. M. (see D. H. Templeton, UCRL-10597)

Word, T. T. (see W. E. Dunn, UCRL-10394)

Worden, E. F., R. G. Gutmacher, E. K. Hulet, J. G. Conway, and M. Fred

The Ground Term of the First Spectrum of Curium
No UCRL number, July 1962 J. Opt. Soc. Am.

Wybourne, B. G.

Electrostatic Interactions in Complex Electron Configuration
UCRL-10443, Aug. 1962 J. Math. Phys.

Wybourne, B. G.

Energy Matrices of the $f^5$ Electron Configuration
UCRL-10448, Sept. 1962

Wybourne, B. G. (see J. G. Conway, UCRL-10566)

Yaffe, L. (see D. J. Horen, UCRL-10413)

Zalkin, A., K. Lee, and D. H. Templeton

Crystal Structure of $CsMnF_3$
UCRL-10149-Abs., March 1962 Abstract for American Crystollagraphic Association, Villanova University, Philadelphia, June 1962

Zalkin, A. (see J. D. Forrester, UCRL-10150-Abs.)

Zalkin, A., K. Lee, and D. H. Templeton

The Crystal Structure of $CsMnF_3$
UCRL-10166, April 1962 J. Chem. Phys. 37, 697 (1962)

Zalkin, A. (see J. D. Forrester, UCRL-10197)

Zalkin, A. (see D. H. Templeton, UCRL-10344)

Zalkin, A. (see D. H. Templeton, UCRL-10485-Abs.)

Zalkin, A. (see D. H. Templeton, UCRL-10597)

## 2. CONTRIBUTIONS TO THIS REPORT

Abraham, M. M. D. 26
Alpert, S. S. A. 10
Asaro, F. A. 25, A. 26, A. 27 A. 28

Barrett, P. H. A. 7, D. 15, D. 16
Bolotin, H. H. A. 16
Bowman, H. R. B. 14
Brandt, R. B. 10, B. 12, D. 9, G. 6
Bromley, L. A. F. 1, F. 2
Budick, B. A. 10, A. 13
Burnett, D. S. B. 13

Cerny, J. C. 9
Cohen, S. B. 15
Conway, J. G. D. 19, D. 20, D. 21 D. 22
Conzett, H. E. C. 4, C. 11
Cunningham, B. B. D. 10

Darriulat, P. C. 7
Diamond, R. M. A. 18, A. 23, D. 4, D. 5, D. 6
Doyle, W. M. A. 13, A. 19, A. 21
Dunn, W. F. 5

Forrester, J. D. D. 11, D. 12, D. 13, D. 14
Fraenkel, Z. B. 9
Frankel, R. B. A. 7
Fred, M. D. 21
Fried, S. M. D. 9

Gatti, R. C. B. 10, B. 12, D. 9
Getzinger, R. W. G. 8
Ghiorso, A. A. 26
Gillet, V. A. 31
Glendenning, N. K. C. 3
Graham, R. J. G. 9
Graham, R. L. E. 1
Grant, R. W. A. 12, A. 15, D. 15, D. 17
Gutmacher, R. C. D. 21

Haines, E. L. B. 11
Harvey, B. G. C. 7, C. 9
Hebert, A. J. G. 7
Heinzelmann, F. J. F. 3
Hollander, J. M. A. 29, E. 1
Horen, D. J. A. 4, A. 5, A. 8, A. 9, A. 16
Hulet, E. K. D. 21
Hyder, M. L. D. 2

Igo, G. C. 2, C. 4, C. 5, C. 6, C. 8

Johansson, S. A. E. A. 30, B. 7, B. 8
Jones, W. B. C. 7
Judd, B. R. A. 14, D. 23, D. 26

Kaplan, M. A. 3, A. 15, D. 15, D. 17
Keller, D. A. A. 15, D. 15, D. 17
Kelly, W. H. A. 4, A. 5, A. 8, A. 9, A. 16
Kim, Y. E. A. 6, A. 24

This report was prepared as an account of Government sponsored work. Neither the United States, nor the Commission, nor any person acting on behalf of the Commission:

A. Makes any warranty or representation, expressed or implied, with respect to the accuracy, completeness, or usefulness of the information contained in this report, or that the use of any information, apparatus, method, or process disclosed in this report may not infringe privately owned rights; or

B. Assumes any liabilities with respect to the use of, or for damages resulting from the use of any information, apparatus, method, or process disclosed in this report.

As used in the above, "person acting on behalf of the Commission" includes any employee or contractor of the Commission, or employee of such contractor, to the extent that such employee or contractor of the Commission, or employee of such contractor prepares, disseminates, or provides access to, any information pursuant to his employment or contract with the Commission, or his employment with such contractor.